8. SITE 762[1]

Shipboard Scientific Party[2]

HOLE 762A

Date occupied: 26 July 1988

Date departed: 26 July 1988

Time on hole: 8 hr, 45 min

Position: 19°53.23′S, 112°15.24′E

Bottom felt (rig floor; m, drill pipe measurement): 1371.3

Distance between rig floor and sea level (m): 11.4

Water depth (drill pipe measurement from sea level, m): 1359.9

Total depth (rig floor; m): 1380.80

Penetration (m): 9.50

Number of cores (including cores with no recovery): 1

Total length of cored section (m): 9.50

Total core recovered (m): 10.04

Core recovery (%): 105

Oldest sediment cored:
Depth (mbsf): 9.50
Nature: foraminifer nannofossil ooze
Age: Quaternary
Measured velocity (km/s): 1.55

HOLE 762B

Date occupied: 26 July 1988

Date departed: 27 July 1988

Time on hole: 16 hr, 30 min

Position: 19°53.24′S, 112°15.24′E

Bottom felt (rig floor; m, drill pipe measurement): 1371.4

Distance between rig floor and sea level (m): 11.4

Water depth (drill pipe measurement from sea level, m): 1360.0

Total depth (rig floor; m): 1546.80

Penetration (m): 175.40

Number of cores (including cores with no recovery): 19

Total length of cored section (m): 175.40

Total core recovered (m): 174.90

Core recovery (%): 99

Oldest sediment cored:
Depth (mbsf): 175.40
Nature: foraminifer nannofossil ooze
Age: lower Oligocene
Measured velocity (km/s): 1.6

[1] Haq, B. U., von Rad, U., et al., 1990. *Proc. ODP, Init. Repts.*, 122: College Station, TX (Ocean Drilling Program).

[2] Shipboard Scientific Party is as given in the list of Participants preceding the contents.

HOLE 762C

Date occupied: 26 July 1988

Date departed: 5 August 1988

Time on hole: 9 days, 5 hr

Position: 19°53.23′S, 112°15.24′E

Bottom felt (rig floor; m; drill pipe measurement): 1371.4

Distance between rig floor and sea level (m): 11.4

Water depth (drill pipe measurement from sea level, m): 1360.0

Total depth (rig floor; m): 2311.40

Penetration (m): 770.00

Number of cores (including cores with no recovery): 91

Total length of cored section (m): 940.00

Total core recovered (m): 534.64

Core recovery (%): 69

Oldest sediment cored:
Depth (mbsf): 940.00
Nature: silty claystone
Age: Berriasian
Measured velocity (km/s): 1.9

Principal results: Site 762 (proposed Site EP12P, 19°53.24′S, 112°15.24′E, water depth 1360 m) is located on the western part of the central Exmouth Plateau. In this area a thick Triassic paralic section is unconformably overlain by a thin upper Jurassic marine succession and lower Cretaceous prodelta sediments, which is in turn covered by mid-Cretaceous to Cenozoic pelagic carbonates. This site was chosen to provide documentation of the Cretaceous and Tertiary depositional sequences and cycles of sea-level change in an area with excellent seismic-stratigraphic control. Together with Site 763 (which is closer to the source of terrigenous influx), this site was expected to furnish data that will help separate the tectonic, sedimentary, and eustatic signals for testing sequence stratigraphic models.

Site 762 was drilled to a total depth (TD) of 940 m and recovered a section ranging in age from Berriasian to Quaternary, with an overall recovery rate of 75%. The upper 182 m of foraminifer-nannofossil and nannofossil oozes of late Oligocene through Quaternary age are underlain by nannofossil oozes and chalks of early Paleocene to late Oligocene age with numerous intervals of cyclic color bands. The Cretaceous/Tertiary boundary occurs at 554.6 mbsf, within the nannofossil chalk, and is marked by a slight color change.

The chalky lithofacies is present to 838.5 mbsf. Clay content is generally greater in the lower part of the section; age ranges from early Albian to latest Maestrichtian. The Cenomanian chalks include abundant pressure-solution contacts (stylolites). The Cenomanian/Turonian boundary is well represented by an interval rich in organic material. Below 838.5 mbsf, a 10-m-thick unit of black shales (equivalent to Muderong Shales on land) of early Aptian age probably represents a period of anoxia on the plateau in an open-marine setting. The mid-Cretaceous to Paleogene section is essentially complete and in large part well preserved. The black shales are unconformably underlain by silty claystones and prodelta claystones of Berriasian to early Valanginian age (equivalent to the Barrow Group on land), which extend to the TD of 940 mbsf. A belemnite-rich horizon below the black shales might

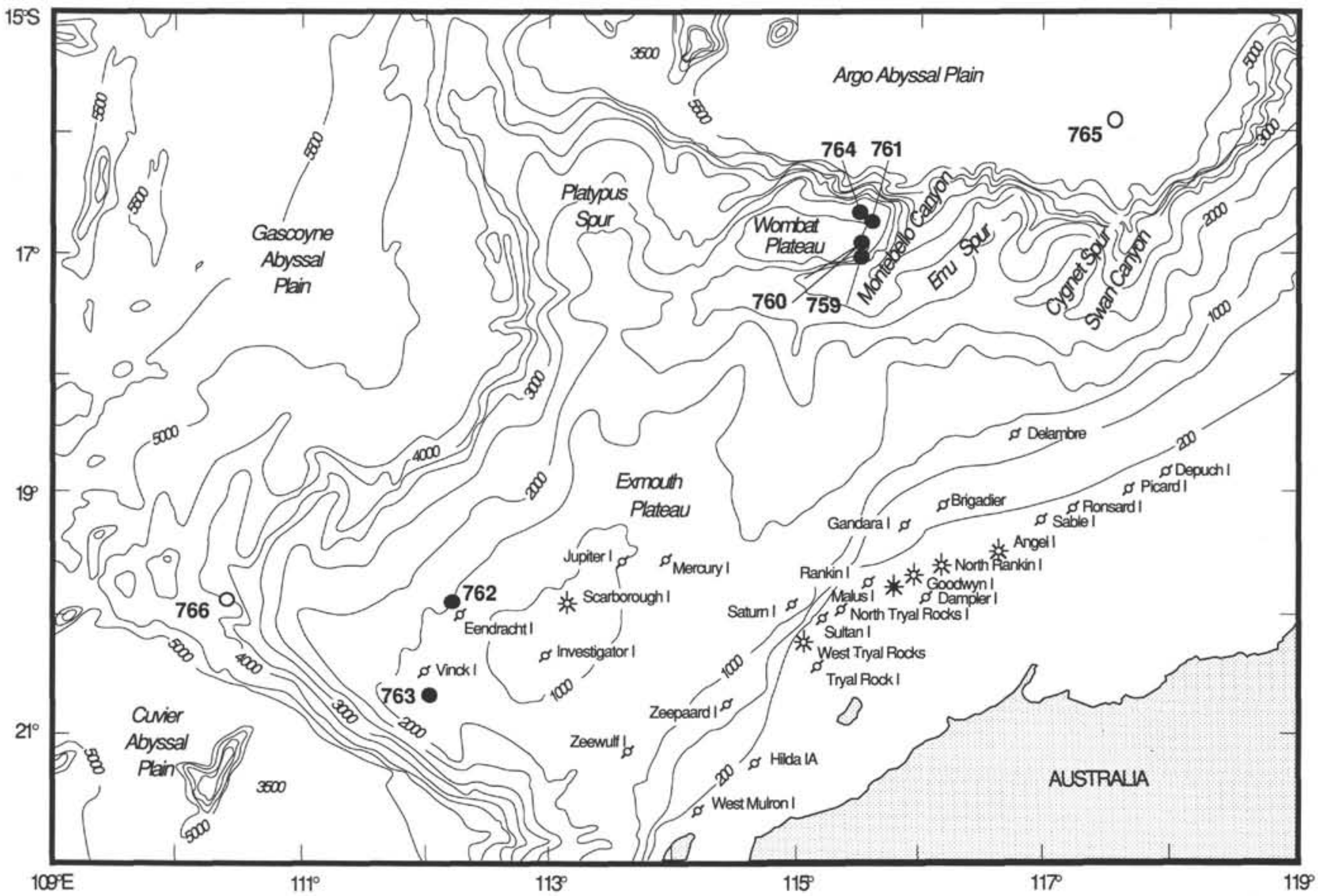

Figure 1. Bathymetric map of Exmouth Plateau showing location of ODP sites (closed circles = Leg 122 sites, open circles = Leg 123 sites) and commercial wells. Leg 122 Sites 759 and 760 are at the position of proposed Site EP10A. Site 761 corresponds to EP9E. Bathymetry is in meters (Exon, unpubl. data).

represent the beginning of a major global late Neocomian transgression.

The site yielded an expanded Maestrichtian-Paleocene succession with well-preserved calcareous microflora and fauna, suitable for detailed magneto-biostratigraphic and stable-isotopic work. Nannofossils, and to some extent, foraminifers, were useful in assigning ages to the pre-Tertiary section. Rich dinoflagellate assemblages were found in the Aptian black shales.

Three logging runs with the seismic-stratigraphic, geochemical, and neutron-density tools generated logs for detailed correlations and for safety considerations regarding the subsequent drilling of Site 763. Careful monitoring of hydrocarbon gases revealed relatively high values of methane between 400 and 850 mbsf, occurring as the dissolved component of sediment pore waters. Traces of ethane were also recorded. Rock-Eval analysis revealed the organic matter to be of type III (woody-coaly, terrestrial), indicating that the gases are of thermogenic origin, sourced from the underlying Triassic.

The interval between 600 and 715 mbsf was determined to be slightly overpressured. Correlation was excellent between the log response, physical properties, and litho- and biostratigraphic data from Site 762; in addition, results from the site compared well with regional seismic data and the well-site data from the Eendracht-1 well. These data will be invaluable for the detailed sequence-stratigraphic analysis of the area.

BACKGROUND AND OBJECTIVES

Site 762 (proposed Site EP12P) is located on the western part of the central Exmouth Plateau in a water depth of about 1360 m (Fig. 1). Proximity to the western margin of the Exmouth Plateau suggests that the site was influenced by the pre-breakup (Triassic to Jurassic) rift tectonics of the margin, which continued as the (Neocomian) breakup occurred and the northwestward migration of "greater India" was initiated by seafloor spreading in the Gascoyne Abyssal Plain (Falvey and Mutter, 1981; Exon et al., 1982). The stratigraphic sequence along the western margin consists of a thick Triassic paralic section, unconformably overlain by a thin upper Jurassic marine succession and upper Cretaceous and Cenozoic pelagic carbonates.

The availability of data from extensive exploratory seismic work and commercial wells on the Exmouth Plateau (including the west-central region in the vicinity of Site 762) makes this a very desirable area for the study of the evolution of passive continental margins. Numerous evolutionary models of margin development have been proposed (Falvey, 1974; Mauffret and Montadert, 1987; Lemoine and Trümpy, 1987) that envision the mechanism of passive-margin evolution in terms of uplift and subsidence cycles, or of varying thermal response of the continental and oceanic lithosphere. Recently, a joint U.S.-Australian two-ship seismic reflection/refraction experiment was conducted on the Exmouth Plateau. This study identified large rotated fault blocks and a set of prominent subhorizontal mid-crustal detachment faults under the central part of the plateau (Mutter et al., 1989; Williamson and Falvey, 1988). These data led Mutter and colleagues to propose that the deformation on the outer part of the plateau (near Site 762) was produced by lithospheric thinning and "pure shear" (high-angle normal faults and McKenzie-type

Table 1. Coring summary, Site 762.

Core no.	Date (July 1988)	Time (local)	Depth (mbsf)	Cored (m)	Recovered (m)	Recovery (%)
122-762A-						
1H	26	1100		9.5	10.04	105.7
Coring totals				9.5	10.04	105.7
122-762B-						
1H	26	1120	0.0–4.4	4.4	4.39	99.8
2H	26	1150	4.4–13.9	9.5	9.92	104.4
3H	26	1210	13.9–23.4	9.5	8.69	91.5
4H	26	1240	23.4–32.9	9.5	9.49	99.9
5H	26	1310	32.9–42.4	9.5	8.65	91.1
6H	26	1340	42.4–51.9	9.5	9.74	102.5
7H	27	1410	51.9–61.4	9.5	9.69	102.0
8H	26	1440	61.4–70.9	9.5	8.83	92.9
9H	26	1500	70.9–80.4	9.5	9.35	98.4
10H	26	1530	80.4–89.9	9.5	9.98	105.1
11H	26	1605	89.9–99.4	9.5	9.68	101.9
	(Pore-water sampling and heat-flow measurement)					
12H	26	1820	99.4–108.9	9.5	9.86	103.8
13H	26	1845	108.9–118.4	9.5	10.18	107.2
14H	26	1935	118.4–127.9	9.5	9.90	104.2
15H	26	2005	127.9–137.4	9.5	9.05	95.3
16H	26	2100	137.4–146.9	9.5	9.07	95.5
17H	26	2155	146.9–156.4	9.5	9.22	97.1
	(Pore-water sampling and heat-flow measurement)					
18H	27	0000	156.4–165.9	9.5	10.31	108.5
19H	27	0030	165.9–175.4	9.5	9.00	94.7
Coring totals				175.4	175.00	99.77
122-762C-						
1C	27	0630	0.0–170.0	(Wash and drill—170.0 m)		
2X	27	0700	170.0–179.5	9.5	7.35	77.3
3X	27	0730	179.5–189.0	9.5	6.10	64.2
4X	27	0800	189.0–198.5	9.5	6.64	69.9
5X	27	0815	198.5–208.0	9.5	2.42	25.5
6X	27	0840	208.0–217.5	9.5	6.82	71.8
7X	27	0910	217.5–227.0	9.5	6.62	69.7
8X	27	0930	227.0–236.5	9.5	7.04	74.1
9X	27	1000	236.5–246.0	9.5	1.15	12.1
10X	27	1025	246.0–255.5	9.5	6.17	64.9
11X	27	1050	255.5–265.0	9.5	9.21	96.9
12X	27	1105	265.0–274.5	9.5	9.38	98.7
13X	27	1130	274.5–284.0	9.5	2.87	30.2
14X	27	1155	284.0–293.5	9.5	9.47	99.7
15X	27	1240	293.5–303.0	9.5	4.33	45.6
16X	27	1305	303.0–312.5	9.5	5.49	57.8
17X	27	1400	312.5–322.0	9.5	7.99	84.1
18X	27	1500	322.0–331.5	9.5	9.51	100.0
19X	27	1540	331.5–341.0	9.5	6.16	64.8
20X	27	1610	341.0–350.5	9.5	5.48	57.7
21X	27	1710	350.5–360.0	9.5	2.95	31.0
22X	27	1805	360.0–369.5	9.5	9.13	96.1
23X	27	1915	369.5–379.0	9.5	4.38	46.1
24X	27	2050	379.0–388.5	9.5	1.97	20.7
25X	27	2300	388.5–398.0	9.5	7.11	74.8
26X	28	0130	398.0–402.5	4.5	8.21	182.0
27X	28	0345	402.5–412.0	9.5	6.29	66.2
28X	28	0540	412.0–421.5	9.5	2.10	22.1
29X	28	0730	421.5–431.0	9.5	4.60	48.4
30X	28	0830	431.0–440.5	9.5	5.67	59.7
31X	28	0915	440.5–450.0	9.5	9.20	96.8
32X	28	1005	450.0–459.5	9.5	3.89	40.9
33X	28	1050	459.5–469.0	9.5	8.73	91.9
34X	28	1615	469.0–478.5	9.5	7.99	84.1
35X	28	1815	478.5–488.0	9.5	3.13	32.9
36X	28	2000	488.0–497.5	9.5	0.78	8.2
37X	28	2215	497.5–507.0	9.5	6.82	71.8
38X	28	2340	507.0–516.5	9.5	9.80	103.0
39X	29	0115	516.5–526.0	9.5	7.94	83.6
40X	29	0250	526.0–535.5	9.5	9.83	103.0
41X	29	0425	535.5–545.0	9.5	9.85	103.0
42X	29	0555	545.0–554.5	9.5	9.70	102.0
43X	29	0715	554.5–564.0	9.5	7.43	78.2
44X	29	0840	564.0–573.5	9.5	9.82	103.0
45X	29	1000	573.5–583.0	9.5	8.03	84.5

Table 1 (continued).

Core no.	Date (July 1988)	Time (local)	Depth (mbsf)	Cored (m)	Recovered (m)	Recovery (%)
46X	29	1050	583.0–592.5	9.5	6.40	67.3
47X	29	1215	592.5–602.0	9.5	9.56	100.0
48X	29	1305	602.0–611.5	9.5	9.86	104.0
49X	29	1710	611.5–621.0	9.5	8.34	87.8
50X	29	1830	621.0–630.5	9.5	9.88	104.0
51X	29	1930	630.5–640.0	9.5	9.25	97.3
52X	29	2040	640.0–649.5	9.5	9.77	103.0
53X	29	2140	649.5–659.0	9.5	9.46	99.6
54X	29	2245	659.0–668.5	9.5	9.92	104.0
55X	30	0000	668.5–678.0	9.5	5.10	53.7
56X	30	0120	678.0–687.5	9.5	9.90	104.0
57X	30	0230	687.5–697.0	9.5	3.73	39.2
58X	30	0325	697.0–706.5	9.5	8.57	90.2
59X	30	0425	706.5–716.0	9.5	8.40	88.4
60X	30	0530	716.0–725.5	9.5	4.87	51.2
61X	30	0620	725.5–735.0	9.5	3.37	35.5
62X	30	0730	735.0–744.5	9.5	7.88	82.9
63X	30	0845	744.5–754.0	9.5	3.46	36.4
64X	30	0945	754.0–760.0	6.0	5.35	89.1
65X	30	1045	760.0–765.0	5.0	0.61	12.2
66X	30	1145	765.0–770.0	5.0	6.98	139.0
67X	30	1245	770.0–775.0	5.0	1.00	20.0
68X	30	1400	775.0–780.0	5.0	1.91	38.2
69X	30	1510	780.0–785.0	5.0	2.57	51.4
70X	30	1710	785.0–790.0	5.0	1.27	25.4
71X	30	1850	790.0–795.0	5.0	3.45	69.0
72X	30	2000	795.0–799.5	4.5	3.02	67.1
73X	30	2120	799.5–804.5	5.0	4.01	80.2
74X	30	2325	804.5–809.5	5.0	3.66	73.2
75X	31	0105	809.5–814.5	5.0	4.19	83.8
76X	31	0250	814.5–819.5	5.0	5.82	116.0
77X	31	0510	819.5–829.0	9.5	9.76	103.0
78X	31	0740	829.0–838.5	9.5	3.13	32.9
79X	31	0855	838.5–843.5	5.0	4.63	92.6
80X	31	1030	843.5–848.5	5.0	0.04	0.8
81X	31	1130	848.5–853.5	5.0	4.88	97.6
82X	31	1300	853.5–858.5	5.0	5.22	104.0
83X	31	1420	858.5–863.5	5.0	1.41	28.2
84X	31	1610	863.5–873.0	9.5	1.51	15.9
85X	31	1810	873.0–882.5	9.5	2.61	27.5
86X	31	2045	882.5–892.0	9.5	6.12	64.4
87X	31	2300	892.0–901.5	9.5	2.49	26.2
88X	01	0135	901.5–911.0	9.5	9.86	104.0
89X	01	0430	911.0–920.5	9.5	7.41	78.0
90X	01	0700	920.5–930.0	9.5	6.31	66.4
91X	01	1020	930.0–940.0	10.0	2.15	21.5
Coring totals				770.0	534.64	69.4
Wash and drill = 170.0 m						

stretching), and postdates the "thin-skinned" deformation with "simple-shear" detachment systems (Wernicke-type deformation) under the central part of the plateau (near Site 763).

The central Exmouth Plateau sediments were deposited in an extension of the Carnarvon Basin, which formed a north-facing Tethyan embayment in Gondwana and received detrital sediments from the south until Neocomian (early Cretaceous) time. On the central plateau some 3000 m of paralic and shallow-marine detrital sediments were deposited during Permian through mid-Jurassic time. After the late Triassic rifting, about 1000 m of deltaic sediments derived from the south and east covered the late Jurassic and early Cretaceous block-faulted surface.

Deposition on Exmouth Plateau can thus be interpreted as having occurred in two distinct phases: (1) a pre-Neocomian phase, during which a large body of synrift and pre-breakup sediments (composed predominantly of detrital terrigenous material shed southward and eastward from the hinterlands) were deposited over thick continental and marginal-marine facies; and (2) a post-Neocomian phase, relatively sediment starved, with decreasingly less terrigenous influence towards the northern and western parts of the plateau.

Site 762 was drilled approximately 2 km northeast of the Eendracht-1 well, to a total depth of 940 mbsf. Eendracht-1 well data indicated an upper 550 m of early Paleocene to Quaternary pelagic ooze overlying the Cretaceous/Tertiary boundary, below which is 114 m of Maestrichtian calcareous mudstones and claystones. The Maestrichtian is unconformably underlain by a 142-m-thick, lower Turonian to upper Middle Campanian section equivalent to the Toolonga Calcilutite on land. An early Turonian regional marker horizon seen on logs from the area is represented by dark green shales with siliceous flecks.

The Toolonga Calcilutite is unconformably underlain by the upper Albian to Cenomanian Gearle Siltstone equivalent, which is approximately 25 m thick in this area. This siltstone unit was deposited in a shelfal setting during a sea-level highstand. An increase in gamma-ray values on the logs from this unit indicates an increased amount of clay. The base of the siltstone is disconformably underlain by a 10-m-thick unit of shales equivalent to the Muderong Shales (Hauterivian to Barremian in age), also deposited in a shelfal setting.

The Berriasian to Valanginian prodelta sediments of the Barrow Group underlie the Muderong Shales and include 150 m of marginal-marine siltstones and claystones. Both lower

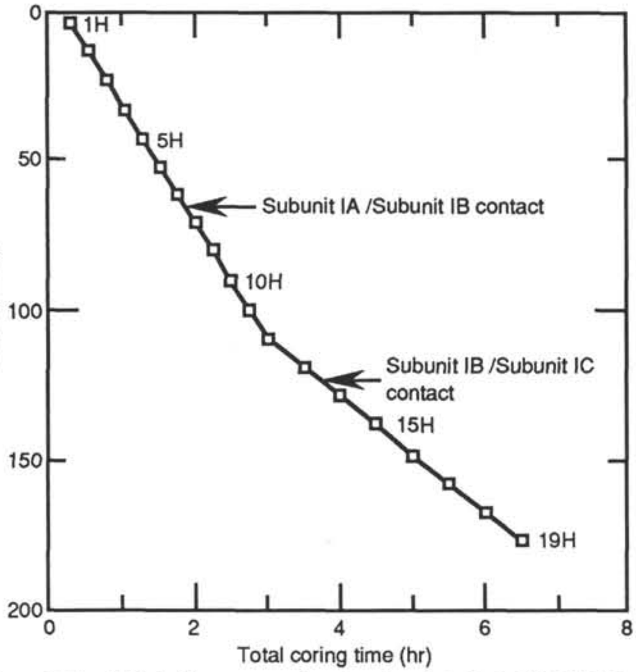

Figure 2. Depth (mbsf) versus total coring time (hr), Hole 762B (APC).

and upper delta sequences are apparently present. The depositional systems of the Barrow Delta are of prime interest for sequence stratigraphy, and represent a prograding clastic wedge bounded by major unconformities. The lower unconformity is characterized by a marked erosion of the underlying shelf (Erskine and Vail, 1988). Drilling at Site 762 provides important information about the age and the nature of these unconformities/sequence boundaries.

The Barrow siltstones and claystones are underlain by a condensed Jurassic section that consists of 28 m of claystones and calcareous claystones equivalent to the Dingo Claystone. The latter is separated from the thick Mungaroo Formation equivalent (which contains deltaic to marginal-marine siltstones and calcareous claystones) by a 45-m-thick Rhaetian-Norian calcareous claystone deposited in an oxidizing marine environment. Because the Dingo Claystone may act as a seal and barrier for the gas shows previously recorded in the Mungaroo section, the JOIDES Pollution Prevention and Safety Panel (PPSP) mandated that the drilling at Site 762 be terminated within the Barrow Group, about 50 m above the top of the Dingo Claystone.

Objectives

The multiple objectives of Site 762 (and nearby Site 763) are listed below:

1. To decipher the post-breakup sedimentary history and paleoenvironmental evolution of the continental margin typified by the central Exmouth Plateau. This starved margin is ideally suited for such studies and will provide important clues about the evolution from a "juvenile" to a "mature" ocean margin. Precision in the reconstruction of subsidence histories depends on the accuracy of the biostratigraphic control and paleodepth indicators. On the central Exmouth Plateau (Sites 762 and 763) we expect good paleontological control for both age and paleodepth determinations.
2. To study the Cretaceous and Tertiary depositional sequences of the clastic (and the subsequent pelagic) depositional system of the central Exmouth Plateau. Because of good biostratigraphic control at Sites 762 and 763 we expect to be able to date the unconformities and the systems tract boundaries within sequences precisely. In addition, sequence analyses of the extensive regional seismic data, the well logs from existing industry well-sites, and the logs obtained during Leg 122 collectively provide a basis for sequence stratigraphic interpretations. The reconstruction of subsidence history using geohistory curves would allow us to evaluate and distinguish between the effects of basin subsidence, sediment input, and the eustatic signal. This could lead to a rigorous testing of

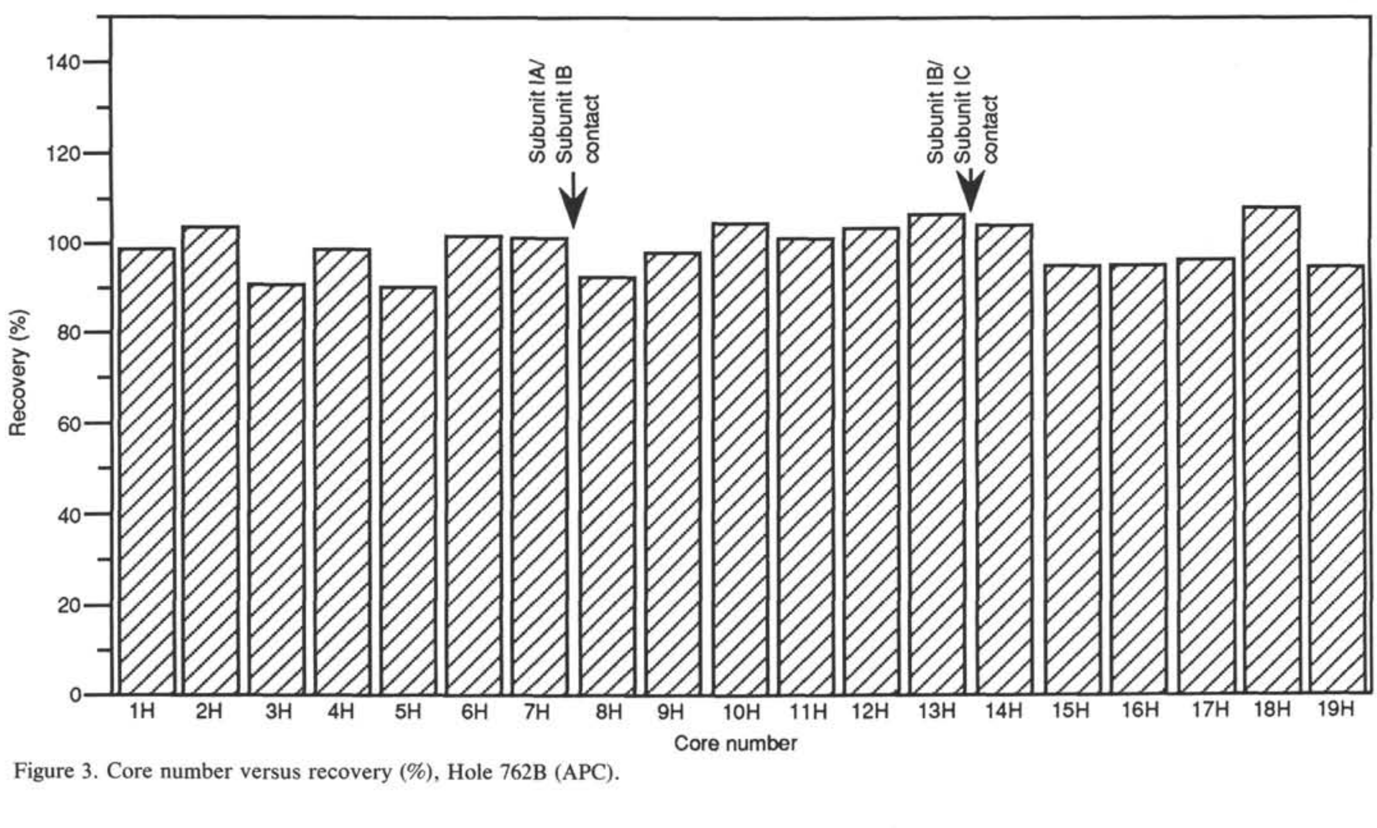

Figure 3. Core number versus recovery (%), Hole 762B (APC).

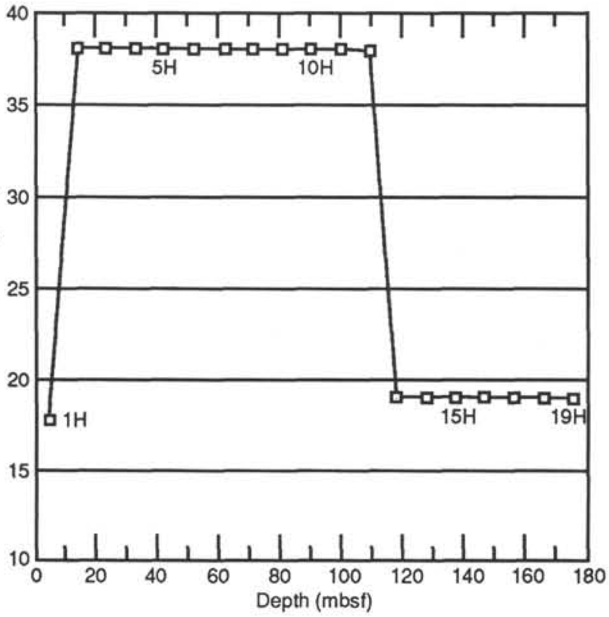

Figure 4. Penetration rate (m/hr) versus depth (mbsf), Hole 762B (APC).

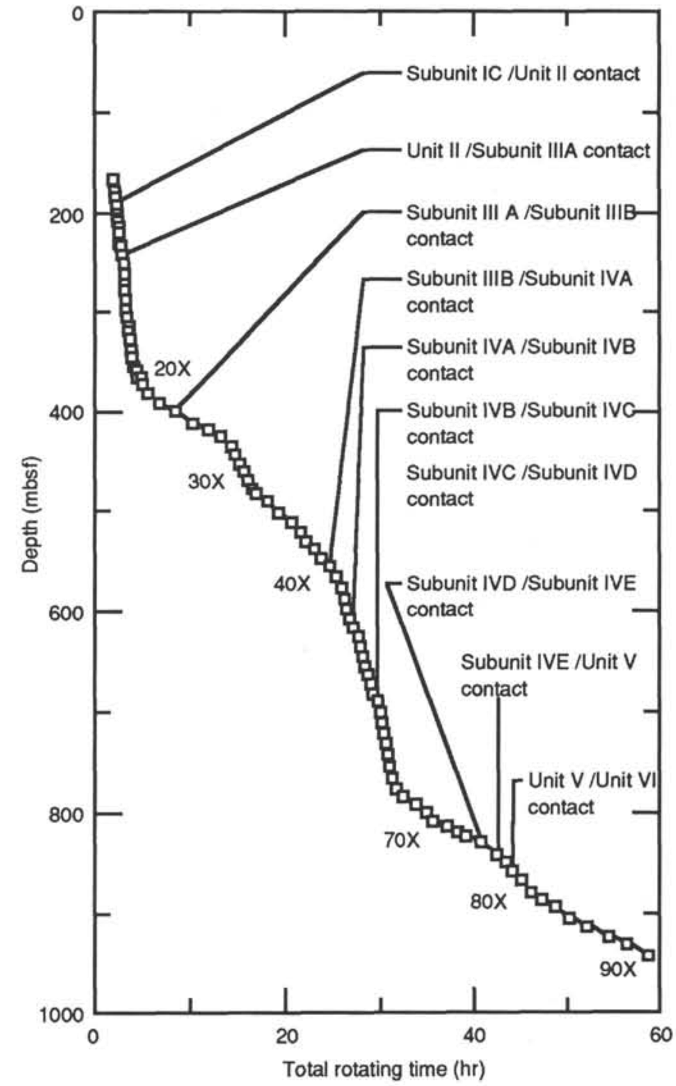

Figure 5. Depth (mbsf) versus total rotating time (hr), Hole 762C (XCB).

both the sequence stratigraphic depositional models and the new eustatic sea-level curves (Haq et al., 1987).

3. To refine Mesozoic magneto- and biochronostratigraphy. Sites 762 and 763 furnish important new biostratigraphic data for the Cretaceous, and magnetostratigraphic studies of the cores provide important first-order ties between bio- and magneto-chrons.

4. To recover complete Cretaceous/Tertiary boundary intervals, where possible. At Site 762 the Cretaceous/Tertiary boundary occurs at about 550 mbsf, within an interval with good fossil assemblages and a lithology suitable for detailed biofacies and isotopic work.

OPERATIONS

Hole 762A

Hole 762A is southwest of Hole 761C. The steaming time between sites was 24-1/4 hr, which included a brief geophysical survey as the site was being approached. The beacon was dropped near 20°35.20'S, 112°12.50'E at 0215 hr (local time, or LT), 26 July 1988. Geophysical gear was recovered, thrusters lowered, and station keeping established. The same bottom-hole assembly (BHA) used on previous advanced-piston-corer/extended-core-barrel (APC/XCB) holes was made up. An 11-7/16 in. Security S86F Code 5-3-7 bit was selected.

The precision-depth recorder (PDR) water depth was 1376.3 m from the dual elevator stool (DES) on the rig floor. As it was anticipated that several reentries might be required to reach total depth, a wash-in test was conducted to determine the amount of 16-in. casing that could be jetted in. The bottom was found to be very soft, and the bit was raised to 74 mbsf with only 0–10,000 pounds of additional weight (overpull) and a circulation rate of 100 gallons per minute (gpm). Our conclusion was that 4 joints (about 160 ft) of 16-in. pipe could be jetted in with little difficulty.

The mud-line core was shot with the bit at 1371.3 m (from the rig floor). The core barrel was full when recovered, indicating that the bit had been below the mud line. The core was curated, and preparations were made for a "B hole."

Hole 762B

The bit was raised to 1366.3 m for the second mud-line shot. The mud line was obtained on this attempt and thus was established to be at 1371.4 m from the DES. A total of 19 APC cores were taken to 175.4 mbsf (Table 1, Fig. 2). Recovery was 99.8% (Fig. 3). No coring problems were encountered for the first 19 cores (Fig. 4). Core 122-762B-19H pulled free with 40,000 lbs overpull, but after pulling on Core 122-762B-20H for 30 min, the piston rod parted at 160,000 lbs (the rod was designed to part at 100,000 lbs). The barrel was left at total depth, terminating the hole.

Hole 762C

The drill pipe was pulled clear of the seafloor, and the ship was moved 20 m north to avoid the lost core barrel.

The planned depth of this hole was 940 mbsf; we believed this to be possible to drill with 2 bits. Our operational plan was to drill as deep as possible with the XCB, launch a free-fall reentry cone, reenter with an RCB assembly, and finish the hole. The alternative was to core as deep as possible with the XCB, make a pipe trip for an RCB bit, drill to the depth where the XCB hole had been terminated, and then core to the total depth.

An 11-7/16 in. Security S86F IADC Code 5-3-7 bit was selected, and the BHA was the standard APC/XCB assembly that had been run on previous holes. Core 122-762C-1C was drilled to 170.0 mbsf, with a rotating time of 89 min with the Atride center bit. Coring conditions from 170.0 through 360.0 mbsf, in calcareous ooze, were excellent; the average rotating time was only 6 min, with a recovery of 67% (Figs. 5 and 6). At 360.0 mbsf the rate of penetration suddenly decreased to less than 20 m/hr (Fig. 7).

The rate of penetration was generally slow in the chalk (between 360.0 and 554.5 mbsf). Below 554.5 mbsf, penetration increased and remained variable but high until 716.0 mbsf. From 765.0 mbsf through 863.5 mbsf, 5-m cores were taken in an effort to improve recovery, with only partially successful results. A wiper trip was made at 611.5 mbsf. There was no excessive drag, and only 8 m of fill was at the bottom of the hole. At 838.5 mbsf, a 10-m thick unit of black to dark gray calcareous claystone was encountered. This material is underlain by black to very dark gray silty claystone and clayey siltstone with minor interbedded limestones (see "Lithostratigraphy," this chapter). The hole had been stable as oozes and chalks were being cored, but we noted that the outer surfaces of claystone and siltstone cores appeared to be disintegrating upon recovery. Some hole fill began to occur between connections, and samples of this material fell apart in a matter of minutes in both seawater and freshwater. Total depth was reached at 940 mbsf, exceeding by 5 m the previous XCB penetration record, set on Leg 116.

After logging was completed, the drill pipe was lowered to 800 mbsf, and 10.2 pounds per gallon (ppg) mud was circulated to 300 mbsf to cover the gassy formation. With the drill pipe at 359 mbsf, a 150-sack cement plug was placed on top of the heavy mud. Hole 762C was abandoned at 0830 hr (LT), 5 August 1988.

LITHOSTRATIGRAPHY

Site 762 consists of three holes, Holes 762A, 762B, and 762C. Hole 762A penetrated only the uppermost 9.5 m of sediments. Hole 762B reached 175.4 mbsf, and Hole 762C was washed to 170 mbsf and cored to 940 mbsf. Lithologic units predominantly consist of Cenozoic and upper Cretaceous nannofossil ooze and chalk, with varying amounts of foraminifers and clay and lower Cretaceous claystone. The sedimentary sequence at Site 762 is divided into six lithologic units on the basis of visual core descriptions, smear slide analysis of sediment composition, and calcium carbonate contents (Table 2; Figs. 8 and 9).

Unit I (0.0–181.5 mbsf)

Cores 122-762B-1H, 0 cm, to 122-762C-3X-3.

Unit I consists of pelagic oozes and is divided into three subunits. These are, from top to bottom: foraminifer nannofossil ooze (Subunit IA), nannofossil ooze with foraminifers (Subunit IB), and foraminifer nannofossil ooze (Subunit IC).

Subunit IA (0.0–61.4 mbsf)

Cores 122-762B-1H-1, 0 cm, to -8H-1, 0 cm.

Subunit IA is represented mainly by light green-gray (10Y 7/0 to 10Y 7/1) foraminifer nannofossil ooze. In addition to nannofossils (more than 50% of the sediment) and pelagic foraminifers (25%–50%) (Fig. 9), radiolarians, sponge spicules, and undifferentiated bioclasts occur in small amounts (usually <10%) in this subunit. Terrigenous material (e.g.,

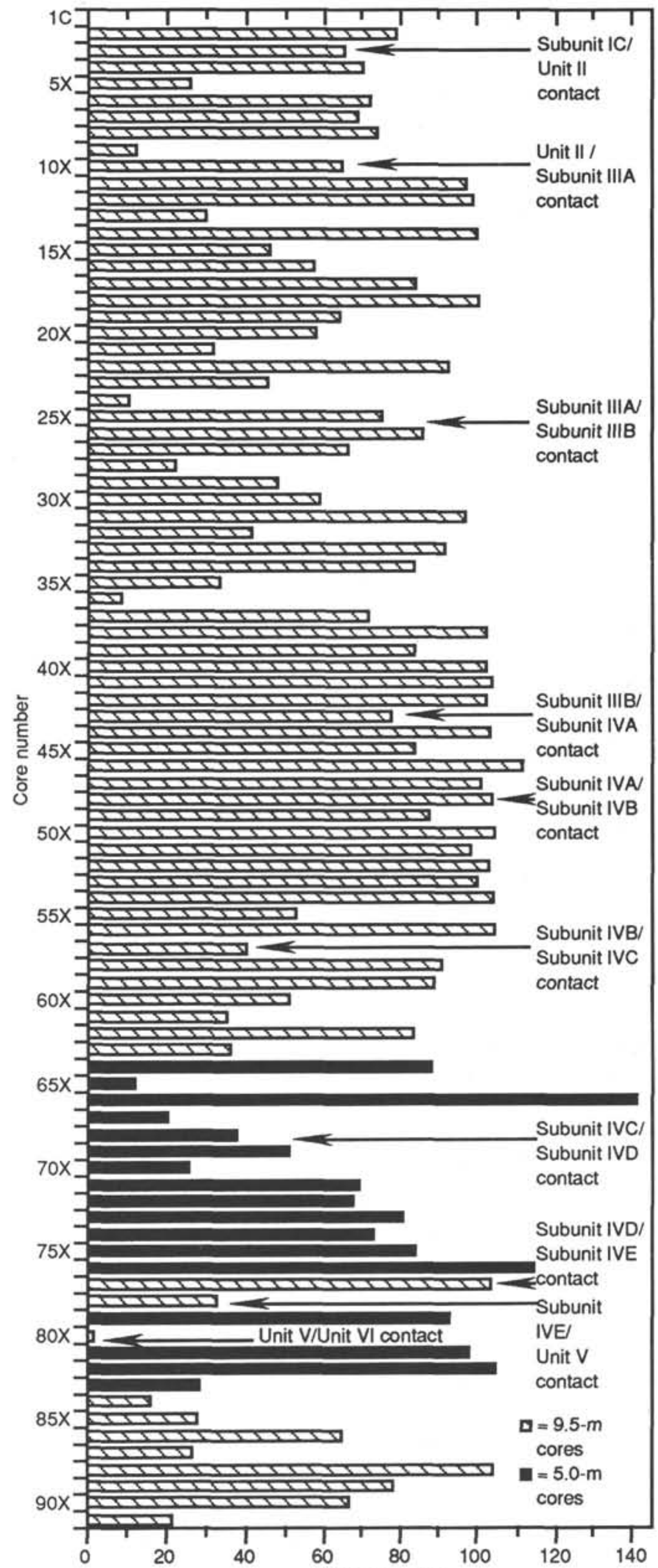

Figure 6. Core number versus recovery (%), Hole 762C (XCB).

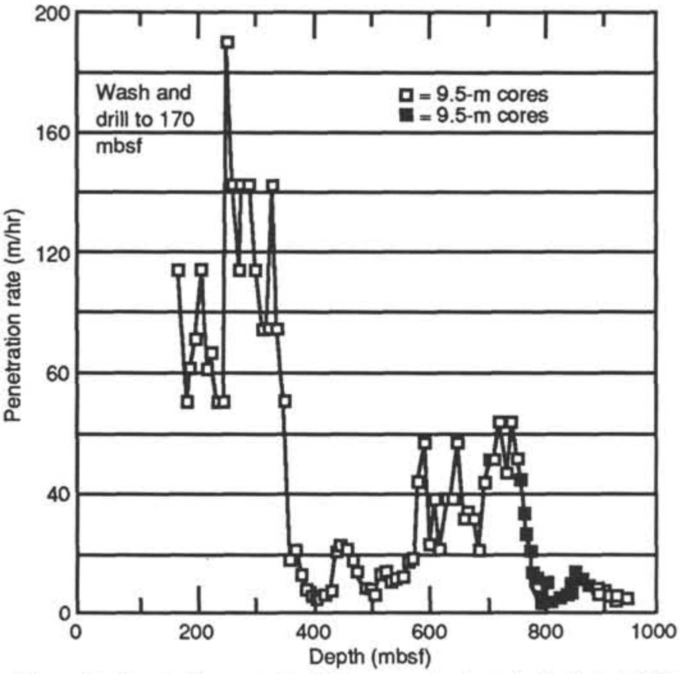

Figure 7. Penetration rate (m/hr) versus depth (mbsf), Hole 762C (XCB).

quartz and clay minerals) occurs in the upper (Cores 122-762B-1H to -3H) and lower (Cores 122-762B-6H and -7H) parts of the unit (Fig. 9). Although it is difficult to estimate the amount of clay minerals in smear slides, they appear to constitute <10% of this sediment. The carbonate content is between 79% and 86%.

The upper part of Subunit IA is largely homogeneous, with no distinct primary sedimentary structures except for slight mottling, weak to moderate bioturbation, and poorly defined laminations. The lower part, however, contains color laminations (i.e., in Cores 122-762B-4H to -7H) that may correspond to increased clay content. The color bands or laminae are commonly mm to a few cm in thickness, and are repeated over an interval ranging from 15 to 30 cm, suggesting cyclic sedimentation (Fig. 10). They are mostly pale green (5G 7/2, 5GY 7/2, 5G 6/2, and 5GY 6/2) and light green-gray (10Y 8/2) in color.

Subunit IA is 61.4 m thick and forms the uppermost part of Hole 762B. It ranges in age from late Pliocene to Quaternary.

Subunit IB (61.4–118.4 mbsf)

Cores 122-762B-8H-1, 0 cm to -14H-1, 0 cm.

The upper boundary of Subunit IB is defined by a slight decrease in the amount of planktonic foraminifers (Fig. 9). This subunit grades downward into the underlying Subunit IC (Fig. 8). Sediments of Subunit IB are, therefore, represented by foraminifer nannofossil ooze, nannofossil ooze with foraminifers, and nannofossil ooze. Nannofossils together with planktonic foraminifers constitute about 90% of the components of these sediments. Minor constituents include quartz, mica, clay, and accessory minerals that appear to be more common both in the upper and lowermost part of the subunit.

Light gray (5Y 7/1) is the dominant sediment color in Subunit IB. Toward the base, however, various shades of white (e.g., 5Y 8/1, 2.5Y 8/0, and 2.5Y 8/2) and light green-gray (5GY 7/1) are also observed (Cores 122-762B-13H and -14H). The main sedimentary structures in these sediments are represented by color bands and laminae. These features occur irregularly and/or in a cyclic manner throughout Subunit IB (Fig. 11). The color laminae are poorly to well defined and are measured in mm (e.g., Cores 122-762B-8H, -10H, and -13H), whereas the color bands are commonly much thicker (up to 30 cm). They are pale green (5G 7/2), light green-gray (5GY 7/1), light gray (10YR 7/1 and 2.5Y 8/0), and white (5Y 8/1) in color. Where they are absent, the sediments largely appear to be homogenous and structureless with rare mottling, bioturbation, and pyrite clusters.

Subunit IB is 57 m thick and of late Middle Miocene to late Pliocene age (Fig. 8).

Subunit IC (118.4–181.5 mbsf)

Cores 122-762B-14H-1, 0 cm, to 122-762C-3X-3, 0 cm.

This subunit is distinguished from the overlying Subunit IB by its color and higher planktonic foraminifer content. It consists generally of foraminifer nannofossil ooze with small amounts (<10%) of sponge spicules, radiolarians, quartz, mica, clay, volcanic glass, and accessory minerals (Fig. 9). It is predominantly white (10YR 8/1 and 10YR 8/2) and pale yellow (5Y 8/3) in the upper part of the subunit (Core 122-762B-14H), and changes downhole to very pale brown (10YR 7/3 and 10YR 7/4) and light gray (5Y 7/2) (Cores 122-762B-16H to 122-762C-2X).

Subunit IC is strikingly homogeneous and structureless, although few areas of weak mottling and bioturbation occur, marked either by color difference or pyrite and glauconite infillings (e.g., Section 122-762B-18H-2). However, in the lower portion of the sequence (Cores 122-762B-19H and 122-762C-2X) there are cyclic color changes between white (5Y 8/1), various shades of light gray (10YR 7/1, 10YR 7/2, 5Y 7/1, and 5Y 7/2), light green-gray (5GY 7/1), and pale green (5G 7/2 and 5G 6/2) sediment bands, which range in thickness from a few mm up to 85 cm (Fig. 12).

Subunit IC includes about 63 m of sediments from Cores 122-762B-14H through -19H and Core 122-762C-2X to Section 122-762C-3X-3. Its age ranges from late Eocene–early Oligocene to Middle Miocene, although the late Early Miocene portion of the subunit is missing (see "Biostratigraphy," this chapter). This depositional break is found in Core 122-762B-15H (132–135 mbsf) and is not detectable as a change in lithology (Fig. 9). Apart from this minor lithologic variation, a slight change in color above and below Core 122-762B-15H may provide an additional clue for this disconformity. The main color in Core 122-762B-15H is white (10YR 8/1 and 10YR 8/2), whereas it is generally white (10YR 8/1 and 10YR 8/2) and pale yellow (5Y 8/3) in the upper portion of the sequence and very pale brown (10YR 7/3 and 10YR 7/4) and light gray (5Y 7/2) in the lower.

Unit II (181.5–265.0 mbsf)

Interval 122-762C-3X-3, 0 cm to -12X-1, 0 cm.

Subunit IC is underlain by more consolidated nannofossil ooze/chalk of Unit II (Fig. 9). This unit differs from the overlying sediments in its hardness and lack of cyclic color change. It is structureless, white (5Y 8/1, 2.5Y 8/1, and N8), and consists mainly of nannofossils (>90%) with <10% planktonic foraminifers. No appreciable amounts of siliciclastic components occur in this lithology (Fig. 9). In Sections 122-762B-6X-2, -8X-3, and -9X-1, it includes light brown gray (2.5Y 6/2) and light gray (5Y 6/1) chert nodules. The nannofossil chalk is characteristically homogeneous, with no visible sedimentary structures (Fig. 13). It is about 83 m thick, and ranges in age from late Eocene–early Oligocene to middle Eocene.

Table 2. Summary of lithologies observed at Site 762.

Unit	Lithology	Cores	Depth (mbsf)	Thick-ness (m)	Environment	Age
IA	Light green-gray foraminifer nannofossil ooze.	762B-1H-1, 0 cm to -8H-1, 0 cm	0–61.4	61.4	Pelagic.	Quaternary to late Pliocene
IB	Light gray nannofossil with foraminifers.	762B-8H-1, 0 cm to -14H-1, 0 cm	61.4–118.4	57.0	Pelagic.	late Pliocene to Middle Miocene
IC	White, pale yellow and light gray foraminifer nannofossil ooze.	762B-14H-1, 0 cm to 762C-3X-3, 0 cm	118.4–181.5	63.1	Pelagic.	Middle Miocene to late Eocene–early Oligocene
II	White nannofossil chalk.	762C-3X-3, 0 cm to -12X-1, 0 cm	181.5–265.0	83.5	Pelagic.	late Eocene–early Oligocene to middle Eocene
IIIA	Light green-gray white and pale green nannofossil chalk with foraminifers.	762C-12X-1, 0 cm to -26X-1, 0 cm	265.0–398.0	133.0	Pelagic.	middle Eocene to early Eocene
IIIB	Light green-gray nannofossil chalk.	762C-26X-1, 0 cm to -43X-1, 30 cm	398.0–554.8	156.8	Pelagic.	early Eocene to early Paleocene
IVA	White to light green-gray nannofossil chalk and green-gray clayey nannofossil chalk.	762C-43X-1, 30 cm to -48X-2, 0 cm	554.8–603.5	48.7	Pelagic.	early to late Maestrichtian
IVB	Light green-gray nannofossil chalk and reddish brown nannofossil claystone.	762C-48X-2, 0 cm to -58X-1, 0 cm	603.5–697.0	93.5	Pelagic.	early Maestrichtian to early Campanian
IVC	White to very light green-gray nannofossil chalk with foraminifers and green-gray nannofossil claystone.	762C-58X-1, 0 cm to -69X-1, 0 cm	697.0–780.0	83.0	Pelagic.	early Campanian to early Santonian
IVD	Light green-gray nannofossil chalk with foraminifers and brown clayey nannofossil chalk.	762C-69X-1, 0 cm to -77X-2, 18 cm	780.0–820.2	40.2	Pelagic.	early Santonian to late Albian
IVE	Light green-gray nannofossil calcareous chalk and green-gray nannofossil chalk with clay.	762C-77X-2, 18 cm to -79X-1, 0 cm	820.2–838.5	18.3	Pelagic.	Albian
V	Black to dark gray calcareous claystone.	762C-79X-1, 0 cm to -81X-1, 0 cm	838.5–848.5	10.0	Epicontinental shelf, hemipelagic.	early Aptian
VI	Black to very dark gray silty claystone and clayey siltstone.	782C-81X-1, 0 cm through -91X-CC	848.5–940.0	91.5	Shelf-margin prodelta.	Berriasian to early Valanginian

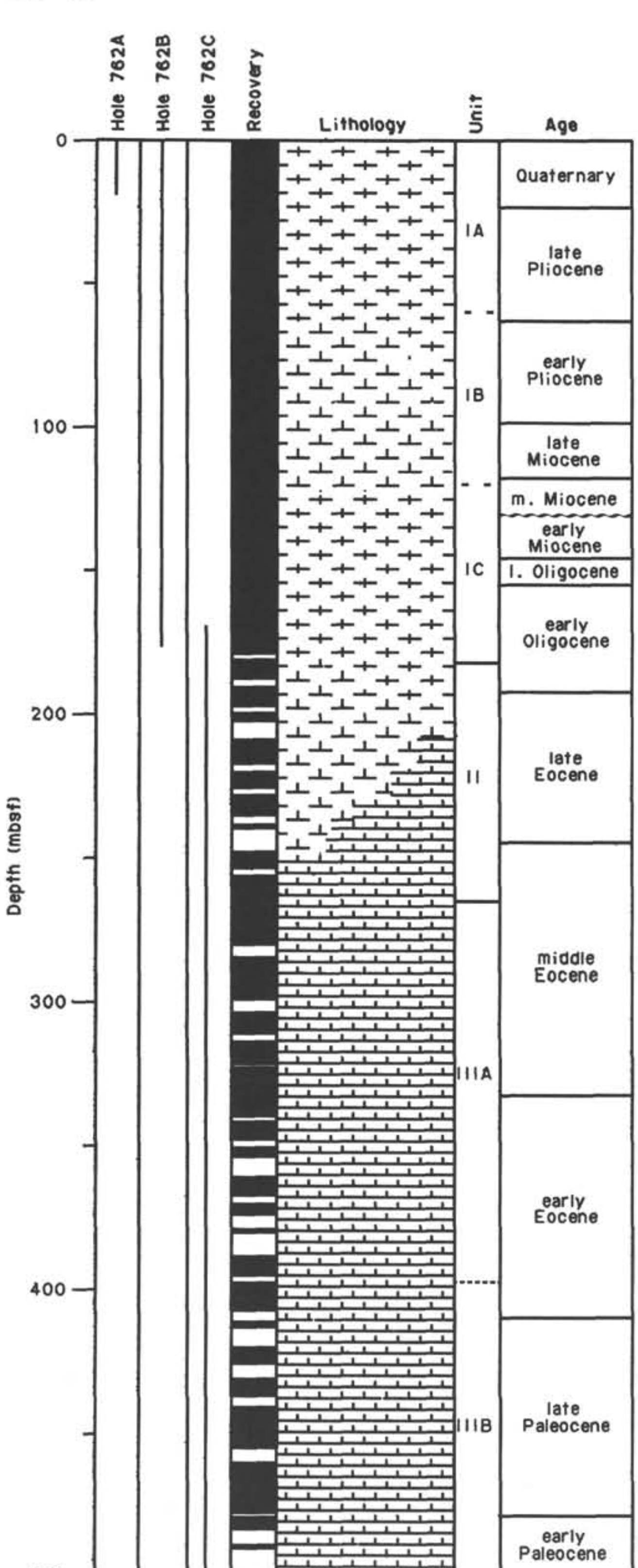

Figure 8. Lithologic column for Site 762, showing core numbers and types, recovery, generalized lithology, lithologic units, and age. A key to lithologic symbols appears in the "Explanatory Notes" chapter (this volume).

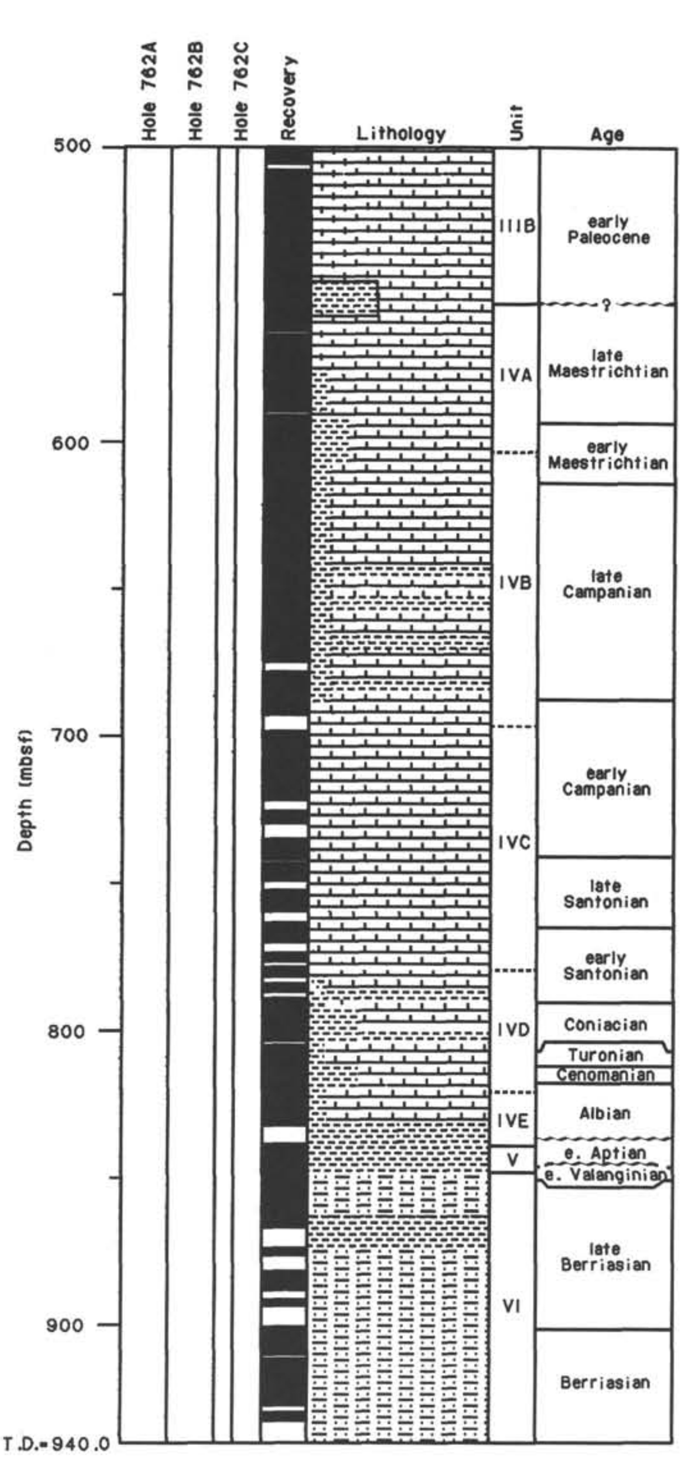

Figure 8 (continued).

Unit III (265.0–554.8 mbsf)

Cores 122-762C-12X-1, 0 cm, to -43X-1, 30 cm.

This unit consists of chalk divided into two subunits: Subunit IIIA and Subunit IIIB. This division is based mainly on downhole variation in the amount of planktonic foraminifers (Fig. 9). Subunit IIIA consists primarily of nannofossil chalk with foraminifers, whereas Subunit IIIB is dominated by nannofossil chalk.

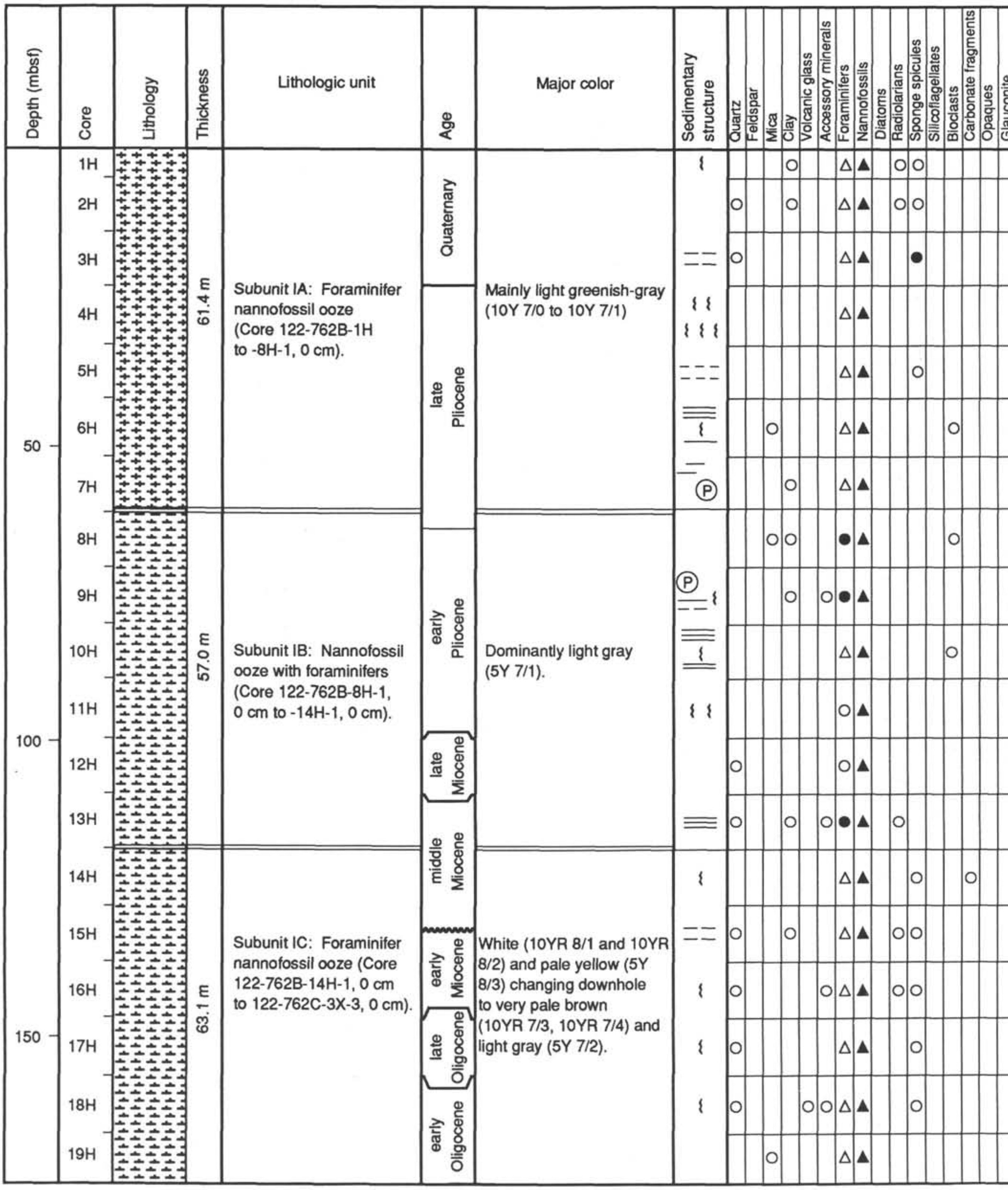

Figure 9. Summary of lithologies and compositions observed in Site 762. A key to lithologic symbols appears in the "Explanatory Notes" chapter (this volume).

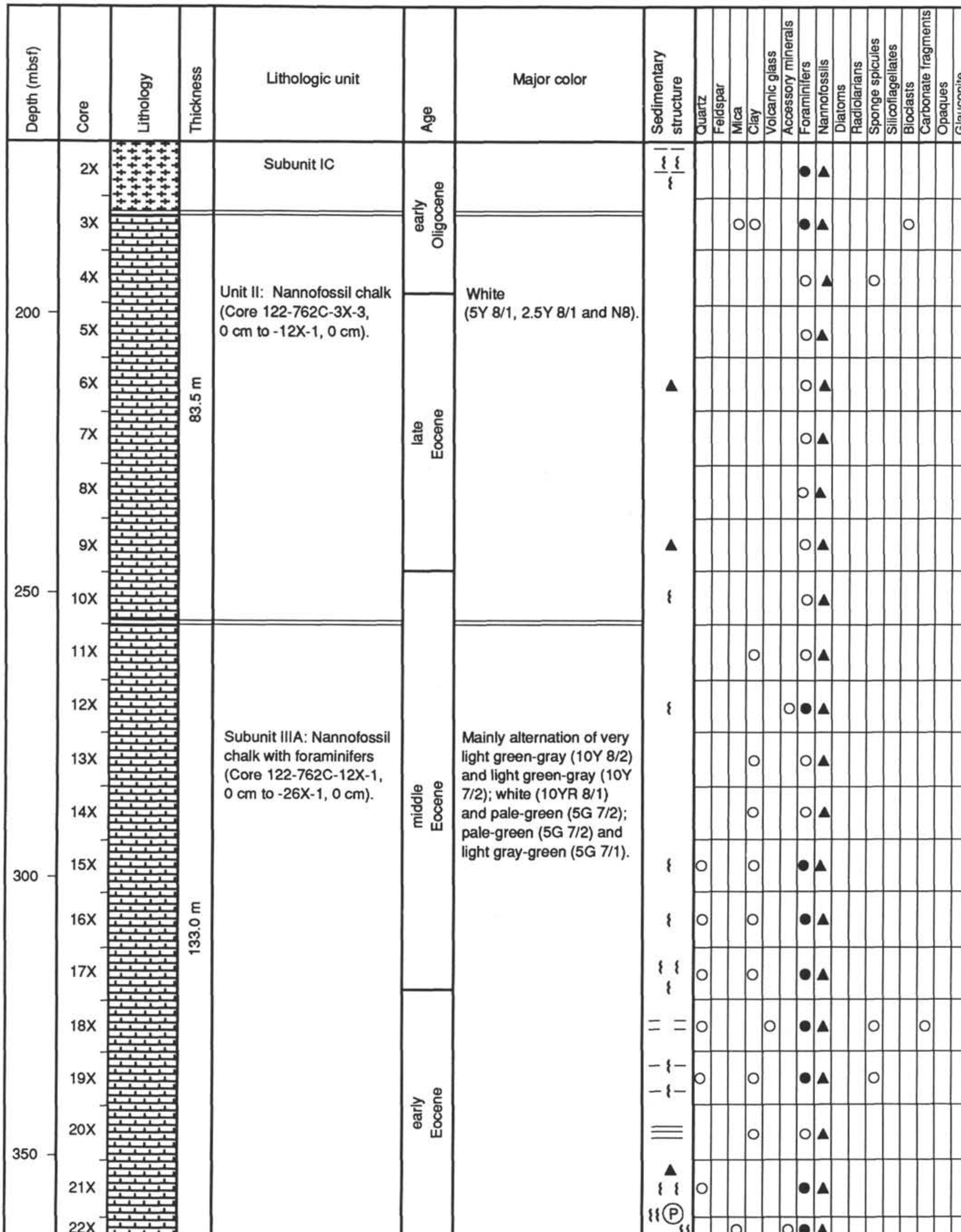

Figure 9 (continued).

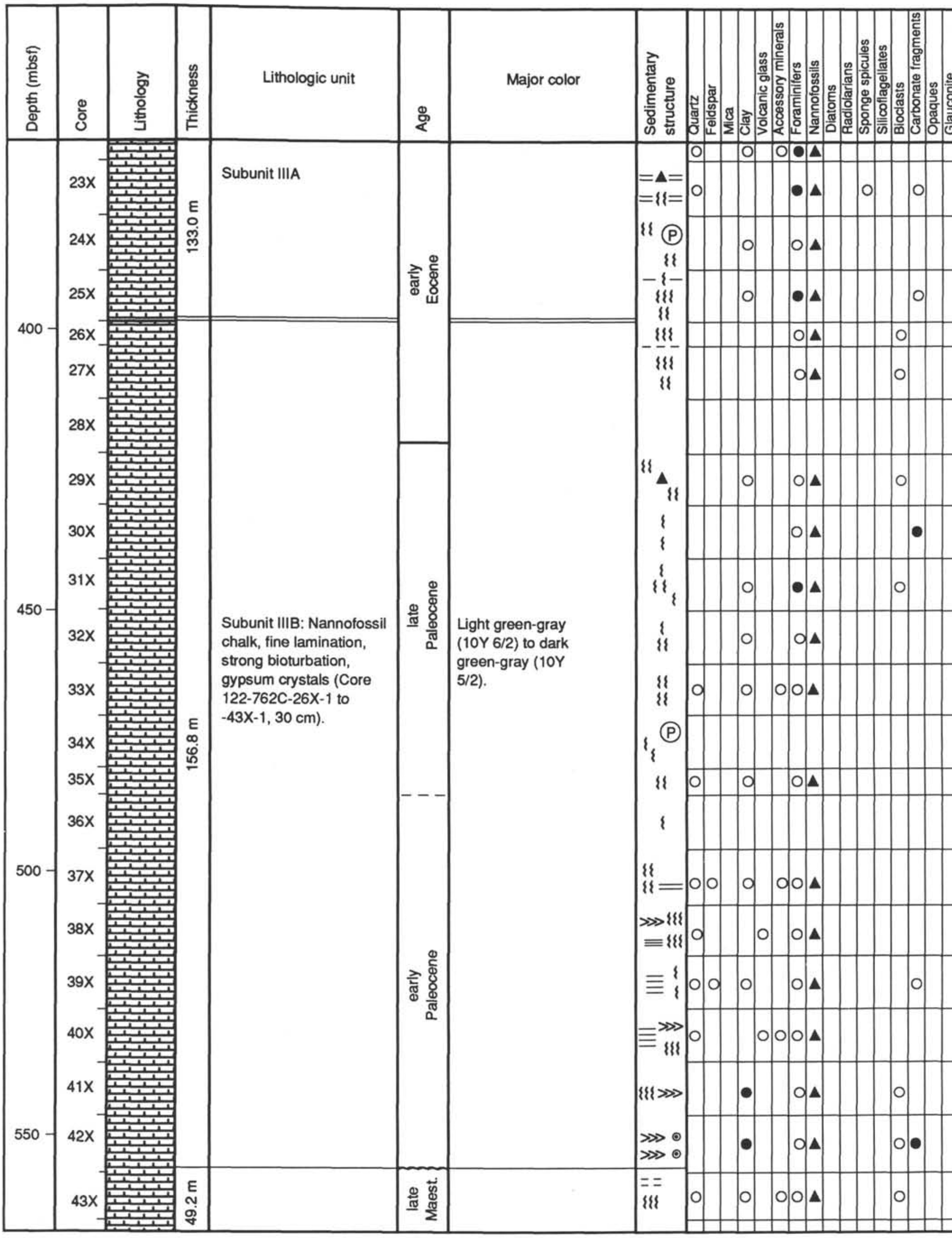

Figure 9 (continued).

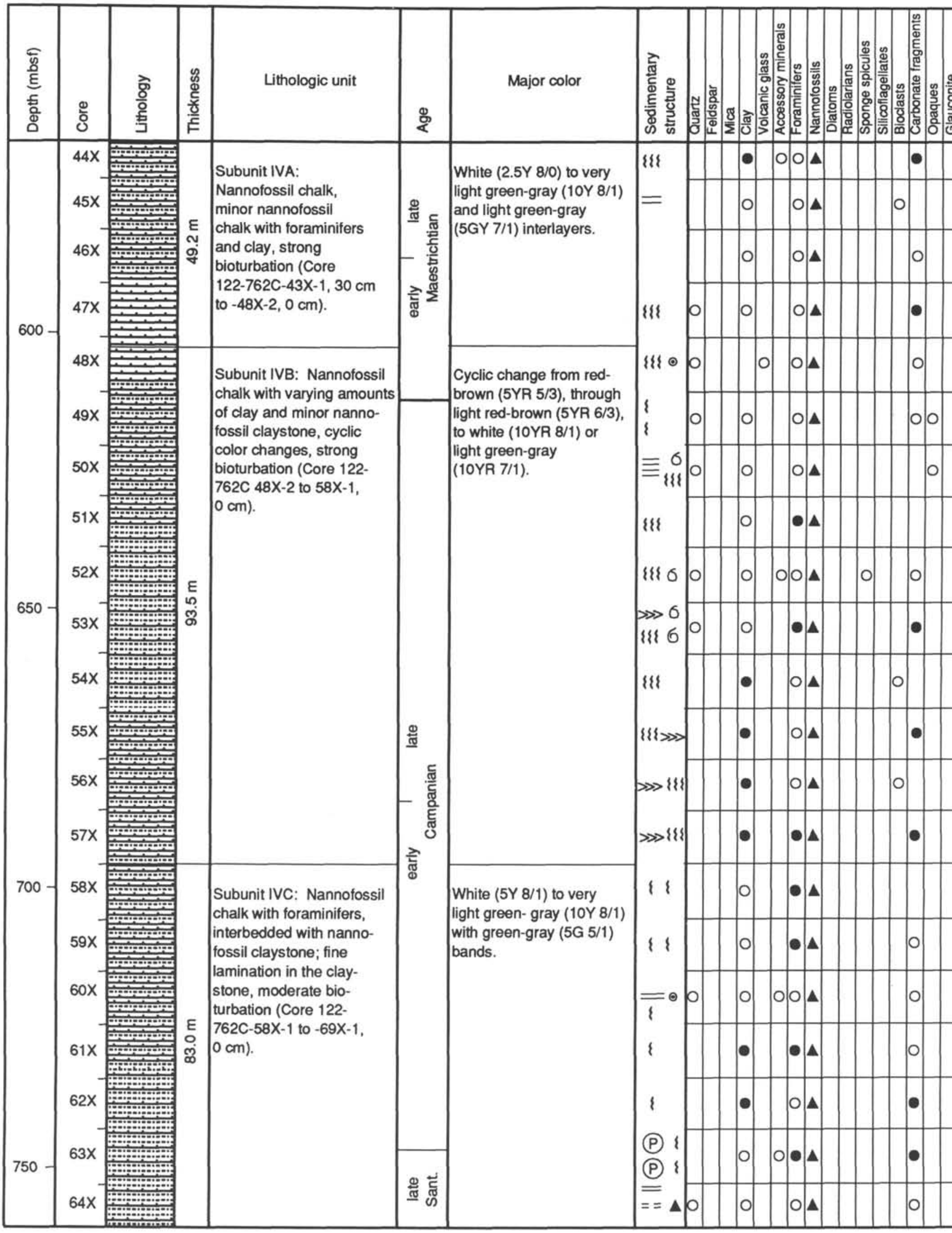

Figure 9 (continued).

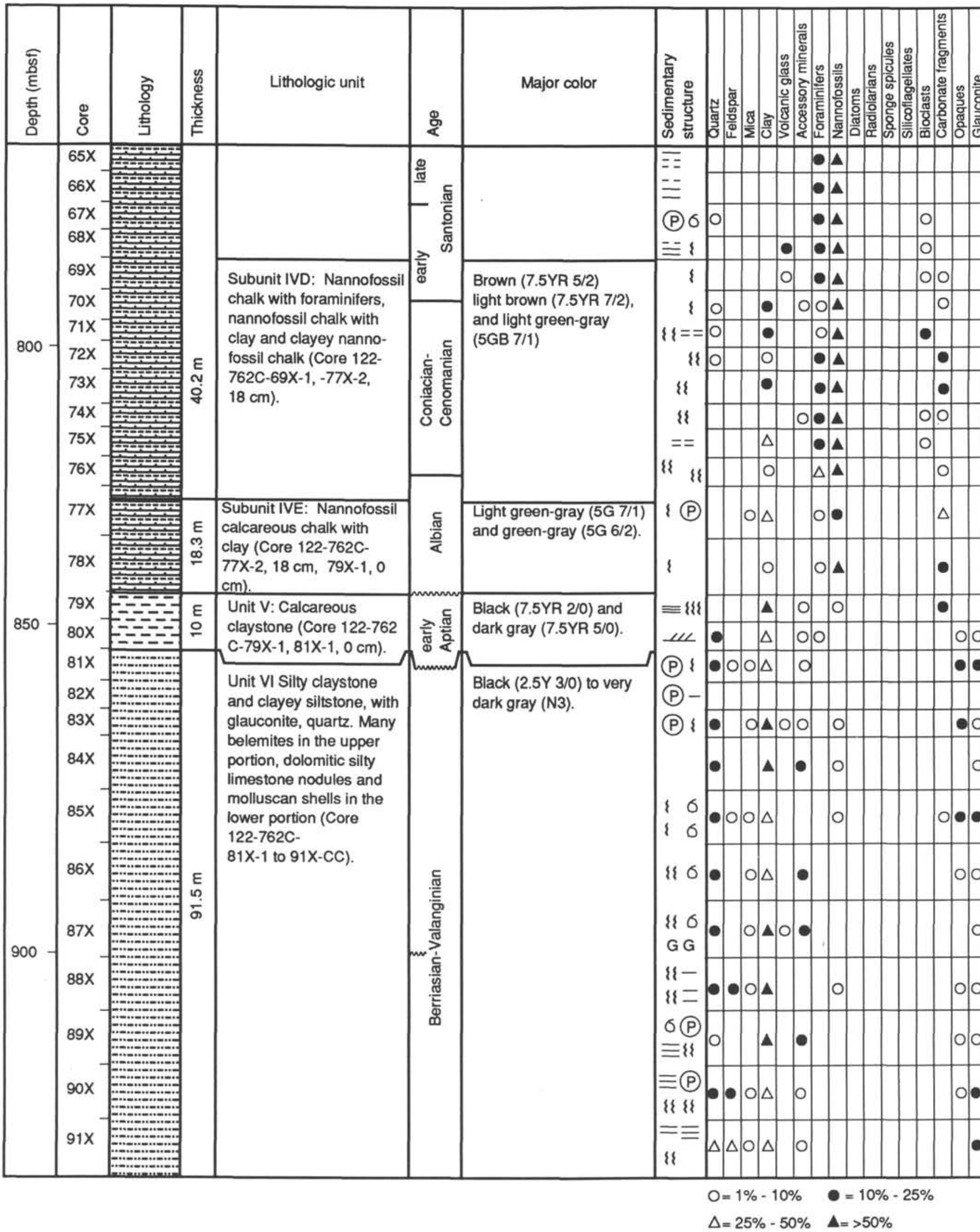

Figure 9 (continued).

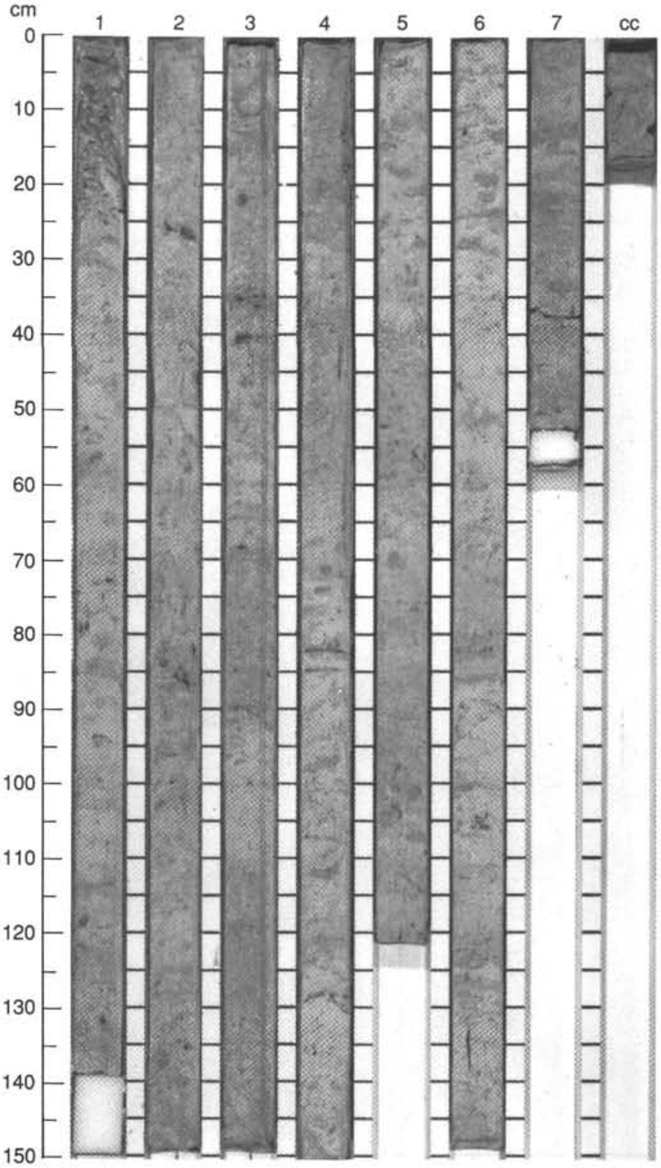

Figure 10. Core 122-762B-6H. Foraminifer nannofossil ooze of Subunit IA, characterized by cyclic color changes and moderate mottling.

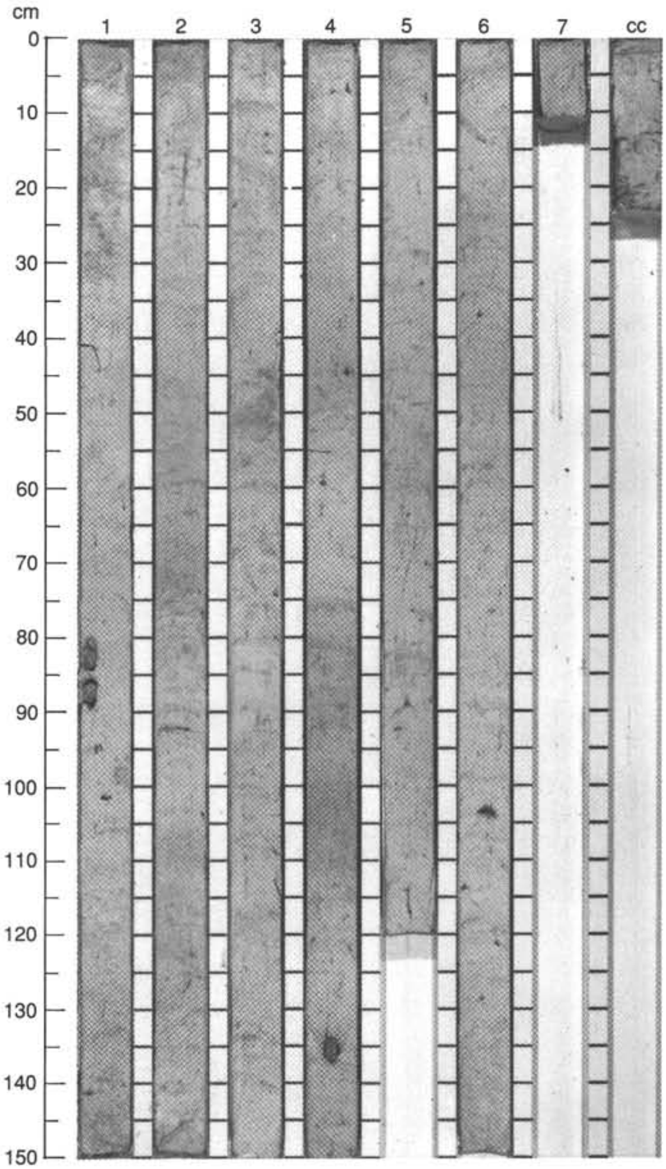

Figure 11. Core 122-762B-9H. Nannofossil ooze with foraminifers of Subunit IB, characterized by cyclic color changes and moderate bioturbation. Pyrite nodules are observed in Intervals 122-762B-9H-1, 80–90 cm and -9H-4, 133–137 cm.

Subunit IIIA (265.0–398.0 mbsf)

Cores 122-762C-12X-1, 0 cm, to -26X-1, 0 cm.

This subunit consists predominantly of nannofossil chalk with foraminifers, although pure nannofossil chalk also occurs in part (i.e., Cores 122-762C-13X, -14X, -20X, and -24X). Other biogenic constituents, such as sponge spicules and undifferentiated bioclasts, are encountered in the middle and lower part of the subunit (Cores 122-762B-18X, -19X, -23X, and -25X) (Fig. 9). Small amounts of inorganic components (i.e., quartz, clay, volcanic glass, and accessory minerals) are found throughout the sequence.

The chalks of Subunit IIIA show a color cyclicity (Fig. 14). From the top of the subunit to the top of Core 122-762C-17X the color cycles are relatively thick and are measured in meters. This is indicated by the alternation of light green-gray (10Y 8/1) and very light green-gray (10Y 8/2) chalks in Cores 122-762C-11X and -16X. However, owing to the great thickness of these cycles they are obvious only upon comparison between sections. Between Cores 122-762C-16X and -21X, the color cycles are thinner and are visible within individual core sections. We observed several color alternation patterns in the chalks: (1) green-gray (10Y 8/2) and light green-gray (10Y 7/2) (Core 122-762C-17X); (2) different shades of very light green-gray (10Y 8/1 and 10Y 8/2) (Core 122-762C-17X), white (10YR 8/1), and pale green (5G 7/2) (Core 122-762C-19X); and (3) pale green (5G 7/2) and light gray-green (5G 7/1) (Core 122-762C-20X). In the portion of the subunit that lacks cyclic color changes the color of the chalk varies from very light green-gray (10Y 8/1) to light green-gray (10Y 7/1) (Cores 122-762C-22X to -25X).

Subunit IIIA is extensively bioturbated in its lower part (Cores 122-762C-22X to -25X) by *Planolites-*, *Chondrites-*, *Zoophycos-*, and *Teichichnus*-type burrows (Fig. 15). These ichnofossils are well preserved, ranging in size from a few mm to a few cm. Pyrite and chert occur as nodules in the heavily

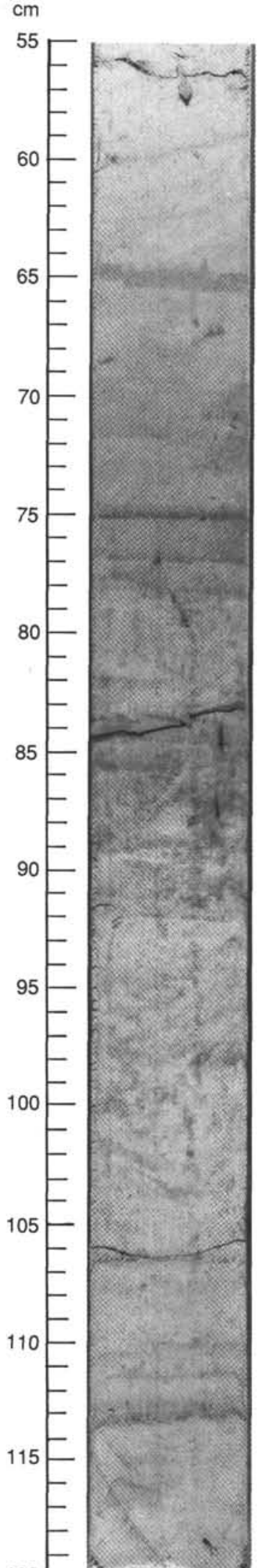

Figure 12. Interval 122-762B-19H-6, 55–120 cm. Foraminifer nannofossil ooze of Subunit IC, characterized by cyclic alternations of light green-gray bands that contain many foraminifers infilled with glauconite. Bioturbation is moderate to strong throughout the core.

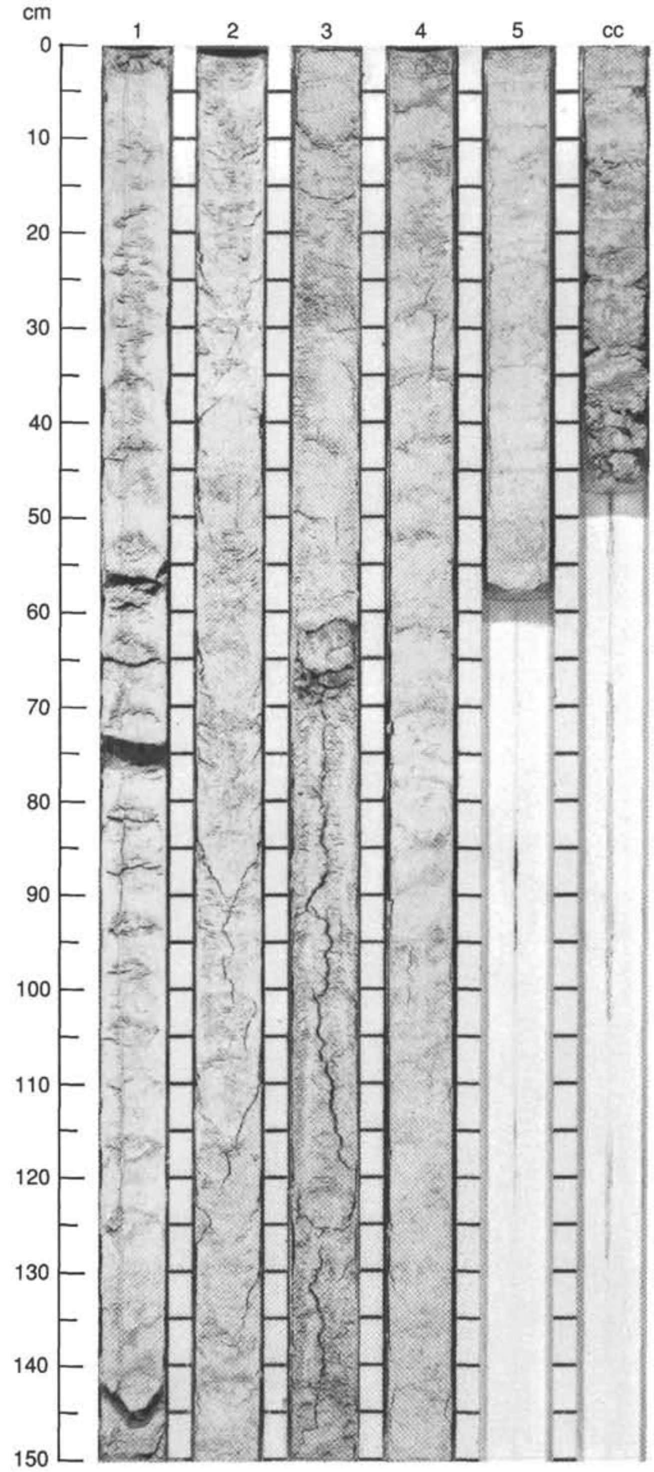

Figure 13. Core 122-762C-8X. Generally structureless white nannofossil chalk of Unit II.

bioturbated lower interval (Cores 122-762C-22X to -25X). The upper part of the subunit appears to be homogenous and contains only a little mottling, bioturbation, and faint lamination.

Subunit IIIA is 133 m thick and ranges in age from early Eocene to middle Eocene (see "Biostratigraphy," this chapter).

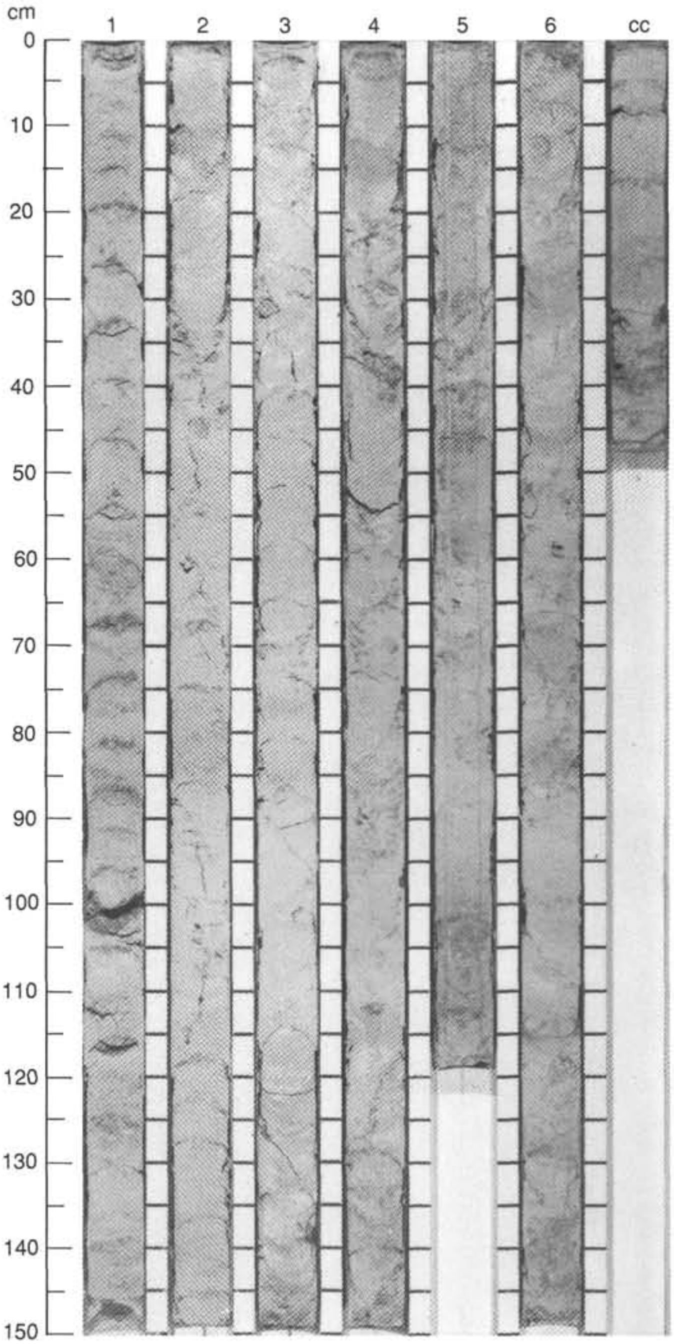

Figure 14. Core 122-762C-14X. Nannofossil chalk with foraminifers of Subunit IIIA, characterized by cyclic alternations of pale green beds.

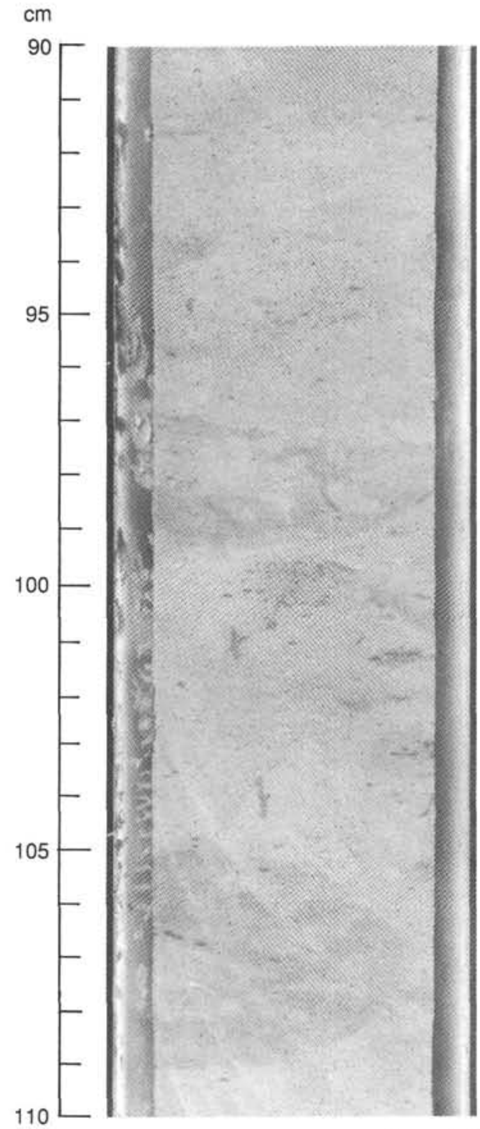

Figure 15. Interval 122-762C-25X-4, 90–110 cm. Strongly bioturbated nannofossil chalk of Subunit IIIA, with many identifiable trace fossils of *Chondrites*, *Zoophycos*, and *Planolites*.

Subunit IIIB (398.0–554.8 mbsf)

Cores 122-762C-26X-1, 0 cm, to -43X-1, 30 cm.

The subunit is composed mainly of light green-gray (5G 7/1, 5GY 7/1, 5Y 7/1, 10Y 7/1, 10Y 7/2, and 10Y 6/2), very light green-gray (10Y 8/1), and white (N8 and 5Y 8/1) nannofossil chalk. It includes nannofossils (>50%), foraminifers (generally <10%), and undifferentiated bioclasts (<10%). The nonbiogenic grains are quartz, feldspar, mica, clay minerals, volcanic glass, accessory minerals, and carbonate fragments. Together, these inorganic components usually constitute <10% of the nannofossil chalk (Fig. 9). However, in the lowermost part of the subunit, just above the Cretaceous/Tertiary boundary, >45% clay minerals and carbonate fragments ($CaCO_3$ = 54.6%) occur together with zeolites, gypsum(?), pyrite, and plant debris.

Subunit IIIB displays a well-developed color cyclicity, predominantly alternating between light green-gray (5G 7/1, 5GY 7/1, 5Y 7/1, 10Y 7/1, 10Y 7/2, and 10Y 6/2) and very light green-gray (10Y 8/1) in thick (on the order of a meter or more) and thin (measured in cm) intervals. The thicker intervals appear at the top of the subunit. A peculiar feature is that these cycles are sometimes separated by a white (N8 and 5Y 8/1) band (e.g., Sections 122-762C-29X-4, -30X-2 to -30X-4, and -32X-1 and -32X-2).

The cyclic sequences are often bioturbated throughout the subunit by *Zoophycos*, *Chondrites*, *Planolites*, *Helm-*

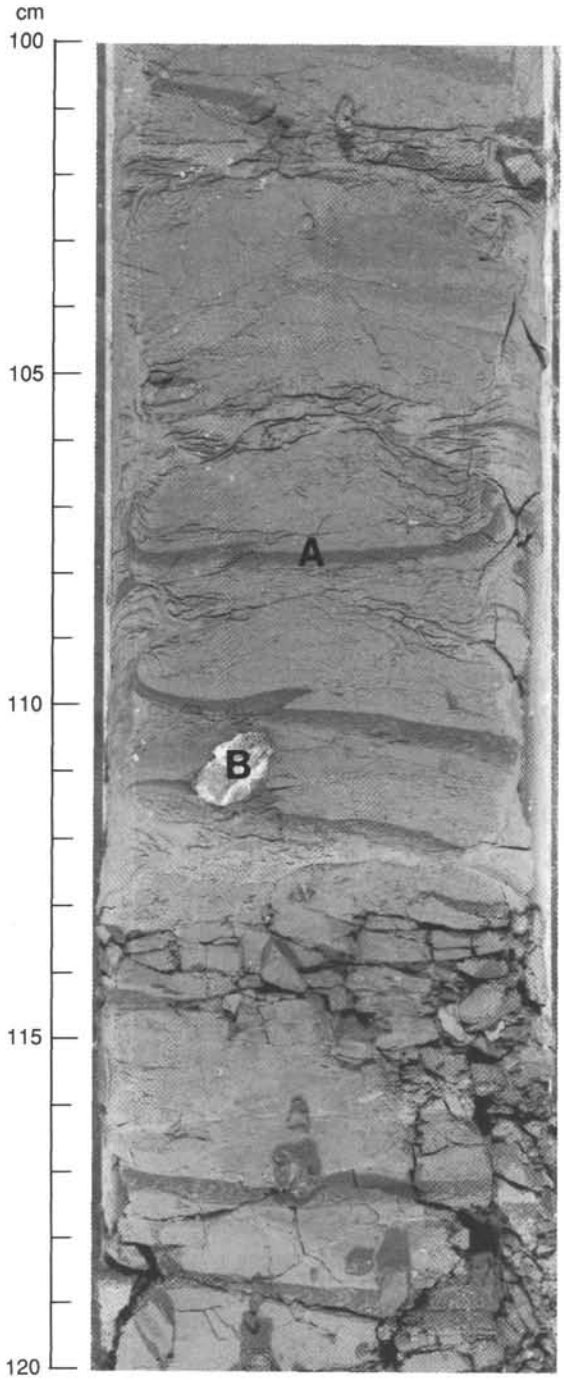

Figure 16. Interval 122-762C-41X-6, 100–120 cm. Basal portion of nannofossil chalk of Subunit IIIB, containing many *Zoophycos* (A) and some gypsum crystals (B).

inthoidea, and other burrows and trails (Fig. 16). Burrows are sometimes more apparent in darker layers. Lighter layers are in part preferentially and intensely fractured (e.g., Core 122-762C-31X). Smear slide data indicate that the darker layers contain relatively more foraminifers and clays, and analyses showed that $CaCO_3$ contents were lower in the darker intervals.

The Subunit IIIB is about 157 m thick and is early Paleocene to early Eocene in age (see "Biostratigraphy," this chapter).

Interpretation of Depositional Environments of Cenozoic Sediments, Site 762

The Cenozoic succession at Site 762 consists of ooze and chalk, rich in nannofossils and planktonic foraminifers. The faunal content indicates that these sediments were deposited in an open-marine pelagic environment.

A distinctive feature of the Cenozoic succession is the alternation of relatively foraminifer-rich and foraminifer-poor units (Fig. 8). Foraminifer-rich facies were generally deposited in the early Eocene to middle Eocene (Subunit IIIA), late Eocene–early Oligocene to middle Miocene (Subunit IC), and late Pliocene to Quaternary (Subunit IA).

Reasons for the changes in foraminiferal content include (but are not limited to):

1. fluctuating rates of nannofossil accumulation—high rates might have diluted the foraminifer component of the sediment;
2. preferential dissolution of foraminifers might have increased the nannofossil content;
3. winnowing by bottom currents might have removed nannofossils and increased the concentration of foraminifers; and
4. changes in foraminifer productivity might have occurred.

A second distinctive feature of the Cenozoic sediments at Site 762 is the development of rhythmic color alternation. This color alternation reflects variation in the conditions of the depositional environment. Color changes might have resulted from variations in the terrigenous clay and organic matter components of the sediments. Sediments with high clay and/or organic matter content tend to be darker, while lighter-colored sediments are more carbonate-rich. The periodicity may reflect the climatic control related to Milankovitch cycles (Arthur et al., 1984).

Extensive bioturbation structures observed throughout the Cenozoic sediments at Site 762 indicate abundant biogenic activity in the depositional environment. The well-preserved laminated parts of these sediments may, however, suggest unfavorable conditions for biogenic activity during or soon after deposition. Episodic oxygen depletion in the bottom water and sediments (possibly resulting from changes in productivity, rate of sedimentation, influx of terrigenous matter, or in the intensity of bottom circulation) could have created such conditions (Ogg et al., 1987).

Unit IV (554.8–838.5 mbsf)

Interval 122-762C-43X-1, 30 cm, to -79X-1, 0 cm.

Unit IV consists of nannofossil chalk with varying amounts of foraminifers and clay and minor nannofossil claystones. The unit is 283.7 m thick and is late Maestrichtian to Albian in age (Table 2; Figs. 8 and 9). The top of Unit IV is defined by the Cretaceous/Tertiary boundary, where the white nannofossil chalk of Unit IV is abruptly overlain by the dark green-gray nannofossil chalk with foraminifers of Unit III. Calcium-carbonate content also abruptly decreases across the Cretaceous/Tertiary boundary, from 95% at the top of Unit IV (Core 122-762C-43X-4, 115–118 cm) to 55% at the base of Unit III (Core 122-762C-42X, 115–118 cm) to (see "Organic Geochemistry," this chapter). The nannofossil chalks of Unit IV are characterized by cyclic color changes (i.e., green to brown) on a scale of 17–94 m.

Color variation, compositional change, and stratigraphic position allow us to divide Unit IV into five subunits (in descending order): Subunit IVA (upper green interval), Subunit IVB (upper brown interval), Subunit IVC (middle green interval), Subunit IVD (lower brown interval), and Subunit IVE (lower green interval) (Fig. 9). Each subunit also includes small-scale, 5–100-cm-thick color cycles of darker and lighter beds without distinct contacts, reflecting the relative abundance of clay and calcium carbonate.

Many cores from Unit IV are highly disturbed, probably because of high gas contents (see "Organic Geochemistry," this chapter).

Subunit IVA (554.8–603.5 mbsf)

Interval 122-762C-43X-1, 30 cm, to -48X-2, 0 cm.

Subunit IVA consists of white (2.5Y 8/0) to very light green-gray (10Y 8/1) nannofossil chalk (lighter beds) with intervals up to 10 cm thick of light green-gray (5GY 7/1) clayey nannofossil chalk (darker beds) (Fig. 17). The age of Subunit IVA is early to late Maestrichtian and the total thickness is 48.7 m (Fig. 9).

The lighter beds (15–100 cm thick) are generally structureless and locally include up to 15% foraminifers (e.g., Section 122-762C-47X-1). Some darker beds show fine laminations and contain 3%–20% more clay than the lighter beds. The couplets generally have gradational boundaries and range in thickness from 15 to 110 cm. The calcium-carbonate content of the lighter beds is 87%–92%, whereas that of the darker beds is 56%–92%. Bioturbation is moderate to strong throughout Subunit IVA, with many identifiable trace fossils such as *Planolites*, *Zoophycos*, and *Chondrites*.

Some pyrite crystals are scattered throughout Sections 122-762C-47X-3, 47X-6, and -47X-7, and a pyritized burrow was observed in Core 122-762C-47X-3, 120 cm.

Subunit IVB (603.5–697.0 mbsf)

Interval 122-762C-48X-2, 0 cm, to -58X-1, 0 cm.

Subunit IVB consists of nannofossil chalk with varying amounts of clay, characterized by 35–130-cm-thick gradational cyclic color changes. The colors range from red brown (5YR 5/3) (beds 5–10 cm thick), through light red brown (5YR 6/3) (beds 10–70 cm thick), to white (10YR 8/1) or light green-gray (10YR 7/1) (beds 20–50 cm thick) (Fig. 9). The thickness is 93.5 m and the age is early Campanian to late Maestrichtian (Fig. 8).

Darker (red brown and light red brown) beds generally contain 7%–27% more clay and 3%–10% more iron oxides than the lighter (white or light green-gray) beds. Furthermore, some darker red-brown beds are composed of 49%–60% clay (e.g., Samples 122-762C-57X-1, 146 cm, and -58X-2, 96 cm) and are classified as nannofossil claystone. Calcium carbonate content is 59%–72% in the darker beds and 86%–93% in the lighter beds. Bioturbation is strong throughout Subunit IVB, with many identifiable trace fossils including *Chondrites*, *Planolites*, *Zoophycos*, and *Teichichnus* (Fig. 18). Downward burrowing has locally mixed lighter-colored material into the darker underlying beds (e.g., Interval 122-762C-56X-3, 30–35 cm; Fig. 19).

Inoceramus fragments are observed in Sections 122-762C-50X-3 and -50X-4, and in Sections 122-762C-53X-1, -53X-2, and -53X-3. A recrystallized silicified shell is also observed in Core 122-762C-51X-5, 105 cm. Smear-slide analysis indicates that the amount of foraminifers varies from 4% to 20% (Fig. 9). However, throughout Subunit IVB (as well as in the other subunits of Unit IV) we recognized many small voids from which foraminifers had been dissolved. The abundance of foraminifers, therefore, might be more variable.

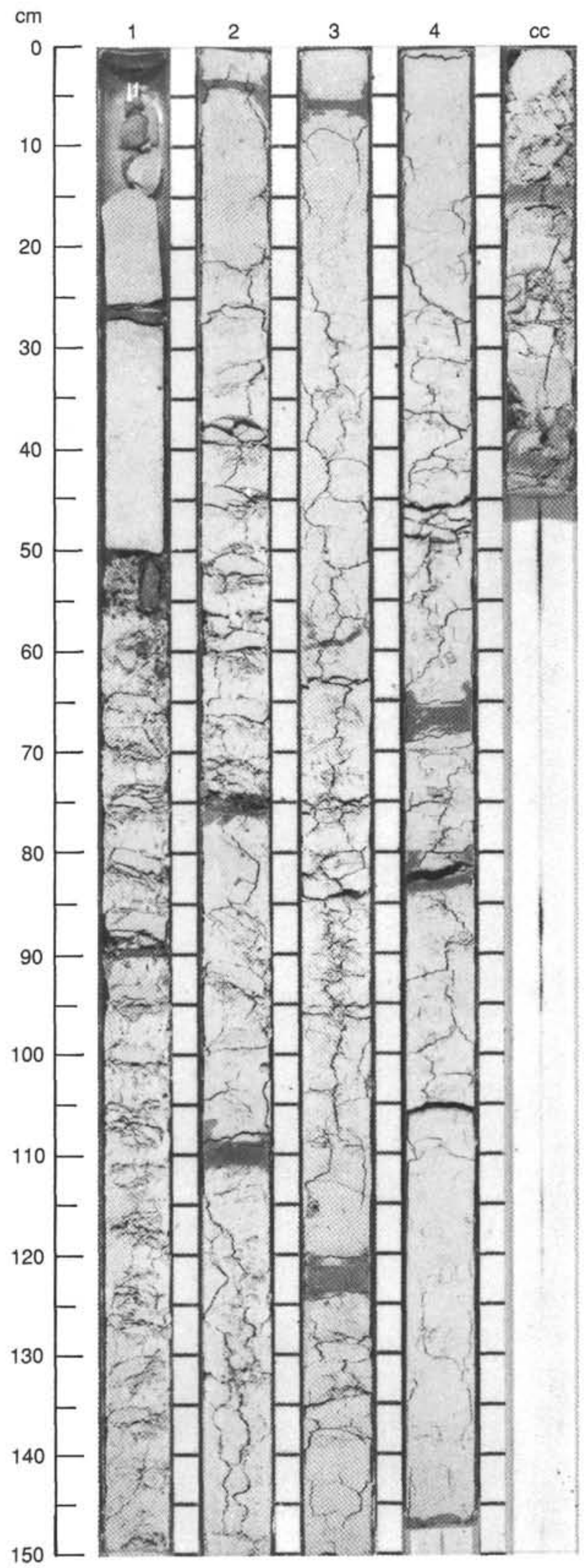

Figure 17. Core 122-762C-46X. Alternation of lighter and darker beds in the nannofossil chalk of Subunit IVA (upper green interval), with gradational basal and upper boundaries.

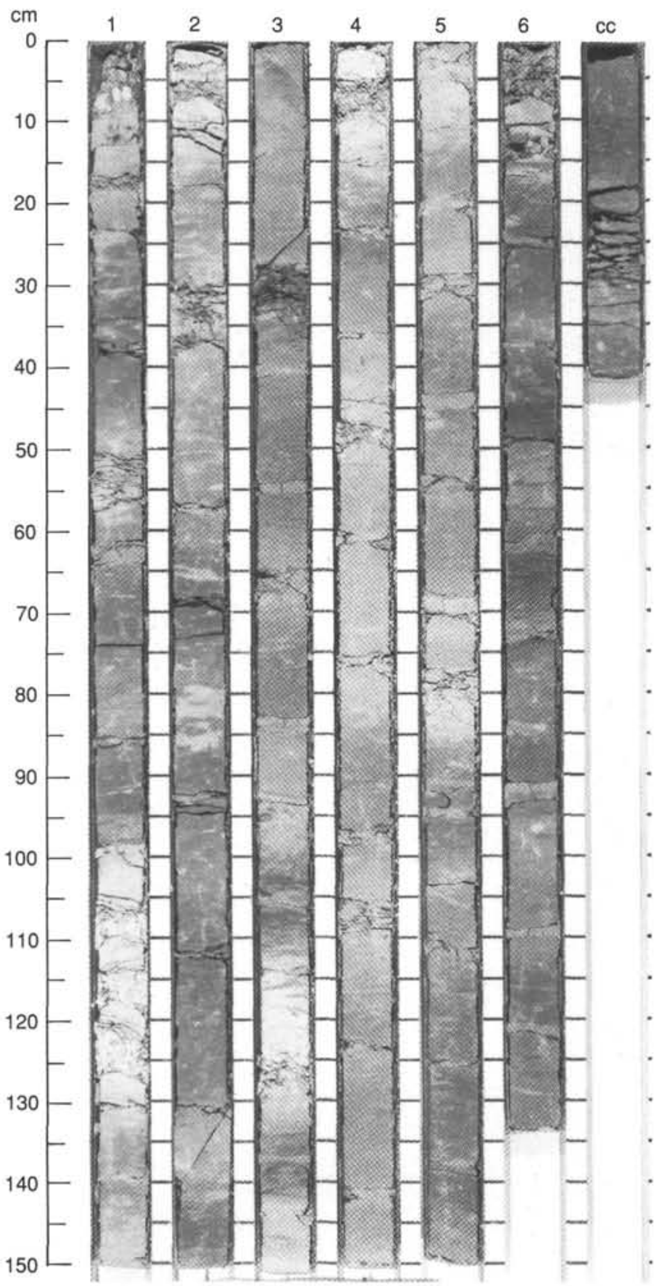

Figure 18. Core 122-762C-51X. Alternation of lighter and darker beds in nannofossil chalk of Subunit IVB (upper brown interval). Darker beds generally contain more clay than lighter beds and have gradational basal and upper boundaries. Bioturbation is strong throughout the core.

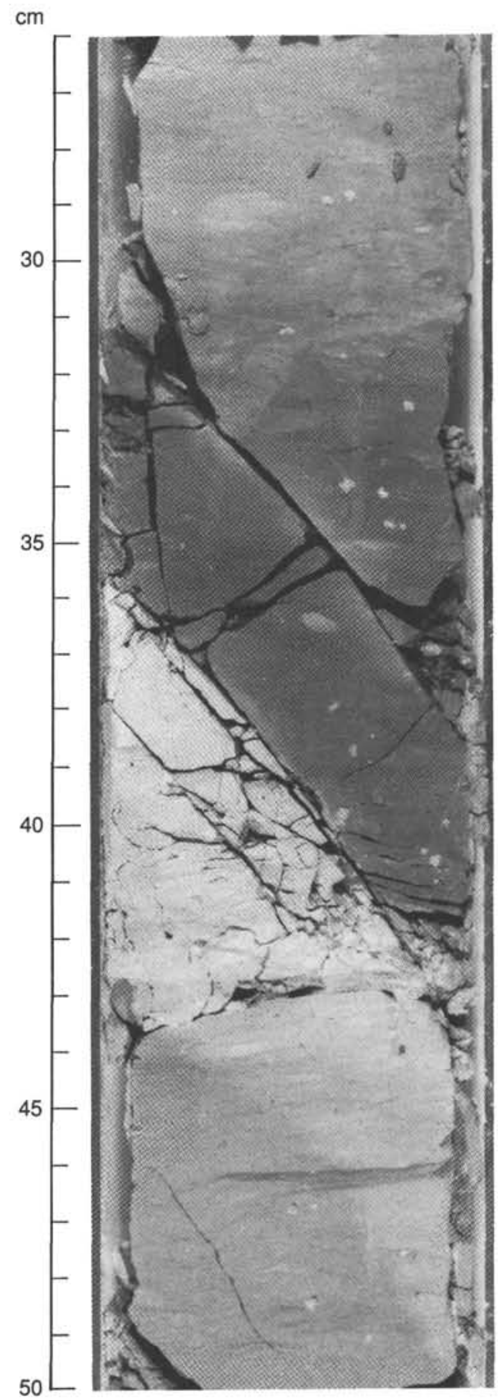

Figure 19. Interval 122-762C-56X-3, 26–50 cm. Gradually alternating darker and lighter beds of Subunit IVB (upper brown interval). Darker beds are disturbed by burrowing from lighter beds. Anastomosing seams run nearly parallel to the bedding.

Many thin anastomosing seams, trending nearly parallel to the bedding, are distinct throughout Subunit IVB (Fig. 19). These cut trace fossils and locally include small boudinage-like and/or microstylolite-like structures (e.g., in Section 122-762C-57X-1). These anastomosing seams are also associated with small veins (e.g., in Core 122-762C-51X-2), and can be interpreted as post-depositional pressure solution structures resulting from early diagenetic compaction, calcium carbonate dissolution, and local reprecipitation during burial.

Subunit IVC (697.0–780.0 mbsf)

Interval 122-762C-58X-1, 0 cm, to -69X-1, 0 cm.

Subunit IVC is an intermediate green interval of Unit IV and is 83.0 m thick. The age is early Santonian to early Campanian (Figs. 8 and 9). Subunit IVC consists of white (5Y 8/1) to very light green-gray (10Y 8/1) nannofossil chalk with foraminifers, which forms interbeds with 1–10-mm-thick layers of green-gray (5G 5/1) nannofossil claystone in an interval of 10–80 cm (Fig. 20).

The nannofossil chalk with foraminifers (lighter beds) is generally structureless. Bioturbation is moderate throughout

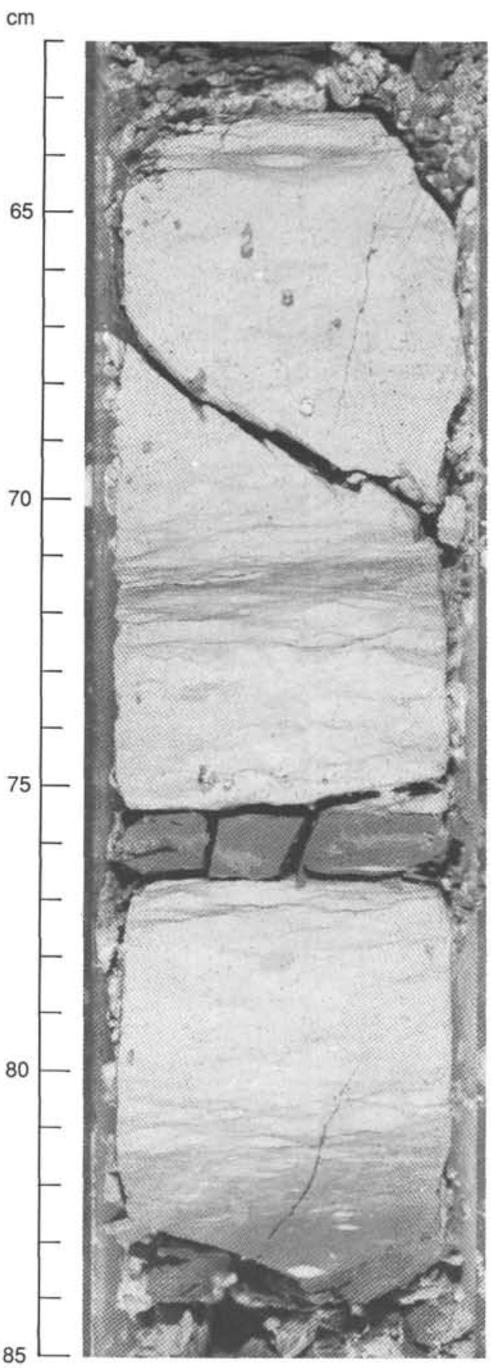

Figure 20. Interval 122-762C-68X-1, 62–85 cm. Alternation of darker and lighter beds of Subunit IVC (middle green interval), with gradational basal and upper boundaries. Bioturbation is moderate throughout the core. Lighter beds are generally classified as nannofossil chalk with foraminifers, while darker beds are nannofossil claystone. Small voids, from which foraminifers have been dissolved or removed, are distinct. Anastomosing seams (microstylolites) include "boudin"-like structures.

Subunit IVC, although identifiable trace fossils are absent. The nannofossil claystones (darker beds) are finely laminated and show slightly sharp or gradational upper and lower contacts. Calcium carbonate content is 89%–94% in the lighter beds and 36%–67% in the darker beds.

Inoceramus fragments are observed in Section 122-762C-62X-2 at 30 cm and -62X-5 at 40 cm. Some pyrite nodules are present throughout the lighter beds of Cores 122-762C-63X and -64X. The lighter beds also contain small chert nodules (e.g., Interval 122-762C-64X-4, 27 cm). Minor anastomosing seams, described in Subunit IVB, are locally present (e.g., Interval 122-762C-58X-6, 53–56 cm, and Section 122-762C-66X-5) (Fig. 20).

Subunit IVD (780.0–820.2 mbsf)

Interval 122-762C-69X-1, 0 cm, to -77X-2, 18 cm.

Subunit IVD is a lower brown interval of Unit IV and is also characterized by 7–85-cm-thick gradational cyclic color changes from brown (7.5YR 5/2) (beds 1–10 cm thick), through light brown (7.5YR 6/2) (beds 3–20 cm), to white (5Y 8/1) or light green-gray (5GB 7/1) (beds 3–55 cm thick) (Fig. 21). The thickness is 41.8 m and the age is late Albian to early Santonian (Figs. 8 and 9). The Turonian/Cenomanian boundary is found in Core 122-762C-75X-1, 115–138 cm (see "Biostratigraphy," this chapter). This interval is represented by dark brown (7.5YR 3/2) fissile claystone with gradational upper and lower boundaries.

Lighter (white or light green-gray) beds mainly consist of nannofossil chalk with up to 24% foraminifers, locally classified as foraminifer nannofossil chalk (e.g., Sample 122-762C-76X-2, 116 cm) (Fig. 9). Clay content is greater in the brown beds than in the light brown beds; these beds are described as nannofossil chalk with clay/clayey nannofossil chalk and clayey nannofossil chalk/nannofossil claystone, respectively. Calcium carbonate content is 92%–93% in the lighter beds and 51%–64% in the darker beds. In addition, there is a minor lithology (claystone) that contains <4% calcium carbonate. Although Subunit IVD is generally structureless, moderate bioturbation is observed throughout, with many identifiable trace fossils including *Planolites*, *Teichichnus*, *Zoophycos*, and *Chondrites*. Many anastomosing seams cut through these trace fossils, and are more distinct in the darker beds than in the lighter beds (Fig. 21).

Subunit IVE (820.2–835.5 mbsf)

Interval 122-762C-77X-2, 18 cm, to -79X-1, 0 cm.

Subunit IVE is the lower green interval of Unit IV and is 18.3 m thick and of Albian age (Figs. 8 and 9). Subunit IVE represents the initial sedimentation of pelagic carbonates over the siliciclastic sediments of Unit V (although the basal contact of Subunit IVE with Unit V was not recovered). It is correlated with the Gearle Siltstone, which is exposed in Barrow Island (Exon and Willcox, 1980). Subunit IVE mainly consists of clayey calcareous chalk (Core 122-762C-77X) and nannofossil chalk with clay (Core 122-762C-78X). Up to 30% μm-size calcite particles are contained in the nannofossil calcareous chalk with clay (Fig. 9). Clay content is variable throughout Subunit IVE, with a range from 3% to 15%. Gradational contacts of alternating light green-gray (5G 7/1) and green-gray (5G 6/2) beds are also typical in Subunit IVE (Fig. 22). Couplets are 15–110 cm thick, and contain many bioturbation structures and anastomosing seams (Fig. 22). Calcium carbonate content is up to 90% in the light green-gray beds, and is about 61.64% in the green-gray beds.

Some *Inoceramus* fragments and a belemnite occur in Samples 122-762C-77X-4, 128 cm, and -77X-5, 110 cm, respectively. Pyrite nodules up to 2 cm in diameter are scattered throughout Sections 122-762C-77X-3 and -77X-5.

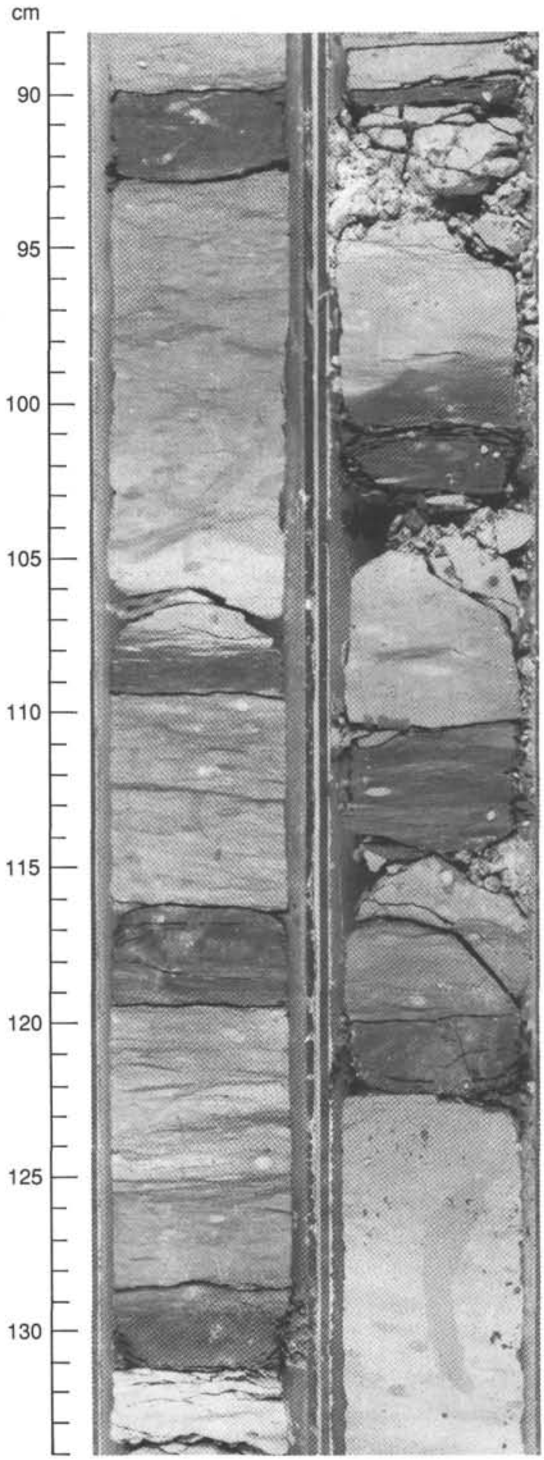

Figure 21. Intervals 122-762C-71X-1, 88–134 cm (left-hand side), and -71X-2, 88–134 cm (right-hand side). Nannofossil chalk with foraminifers (lighter beds) and intercalated nannofossil claystones (darker beds) of Subunit IVD (lower brown interval). Bioturbation is moderate throughout the core and many anastomosing (microstylolites) seams cut the trace fossils.

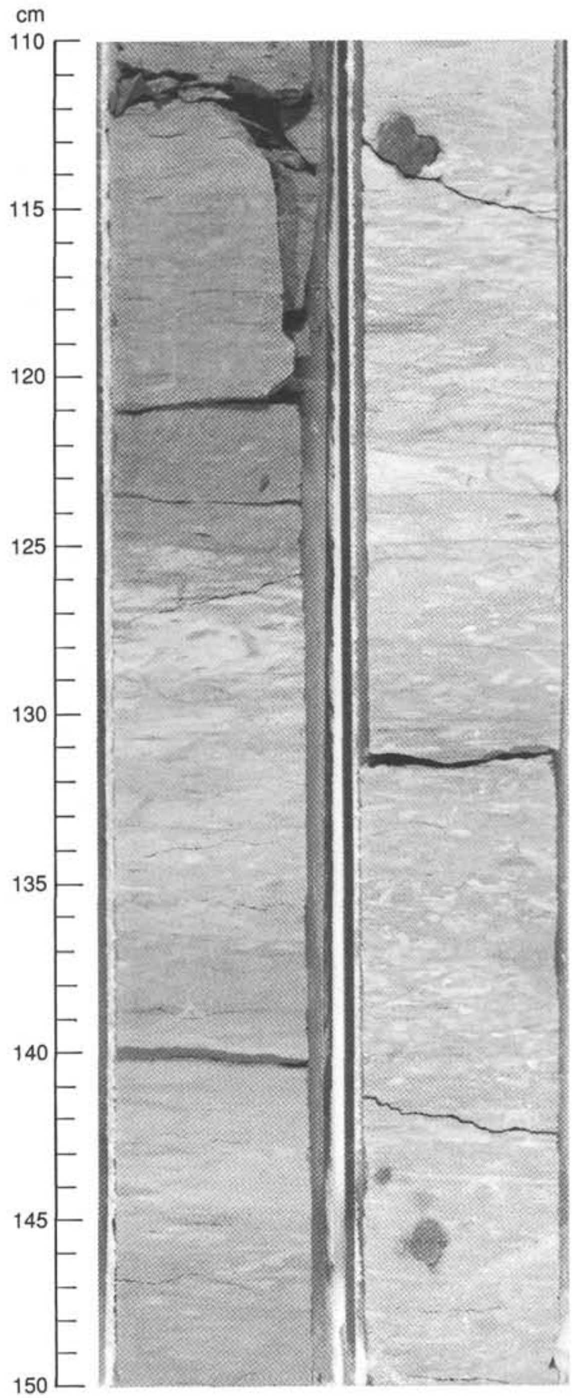

Figure 22. Intervals 122-762C-77X-2, 110–150 cm (left-hand side), and -77X-3, 110–150 cm (right-hand side). Gradually alternating light green-gray and green-gray nannofossil chalk of Subunit IVE, with varying amount of carbonate particles and clay. Bioturbation is strong throughout the core, and some pyrite nodules and *Inoceramus* fragments are present.

Unit V (838.5–848.5 mbsf)

Interval 122-762C-79X-1, 0 cm, to -81X-1, 0 cm.

Unit V consists of parallel-laminated, black (7.5YR 2/0) to dark gray (7.5YR 5/0) calcareous claystones. The recovered thickness is 10 m, with an age of early Aptian (Figs. 8 and 9).

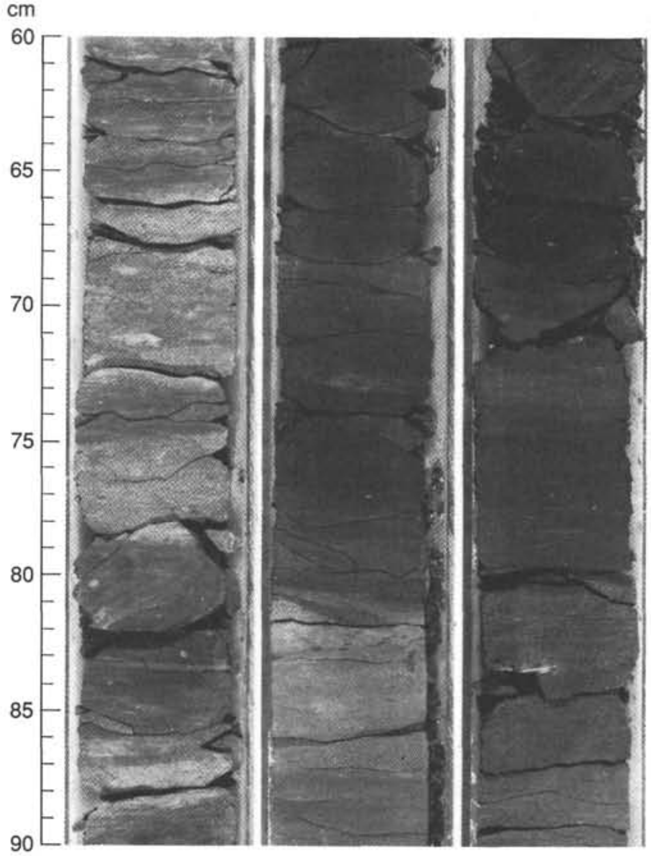

Figure 23. Intervals 122-762C-79X-1, 60–90 cm (left-hand side), -79X-2, 60–90 cm (center), and -79X-3, 60–90 cm (right-hand side), containing parallel-laminated, very dark gray claystone of Unit V. Distinct bioturbation structures are present.

No basal contact with the underlying Unit VI was recovered in this hole. We correlate the calcareous claystones with the Muderong Shale, which was described from Barrow Island (Exon and Willcox, 1980). Minor small cross-laminations occur in Section 122-762C-80X-CC. Bioturbation is moderate to strong throughout Unit V, although identifiable trace fossils are absent (Fig. 23). The calcareous claystones contain many μm-size calcite fragments (20%–30%, determined from smear-slide analyses), and minor glauconite, pyrite, and quartz. Some foraminifers occur in Section 122-762C-80X-CC. Calcium carbonate content in the calcareous claystones averages about 1.9% (see "Organic Geochemistry," this chapter).

Unit VI (848.5–940.0 mbsf)

Interval 122-762C-81X-1, 0 cm, through -91X-CC.

Unit VI consists of black (2.5Y 2/0) to dark gray (5Y 3/1) silty claystone and clayey siltstone; the penetrated thickness is 91.5 m (Figs. 8 and 9). The age is estimated to be Berriasian to early Valanginian. We interpret this unit as the northern extension of the Barrow Group, which was described from Barrow Island (Exon and Willcox, 1980). However, we recognize a distinct hiatus between Cores 122-762C-87X and -88X (see "Biostratigraphy," this chapter).

The silty claystones and clayey siltstones commonly contain glauconite (3%–15%), pyrite (5%–25%), quartz (5%–30%), and feldspar (5%–10%) (Fig. 8). Fine- to medium-grained glauconitic sands are also observed throughout Unit VI.

The upper portion of Unit VI (Sections 122-762C-81X-1 to -83X-CC) is characterized by generally massive silty claystones and contains many belemnites (mainly in Core 122-762C-81X) and pyrite nodules. Minor parallel laminations and bioturbation structures, however, were observed in the upper portion. A 25-cm-thick gray limestone bed is intercalated in the silty claystones in Interval 122-762C-82X-2, 78–103 cm. This limestone, a carbonate mudstone to wackestone, contains some recrystallized shells. The lower portion of the unit includes molluscan shells and gray (N2) dolomitic silty limestone nodules 1–3 cm in diameter (Fig. 24). Some pyrite and minor belemnites are also present in the lower portion of Unit VI (e.g., Section 122-762C-88X-1). Fine laminations and weak-to-moderate bioturbation are much more distinct in the lower portion, and the relative abundance of glauconite increases downhole (up to 10%) (Fig. 9). Log data also suggest that there are 3–4-m-thick intervals of concentrated glauconitic sediments. Plant debris was also observed in Sample 122-762C-85X-2, 58–60 cm. The average calcium carbonate content in the upper portion (except for the limestone bed) is 1.0%, whereas that of the lower portion is 2.3% (see "Organic Geochemistry," this chapter).

Cretaceous Sedimentary Environments

We interpret Unit VI as the distal portion of a deltaic succession (Barrow Group) (Exon and Willcox, 1980) and thus a shelf-margin prodelta deposit. We estimate maximum water depth of the prodelta deposits to be 200–500 m, as determined from seismic profiles of delta clinoforms (see "Seismic Stratigraphy," Site 763 chapter, this volume). Fine laminations in the lower portion of Unit VI may indicate current activity and/or water circulation in the prodelta environment, in response to the episodic supply of silt and minor amounts of plant debris (either by storm waves and/or by flood-water intrusion at a river mouth). Common mollusk shells, glauconite, and bioturbation structures may indicate oxygenated conditions. Numerous dolomitic, silty limestone nodules suggest local concentration of available carbonate materials that may have been derived from marine fauna. In contrast, the upper portion of Unit VI contains less calcium carbonate than the lower part (except for a limestone bed and belemnites) and generally lacks bioturbation structures (suggesting a reduced oxygen supply). Therefore, the upper portion of Unit VI may represent a more distal portion of a prodelta environment where sedimentation rates were very slow and only planktonic fauna (e.g., belemnites) accumulated. The intercalated limestone bed may represent the episodic supply of shallow-marine shell fragments by sediment gravity flows in response to a relative sea-level rise.

We interpret the lithologic change from the lower to upper part of Unit VI to be the result of relative sea-level rise. Alternatively, the lithologic change may represent the transition from the deposition of the lower part of the Barrow Group (derived from a hinterland to the south in the region of the present Cuvier Abyssal Plain) to deposition of the upper part of the group (derived from a hinterland to the east) (Exon and Willcox, 1978). In this scenario, deposition of the lower part of the group ended during the late Neocomian when the Cuvier Abyssal Plain started to form. Eustatic sea-level changes in the Neocomian would thus also be overprinted in the deltaic sedimentation. More precise sequence stratigraphic analyses on the deltaic system will be done after the coring and logging at Site 763.

The calcareous claystones of Unit V represent the end of predominantly terrigenous, siliciclastic sedimentation at this site. The existence of fine parallel laminations and minor

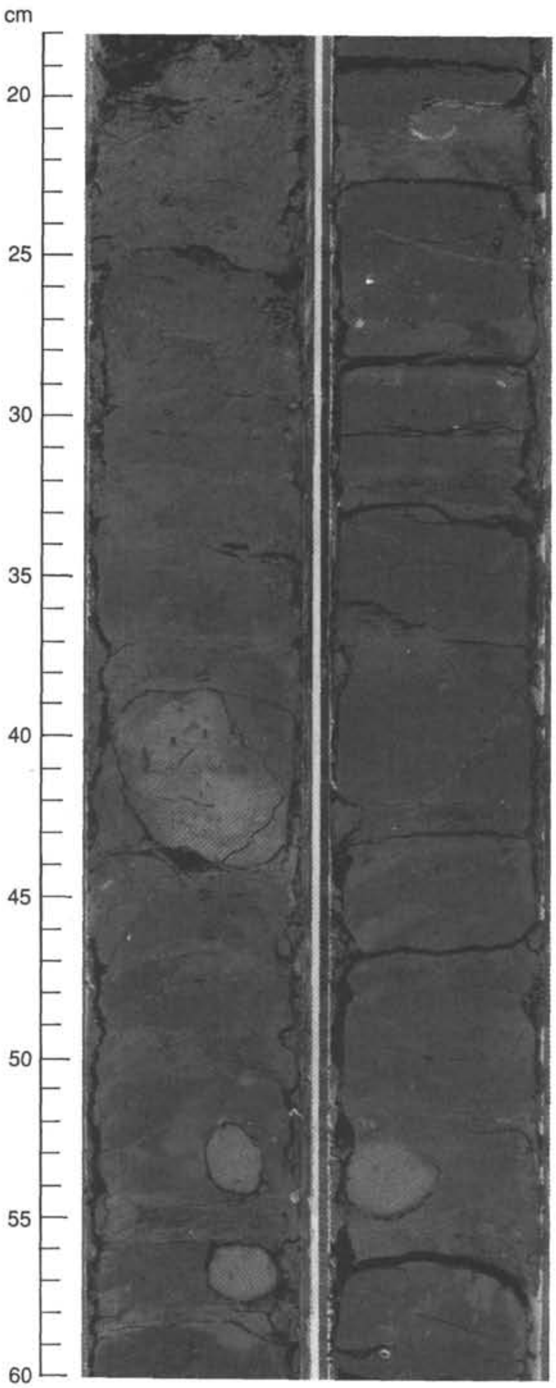

Figure 24. Interval 122-762-85X-1, 18–60 cm (left-hand side), and -85X-2, 18–60 cm (right-hand side), containing finely laminated, black silty claystone of the lower portion of Unit VI. Bioturbation is moderate, and some dolomitic silty limestone nodules and molluscan shells are present.

cross-laminations suggests bottom-water circulation. Strong bioturbation may indicate a slow terrigenous-clastic sedimentation rate and/or the initiation of oxygenated seafloor conditions, following the anoxic conditions recognized in the upper portion of Unit VI. Although there are no available data on paleobathymetry, the depositional environment of Unit V appears to represent a hemipelagic epicontinental sea, and may indicate the start of open-marine bathyal conditions at this site.

Cyclic color changes observed throughout the nannofossil chalk of Unit IV (i.e., small-scale alternations of darker and lighter beds) are controlled by clay and calcium-carbonate contents (as described above). Both the upper and the lower boundaries of each couplet are gradational and no distinct primary sedimentary structures are observed, with the exception of some darker interbeds in Subunit IVC. There is no preliminary evidence to suggest that any of the clay found in these cycles was introduced by sediment gravity flows. Increased suspension of clay in the marine environment, which would have favored the development of darker beds, might have been introduced by other episodic marine processes (e.g., storm waves, mass wasting from continental slopes, bottom current, and/or eolian transport) in response to short-term climatic, eustatic, and tectonic fluctuations during the late Cretaceous.

From the Campanian sedimentation rates determined for the interval from Section 122-762C-49X-1 to -55X-CC (ca. 4 cm/1000 yr; see "Sedimentation Rates," this chapter) we roughly estimate that each cycle (35–130 cm thick) represents 9,000–33,000 yr (average = 21,000 yr). The estimated frequency of the cycles roughly coincides with the orbital cycle of the precession (23,000 yrs) first suggested by Milankovitch (1938) and later by Hays et al. (1976). More detailed petrographic, geochemical, and chronological analyses are needed to decipher the origin of small-scale cyclicity of darker and lighter beds, and the associated pressure-solution structures in the nannofossil chalk. Similar cyclic color patterns in the Cretaceous-Paleocene sediments of the Walvis Ridge area were interpreted to have resulted from fluctuations in bottom-water conditions (Borella, 1984).

Subunit-scale cyclic color changes (i.e., green versus brown cycles) were overprinted by the small-scale cycles of lighter and darker beds. Darker beds of the brown intervals generally contain more iron oxides than those of the green intervals. The brown color, therefore, may reflect ferric iron in clay minerals, whereas the green color may be ferrous iron and thus suggests more reducing pore-water conditions. Pyrite nodules are typically observed in the green intervals and suggest negative-Eh depositional conditions. Bottom-water circulation and enriched oxygen content at and below the sediment/water interface appear to have been required for active oxidation. Strong bioturbation, in which the identifiable trace fossil assemblages indicate bathyal to abyssal environments (Chamberlain, 1978), suggests oxygenated seafloor conditions, and may also suggest a general lack of terrigenous input during transgressions. Sea-level highstands favor active ocean mixing (Ramsay, 1974) and can develop active seafloor oxidation. The subunit-scale cycles of brown and green intervals in Unit IV are therefore best explained in terms of Cretaceous eustatic sea-level changes (Haq et al., 1987). The brown intervals (i.e., Subunits IVB and IVD) may have developed during sea-level highstands at approximately 79 and 92 Ma (Fig. 25).

BIOSTRATIGRAPHY

Introduction

Site 762 is located on the western part of the central Exmouth Plateau at a water depth of 1360 m. Three holes were drilled at this site: Hole 762A consisted of a single 9.5-m core, Quaternary in age; Hole 762B was cored with the APC to a depth of 175.4 mbsf, bottoming in Lower Oligocene sediments Hole 762C was drilled with the XCB to a depth of 940 m, bottoming in Berriasian sediments.

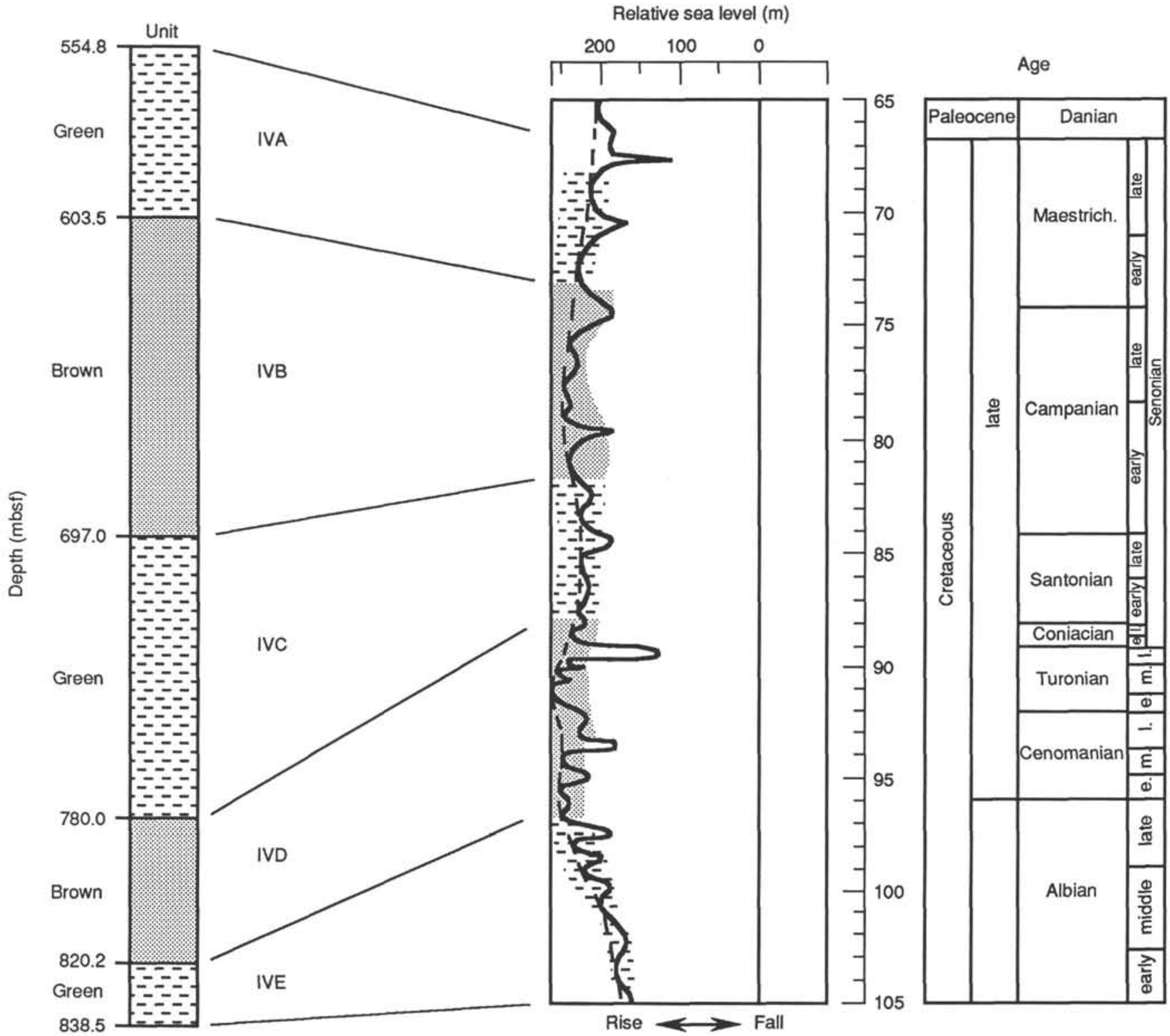

Figure 25. Cyclic sedimentation of green (dashed) and brown (stippled) intervals in Unit VI, compared with global sea-level changes (from Haq et al., 1987). See text for detailed description and age of the subunits.

Biostratigraphic investigations of calcareous nannofossils, foraminifers, radiolarians, and palynomorphs were carried out primarily using core-catcher samples, supplemented by a few samples from higher core sections. The following is a summary of the biostratigraphic results.

Calcareous Nannofossils

Occurrence and Preservation

All cores recovered from Holes 762A and 762B contain abundant, well-preserved Pleistocene to Oligocene calcareous nannofossils. At Hole 762C, Cores 122-762C-1C to -13X (Pleistocene to middle Eocene) also contain abundant, well-preserved nannofossils. Nannofossils are abundant from Cores 122-762C-14X to -23X (middle to lower Eocene), but preservation is mostly moderate to poor. An interval of abundant, well-preserved nannofossils occurs again in Cores 122-762C-24X to -27X (lower Eocene to upper Paleocene) although nannofossils remain abundant, preservation is moderate to poor in Cores 122-762C-28X to -41X. Only in Core 122-762C-42X (lowest Paleocene) are nannofossils rare.

Abundance and preservation increase steadily from the lower to the upper Cretaceous sequence. Cores 122-762C-43X to -50X (mostly Maestrichtian) contain abundant, well-preserved nannofossils. Cores 122-762C-51X to -62X (Campanian) contain abundant, moderately preserved nannofossils. Cores 122-762C-63X to -79X (upper Santonian to lower Aptian) contain common to abundant nannofossils, with preservation varying from poor to moderate. Cores 122-762C-80X to -91X contain only rare, moderately to poorly preserved nannofossils. The assignment of Martini's (1971) biostratigraphic zones to Cenozoic sediments cored at Site 762 is summarized in Figure 26.

Cenozoic Biostratigraphy

Section 122-762A-1H-CC contains a mixed Quaternary (NN19–NN21) assemblage. At Hole 762B, Section 122-762B-1H-CC is in Zones NN20–NN21, as determined by the

Hole 762B

Core	Core, section	Nannofossil zone	Series
1H	1H-CC	NN20-21	Quaternary
2H, 3H	2H-1 to 4H-3	NN19	Quaternary
4H	4H-4 to 5H-2	NN17-18	upper Pliocene
5H, 6H, 7H	5H-3 to 8H-2	NN16	upper Pliocene
8H	8H-3 to 8H-CC	NN14-15	lower Pliocene
9H, 10H	9H-1 to 11H-2	NN13	lower Pliocene
11H	11H-3 to 11H-CC	NN12	lower Pliocene
12H	12H-1 to 13H-2	NN11	upper Miocene
13H	13H-3 to 13H-CC	NN9	upper Miocene
14H	14H-1 to 14H-5	NN6-7	middle Miocene
14H, 15H	14H-6 to 15H-4	NN4-5	middle Miocene
15H, 16H	15H-5 to 16H-5	NN1-2	lower Miocene
16H, 17H	16H-6 to 17H-4	NP24-25	upper Oligocene
17H, 18H	17H-5 to 18H-4	NP23	lower Oligocene
18H, 19H	18H-5 to 19H-5	NP22	lower Oligocene
19H	19H-5 to 19H-CC	NP21	lower Oligocene

Hole 762C

Core	Core, section	Nannofossil zone	Series
2X, 3X, 4X	2X-2 to 5X-1	NP21	lower Oligocene
5X, 6X, 7X	5X-2 to 7X-3	NP19-20	middle Eocene
7X, 8X, 9X	7X-4 to 9X-CC	NP18	middle Eocene
10X, 11X, 12X	10X-1 to 12X-5	NP17	middle Eocene
13X	12X-6 to 13X-CC	NP16	middle Eocene
14X, 15X, 16X	14X-1 to 16X-3	NP15	middle Eocene
16X, 17X, 18X	16X-CC to 18X-5	NP14	middle Eocene
18X, 19X	18X-6 to 19X-2	NP13	lower Eocene
19X, 20X, 21X, 22X	19X-3 to 22X-CC	NP12	lower Eocene

Hole 762C

Core	Core, section	Nannofossil zone	Series
23X, 24X, 25X	23X-1 to 25X-3	NP11	lower Eocene
25X, 26X, 27X	25X-4 to 27X-3	NP10	lower Eocene
27X, 28X	27X-4 to 28X-CC	NP9	upper Paleocene
29X, 30X	29X-1 to 30X-22	NP7-8	upper Paleocene
31X, 32X	31X-1 to 32X-CC	NP6	upper Paleocene
33X, 34X	33X-1 to 35X-1	NP5	upper Paleocene
35X	35X-2 to 36X-1	NP4	upper Paleocene
36X, 37X, 38X, 39X, 40X	36X-CC to 40X-2	NP3-4	lower Paleocene
40X, 41X, 42X	40X-3 to 42X-5	NP2	lower Paleocene
42X	42X-6 to 43X-1	NP1	lower Paleocene
			?
43X	43-1, 31 cm -	CC26	Maestrichtian

Figure 26. Cenozoic calcareous nannofossil stratigraphy of Site 762 modified from Martini's (1971) zonation. Wavy lines indicate hiatuses.

presence of *Emiliania huxleyi* and the absence of *Pseudoemiliania lacunosa*. Sections 122-762B-2H-1 to -4H-3 are placed in Zone NN19, owing to the presence of *P. lacunosa* and the absence of discoasters. Sections 122-762B-4H-4 to -5H-2 are in undifferentiated Zones NN17/NN18, given the presence of *Discoaster brouweri* and the absence of *D. surculus*. Sections 122-762B-5H-3 to -8H-1 are in Zone NN16, on the basis of the presence of *D. surculus* and the absence of *Reticulofenestra pseudoumbilica*. Undifferentiated Zones NN14/NN15 are assigned to Sections 122-762B-8H-CC as determined by the presence of *D. asymmetricus* and *R. pseudoumbilica*.

In Sections 122-762B-9H-1 to -11H-2 the co-occurrence of *Ceratolithus rugosus* and *Ceratolithus acutus* indicates Zone NN13, whereas the presence of *C. acutus* and the lack of *Discoaster quinqueramus* and *C. rugosus* in Section 122-762B-11H-3 to -11H-CC indicates Zone NN12. The presence of *D. quinqueramus* in all sections from Core 122-762B-12H down to -13H-2, 100–101 cm, indicates Zone NN11 for that interval.

Section 122-762B-13H-3, 100–101 cm, down to -13H-CC is in Zone NN9, as determined by the presence of *Discoaster hamatus*. The relatively short Zone NN10 is apparently absent. Samples 122-762B-14H-1 to -14H-5, 100–101 cm, are assigned to undifferentiated Zones NN6/7, indicated by the absence of *Sphenolithus heteromorphus* and *Catinaster coalitus*, and the presence of *Discoaster braarudii*; Zone NN8 is absent. Samples 122-762B-14H-6, 4-6 cm to -15H-4, 100–101 cm, are assigned to undifferentiated Zones NN4/5 according to the presence of *S. heteromorphus* and *Helicosphaera obliqua*. Samples 122-762B-15H-5, 88–90 cm, to -16H-5 contain *Sphenolithus belemnos*, *Sphenolithus conicus*, *Triquetrorhabdulus carinatus*, and rare to very rare *Dictyococcites bisectus* and *Zygrhablithus bijugatus*. This assemblage suggests Zone NN1/2, which implies a hiatus in the middle to upper part of the Lower Miocene.

Sections 122-762B-16H-6 to 17H-4 are in Zone NP25, indicated by the presence of *Sphenolithus ciperoensis*, common *D. bisectus* and *Z. bijugatus*, and the absence of *Sphenolithus distentus*. The lack of *S. ciperoensis* and *Reticulofenestra umbilica* in Sections 122-762B-17H-5 to -18H-4, together with the presence of *S. distentus*, *Discoaster nodifer*, and *Helicosphaera perch-nielsenae*, indicates Zone NP23. Zone NP22 occurs between Section 122-762B-28H-5 and -19H-5. Zone NP21 is present in Section 122-762B-19H-6 and -19H-CC indicated by the co-occurrence of *Ericsonia formosa* and *R. umbilica* and the absence of *Discoaster saipanensis* and *D. barbadiensis*.

The first section recovered at Hole 762C (Section 122-762C-2X-1) is in NP22, on the basis of *Reticulofenestra umbilica* being present and *E. formosa* being absent. Sections 122-762C-2X-2 to -5X-1 are in NP21. Samples 122-762C-5X-2, 36–38 cm, to -7X-3 are in NP19/NP20, as determined by the co-occurrence of *D. saipanensis* and *Isthmolithus recurvus*. Zone NP18 is assigned to Sections 122-762C-7X-4 to -9X-CC, indicated by the presence of *Chiasmolithus oamaruensis* and the absence of *I. recurvus*. Sections 122-762B-10X-1 to -12X-5 are in Zone NP17, according to the presence of *Chiasmolithus grandis* and *Discoaster tanii*, and the lack of *C. oamaruensis* and *C. solitus*.

The presence of *Discoaster nodifer*, together with *Sphenolithus furcatolithoides* and *Campylosphaera dela* in Sections 122-762C-12X-6 to -13X-CC suggests Zone NP16. Sections 122-762C-14X-1 to -16X-3 are in Zone NP15, indicated by the presence of *Nannotetrina* cf. *N. fulgens*, sporadic *Chiasmolithus gigas*, *Sphenolithus furcatolithoides*, *Reticulofenestra umbilica*, and *Pseudotriquetrorhabdulus inversus*.

Sections 122-762C-16X, to -18X-5 are in Zone NP14, suggested by the co-occurrence of *Discoaster lodoensis* and *Discoaster sublodoensis*. Sections 122-762C-18X-6 to -19X-2 are assigned to NP13 because they contain *D. lodoensis* and lack *Tribrachiatus orthostylus*, and Sections 122-762C-19X-3 to -22X-CC are assigned to NP12 because *D. lodoensis* and *T. orthostylus* both occur.

Sections 122-762C-23X-1 to -25X-3 are in NP11, recognized by the presence of *Tribrachiatus bramlettei*, *Chiasmolithus grandis*, and *Discoaster multiradiatus*, and the absence of *Tribrachiatus contortus* and *D. lodoensis*. Sections 122-762C-25X-4 to -27X-3 contain *T. contortus* and are assigned to NP10. Sections 122-762C-27X-4 to -28X-CC are in Zone NP9, as determined by the presence of *D. multiradiatus*, *Fasciculithus tympaniformis*, and *Cruciplacolithus tenuis*, and the absence of *T. contortus*.

Sections 122-762C-29X-1 to -30X-CC contain *Discoaster mohleri*, but *Heliolithus kleinpellii*, *Heliolithus riedelii*, or *D. multiradiatus* could not be found; this interval is therefore assigned to undifferentiated Zones NP7/NP8.

Sections 122-762C-31X-1 to -32X-CC are in Zone NP6, indicated by the presence of *H. kleinpellii*, and the lack of *D. mohleri*. Sections 122-762C-33X-1 to -35X-1 are in Zone NP5, according to the presence of *Fasciculithus tympaniformis* and the absence of *H. kleinpellii*. Sample 122-762C-35X-2, 12–14 cm and Sections 122-762C-35X-CC to -40X-2 are in undifferentiated Zones NP3/NP4, recognized by the presence of *Chiasmolithus danicus*/*Chiasmolithus consuetus* and the lack of *F. tympaniformis*. Section 122-762C-40X-3 to Sample 122-762C-42X-5, 20 cm are placed in NP2, as suggested by the presence of *Cruciplacolithus tenuis* and *Cruciplacolithus edwardsii*, and the lack of *Chiasmolithus danicus*. Samples 122-762C-42X-CC are in NP1, based on the presence of relatively common *Placozygus sigmoides*, *Markalius astroporus*, and *Thoracosphaera* spp., and the lack of *Cruciplacolithus* spp.

Section 122-762C-43X-1, down to 31 cm, contains redrilled NP2; the upper Maestrichtian Zone CC26 occurs in Sample 122-762C-43-1, 34 cm, indicated by the presence of *Nephrolithus frequens*.

Cenozoic Paleoenvironments

The overall nannofossil assemblage suggests a low-latitude, open-ocean environment during the Cenozoic. The only environmental perturbation occurs in Sections 122-762B-15H-5 to -18H-CC (lowest Miocene Zone NN1 to Lower Oligocene Zone NP23). In this interval, *Braarudosphaera bigelowii* is a significant component of the assemblage. Specimens of this species are generally rare to few in this interval, but in Sample 122-762B-15H-5, 88–90 cm, *B. bigelowii* is common to abundant. Very large specimens occur throughout this interval (up to 22 μm), coexisting with specimens in the normal size range of about 10–14 μm. *Braarudosphaera bigelowii* was not found in cores from this stratigraphic interval recovered from the Wombat Plateau (Sites 760 and 761), nor was this interval recovered at the nearby Deep Sea Drilling Project (DSDP) Sites 259 or 263 (Leg 27, eastern Indian Ocean–Western Australia).

In today's oceans, *Braarudosphaera bigelowii* has been found living in nearshore waters, but not in open-ocean conditions. It has been suggested (e.g., Bukry, 1974) that this distribution may reflect its preference for low-salinity waters. Certainly *B. bigelowii* seems to be able to tolerate salinities lower than those in which most calcareous nannoplankton can survive (*B. bigelowii* has been found living in the Black Sea in salinities as low as 11 g/kg, compared to normal seawater at 36 g/kg; Bukry, 1974).

In fossil assemblages, *B. bigelowii* is most common in sediments deposited in nearshore environments, and it is assumed that low nearshore salinities also controlled the abundance of this species in the past.

More difficult to explain is the widespread occurrence in the Oligocene of the "*Braarudosphaera* chalk," which was deposited under apparently open-ocean conditions, primarily in the South Atlantic. Bukry (1981) summarized the known occurrences of *Braarudosphaera*-rich sediments as follows: from the Quaternary of the Black Sea, the upper Oligocene of the North Atlantic, the lower Oligocene of the South Atlantic, the middle Eocene of the Gulf of Mexico, the lower Paleocene of Spain, and the Hauterivian of the North Atlantic.

The most extensive deposits are the thin *Braarudosphaera* chalk beds which occur in a lower Oligocene trans-oceanic belt across the South Atlantic, roughly between 20°S and 30°S (Bukry, 1981). It should be noted that this belt occurs in Bukry's *Sphenolithus distentus* Zone, correlatable to NP23, within which *Braarudosphaera* became prominent at Site 762.

Bukry (1981) and others have speculated on the conditions necessary to have created an open-ocean bloom of *Braarudosphaera*. Low salinities could have resulted from the addition of unusual amounts of freshwater to oceanic surface waters, possibly caused by a long interval of heavy rainfall or the influence of Antarctic meltwater.

Cretaceous Biostratigraphy

A thick upper Cretaceous sequence was drilled in Hole 762C. As at other Leg 122 sites, the zonations of Sissingh (1977) and Roth (1978) were not applicable for the whole section because many of the zonal markers are not present. We have therefore used biohorizons as a basis for stratigraphy (Fig. 27), allowing us to define combined zonal units of Sissingh (1977) and Roth (1978). We examined one sample in every other section recovered. However, it remains difficult to determine the completeness of the upper Cretaceous sequence because of the different order of events compared to other areas, and because of the limited size of the sample set. The lack of clustering of events suggests that the sequence is quite complete, although our resolution is poor in certain intervals, most notably the Campanian. There are condensed intervals, and intervals of quite rapid sedimentation. A particularly condensed interval is that around the Cenomanian/Turonian boundary, where Turonian markers (*Quadrum gartneri* and *Eiffellithus eximius*) are separated from a Cenomanian assemblage (including *Microstaurus chiastius*) by less than a meter. It is quite likely that part of the lower Turonian is missing.

Because most upper Cretaceous stage boundaries fall between two nannofossil events (Fig. 27), it is difficult to determine their position in Hole 762C with accuracy. Exceptions are the Cenomanian/Turonian and Santonian/Campanian boundaries, which lie close to events. These boundaries lie within Section 122-762C-63X-1 and between Samples 122-762C-75X-1, 113 cm and -75X-1, 143 cm, respectively. The position of the Campanian/Maestrichtian and Albian/Cenomanian boundaries was determined with less precision (indicated by the last occurrence of *Eiffellithus eximius* and *Corollithion kennedyi*, respectively; Fig. 27). Considerable inaccuracies in boundary assignments could result from differences in the ranges of marker species between the European stratotypes and their occurrences offshore of Northwest Australia.

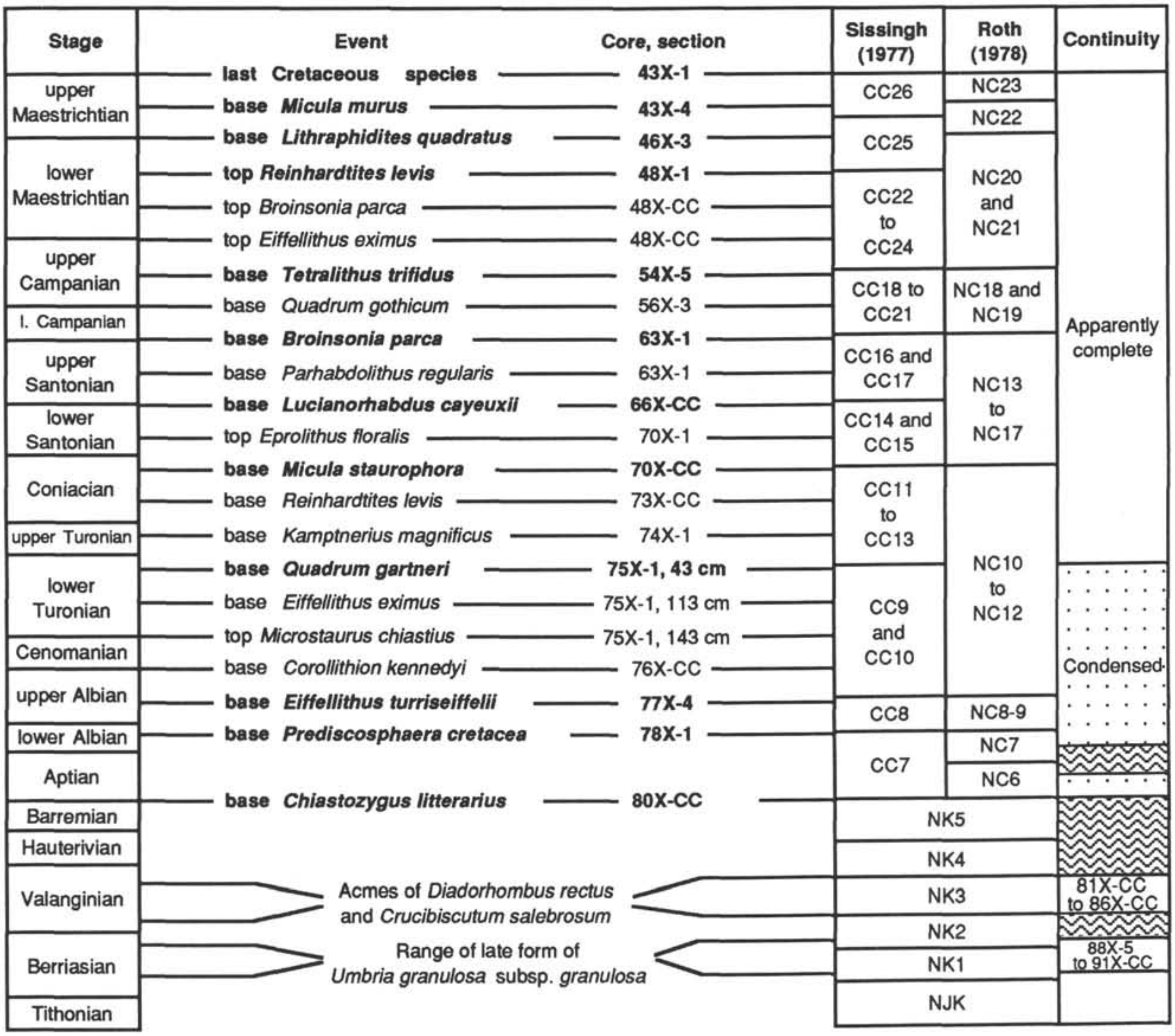

Figure 27. Cretaceous calcareous nannofossil stratigraphy of Site 762 and correlation with the zonations of Sissingh (1977) and Roth (1978). Zonal events are indicated in bold type. Ages of recovered sections are shown in the column on the right with the inferred positions of hiatuses (wavy pattern) and condensed sections (dotted pattern). Lower Cretaceous zonation is that of Bralower (1987) and Bralower et al. (1989); see text for details.

The lower Cretaceous section contains two distinct hiatuses, corresponding to the upper Aptian–lower Albian and the Hauterivian-Barremian (Fig. 27). The former break extends from the *Chiastozygus litterarius* Zone (CC7) to the *Prediscosphaera cretacea* Zone (CC8), and corresponds to the contact between the Muderong Shale equivalent sediments (Unit IVE) and the overlying Gearle Siltstone equivalent sediments (Unit IVD). The *C. litterarius* Zone is indicated by the presence in Muderong equivalent samples of *Rucinolithus irregularis* and *Vagalapilla metalosa*, which first occur in the early Aptian, and of *Conusphaera mexicana* and *Micrantholithus hoschulzii*, which are absent in this interval.

The age of the Barrow Group equivalent sediments (Unit V) drilled in Hole 762C is more difficult to establish owing to the paucity of nannofossil markers in this unit. Many nannofossiliferous samples were found, however, and the presence of a few marker specimens has enabled the age of this unit to be tightly constrained. Section 122-762C-82X-CC contains *Cruciellipsis cuvillieri*, *Crucibiscutum salebrosum*, and *Diadorhombus rectus*, and Section 122-762C-86X-CC contains the former two markers. The ranges of these two taxa overlap from the uppermost Ryazanian to the upper Hauterivian, but *C. salebrosum* has a pronounced acme in the Valanginian. *D. rectus* has been observed in the Berriasian and Aptian in well-preserved material, and has been used as a marker in the middle Valanginian, where its range is restricted in most sequences (Thierstein, 1976) within the *Tubodiscus verenae* Zone (NK3) (Roth, 1978). Although more detailed investigations are clearly warranted, this assemblage indicates a middle Valanginian age. Samples 122-762C-88X-5, 53 cm, and -91X-CC, 13 cm, contain a different assemblage, including the late form of the nannofossil *Umbria granulosa* subsp. *granulosa*, which has a restricted range in the lower to middle Berriasian (*Nannoconus steinmannii steinmannii* Zone, = NK1; and lower part of *Cretarhabdus angustiforatus* Zone, = NK2) (Bralower et al., 1989). From the biostratigraphy, it is not clear at present whether the Barrow Group equivalent was characterized by continuous sedimentation, or whether there is an intraformational hiatus, as suggested by the seismic stratigraphy.

Cretaceous Paleoenvironments

Most of the Cretaceous coccolith assemblages indicate either tropical or temperate conditions with open-ocean circulation. There are a few exceptions, however, which deserve mention. Occurrences of *Nephrolithus frequens*, *Kamptnerius magnificus*, and *Lucianorhabdus cayeuxii* in the Santonian to late Maestrichtian interval may indicate influxes of colder waters. The latter species may indicate a marginal-marine environment (Thierstein, 1976).

Several layers of green claystone in Sections 122-762C-45X-CC to -47X-CC contain unusually high abundances of the nannofossil genus *Micula* (species *Micula staurophora*, *Micula concava*, and *Micula murus*). These occurrences, which are unrelated to preservation, appear to represent plankton blooms and may have a similar origin to the *Braarudosphaera* blooms in the Cenozoic.

Foraminifers

Occurrence and Preservation

In Holes 762A, 762B, and 762C, an almost complete succession of Aptian to Recent pelagic sediments was recovered in predominantly carbonate sediments overlying older Cretaceous restricted marine clastics. The carbonates yielded generally abundant planktonic foraminiferal faunas, of typical low-latitude character in the younger Cenozoic, to more temperate, higher-latitude faunas in the Cretaceous, where tropical influence was only intermittently present.

Preservation varies with induration of the sediments, but is generally moderate to good. In chalks, foraminifers are often difficult to extract from the nannofossil matrix.

In the lower Cretaceous clastics, most samples are barren or yielded only poorly preserved, pyritized foraminifers or glauconitic molds.

The planktonic foraminiferal faunas were studied using core-catcher samples and additional core samples from condensed intervals.

Cenozoic Biostratigraphy

Neogene

Quaternary faunas were recovered from Section 122-762B-1-CC down to and including Section 122-762B-4H-CC. These all contain *Globorotalia truncatulinoides* and are dominated by low-latitude forms such as *Globigerinoides sacculifer*, *Globorotalia tumida*, *Globorotalia menardii*, *Pulleniatina obliquiloculata*, and *Sphaeroidinella dehiscens*. *Globorotalia inflata*, a more temperate form, was also found. Section 122-762B-4H-4 contains a transitional form between *G. truncatulinoides* and *Globorotalia tosaensis*, suggesting placement near the Pleistocene/Pliocene boundary.

Pliocene ages were obtained from planktonic assemblages in Section 122-762B-5H-CC through -11H-CC. A detailed subdivision of the Pliocene will be the subject of further investigation. Provisionally, we place the boundary between Lower and Upper Pliocene at the highest occurrence of *Globorotalia margaritae* in Section 122-762B-8H-3. No hiatuses are apparent from the Pliocene succession of faunas.

Sections 122-762B-12H-CC and -13H-CC are of late Miocene age, as indicated by the presence of *Neogloboquadrina humerosa* in Section 122-762B-12H-CC (Zone N17), and of *Globigerina nepenthes* and *Globigerinoides bollii*, among others, in both samples. Detailed shore-based sampling is required to establish the zonal succession in this interval.

Detailed analysis was carried out on a condensed middle Miocene interval in Core 122-762B-14H. Sample 122-762B-14H-2, 18–20 cm, contains both *Globorotalia siakensis* and *G. nepenthes*, indicating Zone N14. Below that, successive members of the *Globorotalia fohsi* lineage, in the presence of *Orbulina* spp., indicate Zones N11–N9. This rapid succession of zones may include N12 and N13. The lowest sample to contain *Orbulina suturalis*, Sample 122-762B-14H-7, 18–20 cm, marks the base of the middle Miocene Zone N9.

The upper part of Core 122-762B-15H belongs to Zone N8. This is indicated by the presence of the successive members of the *Globigerinoides sicanus-Praeorbulina* lineage in Samples 122-762B-15H-1, 88–90 cm, and -15H-3, 88–90 cm. However, this uppermost Lower Miocene zone is immediately followed by an assemblage including *Globigerinoides immaturus* and *Globoquadrina binaiensis*, which characterize Zone N5 in the absence of *Globorotalia kugleri*. Lowermost Miocene Zone N4 was recognized in Section 122-762B-16H-CC on the basis of *G. kugleri* being present.

Paleogene

Section 122-762B-17H-CC contains *Globigerina tripartita*, *Globigerina* cf. *sellii*, and *Neogloboquadrina opima nana* without *G. kugleri*, and seems to belong to upper Oligocene Zones P22 or P21. The combined occurrence of *Turborotalia ampliapertura* and *Pseudohastigerina* spp. in Sections 122-762B-18H-CC and -19H-CC assigns these samples to lower Oligocene Zone P18. In Hole 762C, a lower Oligocene (Zone P18) fauna with *T. ampliapertura* and *Pseudohastigerina micra* was found in Sections 122-762C-2X-CC and -3X-CC.

Section 122-762C-4X-CC is the uppermost section to contain *Turborotalia cerroazulensis cocoaensis* and *Turborotalia cerroazulensis* s.s., and marks the top of uppermost Eocene Zone P17. Below that, Section 122-762C-5X-CC through -9X-CC are characterized by the occurrence of the *T. cerroazulensis* group (*Turborotalia cerroazulensis pomeroli*, *T. cerroazulensis* s.s., and *T. cerroazulensis cocoaensis*), *Hantkenina* spp., and *Globigerinatheka* spp., indicating that they are late Eocene (Zone P15–P17) in age.

Section 122-762C-10X-CC contains both *T. cerroazulensis* s.s. and *Truncorotaloides* spp., and therefore is of middle Eocene (Zone P14) age. Below that, Sections 122-762C-11X-CC through -16X-CC are middle Eocene. This interval is characterized by the occurrence of the *Truncorotaloides* group (e.g., *Truncorotaloides rohri*) and of *Globigerinatheka tropicalis*. Sample 122-762C-15X-CC is the highest one to contain *Morozovella aragonensis* and marks the top of lower Middle Eocene Zone P11.

The combined occurrence of *Morozovella caucasica* and *M. aragonensis* in Sections 122-762C-17X-CC and -18X-CC assigns these samples to upper Lower Eocene Zones P9 and P8. Sections 122-762C-19X-CC down through -22X-CC are characterized by presence of *Morozovella formosa formosa* and *M. aragonensis* and therefore belong to lower Eocene Zones P8 and P7. Further down, *Morozovella marginodentata* was found in Sections 122-762C-23X-CC through -25X-CC in the absence of *M. aragonensis*, indicating lower Eocene Zone P6. *Morozovella aequa* was also found in Section 122-762C-25X-CC and occurs down to and including Section 122-762C-28X-CC.

The Eocene/Paleocene boundary was placed within Zone P6, at the highest occurrence of *Morozovella velascoensis*, probably marking the top of an undifferentiated P6A–P5 interval in Section 122-762C-28X-CC. Sections 122-762C-29X-CC down to and including 762C-33X-CC belong to upper Paleocene Zone P4, given the occurrence of *Planorotalites pseudomenardii*. Section 122-762C-34X-CC is the lowest to contain *Morozovella angulata*, and marks the base of Zone P3.

Cores 122-762C-35X through -41X belong to the lower Paleocene (Zones P2 and P1). This is indicated by the occurrence of *Planorotalites compressus*, *Morozovella pseudobulloides*, and *Subbotina triloculinoides*. Section 122-762C-42X-CC is barren of foraminifers.

Cretaceous Biostratigraphy

Upper Cretaceous

Sections 122-762C-43X-CC through -46X-CC all contain *Abathomphalus mayaroensis* and therefore belong to the upper Maestrichtian *A. mayaroensis* Zone. Section 122-762C-47X-CC yielded rare *Abathomphalus intermedius*, indicating the *Rosita contusa* Zone. Lower in the section, Maestrichtian dates (as indicated by nannofossils) coincide with the presence of *Gueblerina* spp. down to and including Section 122-762C-53X-CC. However, other Maestrichtian markers are absent in the *Rugoglobigerina*-dominated faunas, and the standard Tethyan zonation could not be applied.

From Section 122-762C-54X-CC downward, *Gueblerina* was not found and we tentatively assign the entire interval containing *Globotruncana* spp. (including *Globotruncana arca*) but lacking *Dicarinella asymetrica* to the Campanian. Again, the standard Tethyan zonation could not be applied. This is partly because markers (e.g., *Globotruncanita calcarata*) are absent, but also because *Globotruncana ventricosa*, commonly considered to be an upper Campanian marker, extends into the *Dicarinella asymetrica* Zone.

An earliest Campanian to Santonian age is assigned to Section 122-762C-62X-CC through -66X-CC on the basis of *Dicarinella asymetrica* occurring regularly, marking the *D. asymetrica* Zone. Below these occurrences, *Globotruncanita elevata* was found together with *Globotruncana ventricosa* in several samples as far down as Section 122-762C-69X-CC. Application of the standard Tethyan zonation scheme places the entire interval containing *G. elevata* in the upper part of the *D. asymetrica* Zone, but evidently *G. elevata* appears earlier than usual in this area. Therefore, we assign an undifferentiated Santonian age to all sediments from Section 122-762C-64X-CC to -70X-CC (the highest occurrence of *Whiteinella archaeocretacea*).

The first occurrence of *W. archaeocretacea* is in Section 122-762C-70X-CC and marks the top of a Coniacian to upper Turonian interval which continues down to Sample 122-762C-73X-2, 50–52 cm. This interval corresponds to the lower part of the *Dicarinella primitiva* Zone and the entire *Marginotruncana sigali* Zone.

The mid-Turonian marker *Helvetoglobotruncana helvetica* was seen in Section 122-762C-73X-CC only. However, Section 122-762C-74X-CC was also assigned to the *H. helvetica* Zone on the basis of *Marginotruncana sigali* being present.

Three closely spaced samples were studied across the Turonian/Cenomanian boundary. Of these, Sample 122-762C-75X-1, 92–93 cm, yielded a typical assemblage with *W. archaeocretacea* and *Praeglobotruncana* spp. but without *Marginotruncana* and *H. helvetica*, and could thus be assigned to the *W. archaeocretacea* Zone. Sample 122-762C-75X-1, 134–135 cm, is barren; this is common for basinal black shales at or near the Turonian/Cenomanian boundary. Sample 122-762C-75X-1, 142–143 cm, contains abundant *Thalmanninella deeckei* as the only keeled planktonic species, which proves a latest Cenomanian age and shows that the succession across the boundary is complete within the accuracy limits of biostratigraphic resolution.

The Cenomanian is thin but no hiatuses are apparent in the succession of rotaliporid faunas, with which it can be subdivided into the *Rotalipora cushmani* Zone (down to Sample 122-762C-76X-2, 130–131 cm) and the *Thalmanninella reicheli* Zone (Samples 122-762C-76X-3, 129–130 cm, and -76X-CC). The *Thalmanninella brotzeni* Zone may be present in an unsampled portion of the upper part of Core 122-762C-77X.

Lower Cretaceous

Albian and Aptian pelagic sediments are present in Hole 762C, presumably continuous with the overlying Cenomanian. These are marked by the occurrence of *Planomalina buxtorfi* in Sample 122-762C-77X-4, 50–52 cm, together with abundant *Hedbergella* spp. Almost immediately below this, in Section 122-762C-77X-CC, *P. buxtorfi* is absent, and only abundant *Hedbergella* spp. occur (including *H. delrioensis* and *H. planispira*). This fauna is most probably early or middle Albian in age, although the species range well into the Aptian.

Section 122-762C-78X-CC yielded an abundance of very small planktonic species, including *Globigerinelloides blowi* and *Hedbergella sigali*, indicating the lower Aptian *G. blowi* Zone. This is confirmed by the presence of *Gavelinella barremiana*, which has its top in the lower Aptian.

Most core-catcher samples below and including Section 122-762C-79X-CC are barren. It is possible that detailed sampling may provide more foraminiferal material for study, but as yet only a few indeterminate nodosariids and questionable, poorly preserved epistominids were found in Sections 122-762C-82X-CC through -84X-CC. In the latter sample, one specimen of what is possibly *Lenticulina nodosa* may indicate a Valanginian age.

Cretaceous Paleoenvironments

For a thorough paleoenvironmental analysis, a detailed and preferably quantitative study of the benthic foraminifers is required. The following notes are based on a qualitative impression obtained during the study of the planktonic assemblages.

Little can be said about the paleoenvironment of the pre-Aptian clastics. It is obvious that the environment, presumably marine, was very restricted and to a large extent anoxic, as indicated by the presence of abundant pyrite and glauconite, and the scarcity of marine fauna. The few foraminifers found could not be identified with certainty and their paleoenvironmental significance is therefore totally unknown.

Apart from the one sample at the Cenomanian/Turonian boundary interval, no evidence was found of any sediment having been deposited below the CCD. The present water depth at the site is only about 1350 m, and we assume that no significant uplift occurred on the Exmouth Plateau during deposition of the continuous carbonate succession that would warrant the possibility of the seabed ever having been below a normal CCD depth. However, we note that during the Aptian and Albian bathyal depths prevailed at Site 762. This is clearly indicated by the consistent presence in the benthic assemblages of *Gyroidinoides crassa* and *Osangularia* ex gr. *utaturenis* (= *O.* aff. *brotzeni* Auctt.). Both forms were considered by Moullade (1984) to be upper bathyal indicators for the southern Atlantic Ocean. Moreover, typical shelf dwellers, especially epistominids, are noticeably absent in the Albian and Aptian in spite of the diverse benthic assemblages in all samples studied. A planktonic formaniniferal group associated with shelf environments, the *Favusellidae*, are also absent. Scheibnerova (1974) attempted to use *Osangularia utaturensis* as a shallow-water indicator in the Albian of DSDP Sites 259 and 260. A full critique of her interpretation is beyond the scope of this report, but we note that the much more distal settings of the DSDP sites is in obvious contradiction to a shallow-water origin for their Albian sediments even if the Albian on the Exmouth Plateau is bathyal.

The Cenomanian/Turonian boundary is of the basinal type, with a noncalcareous, pelagic black shale that in the chalk environments of Northwest Europe only occurs in intra-shelf basinal and deeper settings.

The upper Maestrichtian fauna shows signs of diversification and more tropical influence than that of the lower Maestrichtian, contrary to the regressive trend that one would expect in a shallower setting.

In summary, bathyal environments prevail throughout the deposition of the Cretaceous pelagic carbonate succession at Site 762. However, the planktonic faunas are not typically Tethyan, probably owing to deposition at relatively high latitudes. This is especially noteworthy in the Santonian to lower Maestrichtian, where species of *Globotruncanita* and *Rosita* are often poorly (if at all) represented, as are the more complex heterohelicids such as *Sigalia*, *Planoglobulina*, *Racemiguembelina*, and *Pseudoguembelina*. This holds to a far lesser extent for the Albian to Coniacian interval, in which most Tethyan forms are present, although in some cases in rather low proportions. We think that this may be the result of a homogeneous, generally warm climate that led to sluggish circulation in the mid-Cretaceous oceans.

Cenozoic Paleoenvironments

Site 762 offered a fairly complete Cenozoic planktonic foraminiferal succession, with one hiatus in the lower Miocene. Throughout the Cenozoic section, percentages of planktonic foraminifers relative to benthic foraminifers are high, as expected for an open-ocean, pelagic environment.

The Paleocene has normal planktonic formaniniferal faunas, except that the *Morozovella* group is poorly represented, and *Planorotalites* in the *Planorotalites pseudomenardii* zone are of the inflated, *chapmani*-type rather than of the typical *pseudomenardii*-type. This peculiarity in the faunas is less apparent in the uppermost Paleocene and in the lower Eocene, in which normal, low-latitude forms predominate. Middle Eocene assemblages are dominated by *Acarinina* spp. and are characterized by a lack of low-latitude species such as *Hantkenina* spp., *Morozovella lehneri*, and *Orbulinoides beckmanni*. According to Jenkins (1985), high abundances of acarininids are typical for austral/temperate areas. Upper Eocene assemblages are of a warm-water nature as represented by species belonging to the genera *Globigerinatheka*, *Hantkenina*, and *Turborotalia*. In addition, normal tropical faunas are also found in the Oligocene (to the extent that Oligocene planktonic faunas can be regarded as normal and tropical).

In the lower Miocene, the assemblages contain up to 10% poorly preserved, reworked Oligocene and Eocene brown-colored forms. These forms are probably the result of repeated mixing and winnowing in a deep marine environment. An associated hiatus was recognized within Core 122-762B-15H, in the lower Miocene.

During the middle Miocene, only the temperate to subtropical early forms of the *Globorotalia fohsi* evolutionary lineage are present and the more advanced forms are lacking. This is probably a result of climatic deterioration, which is also expressed by low average sedimentation rates. The upper Miocene–Quaternary assemblages are predominantly subtropical to tropical. However, it is noteworthy that temperate forms such as *Globorotalia* of the *G. conoidea/conomiozea* group occurs in the Pliocene, as does *Globorotalia inflata* in the Quaternary. Again, this suggests some cool-temperate influence in a predominantly tropical pelagic environment, very much like the present-day waters over the Exmouth Plateau.

Radiolarians

Radiolarian recovery from Holes 762B and 762C was generally poor, and the faunas were studied as wet-sieved residues instead of as strewn slides. Section 122-762A-1H-CC contains a few, well-preserved radiolarians of undifferentiated Quaternary age, including *Arcosphaera spinosa*, *Didymocyrtis prismatica*, *Lamprocyrtis maritalis*, *Lamprocyrtis* sp. cf. *L. nigriniae*, and *Theocorythium trachelium*. Samples 122-762B-1H-1, 90–92 cm, to -1H-3, 90–92 cm, contain radiolarians assignable to the upper Quaternary *Buccinosphaera invaginita* Zone of Sanfilippo et al. (1985). Characteristic taxa include *Buccinosphaera invaginita*, *Didymocyrtis tetrathalamus*, *Lamprocyrtis nigrinae*, and *Stylocontarium acquilonium*. Section 122-762B-1H-CC contains relatively well-preserved radiolarians assignable to either the upper Quaternary *Buccinosphaera invaginita* Zone or *Collosphaera tuberosa* Zone (Sanfilippo et al., 1985), and includes the radiolarian marker taxa *Arcosphaera spinosa*, *Collosphaera tuberosa*, *Lamprocyrtis nigriniae*, *Stylacontarium acquilonium*, and *Theocorythium trachelium*. Samples 122-762B-2H-1, 76–78 cm to -2H-CC contain undifferentiated middle Quaternary radiolarians, including *Axoprunum angelinum*, *Anthrocyrtidium* spp., *Phormostichoartus doliolum*, and *Theocorythium trachelium*. Samples 122-762B-3H-1, 74–76 cm to -3H-5, 74–76 cm contain radiolarians assignable to the lower Quaternary *Amphirhopalum ypsilon* or *Anthrocyrtidium angulare* Zones of Sanfilippo et al. (1985).

Radiolarians are absent in Sections 122-762B-3H-CC down to -17H-CC, and in Sections 122-762C-2X-CC and -3X-CC. Sample 122-762C-4X-3, 75–77 cm, contains the lower Oligocene marker taxon *Theocyrtis tuberosa*(?). Section 122-762C-4X-CC contains a relatively well-preserved fauna assignable to the upper Eocene *Thyrsocyrtis bromia* Zone of Sanfilippo et al. (1985). Marker taxa include *Carpocanistrum azyx*, *Dictyopora pirum*, and *Theocyrtis tuberosa*, as well as undescribed *Axoprunum* spp. and *Theocotyle* spp. Sections 122-762C-5X-CC down to -19X-CC are barren of all siliceous microfossils with the exception of sponge spicules. Samples 122-762C-20X-3, 74–76 cm, and -20X-CC contain poorly preserved lower Eocene radiolarians questionably assigned to the *Buryella clinata* Zone (Sanfilippo et al., 1985), including undescribed *Axoprunum* spp., *Buryella clinata*, *Buryella tetradica*, *Calocycloma castrum*, *Podocyrtis papalis*, and *Spongatractus* sp. cf. *S. balbis*.

Although Sections 122-762C-21X-CC down to -42X-CC contain radiolarian debris, it is too fragmental and poorly preserved to be identified. These samples were processed by two separate methods in order to maximize preservation, but recovery was severely hampered by dissolution affects, the recrystallization of the skeletal fragments into quartz, and the partial replacement of the skeletons to pyrite. Sections 122-762C-43X-CC and -45X-CC yielded poorly preserved Maestrichtian or Campanian radiolarians as determined by the occurrence of *Dictyomitra* cf. *D. densicostata*, as well as the presence of the genus *Phaseliforma* Pessagno. Sections 122-762C-46X-CC, -47X-CC, -58X-CC, and -64X-CC all contain poorly preserved forms of undifferentiated late Cretaceous age. Section 122-762C-44X-CC and most sections from 122-762C-48X-CC down to -63X-CC not mentioned above are barren of identifiable radiolarians. An undifferentiated early Cretaceous age was assigned to Sections 122-762C-66X-CC, as indicated by the presence of the radiolarian genus *Pseudodictyomitra*. With the exception of Section 122-762C-79X-CC, which contains undifferentiated early Cretaceous age forms assignable only to *Pseudodictyomitra* spp. and *Stichomitra* spp., all of the remaining cores from Core 122-762C-67X to -89X-CC are barren of radiolarians.

Palynology

Mesozoic Biostratigraphy

All cores in Holes 762A and 762B, and cores in Hole 762C through Core 122-762C-78X are barren of palynomorphs. The first evidence of palynomorphs is in Section 122-762C-79X-1, 14–17 cm. Cores 122-762C-79X through -80X are dominated by dinoflagellates. Only a few spores and pollen grains are present. Cuticles and the organic coatings of foraminifers (foraminifer liners) are absent. The dinoflagellate assemblage is dominated by the *Circulodinium* group (*C. colliveri* and *C. deflandrei*). The presence of *Dingodinium cerviculum*, *Chlamydophorella ambigua*, *Batiacasphaera imperfecta*, *Impagidinium phlyctaena*, and *Herendeenia postprojecta* suggests a Barremian to Aptian age (the upper part of the *Muderongia australis* Zone to the lower part of the *Odontochitina operculata* Zone).

Sample 122-762C-81X-CC contains only a few poorly preserved dinoflagellates, spores, and pollen grains. Wood is rare, and foraminifer linings are absent. The dinoflagellate assemblage contains *Egmontodinium torynum*, *Tubotuberella vlamingii*, *Apteodinium granulatum*, and *Scriniodinium attadalense*, which suggest a late Berriasian to early Valanginian age (*Batioladinium reticulatum* to *Egmontodinium torynum* Zone).

Cores 122-762C-82X through -87X contain an assemblage dominated by terrestrial palynomorphs. Dinoflagellates are common and foraminifer liners are rare. The presence of the dinoflagellates *Egmontodinium torynum* and *Apteodinium granulatum*, and the absence of *Kaiwaradinium scrutillinum* and *Dissimulidinium lobispinosum* indicate a late Berriasian age (*Batioladinium reticulatum* Zone).

Cores 122-762C-88X through -91X contain terrestrial organic material (spores, pollen, wood/cuticles) and marine palynomorphs (dinoflagellates, acritarchs, and foraminifer liners) in nearly equal abundance. The presence of *Dissimulodinium lobispinosum* and *Canninginopsis* sp. cf. *C. tabulata* (Helby et al., 1987), and the absence of *Apteodinium granulatum* suggest a middle to early late Berriasian age (*Dissimulidinium lobispinosum* Zone).

Summary

An almost complete Cenozoic sedimentary section was cored at Site 762. Calcareous nannofossils and planktonic foraminifers are abundant and well preserved in the Cenozoic, and zonal assignments for the two groups correspond well. Abundance and preservation of both groups are poorer in the Cretaceous, and stratigraphic assignments are not as tightly constrained as they are in the Cenozoic. Nannofossil and foraminiferal evidence both indicate a hiatus during the late Early Miocene and at the Cretaceous/Tertiary boundary. Nannofossil evidence also suggests that a stressed environment (low salinity?) may have occurred in the early Oligocene to earliest Early Miocene interval, indicated by blooms of *Braarudosphaera*.

Radiolarians occur in the Quaternary and Eocene, as well as a few poorly preserved forms in the Cretaceous. Except in the Quaternary, radiolarian preservation was too poor for accurate biostratigraphy.

No Cenozoic palynomorphs were found at Site 762. Marine palynomorphs (primarily dinoflagellates) are present in the Aptian through late Berriasian. Terrestrial palynomorphs are also present and are more common in the Valanginian to Berriasian interval.

PALEOMAGNETICS

Remanent Magnetization Measurements

Measurement of the archive halves of Cores 122-762B-1H through -19H and 122-762C-2X through -91X was performed at either 5- or 10-cm intervals. These cores were demagnetized with alternating magnetic fields, peaking at 9 mT. Despite a slight overprint (not entirely removed by 9 mT-demagnetization) and coring disturbance, an attempt was made to define a reversal sequence for Site 762.

Polarity assignments were made primarily on the basis of pattern recognition, but are supported by magnetic behavior and biostratigraphic zonations. Study of magnetic behavior can provide clues to polarity if we assume that reversed directions are more likely to be affected by viscous overprinting than are normal ones. The removal of normal overprinting of viscous origin results in an intensity increase during early demagnetization. We illustrate the difference between "normal" and "reversed" behavior in Figure 28. The data shown in Figures 28A and 28B is typical of "normal" samples at this site, displaying a smooth decay to the origin; "reversed" behavior is shown in Figures 28C and 28D, which have more complicated demagnetization paths. The combined magnetostratigraphic and biostratigraphic data intervals are shown in Figure 29. The Brunhes/Matuyama chron boundary is found at 10.2 mbsf (Fig. 29A).

Correlation of the reversal pattern in Cores 122-762B-9H through -12H with the geomagnetic reversal time scale (GRTS) (Haq et al., 1987) allows Chrons C5 and C5A to be identified at Site 762 (Fig. 29B). Despite the complicated reversal-sequence pattern in Cores 122-762C-10X through -17X, a speculative correlation of those reversals to the GRTS is also carried out. Chrons C13 and C15 (Fig. 29C) as well as C16 may occur at Site 762. Further refinement will require careful demagnetization of discrete samples; this will be conducted during shore-based investigations.

The main features of the upper Cretaceous magnetic-polarity sequence occur in Hole 762C. The base of Chron C29 occurs at the base of Core 122-762C-43X. A short reversed-polarity zone is found at the top of Core 122-762C-45X, and may correspond to the base of Chron C30. The data for Cores 122-762C-46X through -48X are somewhat difficult to interpret because of coring disturbance, and no polarity-chron assignments could be made on the basis of whole-core measurements. Core 122-762C-51X (which is of reversed polarity) may correspond to the base of Chron C32; the base of Chron C33 (which corresponds approximately to the Campanian/Santonian boundary) occurs at the base of Core 122-762C-62X.

Cores 122-762C-63X through -67X have not been measured because of their highly disturbed state. Cores 122-762C-68X through -88X are of normal polarity and correspond for most part to long-normal-polarity Chron C34. Some reversed-magnetic-polarity zones occur in Cores 122-762C-89X through -91X but no assignment to the magnetic-polarity time scale can be made at present.

Magnetic Susceptibility Measurements

At Hole 762B the whole-core volume susceptibility records exhibit a pattern of high-frequency variations, with values in the range of $0.1–17.0 \times 10^{-6}$ cgs units (Fig. 30). The susceptibility measurements have low values, about 3×10^{-6} cgs, in the upper Pleistocene foraminifer nannofossil ooze (0–5 mbsf). The interval between 5–30 mbsf has much lower susceptibility values, around 1×10^{-6} cgs, and the fluctuations are of relatively low amplitude. The lower values reflect a

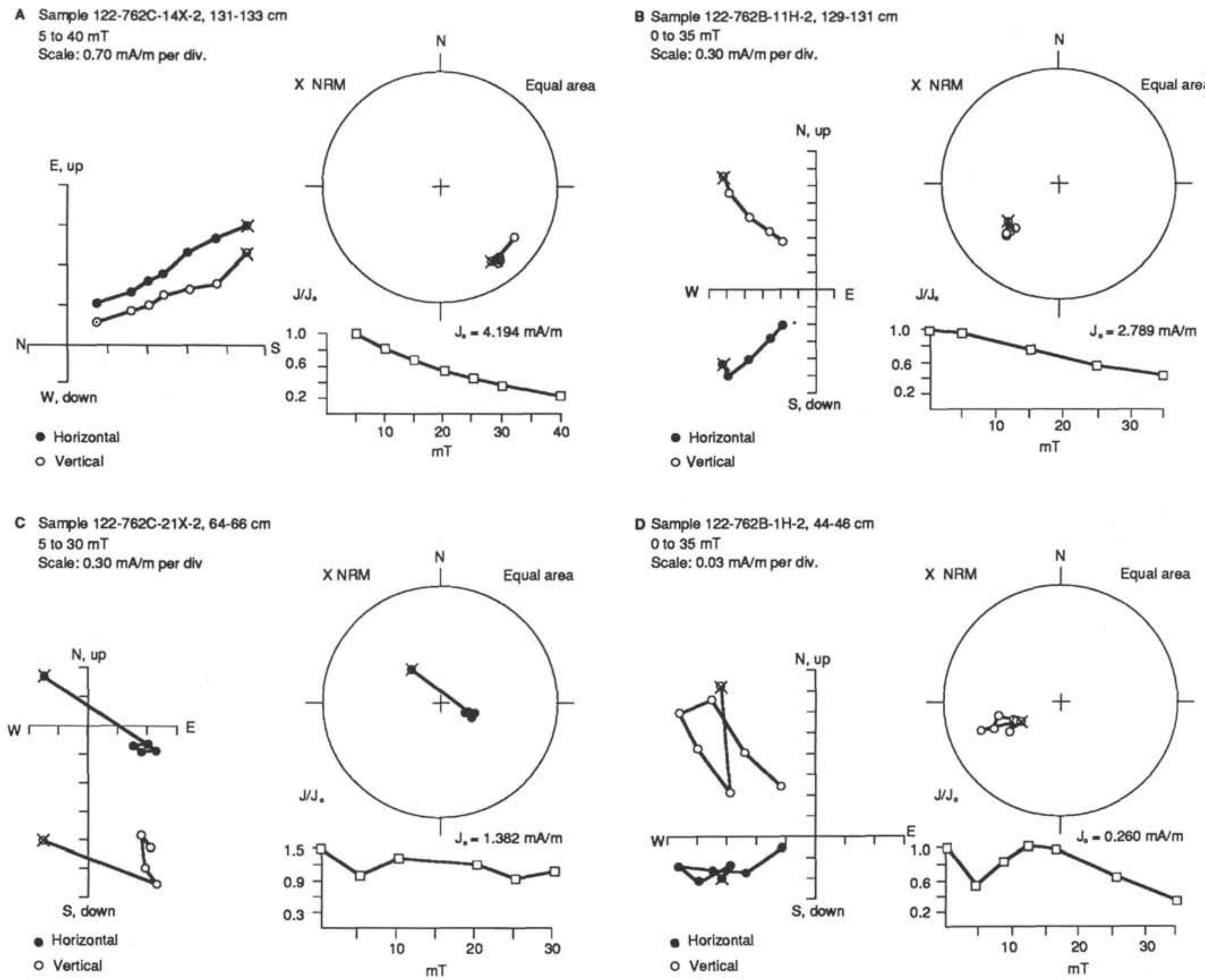

Figure 28. Vector endpoint diagram, equal area stereographic projection and intensity decay curves. **A.**, **B.** Single component of magnetization. **C.**, **D.** More complicated demagnetization paths.

lower magnetic-mineral content. This means that the NRM intensity is very close to the noise level of the cryogenic magnetometer and probably causes the scatter in the inclination measurements from Cores 122-762B-2H to -4H. The susceptibility values average around 5–10 × 10^{-6} cgs from Cores 122-762B-5H to -12H. Between 120 and 137 mbsf, susceptibility values are considerably lower (0.1 × 10^{-6} cgs). A sharp change in susceptibility (up to 17 × 10^{-6} cgs) is observed at 137 mbsf. A few high-amplitude spikes are also found between Cores 122-762B-14H to -19H.

SEDIMENTATION RATES

Figures 31 and 32 show sedimentation rates for the Cenozoic and Mesozoic, respectively. Techniques used to estimate these rates are described in the "Explanatory Notes" (this volume).

Cretaceous sedimentation rates are difficult to ascertain and consequently have large error bars (Fig. 32). Between the lower Santonian (794 mbsf) and the Albian, the lowermost interval where reasonable biozonal assumptions can be made, sedimentation rates are about 0.2 cm/k.y. They are higher throughout the remainder of the Cretaceous, averaging between 1.0 and 1.5 cm/k.y. until the brief Danian-Maestrichtian hiatus.

Sedimentation rates are about 1.0 cm/k.y. from the base of the Tertiary to the Lower Eocene, resulting in an expanded sedimentary section. They decrease, and are on the order of 0.5 cm/k.y. in the Upper Eocene to Lower Oligocene to upper Late Eocene interval.

Sedimentation rates for the remainder of the Cenozoic are variable (Fig. 31). They decrease markedly (to about 0.2 cm/k.y.) from the Upper Miocene to the Lower Oligocene, suggesting a condensed interval. There is also a brief hiatus at 130 mbsf in the upper part of the Lower Miocene, which is supported both by calcareous nannofossil and foraminifer biostratigraphic results (see "Biostratigraphy," this chapter). Rates increase and are higher from the lower Pliocene to Quaternary, averaging about 2 cm/k.y.

In summary, sedimentation rates show generally normal values for pelagic environments from Santonian to the Lower Oligocene. An upper Lower Oligocene to Upper Miocene condensed interval is followed by normal pelagic rates until

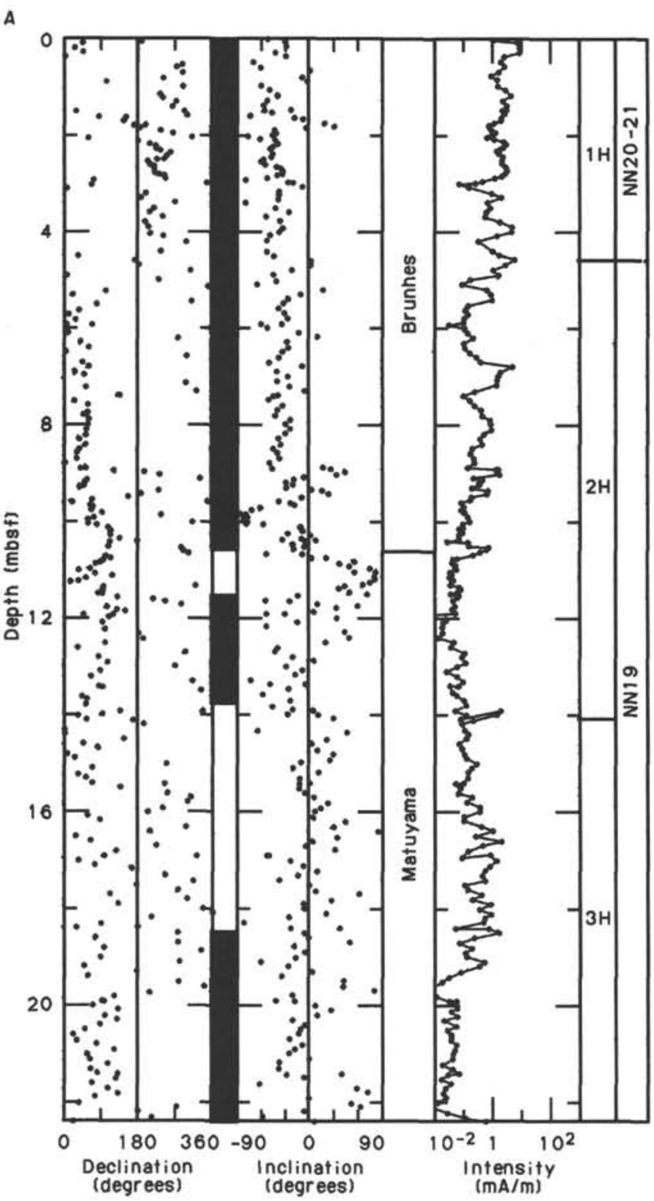

Figure 29. Data from 9-mT demagnetization, Hole 762B. **A.** Cores 122-762B-1H to -3H. **B.** Cores 122-762B-9H to -12H. **C.** Cores 122-762C-10X to -13X. **D.** Cores 122-762C-14X to -17X. An "X" in the polarity column indicates no recovery.

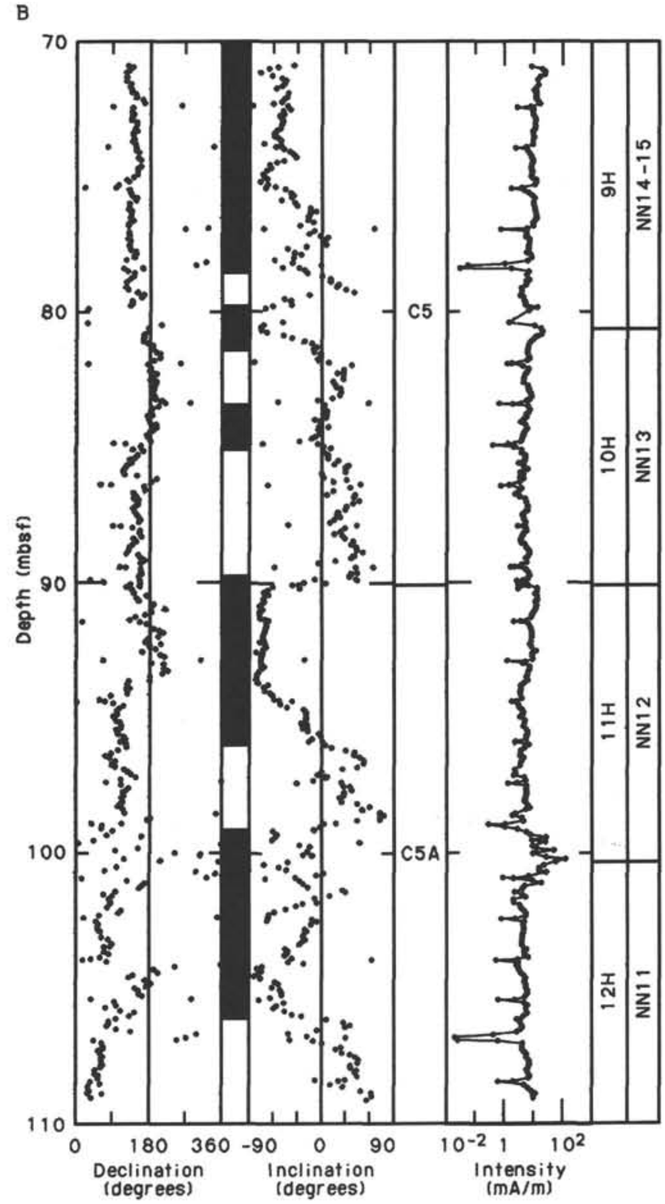

Figure 29 (continued).

the Holocene. The Middle Cretaceous sequence is characterized by very low sedimentation rates.

ORGANIC GEOCHEMISTRY

Shipboard organic geochemical analyses at Site 762 consisted of 246 determinations of inorganic carbon, 131 Rock-Eval and total organic carbon (TOC) analyses, 113 measurements of low-molecular-weight hydrocarbons, and 2 determinations of high-molecular-weight hydrocarbons. The procedures used for these determinations are outlined in the "Explanatory Notes" (this volume) and are described in detail by Emeis and Kvenvolden (1986).

Inorganic and Organic Carbon

Results of analyses of inorganic carbon in samples from Holes 762B and 762C are listed in Table 3. Calculated estimates of percentages of calcium carbonate percentages are given, assuming that the inorganic carbon occurs only as calcite. The upper 830-m-thick section of these sediments and rocks is made up of calcareous oozes and chalks. Below ca. 830 mbsf, few carbonate-rich rocks were encountered. Little organic carbon is found in the carbonate sequence, but percentages of organic carbon are relatively greater (between 0.2% and 1.5%, determined on a sample dry-weight basis) in the lower 100 m of Hole 762C.

Rock-Eval Pyrolysis

The results of Rock-Eval pyrolysis and total organic carbon (TOC) analysis of samples from Holes 762B and 762C are listed in Table 4. In samples from the uppermost 840 mbsf, pyrolysis yields and TOC contents are very low (generally less than 0.30 and 0.15, respectively). Because of these low values, all parameters subsequently derived from them as ratios, such as PI (production index), HI (hydrogen index), and OI (oxygen index), cannot be considered as exact. Similarly, the

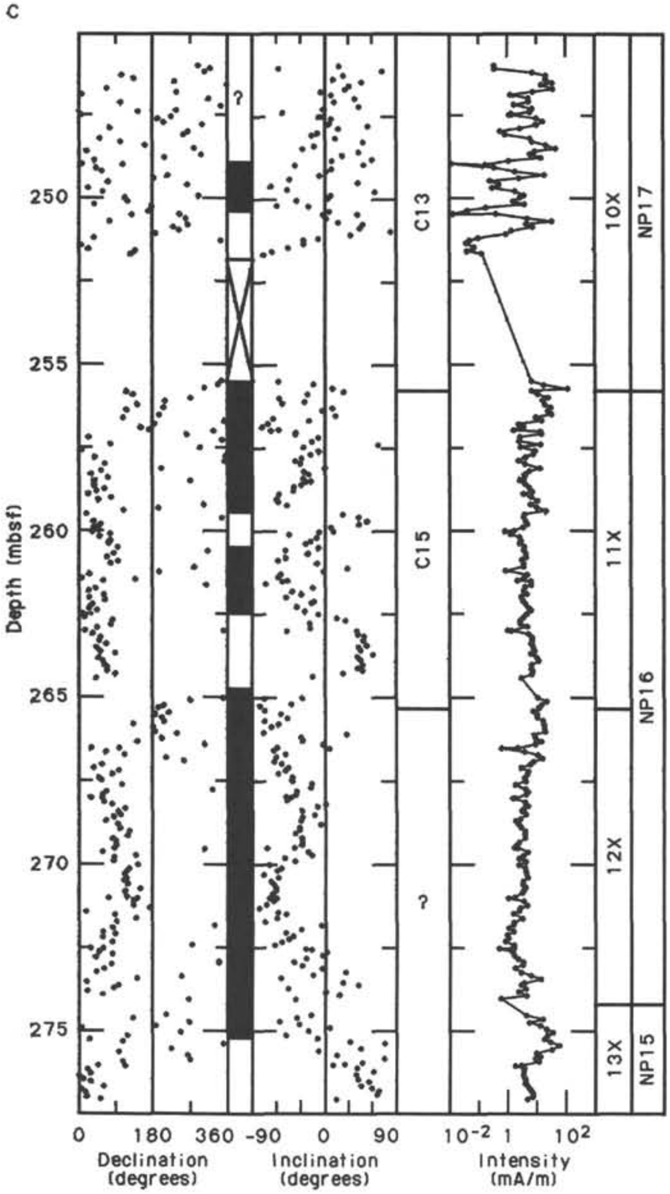

Figure 29 (continued).

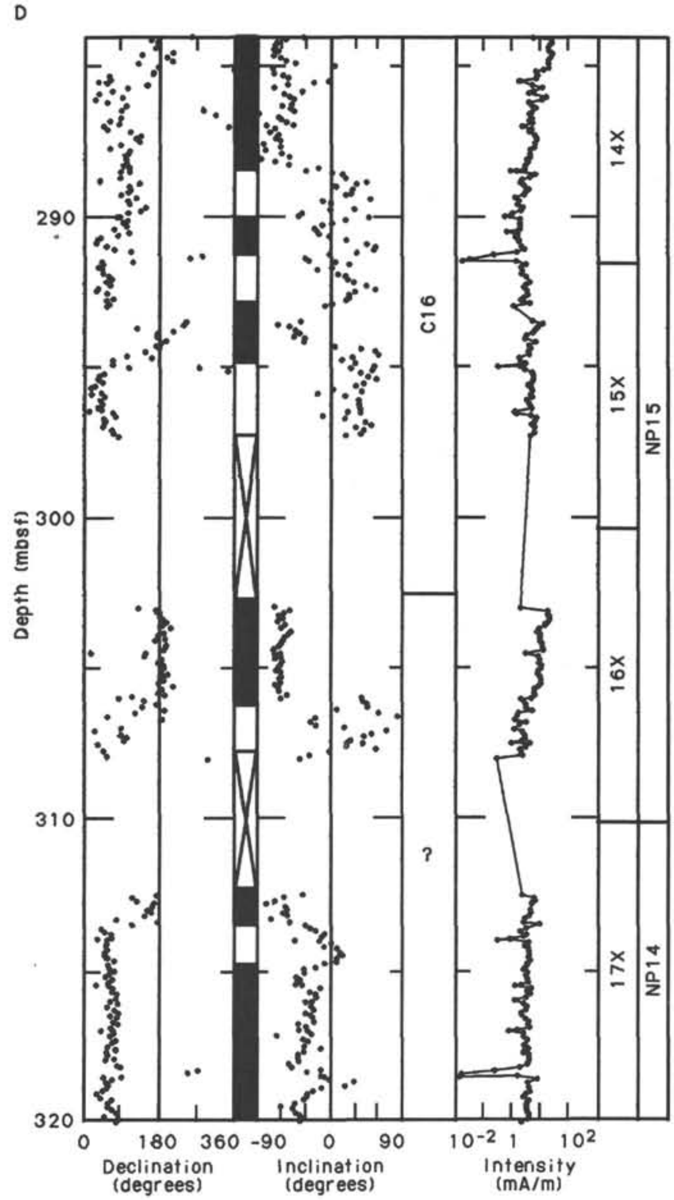

Figure 29 (continued).

pyrolyzable hydrocarbon yield (S_2) is too small and too variable to provide a truly meaningful T_{max} determination.

In the lowermost 100 m of Hole 762C, the pyrolysis yields and TOC contents are somewhat higher, and the Rock-Eval results can be interpreted with some confidence. The organic matter in samples from this interval is of type III (Fig. 33) and was probably derived from land plants. These rocks represent the distal equivalents of the Muderong Shale and the Barrow Group and are predominantly clastic in content.

TOC concentrations throughout Holes 762B and 762C are generally low (Table 4). The upper ca. 810 m of calcareous sediments contain <0.1% organic carbon, as determined by whole-sediment dry weight. Although most of the TOC concentrations in the bottom of Hole 762C are <1% of sample dry weight, several samples, especially from the Upper Barrow Group, have values ranging up to about 1.5% (Fig. 34). The very dark to black color of the cores indicates the presence of relatively large amounts of finely dispersed metal sulfides (such as pyrite) rather than the presence of organic matter. Even so, organic carbon concentrations are higher in this interval than in the upper parts of this hole.

Because of the low organic carbon content of the upper, calcareous sections of this site, their organic matter type could not be assessed by Rock-Eval pyrolysis. In the lowermost section, however, the hydrogen index values and the S_2/S_3 ratios clearly indicate that the organic matter is dominated by type III land-plant debris.

T_{max} values of 420°C–425°C indicate that the Barrow Group samples from the bottom of Hole 762C are thermally immature, equivalent to a vitrinite reflectance of about 0.4%–0.5% R_o. This interpreted level of thermal maturation is consistent with the occurrence of higher-molecular-weight hydrocarbon gases (C_2–C_4) (Powell, 1978) as indigenous products of catagenesis, observed in the headspace gas samples (Table 5).

Low-Molecular-Weight Hydrocarbons

High concentrations of headspace gas (up to 100,000 ppm) were noted in samples from about 500 to 800 mbsf in Hole

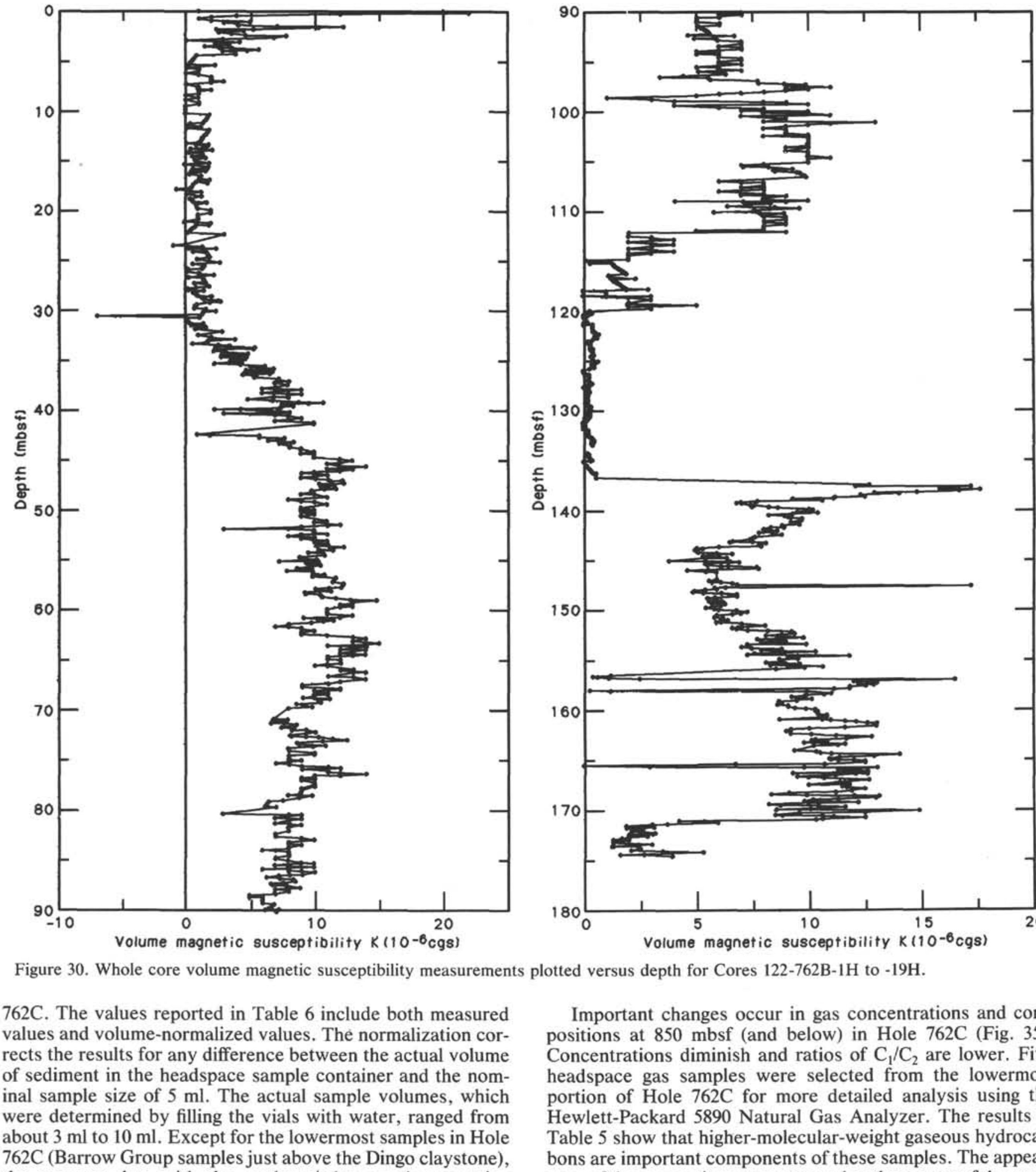

Figure 30. Whole core volume magnetic susceptibility measurements plotted versus depth for Cores 122-762B-1H to -19H.

762C. The values reported in Table 6 include both measured values and volume-normalized values. The normalization corrects the results for any difference between the actual volume of sediment in the headspace sample container and the nominal sample size of 5 ml. The actual sample volumes, which were determined by filling the vials with water, ranged from about 3 ml to 10 ml. Except for the lowermost samples in Hole 762C (Barrow Group samples just above the Dingo claystone), the gas was dry, with the methane/ethane ratio averaging about 10,000. The most gas-rich cores expanded somewhat after arrival on deck, and developed gas-filled voids. Vacutainer samples (taken through the core liner) of the gas from the expansion voids yielded from 20% to 90% methane by volume, with very high C_1/C_2 ratios (ca. 10,000). High C_1/C_2 values are usually interpreted as indicative of biogenic gas (cf. Claypool and Kvenvolden, 1983), although they may also indicate a thermogenic origin from gas-prone organic matter (Hunt, 1979, p. 438).

Important changes occur in gas concentrations and compositions at 850 mbsf (and below) in Hole 762C (Fig. 35). Concentrations diminish and ratios of C_1/C_2 are lower. Five headspace gas samples were selected from the lowermost portion of Hole 762C for more detailed analysis using the Hewlett-Packard 5890 Natural Gas Analyzer. The results in Table 5 show that higher-molecular-weight gaseous hydrocarbons are important components of these samples. The appearance of these constituents suggests that the source of the gases found through much of Hole 762C was being approached at the total depth of the hole.

The Natural Gas Analyzer results revealed, predictably, that air is the major fraction of the headspace samples, making up about 90% of their total volumes. The concentrations of CO_2 listed in Table 5, however, are enriched on the order of 100 times over the proportion of this gas in the atmosphere, implying that the sediment gases contain large amounts of CO_2. As further evidence of this, ratios of CO_2 to CH_4 range

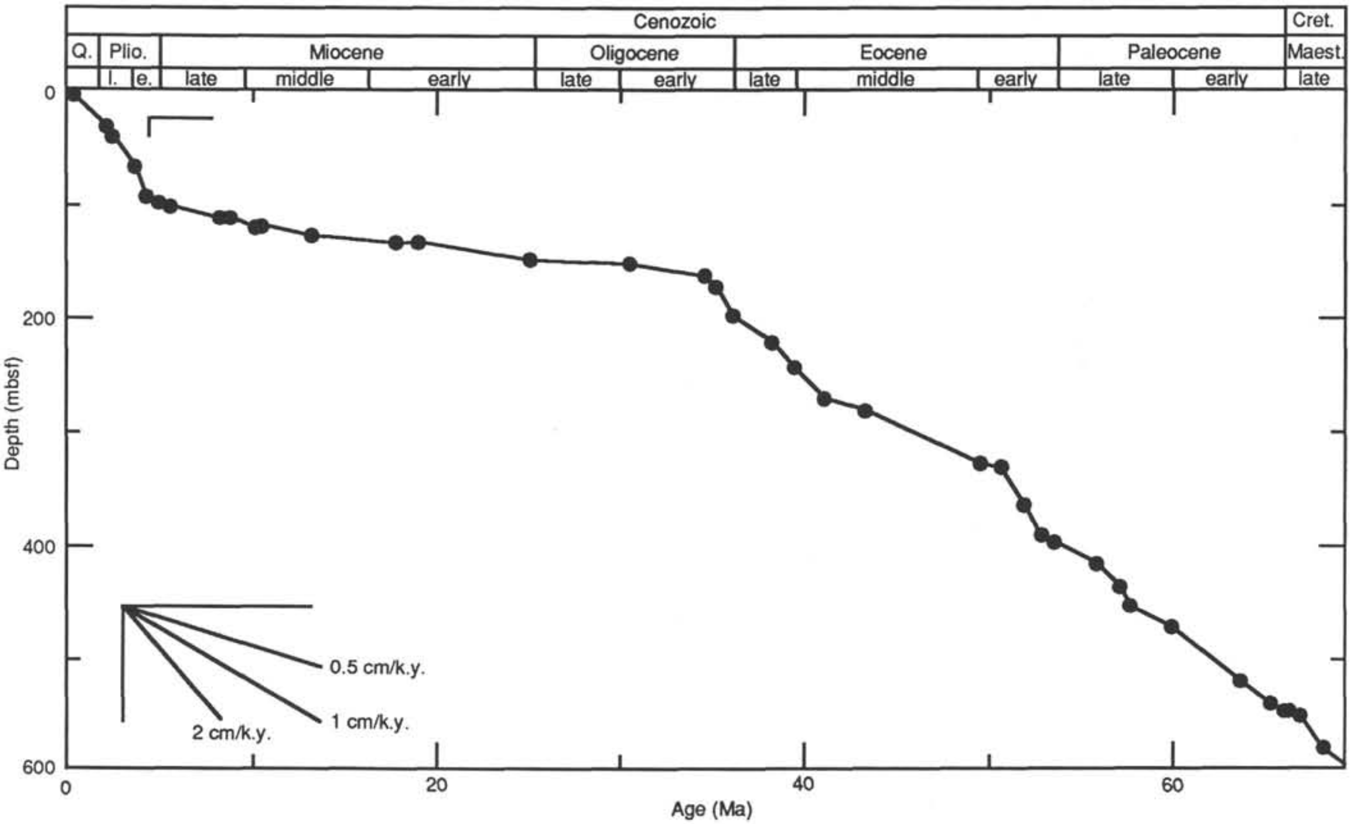

Figure 31. Cenozoic sedimentation rates at Site 762. Standard depth and age error bars are shown at top left. See "Explanatory Notes" (this volume) for full discussion of the techniques used to calculate sedimentation rates.

from ca. 8 to 36. The origin of the CO_2 in these samples cannot be verified without isotopic measurements, yet it may be assumed that postdepositional oxidation of organic matter is involved.

The high concentrations of gas from this site are interpreted to have resulted from migrated thermogenic gas derived from a deep-seated source, possibly the Triassic Mungeroo Formation or Jurassic coal seams. Vertical migration is inferred from: (1) the gas chimneys visible on reflection seismic profiles, (2) the very low concentration of organic carbon over the entire upper portion of the site, and (3) the increase in gas concentrations by about three orders of magnitude over a relatively short depth interval. The high C_1/C_2 ratio is interpreted to have been the product both of the generation from type III (woody or coaly) organic matter and of migration differentiation, which favors the movement of methane over heavier gas components (Leythaeuser et al., 1982, 1983). Stable carbon isotopic measurements of the methane were not available on the ship, but would almost certainly clarify the nature of the gas source.

The rapid rise in the gas concentration at about 350 mbsf (Fig. 35) coincides with a lithologic transition from about 85%–90% carbonate to about 75%–80% carbonate. Gas may be trapped due to the establishment of a critical level of lithification and/or reduction of the effective permeability caused by the presence of small amounts of clay. Above about 350 mbsf there is no seismic expression of gas chimneys, and it appears that gas is dispersed from this zone faster than it can migrate out of the underlying zone.

The level of gas saturation in the pore water was estimated by using measured gas concentrations in the headspace samples, porosity measurements, a methane-solubility curve (Hunt, 1979; p. 209 and p. 447), and estimated pressure and temperature conditions in Hole 762C. These calculations indicate that 100,000 ppm methane in a headspace sample represents less than half the gas necessary to saturate distilled water. We would expect the actual level of saturation to be somewhat higher owing to a 10%–20% reduction in solubility for salt water and some gas loss during drilling and core recovery. On the basis of the observations made during the drilling of the nearby Eendracht-1 well, no free gas phase was expected. Similarly, normal (hydrostatic) pressures (as used in Hole 762C saturation determinations) were noted in the Eendracht-1 well.

Safety Considerations

The decision to continue open-hole drilling in the presence of relatively large amounts of inferred thermogenic gas was predicated on a number of important factors. The results from the Eendracht-1 well (in a somewhat structurally higher position than Site 762) showed no indication of a free gas phase or pressures above the hydrostatic gradient. Secondly, the section above the Dingo Claystone did not contain a porous reservoir unit. The onset of significant amounts of ethane and propane in the headspace gas at about 880 mbsf coincided precisely with the same observation in the Eendracht well. The increase in concentration of "wet gas" has been interpreted herein to indicate that the level of thermal maturation attained a threshold level equivalent to a vitrinite reflectance level of about 0.45% R_o (Powell, 1978). Because of the presence of inferred epigenetic gases in the overlying rocks, it must be assumed that some of the gas in the lowermost 100 m of Site 762 is also migrated dry gas. As a result, the C_1/C_2 ratio observed for the bottom of Hole 762C may be somewhat

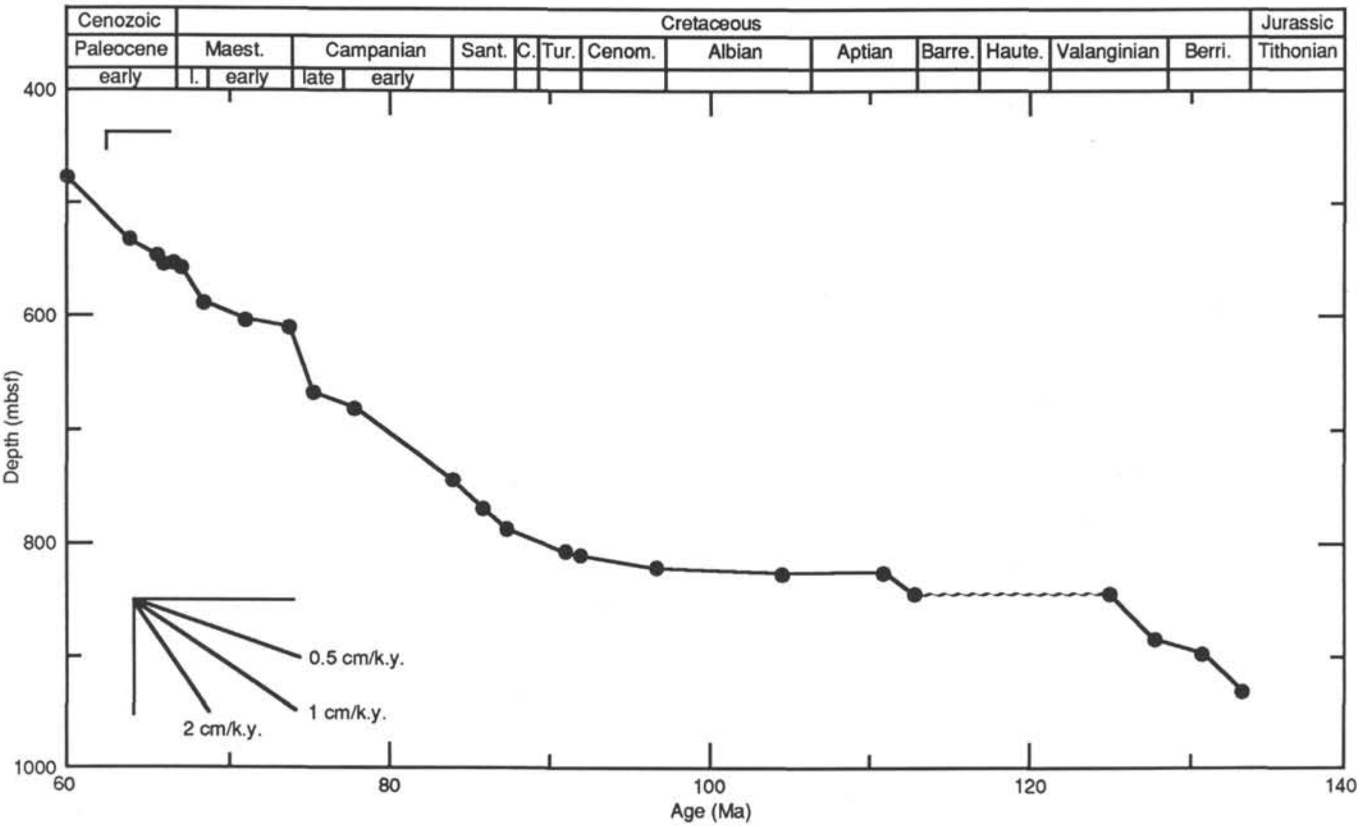

Figure 32. Cretaceous sedimentation rates at Site 762. Hiatuses shown in wavy lines. Standard depth and age error bars are shown at top left. See "Explanatory Notes" (this volume) for full discussion of the techniques used to calculate sedimentation rates.

higher than would be expected for a situation in which only syngenetic gases were present.

High-Molecular-Weight Hydrocarbons

Two samples of Barrow Group siltstone were extracted and analyzed for their contents of high-molecular-weight hydrocarbons. Interstitial-water squeeze cakes from Samples 122-762C-82X-3, 140–150 cm, and -89X-4, 140–150 cm, were freeze-dried and refluxed with azeotropic chloroform/methanol (ratio = 87:13) for 12 and 18 hr, respectively. The extracts were filtered, and the solvent was rotary evaporated almost to dryness. The saturate fraction was eluted from a silica-gel chromatography column using hexane and was analyzed by gas chromatography.

The resulting chromatograms (Fig. 36) show the presence of a relatively large amount of C_{15}–C_{17} normal alkanes in the shallower sample, indicating that the precursor organic matter contained a significant amount of algal material. The large odd/even *n*-alkane predominance over this interval (especially from about C_{20} to C_{30}) indicates a low level of thermal maturity, consistent with the Rock-Eval results. The level of maturity is probably too low to interpret the pristane/phytane ratio (about 1.7) reliably. The discrepancy between the organic-matter type as inferred from the Rock-Eval results (continental source) and the shipboard extract data (marine source) probably relates to the level of thermal maturity, which is just sufficient to yield a small amount of bitumen from the most reactive phase (i.e., the lipid-rich material), but a much smaller relative amount from the type III organic matter.

The presence of a small proportion of lipid-rich material in the Barrow Group sediments is also consistent with the relatively low C_1/C_2 ratio observed at the bottom of Hole 762C. An additional factor that may help to explain the discrepancy in organic-matter character is the selective loss of the higher molecular weight components of the hydrocarbon fractions observed during gas chromatography of standard mixtures. This factor was not quantitatively evaluated in the shipboard laboratory. Subsequent shore-based gas chromatography confirmed that the shipboard instrument discriminated in favor of low-molecular-weight hydrocarbons and against high-molecular-weight (terrigenous) compounds (Meyers and Snowdon, unpubl. data in preparation for Leg 122 *Scientific Results* volume).

The second chromatogram (Sample 122-762C-89X-4, 140–150 cm; Fig. 36) has a much higher proportion of higher-molecular-weight *n*-alkanes (as would be expected from land plant debris) and is interpreted to contain a smaller amount of lipid-rich material than Sample 122-762C-82X-3, 140–150 cm. It, too, shows a relatively low degree of diagenetic alteration of the odd-to-even predominance of the original source material.

Calculation of Percentage of Saturation of Pore Water by Methane

In order to determine if an *in-situ* free gas phase was present over the interval of high gas recoveries, volumetric calculations were made using the headspace gas analysis results and published methane solubility data (Hunt, 1979). The headspace sample vials had a nominal volume of 20 cm^3 (actual volume was closer to 21.5 cm^3) and the nominal sample size was 5 cm^3. Individual actual sample sizes were deter-

Table 3. Concentrations of inorganic carbon, calcium carbonate, and total organic carbon (TOC) in samples from Holes 762B and 762C. Inorganic carbon concentrations were measured coulometrically. Calcium carbonate percentages were calculated assuming the carbonate contents to be pure calcite. TOC values were determined by Rock-Eval analysis. All percentages are on a whole-sediment, dry-weight basis.

Core, section, interval (cm)	Depth (mbsf)	Inorganic carbon (%)	$CaCO_3$ (%)	TOC (%)	Unit	
122-762B-						
1H-1, 104–106	1.04	10.36	86.33			
1H-3, 62–64	3.62	10.34	86.16	0.07		
2H-2, 94–96	6.84	10.17	84.74			
2H-4, 90–93	9.80	10.16	84.66	0.05		
3H-2, 96–98	16.36	9.99	83.24			
3H-4, 83–86	19.23	10.05	83.74		IA	Quaternary to
3H-6, 54–56	21.94	9.65	80.41	0.08		upper Pliocene
4H-2, 95–97	25.85	9.52	79.33			foraminifer-
4H-4, 97–99	28.87	9.69	80.74			nannofossil ooze
4H-6, 92–94	31.82	9.81	81.74	0.05		
5H-2, 92–94	35.32	10.24	85.33			
5H-4, 93–95	38.33	9.41	78.41			
5H-6, 91–93	41.31	9.73	81.08	0.06		
6H-2, 90–92	44.80	9.58	79.83			
6H-4, 90–92	47.80	10.03	83.58			
6H-6, 90–92	50.80	10.00	83.33	0.03		
7H-2, 92–94	54.32	9.73	81.08			
7H-4, 92–94	57.32	9.82	81.83			
7H-6, 92–94	60.32	9.81	81.74	0.02	------	------
8H-2, 53–54	63.43	9.25	77.08	0.03		
8H-4, 95–97	66.85	9.35	77.91			
8H-6, 71–73	69.61	9.93	82.74			
9H-2, 90–92	73.30	9.90	82.49			
9H-4, 89–91	76.29	8.80	73.33	0.03		
9H-6, 87–89	79.27	9.98	83.16		IB	upper Pliocene to
10H-2, 90–92	82.80	10.30	85.83			middle Miocene
10H-4, 90–92	85.80	9.97	83.08	0.15		nannofossil ooze
10H-6, 84–86	88.74	10.73	89.41			
11H-2, 75–75	92.15	10.62	88.49			
11H-4, 64–66	95.04	10.29	85.74			
11H-6, 88–90	98.28	10.57	88.08	0.03		
12H-2, 88–90	101.78	10.57	88.08			
12H-4, 88–90	104.78	10.37	86.41			
12H-6, 88–90	107.78	10.46	87.16			
13H-1, 75–76	109.65	10.46	87.16	0.09		
13H-3, 80–83	112.70	10.47	87.24			
13H-5, 64–66	115.54	11.11	92.58		------	------
14H-2, 83–85	120.73	10.51	87.58			
14H-4, 87–89	123.77	10.88	90.66	0.03	IC	middle Miocene to
14H-6, 87–89	126.77	11.11	92.58			upper Eocene–
15H-2, 34–36	129.74	10.95	91.24			lower Oligocene
15H-4, 57–59	132.97	10.46	87.16	0.01		foraminifer
16H-1, 60–62	138.00	7.67	63.91			nannofossil ooze
16H-3, 70–74	141.10	9.08	75.66	0.01		
16H-5, 70–74	144.10	10.48	87.33			
17H-2, 70–74	149.10	10.40	86.66	0.06		
17H-4, 62–64	152.02	10.72	89.33			
17H-6, 62–64	155.02	10.47	87.24			
18H-3, 76–80	160.16	8.81	73.41			
18H-5, 60–64	163.00	9.42	78.49	0.03		
19H-1, 72–74	166.62	9.50	79.16	0.01		
19H-3, 62–64	169.52	9.88	82.33			
19H-5, 49–50	172.39	10.28	85.66			
122-762C-						
2X-2, 109–111	172.59	10.51	87.58	0.01		
2X-4, 83–85	175.33	9.85	82.08			
3X-1, 82–83	180.32	10.08	83.99			
3X-3, 111–113	183.61	10.53	87.74	0.00	------	------
4X-2, 84–86	191.34	10.62	88.49			
4X-4, 88–90	194.38	10.63	88.58	0.01		
5X-1, 90–95	199.40	10.72	89.33	0.03		
6X-2, 18–21	209.68	11.01	91.74			
6X-2, 115–120	210.65	3.47	28.91	0.01	II	upper Eocene–
6X-4, 108–110	213.58	10.75	89.58			lower Oligocene
7X-1, 86–88	218.36	10.43	86.91			to middle Eocene
7X-4, 85–90	222.85	10.50	87.49	0.00		nannofossil
8X-2, 84–86	229.34	10.81	90.08			chalk
8X-4, 90–92	232.40	9.88	82.33	0.01		

Table 3 (continued).

Core, section, interval (cm)	Depth (mbsf)	Inorganic carbon (%)	$CaCO_3$ (%)	TOC (%)	Unit	
9X-1, 51–53	237.01	10.98	91.49	0.00		
10X-2, 95–97	248.45	10.88	90.66	0.03		
10X-4, 88–90	251.38	10.83	90.24			
11X-2, 80–82	257.80	10.98	91.49			
11X-4, 48–50	260.48	10.77	89.74	0.02		
11X-6, 100–101	263.50	10.44	86.99		------------	
12X-2, 88–90	267.38	10.27	85.58			
12X-6, 88–90	273.38	10.48	87.33			
13X-2, 88–90	276.88	10.70	89.16	0.03		
14X-2, 64–66	286.14	10.41	86.74			
14X-2, 78–80	286.28	10.23	85.24	0.00		
14X-4, 88–90	289.38	10.43	86.91		IIIA	middle to lower
14X-6, 98–100	292.48	10.34	86.16			Eocene
15X-1, 94–96	294.44	10.30	85.83			foraminifer
15X-3, 30–32	296.80	10.33	86.08	0.00		nannofossil
16X-1, 92–94	303.92	10.65	88.74			chalk
16X-3, 83–85	306.83	10.42	86.83	0.04		
17X-2, 123–125	315.23	10.56	87.99			
17X-4, 98–100	317.98	10.80	89.99	0.01		
17X-5, 128–130	319.78	10.44	86.99			
18X-2, 70–72	324.20	10.43	86.91	0.01		
18X-4, 70–72	327.20	10.85	90.41			
18X-6, 70–72	330.20	10.77	89.74			
19X-4, 62–64	336.62	10.38	86.49	0.00		
20X-2, 60–62	343.10	10.02	83.49			
20X-4, 32–34	345.82	10.40	86.66	0.05		
21X-CC, 18–20	359.00	10.08	83.99			
22X-1, 22–24	360.22	10.31	85.91			
22X-3, 40–44	363.40	9.89	82.41			
22X-5, 40–44	366.40	9.09	75.74	0.04		
23X-2, 61–63	371.61	8.99	74.91	0.04		
23X-4, 20–23	374.20	9.34	77.83			
24X-1, 40–43	379.40	10.04	83.66	0.03		
25X-2, 30–32	380.80	10.05	83.74			
25X-4, 40–44	393.40	8.99	74.91	0.04		
26X-1, 32–34	398.32	9.76	81.33		------------	
27X-1, 48–51	402.98	8.56	71.33			
26X-6, 12–14	405.62	9.25	77.08	0.06		
27X-3, 60–62	406.10	8.51	70.91	0.05		
28X-2, 5–8	413.55	9.97	83.08			
29X-1, 3–5	421.53	10.43	86.91	0.05		
30X-1, 77–79	431.77	10.83	90.24			
31X-2, 85–88	42.85	10.35	86.24	0.06		
31X-4, 85–88	445.85	10.55	87.91			
31X-6, 85–88	448.85	10.35	86.24			
32X-1, 91–93	450.91	10.83	90.24			
32X-2, 63–65	452.13	10.58	88.16		IIIB	lower Eocene
33X-1, 90–92	460.40	10.34	86.16			to lower
33X-2, 11–12	461.11	10.73	89.41	0.01		Paleocene
33X-3, 90–92	463.40	10.53	87.74	0.01		nannofossil
33X-5, 88–90	466.38	9.44	78.66			chalk
33X-CC, 8–9	468.00	8.38	69.83	0.02		
34X-2, 118–120	471.68	10.11	84.24			
34X-4, 29–31	473.79	10.74	89.49			
35X-1, 107–109	479.57	9.21	76.74			
36X-1, 22–24	488.22	10.14	84.49	0.02		
37X-1, 102–105	498.52	9.62	80.16			
37X-3, 98–100	501.48	8.64	71.99			
37X-5, 16–19	503.66	8.80	73.33			
38X-2, 17–18	508.67	7.59	63.24			
38X-4, 42–43	511.92	8.20	68.33			
38X-6, 40–42	514.90	6.40	53.33			
39X-2, 42–44	518.42	6.67	55.58	0.09		
39X-4, 42–44	521.42	5.18	43.16			
40X-2, 51–53	528.01	6.51	54.24			
40X-4, 46–48	530.96	7.62	63.49			
40X-6, 38–40	533.88	6.87	57.24			
41X-2, 40–43	537.40	6.45	53.74	0.08		
41X-4, 23–26	540.23	5.92	49.33			
42X-1, 115–118	546.15	6.55	54.58		------------	
43X-4, 115–118	560.15	11.38	94.83	0.02		
44X-1, 115–117	565.15	10.25	85.41			
44X-3, 33–35	567.33	9.99	83.24			
44X-5, 94–96	570.94	10.06	83.83			
45X-1, 9–10	573.59	10.88	90.66		IVA	upper to lower
45X-4, 95–97	578.95	10.97	91.41	0.02		Maestrichtian

Table 3 (continued).

Core, section, interval (cm)	Depth (mbsf)	Inorganic carbon (%)	$CaCO_3$ (%)	TOC (%)	Unit	
46X-1, 35–37	583.35	11.29	94.08			nannofossil
46X-2, 75–75	585.25	6.73	56.08	0.04		chalk
46X-2, 130–132	585.80	11.20	93.33			
46X-3, 116–116	587.16	11.07	92.24	0.03		
46X-4, 65–67	588.15	7.12	59.33			
47X-2, 81–83	594.81	9.93	82.74			
47X-2, 140–140	595.40	8.64	71.99	0.02		
47X-4, 71–73	597.71	10.12	84.33			
47X-4, 106–106	598.06	10.49	87.41	0.02		
47X-6, 66–68	600.66	9.93	82.74			
48X-1, 90–92	602.90	10.61	88.41		------	------
48X-3, 94–96	605.94	10.10	84.16			
48X-5, 55–57	608.55	9.16	76.33			
48X-6, 68–70	610.18	10.73	89.41			
49X-1, 9–11	611.59	10.85	90.41			
49X-3, 78–80	615.28	8.38	69.83			
49X-4, 19–21	616.19	11.07	92.24			
49X-5, 132–134	618.82	9.51	79.24			
50X-2, 48–50	622.98	9.76	81.33	0.01	IVB	lower
50X-4, 94–96	626.44	10.49	87.41			Maextrichtian
50X-6, 116–118	629.66	10.22	85.16			to lower
51X-2, 66–68	632.66	8.77	73.08			Campanian
51X-4, 142–144	636.42	10.26	85.49	0.04		clayey nannofossil
51X-5, 142–144	637.92	9.77	81.41			chalk
52X-2, 50–52	642.00	10.28	85.66			
52X-4, 76–78	645.26	9.83	81.91	0.01		
53X-2, 20–22	651.20	9.89	82.41			
54X-2, 31–33	660.81	10.47	87.24			
54X-4, 49–52	663.99	9.70	80.83	0.02		
54X-4, 86–88	664.36	9.21	76.74			
53X-4, 94–97	654.94	9.78	81.49	0.00		
53X-6, 8–10	657.08	10.64	88.66			
54X-6, 104–106	667.54	10.16	84.66			
55X-2, 67–69	670.67	10.62	88.49			
55X-4, 7–9	673.07	10.24	85.33			
56X-1, 63–65	678.63	10.24	85.33			
56X-3, 90–92	681.90	10.13	84.41	0.00		
56X-5, 56–58	684.56	10.25	85.41			
57X-2, 56–58	689.56	10.48	87.33		------	------
58X-3, 103–105	701.03	11.06	92.16			
58X-5, 12–15	703.12	11.03	91.91			
59X-2, 109–111	709.09	10.65	88.74			
59X-3, 148–150	710.98	11.08	92.33	0.00		
60X-1, 26–28	716.26	11.14	92.83			
60X-4, 7–9	720.57	11.05	92.08		IVC	lower Campanian
61X-1, 3–5	725.53	10.97	91.41			to lower
61X-2, 35–37	727.35	10.95	91.24			Santonian
62X-2, 127–129	737.77	11.05	92.08			nannofossil chalk
62X-3, 86–89	738.86	11.05	92.08	0.00		
62X-4, 35–37	739.85	11.29	94.08			
62X-5, 39–42	741.39	11.14	92.83			
63X-1, 43–45	744.93	11.43	95.24			
64X-1, 13–15	754.13	11.41	95.08			
64X-3, 7–9	757.07	11.36	94.66			
64X-4, 2–4	758.52	11.20	93.33			
66X-1, 29–30	765.29	11.42	95.16			
66X-3, 90–92	768.90	11.25	93.74	0.01		
67X-CC, 34–36	771.34	11.39	94.91			
68X-1, 140–142	776.40	11.09	92.41		------	------
69X-1, 42–44	780.42	10.59	88.24	0.00		
70X-2, 144–146	787.94	10.93	91.08			
71X-1, 56–58	790.56	10.37	86.41			
71X-2, 144–146	792.94	11.26	93.83			
72X-1, 42–44	795.42	10.87	90.58	0.00	IVD	lower Santonian
73X-2, 84–86	801.84	11.07	92.24			to upper Albian
73X-3, 6–8	802.56	10.41	86.74	0.00		nannofossil chalk
74X-2, 47–49	806.47	10.40	86.66			
74X-3, 24–27	807.74	10.67	88.91			
75X-1, 2–5	809.52	10.37	86.41			
76X-CC, 2–3	820.34	9.37	78.05			
76X-1, 82–85	815.32	10.73	89.41			
76X-3, 99–101	818.49	9.34	77.83	0.02		
76X-4, 82–85	819.82	7.68	63.99			
76X-4, 82–85	819.82	6.50	54.16			
77X-1, 134–136	820.84	6.80	56.66		------	------
77X-3, 129–131	823.79	8.52	70.99	0.01	IVE	Albian clayey

Table 3 (continued).

Core, section, interval (cm)	Depth (mbsf)	Inorganic carbon (%)	$CaCO_3$ (%)	TOC (%)	Unit
77X-5, 147–149	826.97	8.23	68.58		nannofossil chalk
78X-1, 91–93	829.91	10.03	83.58	0.01	------------
79X-1, 64–66	839.14	0.52	4.33	0.21	V lower Aptian
79X-2, 109–111	841.09	0.22	1.83	0.84	black claystone
81X-1, 22–24	848.72	0.20	1.66	1.02	------------
81X-3, 107–109	852.57	0.09	0.74	1.50	
81X-3, 116–118	852.66	0.12	0.99	1.17	
82X-1, 112–114	854.62	0.07	0.58	1.42	
82X-2, 84–85	855.84	8.99	74.91	0.23	
82X-3, 71–73	857.21	0.18	1.49	1.23	
83X-1, 59–60	859.09	0.18	1.49	1.21	
84X-1, 70–74	864.20	0.10	0.83	0.68	
85X-1, 114–116	874.14	0.36	2.99	1.28	VI Berriasian to
86X-2, 113–117	885.13	0.23	1.91	0.89	lower Valanginian
86X-4, 84–89	887.84	0.56	4.66	0.75	black to dark gray
87X-2, 21–23	893.71	0.30	2.49	0.80	clayey siltstone
88X-2, 126–128	904.26	0.10	0.83	0.75	
88X-4, 65–67	906.65	0.07	0.58	0.66	
88X-6, 100–102	910.00	0.43	3.58	0.64	
89X-2, 84–86	913.34	0.10	0.83	0.79	
89X-4, 27–28	915.77	0.27	2.24	0.62	
90X-2, 82–83	922.82	0.32	2.66	0.86	
90X-4, 86–87	925.86	0.30	2.49	0.92	
91X-1, 85–87	930.85	0.15	1.24	1.15	
91X-2, 21–23	931.71	0.12	0.99	0.98	

mined after the gas analysis was completed by noting the volume of water needed to fill the vial. The actual volume of methane could easily be determined by noting the proportion of methane (in ppm or %) and multiplying by the total air volume (15 cm^3) in the headspace vial.

$$\begin{aligned}\text{Methane volume} &= \text{vial headspace volume} \times \%\ \text{methane in vial}\\ &= \text{vial headspace volume} \times \text{ppm } C_1 / 1{,}000{,}000\\ &= 15\ cm^3 \times 100{,}000 / 1{,}000{,}000\\ &= 1.5\ cm^3\end{aligned}$$

The pore water volume was estimated by using the physical-properties measurements of porosity, which in this case were about 35%.

$$\begin{aligned}\text{Pore water volume} &= \text{sediment volume} \times \text{porosity}\\ &= 5\ cm^3 \times 35\%\\ &= 1.75\ cm^3\end{aligned}$$

Thus the gas-to-water volume ratio (methane volume/pore water volume [v/v] = 1.5/1.75) for this example is about 0.86. This value was compared with the v/v saturation solubility curve of Figure 37 (Hunt, 1979, fig. 6-9, p. 209) which assumes normal pressure and temperature gradients of about 100 atm/km (0.46 psi/ft) and 27°C/km (1.5°F/100 ft). At a depth of 2000 m, the v/v saturation solubility ratio was noted to be about 2.5 cm^3 gas/cm^3 water, or about 2 cm^3 gas/cm^3 water if a 20% reduction in solubility is applied because of the salinity of the pore water = 35 g/kg, approximating normal seawater values. The estimated level of saturation is thus 0.86/2, or about 43%.

Several possible errors must be considered when applying this calculation and interpreting the results. First, the headspace gas concentration is measured on a sediment sample which is sealed in a vial after the core is retrieved and cut into 1.5-m sections. Thus gas may be lost during the transit of the core up the drill string and during degassing on the deck. This error is not thought to be significant in fine-grained rocks because the cores rarely exceed their drilled length (usually 9.5 m) before they arrive on deck. A second possible error (but with the opposite effect) arises because the temperature of sections drilled in the deep ocean is typically lower than those drilled on land or in shallow water. This results from the decrease in temperature with depth through the water column and the commensurate reduction in absolute temperature for any given depth (below sea level). These errors tend to offset one another. Two other sources of error include the possibility that the gas is not pure methane (i.e., ethane and higher homologs have lower solubilities) and that the pore water has higher-than-normal salinity. Shipboard analyses of both headspace and vacutainer gas and also of interstitial-water salinities are routinely made, and any serious deviations from normal conditions should be immediately obvious.

INORGANIC GEOCHEMISTRY

Introduction

The shipboard inorganic geochemistry procedures at Site 762 included (1) chemical analyses of interstitial waters (Fig. 38, Table 7) and (2) mineralogical (XRD) analyses (Table 8) of the corresponding squeeze cakes and several other sediment samples of special interest to shipboard sedimentologists. Surface seawater was collected in addition to two *in-situ* pore-water samples obtained during downhole heat-flow measurements. Thirty-two whole-round (5- or 10-cm-long) samples were squeezed for interstitial waters. One of these (Sample 122-762C-69X, 140–150 cm) did not yield any pore water; another (Sample 122-762C-72X, 140–150 cm) yielded only enough fluid (0.5 cm^3) to allow the determination of salinity, chlorinity, sulfate, and silica. In two other cases (Samples 122-762C-82X, 140–150 cm, and -89X, 140–150 cm) insufficient interstitial water was obtained to allow the measurement of alkalinity. All samples from which little or no water was obtained came from the lower section of Hole 762C where the highly compacted Gearle Siltstone equivalent, Muderong Shale equivalent, and prodelta mudstones of the Barrow Group equivalent occur. Thirty-six solid samples were subjected to XRD analysis; 28 of these were from squeeze cakes. XRD data for samples from Site 763, which

Table 4. Rock-Eval data from samples from Holes 762B and 762C. Total organic carbon (TOC) percentages were determined on a whole-sediment, dry-weight basis.

Core, section, interval (cm)	Depth (mbsf)	Wt. (mg)	T_{max} (°C)	S_1	S_2	S_3	PI	S_2/S_3	PC	TOC (%)	HI	OI
122-762B-												
1H-3, 62–64	3.6	100.8	406	0.07	0.20	1.93	0.27	0.10	0.02	0.07	285	2757
2H-4, 90–93	9.8	101.4	397	0.10	0.20	1.88	0.33	0.10	0.02	0.05	400	3760
3H-6, 54–56	21.9	100.0	381	0.10	0.15	2.02	0.42	0.07	0.02	0.08	187	2525
4H-6, 92–94	31.8	100.6	390	0.06	0.21	1.75	0.23	0.12	0.02	0.05	420	3500
5H-5, 0–5	38.9	101.1	404	0.03	0.00	1.74	1.00	0.00	0.00	0.02	0	8700
5H-6, 91–93	41.3	100.6	397	0.13	0.43	4.93	0.23	0.08	0.04	0.06	716	8216
6H-6, 90–92	50.8	100.2	304	0.09	0.23	1.44	0.28	0.15	0.02	0.03	766	4800
7H-6, 92–94	63.3	101.8	331	0.09	0.20	1.60	0.32	0.12	0.02	0.02	1000	8000
8H-2, 53–54	63.4	100.1	325	0.08	0.23	1.52	0.27	0.15	0.02	0.03	766	5066
9H-4, 89–91	76.3	100.0	304	0.07	0.22	1.56	0.25	0.14	0.02	0.03	733	5200
10H-4, 90–92	85.8	101.4	304	0.04	0.14	1.37	0.22	0.10	0.01	0.15	93	913
11H-6, 88–90	98.3	101.5	315	0.05	0.28	1.33	0.16	0.21	0.02	0.03	933	4433
13H-1, 75–76	109.7	102.5	304	0.05	0.23	1.06	0.18	0.21	0.02	0.09	255	1177
14H-4, 87–89	123.8	100.2	431	0.03	0.31	1.24	0.09	0.25	0.02	0.03	1033	4133
15H-4, 57–59	133.0	99.7	304	0.01	0.04	1.16	0.25	0.03	0.00	0.01	400	11600
16H-3, 70–74	141.1	99.5	413	0.04	0.08	1.25	0.33	0.06	0.01	0.01	800	12500
17H-2, 70–74	149.1	101.2	348	0.04	0.42	1.05	0.09	0.40	0.03	0.06	700	1750
18H-5, 60–64	163.0	99.5	304	0.02	0.03	1.01	0.50	0.02	0.00	0.03	100	3366
19H-1, 72–74	166.6	100.2	394	0.07	0.11	1.05	0.39	0.10	0.01	0.01	1100	10500
122-762C-												
2X-2, 109–111	172.6	99.8	396	0.01	0.01	0.96	0.50	0.01	0.00	0.01	100	9600
3X-3, 111–113	183.6	99.9	265	0.00	0.01	0.99	0.00	0.01	0.00	0.00	0	0
4X-4, 88–90	194.4	102.3	385	0.01	0.04	0.78	0.25	0.05	0.00	0.01	400	7800
5X-1, 90–95	199.4	101.9	379	0.01	0.23	0.85	0.04	0.27	0.02	0.03	766	2833
6X-2, 115–120	210.7	101.8	367	0.01	0.05	0.55	0.17	0.09	0.00	0.01	500	5500
7X-4, 85–90	222.9	100.3	304	0.00	0.00	0.72	0.00	0.00	0.00	0.00	0	0
8X-4, 90–92	232.4	100.3	419	0.00	0.00	0.61	0.00	0.00	0.00	0.01	0	6100
9X-1, 51–53	237.0	100.5	333	0.00	0.00	0.58	0.00	0.00	0.00	0.00	0	0
10X-2, 95–97	248.5	102.8	383	0.00	0.03	0.57	0.00	0.05	0.00	0.03	100	1900
13X-2, 88–90	249.9	100.1	403	0.01	0.16	0.66	0.06	0.24	0.01	0.03	533	2200
11X-4, 48–50	260.5	100.9	383	0.00	0.15	0.70	0.00	0.21	0.01	0.02	750	3500
12X-4, 88–90	270.4	99.3	310	0.04	0.10	1.55	0.29	0.06	0.01	0.03	333	5166
14X-2, 78–80	286.3	99.9	348	0.01	0.04	0.82	0.25	0.04	0.00	0.00	0	0
15X-3, 30–32	296.8	100.1	394	0.00	0.06	0.68	0.00	0.08	0.00	0.00	0	0
16X-3, 83–85	306.8	100.3	356	0.02	0.18	0.58	0.10	0.31	0.01	0.04	450	1450
17X-4, 98–100	318.0	101.3	340	0.00	0.01	0.54	0.00	0.01	0.00	0.01	100	5400
18X-2, 70–72	324.2	101.0	303	0.01	0.02	0.60	0.50	0.03	0.00	0.01	200	6000
19X-4, 62–64	336.6	100.2	275	0.00	0.00	0.49	0.00	0.00	0.00	0.00	0	0
20X-4, 32–34	345.8	102.0	302	0.01	0.00	0.55	0.00	0.00	0.00	0.05	0	1100
22X-5, 40–44	366.4	100.2	387	0.00	0.02	0.81	0.00	0.02	0.00	0.04	50	2025
23X-2, 61–63	371.6	99.8	343	0.02	0.23	0.86	0.08	0.26	0.02	0.04	575	2150
24X-1, 40–43	379.4	102.0	304	0.03	0.17	0.57	0.15	0.29	0.01	0.03	566	1900
25X-4, 40–44	393.4	99.1	415	0.03	0.10	0.77	0.25	0.12	0.01	0.04	250	1925
26X-6, 12–14	405.6	100.8	456	0.12	0.14	0.98	0.46	0.14	0.02	0.06	233	1633
27X-3, 60–62	406.1	99.7	403	0.01	0.24	1.25	0.04	0.19	0.02	0.05	480	2500
29X-1, 3–5	421.5	101.6	391	0.01	0.30	0.86	0.03	0.34	0.02	0.05	600	1720
31X-2, 85–88	442.9	100.9	331	0.02	0.22	0.76	0.08	0.28	0.02	0.06	366	1266
33X-2, 11–12	461.1	102.7	335	0.00	0.08	0.45	0.00	0.17	0.00	0.01	800	4500
33X-3, 90–92	463.4	100.2	304	0.02	0.13	0.54	0.14	0.24	0.01	0.01	1300	5400
33X-CC, 8–9	468.3	101.0	357	0.00	0.13	0.93	0.00	0.13	0.01	0.02	650	4650
36X-1, 22–24	488.2	100.3	339	0.02	0.11	0.57	0.17	0.19	0.01	0.02	550	2850
39X-2, 42–44	518.4	100.6	328	0.04	0.14	1.48	0.22	0.09	0.01	0.09	155	1644
41X-2, 40–43	537.4	99.5	356	0.07	0.15	1.40	0.32	0.10	0.01	0.08	187	1750
42X-5, 0–2	551.0	100.3	334	0.00	0.00	1.63	0.00	0.00	0.00	0.03	0	5433
43X-4, 115–117	560.1	100.7	287	0.00	0.00	0.52	0.00	0.00	0.00	0.02	0	2600
44X-4, 140–150	569.9	101.8	529	0.09	0.24	0.58	0.28	0.41	0.02	0.03	800	1933
45X-4, 95–97	579.0	99.7	304	0.03	0.09	0.67	0.25	0.13	0.01	0.02	450	3350
46X-2, 75–75	585.3	99.7	304	0.01	0.09	0.62	0.10	0.14	0.00	0.04	225	1550
46X-2, 75–75	585.3	100.1	304	0.03	0.25	0.65	0.11	0.38	0.02	0.05	500	1300
46X-3, 116–116	587.2	100.9	344	0.00	0.00	0.38	0.00	0.00	0.00	0.03	0	1266
46X-3, 116–116	587.2	99.3	326	0.04	0.22	0.42	0.15	0.52	0.02	0.02	1100	2100
47X-2, 140–140	595.4	101.3	330	0.01	0.20	0.75	0.05	0.26	0.01	0.03	666	2500
47X-2, 140–140	595.4	102.7	333	0.00	0.07	0.73	0.00	0.09	0.00	0.02	350	3650
47X-4, 106–106	598.1	101.0	411	0.00	0.17	0.53	0.00	0.32	0.01	0.02	850	2650
47X-4, 106–106	598.1	99.6	327	0.00	0.04	0.57	0.00	0.07	0.00	0.00	0	0
47X-5, 140–150	599.9	101.8	337	0.03	0.19	0.41	0.14	0.46	0.01	0.02	950	2050
50X-2, 48–50	623.0	100.3	229	0.00	0.00	1.50	0.00	0.00	0.00	0.01	0	15000
50X-2, 140–150	623.9	99.6	346	0.03	0.18	0.60	0.15	0.30	0.01	0.02	900	3000
51X-4, 142–144	636.4	99.8	255	0.00	0.00	1.11	0.00	0.00	0.00	0.04	0	2775
52X-4, 76–78	645.3	100.2	225	0.00	0.00	0.97	0.00	0.00	0.00	0.01	0	9700
53X-4, 94–97	654.9	100.3	261	0.00	0.00	1.29	0.00	0.00	0.00	0.00	0	0
53X-4, 140–150	655.4	100.8	387	0.01	0.08	0.71	0.12	0.11	0.00	0.03	266	2366
53X-5, 0–2	655.5	101.9	390	0.00	0.08	1.42	0.00	0.05	0.00	0.05	160	2840

Table 4 (continued).

Core, section, interval (cm)	Depth (mbsf)	Wt. (mg)	T_{max} (°C)	S_1	S_2	S_3	PI	S_2/S_3	PC	TOC (%)	HI	OI
54X-4, 49–52	664.0	101.0	283	0.00	0.00	0.98	0.00	0.00	0.00	0.02	0	4900
56X-3, 90–92	681.9	100.8	304	0.00	0.00	0.93	0.00	0.00	0.00	0.00	0	0
56X-5, 113–115	685.1	99.9	301	0.01	0.00	0.81	0.00	0.00	0.00	0.02	0	4050
56X-5, 140–150	685.4	99.2	295	0.07	0.06	0.90	0.58	0.06	0.01	0.04	150	2250
59X-3, 148–150	711.0	100.4	325	0.02	0.06	0.81	0.25	0.07	0.00	0.00	0	0
59X-4, 140–150	712.4	101.0	304	0.10	0.03	0.64	0.83	0.04	0.01	0.02	150	3200
62X-3, 86–89	738.9	101.6	304	0.00	0.06	0.48	0.00	0.12	0.00	0.00	0	0
62X-4, 140–150	740.9	100.4	304	0.03	0.05	0.26	0.37	0.19	0.00	0.01	500	2600
66X-3, 90–92	768.9	99.6	325	0.06	0.18	0.58	0.00	0.31	0.02	0.01	1800	5800
66X-4, 140–150	770.9	101.6	266	0.01	0.00	0.24	0.00	0.00	0.00	0.00	0	0
69X-1, 42–44	780.4	99.2	342	0.02	0.05	0.56	0.33	0.08	0.00	0.00	0	0
72X-1, 42–44	795.4	101.7	333	0.00	0.03	0.59	0.00	0.05	0.00	0.00	0	0
72X-1, 140–150	796.4	101.7	269	0.01	0.00	0.58	0.00	0.00	0.00	0.00	0	0
73X-3, 6–8	802.6	100.8	267	0.00	0.00	1.13	0.00	0.00	0.00	0.00	0	0
76X-3, 99–101	818.5	101.8	267	0.00	0.00	1.04	0.00	0.00	0.00	0.02	0	5200
77X-3, 0–2	822.5	100.0	255	0.00	0.00	0.72	0.00	0.00	0.00	0.01	0	7200
77X-3, 129–131	823.8	98.4	221	0.00	0.00	1.04	0.00	0.00	0.00	0.01	0	10400
77X-7, 0–2	828.5	101.6	241	0.00	0.00	1.02	0.00	0.00	0.00	0.13	0	784
78X-1, 91–93	829.9	100.8	270	0.00	0.00	1.06	0.00	0.00	0.00	0.01	0	10600
79X-1, 64–66	839.1	101.6	404	0.02	0.07	0.95	0.25	0.07	0.00	0.21	33	452
79X-2, 109–111	841.1	101.2	414	0.01	0.48	0.69	0.02	0.69	0.04	0.84	57	82
79X-3, 0–2	841.5	101.0	372	0.00	0.10	0.46	0.00	0.21	0.00	0.25	40	184
79X-3, 65–66	842.2	98.9	416	0.02	0.33	0.81	0.06	0.40	0.02	0.42	78	192
81X-1, 22–24	848.8	101.9	415	0.02	0.51	1.05	0.04	0.48	0.04	1.02	50	102
81X-3, 0–2	851.5	100.6	461	0.00	0.80	0.42	0.00	1.90	0.06	0.99	80	42
81X-3, 0–2	851.5	100.1	415	0.02	0.48	0.51	0.04	0.94	0.04	1.00	48	51
81X-3, 107–109	852.6	100.4	415	0.01	0.87	0.75	0.01	1.16	0.07	1.50	58	50
81X-3, 116–118	852.7	100.8	415	0.02	0.50	0.98	0.04	0.51	0.04	1.17	42	83
82X-1, 114–114	854.6	100.3	419	0.01	0.81	1.20	0.01	0.67	0.06	1.42	57	84
82X-2, 84–85	855.8	98.8	409	0.00	0.08	2.16	0.00	0.03	0.00	0.23	34	939
82X-3, 71–73	857.2	101.6	419	0.08	1.48	1.75	0.05	0.84	0.13	1.23	120	142
82X-3, 140–150	857.9	100.8	426	0.06	1.57	0.41	0.04	3.82	0.13	1.14	137	35
83X-1, 0–2	858.5	100.4	414	0.00	0.35	1.12	0.00	0.31	0.02	0.86	40	130
83X-1, 59–60	859.1	100.6	422	0.02	1.42	2.11	0.01	0.67	0.12	1.21	117	174
84X-1, 0–2	863.5	100.4	425	0.00	0.82	0.37	0.00	2.21	0.06	0.72	113	51
84X-1, 70–74	864.2	101.2	416	0.01	0.68	1.96	0.01	0.34	0.05	0.68	100	288
85X-1, 114–116	874.1	102.0	426	0.10	1.07	2.12	0.09	0.50	0.09	0.83	128	255
85X-1, 148–150	874.5	102.3	431	0.00	1.08	0.71	0.00	1.52	0.09	0.79	136	89
86X-2, 113–117	885.1	98.8	424	0.06	0.84	1.88	0.07	0.44	0.07	0.89	94	211
86X-3, 140–150	886.9	100.8	426	0.01	0.93	0.87	0.01	1.06	0.07	0.85	109	102
86X-4, 0–2	887.0	100.4	427	0.00	0.64	0.93	0.00	0.68	0.05	0.71	90	130
86X-4, 84–86	887.8	98.9	423	0.03	0.64	1.88	0.05	0.34	0.05	0.75	85	250
87X-2, 0–2	893.5	100.9	425	0.00	0.31	0.90	0.00	0.34	0.02	0.55	56	163
87X-2, 21–23	893.7	101.6	427	0.02	0.84	1.58	0.02	0.53	0.07	0.80	105	197
88X-2, 126–128	904.3	101.8	418	0.04	1.06	1.19	0.04	0.89	0.09	0.75	141	158
88X-4, 65–67	906.7	99.9	438	0.04	0.65	1.05	0.06	0.61	0.05	0.66	98	159
88X-6, 0–2	909.0	100.0	422	0.02	0.66	0.84	0.03	0.78	0.05	0.63	104	133
88X-6, 100–102	910.0	101.3	415	0.01	0.48	1.42	0.02	0.33	0.04	0.64	75	221
89X-2, 0–2	912.5	101.7	425	0.00	0.62	1.05	0.00	0.59	0.05	0.67	92	156
89X-2, 84–86	913.3	100.5	420	0.02	0.72	1.37	0.03	0.52	0.06	0.79	91	173
89X-4, 27–28	915.8	99.8	416	0.03	0.38	1.56	0.07	0.24	0.03	0.62	61	251
89X-5, 0–2	917.0	100.2	423	0.00	0.57	0.80	0.00	0.71	0.04	0.68	83	117
90X-2, 0–2	922.0	100.4	423	0.00	0.84	0.77	0.00	1.09	0.07	0.87	96	88
90X-2, 82–83	922.8	101.0	425	0.02	1.12	1.23	0.02	0.91	0.09	0.86	130	143
90X-4, 0–2	925.0	100.6	433	0.00	1.17	0.77	0.00	1.51	0.09	1.10	106	70
90X-4, 86–88	925.9	101.4	428	0.03	1.08	1.15	0.03	0.93	0.09	0.92	117	125
91X-1, 85–87	930.9	101.3	428	0.01	1.15	0.98	0.01	1.17	0.09	1.15	100	85
91X-2, 0–2	931.5	100.8	427	0.02	1.34	0.85	0.01	1.57	0.11	1.08	124	78
91X-2, 21–23	931.7	101.6	428	0.02	0.94	0.81	0.02	1.16	0.08	0.98	95	82

were analyzed during transit to Singapore, are also included in Table 8.

Smooth concentration gradients for most constituents between 0 and 372.4 mbsf suggest slow diffusion of dissolved species through the poorly consolidated sediments of Site 762. Below 372.4 mbsf, the local lithology appears to exercise greater control on the pore-water composition, and diffusion processes appear to play a more limited role.

Interstitial Waters

Magnesium (Mg^{2+}) and Calcium (Ca^{2+})

Dissolved Mg^{2+} at Site 762 decreases steadily from a near-surface-seawater concentration (52.3 mM) at 3.0 mbsf to 11.7 mM by 916.9 mbsf (Table 7 and Fig. 38). Two deviations from this trend occur: (1) a large concentration drop from 32.9 to 25.3 mM between 372.4 and 403.9 mbsf, and (2) a reversal from 9.4 to 11.7 mM between 886.9 and 916.9 mbsf. The former is associated with large spikes in dissolved Ca^{2+}, SO_4^{2-}, SiO_2, and alkalinity, and coincides with the top of Subunit IIIB, which is characterized by nannofossil chalk that becomes darker with depth, from white to dark green-gray (see "Lithostratigraphy," this chapter). The Mg^{2+} concentration reversal at 916.9 mbsf is accompanied by only subtle changes in the concentration of other pore-water constituents.

Very good agreement is observed between *in-situ* pore water samples and those obtained by shipboard squeezing of whole-round cores (see Table 7, Samples 122-762B-12H-1,

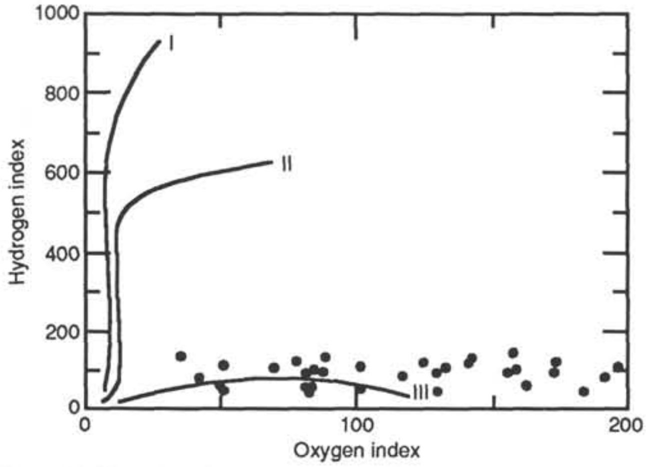

Figure 33. Van Krevelen-type plot of Rock-Eval hydrogen index (HI) and oxygen index, (OI) of samples from Holes 762B and 762C. Units for HI are mg total hydrocarbons/g total organic carbon; for OI, mg CO_2/g total organic carbon.

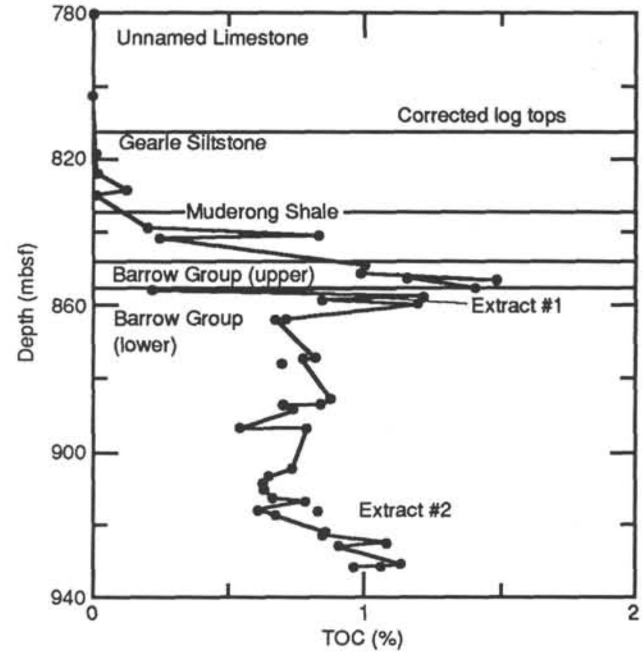

Figure 34. Concentrations of total organic carbon (TOC) in samples from the lower 150 m of Hole 762C. Equivalent lithologic formations on land are indicated. Values are from the Rock-Eval data listed in Table 4.

0–10 cm, -12H-5, 145–150 cm, -18H-1, 0–10 cm, and -18-5, 145–150 cm).

The Mg^{2+} concentration gradient observed in the upper 100 m of Site 762 (−10.7 mM/100 m) is greater than that below 106.9 mbsf, where it remains nearly constant (−4.5 mM/100 m) down to 770.9 mbsf. The larger gradient occurs within Subunits IA and IB, which consist primarily of calcareous ooze (see "Lithostratigraphy," this chapter). The reduced Mg^{2+} gradient observed between 106.9 and 770.9 mbsf corresponds with Subunits IC through IVC, which includes the transition from ooze to chalk with variable amounts of clay in the lower units (see "Lithostratigraphy," this chapter). In the deepest section, sampled between 796.4 and 916.9 mbsf (Gearle Siltstone through Barrow Group), no significant Mg^{2+} concentration gradient is observed. The overall observed gradient is attributed to carbonate diagenesis and has been observed at many DSDP sites (Gieskes, 1981).

In contrast to the relatively smooth downhole concentration profile exhibited by Mg^{2+}, the Ca^{2+} profile (Fig. 38) is characterized by numerous reversals. A slight but unexpected decrease from 10.7 to 9.7 mM is observed between 3.0 and 49.9 mbsf; this is followed by an increase to 12.8 mM at 193.5 mbsf. Between 193.5 and 344.0 mbsf Ca^{2+} remains nearly constant (12.8–12.2 mM). Below 372.4 mbsf a series of concentration reversals are observed, with the largest single downward increase (13.1–18.3 mM) occurring between 372.4 and 403.4 mbsf. Although additional fluctuations exist downhole, they decrease in magnitude, and there is an overall decreasing trend in dissolved Ca^{2+} with an average gradient of 0.51 mM/100 m between 422.4 and 916.9 mbsf.

The Ca^{2+} gradient between 49.9 and 193.5 mbsf (2.16 mM/100 m) is less than half that of Mg^{2+} in the same interval, indicating that a direct one-to-one ion exchange of Mg^{2+} for Ca^{2+} associated with carbonate diagenesis is not the only process taking place. From 193.5 to 344.0 mbsf the constant level of Ca^{2+} coincides with a near doubling of the dissolved-SiO_2 concentration and the appearance of zeolites and smectites in the sediments (Tables 7 and 8). We interpret this to reflect silica diagenesis. Between 403.9 and 569.9 mbsf (Subunit IIIB; see "Lithostratigraphy," this chapter), the irregular pattern displayed by Ca^{2+} is almost perfectly paralleled by SiO_2. The X-ray mineralogy of samples from this interval reveals abundant clay minerals, as well as the presence of opal-CT in Sample 122-762C-42X-5, 100–101 cm (Table 8).

The smooth downhole trend in the Mg^{2+}/Ca^{2+} ratio (Fig. 38), except for the deviations associated with the concentration spikes and reversals discussed above, suggests that their concentrations in the interstitial waters of Site 762 are influenced by carbonate diagenesis and that Ca^{2+} is also influenced, to lesser extent, by reactions related to the formation of smectite clays and zeolites.

Sulfate (SO_4^{2-})

The concentration of SO_4^{2-} decreases sharply from near-surface-seawater values (28.1 mM) at 3.0 mbsf to 17.6 mM at 99.4 mbsf, displaying a behavior similar to that of Mg^{2+} in the uppermost 100 m of Site 762. Between 106.9 and 372.4 mbsf, SO_4^{2-} reduction is less pronounced and its concentration decreases to 7.1 mM. A small increase in SO_4^{2-} occurs at 403.9 mbsf along with the previously mentioned sharp increases observed for other constituents. Between 424.4 and 479.9 mbsf the SO_4^{2-} concentration is nearly constant, but resumes its decline to 1.6 mM by 623.9 mbsf. Between this depth and 712.4 mbsf a small increase to 5.0 mM occurs, followed by a decrease to 1.8 mM by 770.9 mbsf, and nearly constant values to 916.9 mbsf.

The large SO_4^{2-} gradient of −10.9 mM/100 m in the upper 100 m of Site 762 (nearly identical to the Mg^{2+} gradient over this interval) suggests rapid consumption of SO_4^{2-} associated with the oxidation of organic matter in the calcareous oozes of Subunits IA and IB. The smaller gradient observed from 106.9 to 372.4 mbsf (−3.05 mM/100 m, also similar in magnitude to that of Mg^{2+} in the same depth range) may reflect the decreased fraction of organic matter remaining in the biogenic sediments downhole through Subunit IC, Unit II, and Subunit IIIA. There is no further evidence of SO_4^{2-} reduction in the clay-enriched sediments of Subunit IIIB, but it appears to resume somewhat in Subunit IVA. Below 770.9 mbsf (coinciding with the occurrence of predominantly clay-rich sediments), no further changes in SO_4^{2-} are observed although this

Table 5. Concentrations and compositions of low-molecular-weight hydrocarbons of selected samples from the lowermost portion of Hole 762C. Analyses were done with the Hewlett Packard 5890 Natural Gas Analyzer. Data from both flame ionization detection (FID) and thermal conductivity detection (TCD) of gas components are given. Concentrations are in parts per million (ppm) of headspace volume.

	Sample 122-762C-				
Conc. (ppm)	86X-4, 0–2 cm	89X-2, 0–2 cm	89X-5, 0–2 cm	90X-2, 0–2 cm	90X-4, 0–2 cm
FID:					
Methane	4618	710	426	35	589
Ethane	29	17	14	12	26
Propane	12	16	18	11	20
n-butane	6	4	6	4	8
Isobutane	—	7	8	6	5
n-pentane	—	—	9	—	9
C_1/C_2	159	41	26	3	23
TCD:					
Methane	3901	926	735	481	944
Ethane	38	30	18	19	32
Propane	17	13	19	12	24
CO_2	33245	21385	26563	13350	9984
C_1/C_2	102	31	40	26	26
CO_2/C_1	8.5	23.1	36.1	27.8	10.6

Table 6. Concentrations of low-molecular-weight hydrocarbons of samples from Holes 762B and 762C. Analyses were done with the Carle gas chromatograph. Data are from headspace samples. Concentrations are given in parts per million (ppm) of headspace volume.

Core, section, interval (cm)	Depth (mbsf)	C_1 (ppm)	C_2 (ppm)	C_1/C_2	Normalized
122-762B-					
1H-3, 0–5	3.00	2.9			
2H-7, 0–5	13.40	2.3			2
3H-5, 0–5	19.90	3.1			2
4H-6, 145–150	32.35	3.9			3
5H-5, 0–5	38.90	4.6			
6H-6, 0–5	49.90	4.0			3
7H-6, 0–5	59.40	5.0			
8H-6, 0–5	68.90	3.3			
9H-6, 0–5	78.40	5.5			
10H-6, 0–5	87.90	5.6			3
11H-6, 0–5	97.40	3.9			
12H-6, 0–5	106.90	5.4			
13H-6, 0–5	116.40	3.8			
14H-6, 0–5	125.90	3.7			2
15H-6, 0–5	135.40	5.0			
16H-6, 0–5	144.90	3.0			
17H-6, 0–5	154.40	4.0			
18H-5, 113–115	163.53	3.2			
19H-5, 0–3	171.90	4.2			
122-762C-					
2X-5, 0–2	176.00	4.6			
3X-3, 0–3	182.50	3.9			6
4X-4, 0–2	193.50	4.8			5
5X-2, 0–2	200.00	4.2			5
6X-6, 0–2	215.50	3.9			3
7X-4, 0–2	222.00	5.2			6
8X-4, 0–2	231.50	6.2			7
9X-1, 95–96	237.45	4.1			6
10X-4, 0–2	250.50	4.8			6
11X-5, 0–2	261.50	5.0			6
12X-5, 0–2	271.00	5.6			4
13X-2, 0–2	276.00	6.2			5
14X-6, 0–5	291.50	4.0			2
15X-3, 0–5	296.50	8.2			5
16X-3, 0–5	306.00	14.3			

Table 6 (continued).

Core, section, interval (cm)	Depth (mbsf)	C_1 (ppm)	C_2 (ppm)	C_1/C_2	Normalized
17X-5, 0–5	318.50	16.8			12
18X-6, 0–5	329.50	30.3			18
19X-4, 0–5	336.00	60.1			32
20X-3, 0–0	344.00	31.1			19
21X-2, 0–5	352.00	277.1			301
22X-6, 0–5	367.50	2083.1			1197
23X-3, 0–5	372.50	1311.9			994
24X-1, 0–5	379.50	1460.0			1404
25X-5, 0–5	394.50	3717.0			3319
26X-5, 0–5	404.00	2446.0	1.0	2446.0	3494
27X-4, 0–2	407.00	2315.0			3215
28X-1, 0–2	412.00	2209.0			2084
29X-3, 0–2	424.50	1812.0			1812
30X-3, 0–2	434.00	6533.0			4083
31X-5, 0–2	446.50	4470.0	0.6	7450.0	5198
32X-3, 0–2	453.00	7661.0	0.7	10944.2	8512
33X-5, 0–2	465.50	4996.0	0.7	7137.1	5809
34X-5, 0–2	475.00	13853.0	1.6	8658.1	
35X-2, 0–2	480.00	7334.0	1.7	4314.1	4584
36X-1, 0–2	488.00	9164.0	2.0	4582.0	5800
37X-4, 0–2	502.00	52414.0	4.6	11394.3	
38X-6, 0–2	514.50	9350.0	3.0	3116.6	5313
39X-5, 0–2	522.50	8616.0	2.5	3446.4	
40X-5, 0–2	532.00	2467.0	1.2	2055.8	3246
41X-5, 0–2	541.50	9407.0	1.8	5226.1	
42X-5, 0–2	551.00	28743.0	1.9	15127.8	
43X-4, 0–2	559.00	7989.0	0.9	8876.6	6887
44X-5, 0–2	570.00	4016.0			4016
45X-5, 0–5	579.50	5412.0	0.5	10824.0	6765
46X-4, 0–2	587.50	6095.0			7814
47X-6, 0–2	600.00	88821.0	3.0	29607.0	77913
49X-5, 0–2	617.50	85871.0	3.5	24534.5	84187
50X-3, 0–2	624.00	39511.0	2.5	15804.4	24092
51X-6, 0–2	638.00	8158.0	1.2	6798.3	8324
52X-6, 0–5	647.50	50123.0	2.9	17283.7	26381
53X-5, 0–5	655.50	86450.0	5.9	14652.5	56875
54X-6, 0–5	666.50	128396.0	13.0	9876.6	57320
55X-3, 0–5	671.50	56808.0	3.8	14949.4	45813
56X-5, 0–5	684.00	6537.0	1.2	5447.5	10214
57X-2, 0–5	689.00	8055.0	1.3	6196.1	5923
58X-5, 0–5	703.00	64755.0	4.4	14717.0	66077
59X-5, 0–5	712.50	42056.0	3.6	11682.2	51288
60X-3, 0–5	719.00	8365.0	1.6	5228.1	8043
61X-3, 0–5	728.50	73957.0	5.4	13695.7	102718
62X-5, 0–5	741.00	9126.0	1.9	4803.1	11129
63X-2, 0–5	746.00	80901.0	6.0	13483.5	73546
64X-4, 0–2	758.50	27332.0	2.8	9761.4	26796
66X-5, 0–2	771.00	18742.0	2.7	6941.4	24661
67X-1, 0–2	770.00	41054.0	3.7	11095.6	44624
68X-1, 0–2	775.00	22628.0	2.7	8380.7	23571
69X-2, 0–2	781.50	9123.0	2.2	4146.8	6516
70X-1, 0–2	785.00	9556.0	2.0	4778.0	13651
71X-2, 0–2	791.50	49874.0	4.6	10842.1	44530
72X-2, 0–2	796.50	33402.0	3.5	9543.4	32747
73X-3, 0–2	802.50	98904.0	9.4	10521.7	83817
74X-2, 0–2	806.00	60343.0	5.5	10971.4	50286
75X-2, 0–2	811.00	3996.0	1.3	3073.8	6055
76X-3, 0–2	817.50	794.0	2.4	330.8	3970
77X-3, 0–2	822.50	6324.0	1.5	4216.0	10200
77X-7, 0–2	828.50	1041.0			1157
78X-2, 0–2	830.50	8409.0	2.3	3656.0	11364
79X-3, 0–2	841.50	7637.0	3.3	2314.2	10320
81X-3, 0–2	851.50	1005.0	2.3	436.9	1523
83X-1, 0–2	858.50	9815.0	13.3	737.9	6373
84X-1, 0–2	863.50	6697.0	18.1	370.0	5489
85X-1, 148–150	874.48	1120.0	11.0	101.8	836
86X-4, 0–2	887.00	3277.0	30.8	106.3	3344
87X-2, 0–2	893.50	72.2	0.8	90.2	41
88X-6, 0–2	909.00	472.1	8.6	54.8	874
89X-2, 0–2	912.50	719.0	12.4	57.9	972
89X-5, 0–2	917.00	701.0	14.2	49.3	1062
90X-2, 0–2	922.00	781.0	26.6	29.3	868
90X-4, 0–2	925.00	688.0	23.7	29.0	905
91X-2, 0–2	931.50	1407.0	26.8	52.5	2010

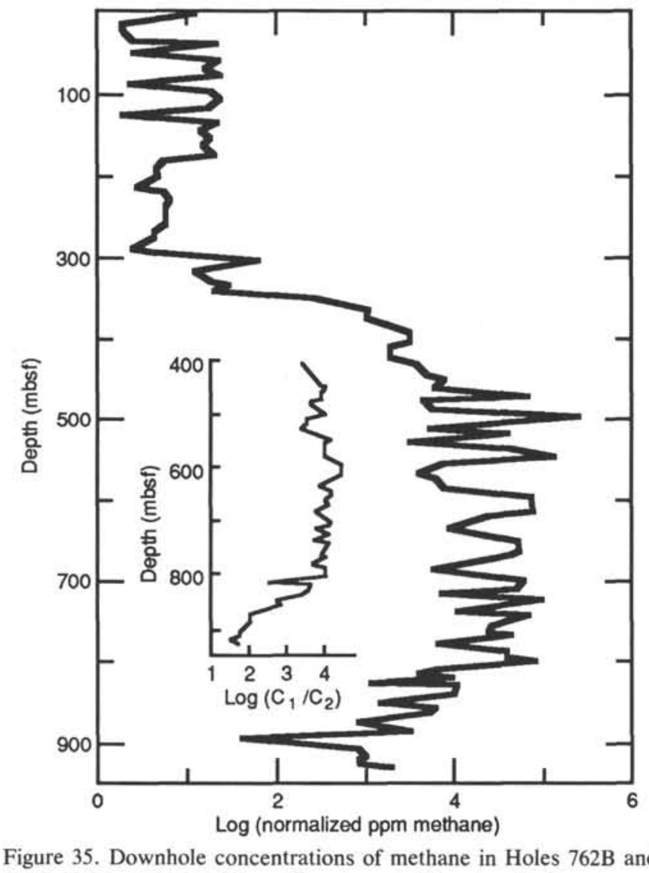

Figure 35. Downhole concentrations of methane in Holes 762B and 762C, in base ten logarithms of parts per million (ppm) of headspace volume. Inset shows C_1/C_2 ratios of headspace samples from Table 6, also in logarithmic notation.

constituent is incompletely depleted (approximately 93%) relative to seawater.

Silica (SiO_2)

Silica concentrations at Site 762 vary considerably with depth (Fig. 38). Between 3.0 and 19.9 mbsf dissolved SiO_2 remains near 1.0 mM, drops sharply to 0.4 mM at 49.9 mbsf, then remains nearly constant to 135.4 mbsf. Between 135.4 and 193.5 mbsf a sharp increase to 1.8 mM occurs. Below this depth and down to 569.9 mbsf, SiO_2 ranges between 1.3 and 1.8 mM except at 403.9 mbsf, where a maximum concentration of 2.4 mM is observed. The latter corresponds to the previously discussed spikes in other dissolved constituents. From 599.9 to 916.9 mbsf, SiO_2 ranges between 0.3 and 0.9 mM; within this interval two series of regular increases are observed. The first occurs between 685.4 and 770.9 mbsf (0.4–0.9 mM) and the second between 796.4 and 916.9 mbsf (0.3–0.6 mM).

The sharp dissolved-SiO_2 decrease at 49.9 mbsf from near-mudline high concentrations is reminiscent of Site 761 and is also consistent with the disappearance of radiolarians over this interval (Core 122-762B-2H to -4H; see "Biostratigraphy," this chapter) resulting from early-diagenetic dissolution of opaline silica. The first SiO_2 maximum observed at 193.5 mbsf coincides with a zone in which the abundance of radiolarians peaks. Subsequent downhole variations are difficult to relate directly to siliceous organisms but are probably associated with mobilization of SiO_2 and reprecipitation of authigenic silica. The sediments in the broad interval (193.5–569.9 mbsf) over which SiO_2 concentrations fluctuate are of early Paleocene to middle Eocene age (see "Biostratigraphy," this chapter); Riech and von Rad (1979) have suggested that silicification by precipitation of opal-CT (intermediate diagenesis) often occurs during this period. The presence of opal-CT in Sample 122-762C-42X, 100–101 cm (Table 8), supports this hypothesis.

Although dissolved SiO_2 concentrations remain high in the interval discussed above, this is not inconsistent with the proposed mechanism as there is ample evidence from DSDP sites that high concentrations persist after the precipitation of opal-CT (Gieskes, 1981). Below 403.9 mbsf, uptake of SiO_2 into authigenic clays should result in lower dissolved concentrations of SiO_2 (Kastner and Gieskes, 1976). Indeed, we observed a decreasing trend that corresponds to the greater downhole abundance of clays (Table 8) in sediments from Subunits IIIB and IVA. However, only presently active diagenetic transformations and not fossilized diagenetic transformations (e.g., clinoptilolite possibly formed 50 m.y. ago) are likely to be reflected in the pore-water chemistry. Despite the increased abundance of clays the SiO_2 concentrations remain relatively high, in agreement with observations by Gieskes (1981) that only after diagenetic reactions have led to the complete conversion of opal-CT to quartz do SiO_2 concentrations drop significantly. Below 599.9 mbsf the lower SiO_2 concentrations and the presence of primarily detrital silicates (see "Lithostratigraphy," this chapter, and Table 8) suggest that no further silicification reactions occur. The lowest concentrations at the bottom of the hole reflect the mineralogy of terrigenous Barrow Group equivalent sediments dominated by resistant crystalline detrital silicates (Table 8).

Salinity and Chlorinity

Chloride concentrations at Site 762 remain essentially constant (555–560 mM) for the first 480 m (Fig. 38), exhibit a very slight drop to 552 mM by 479.9 mbsf, then decrease progressively downhole. The onset of the Cl^- concentration drop coincides approximately with the Cretaceous/Tertiary boundary at 554.3 mbsf, and an average gradient of −8.1 mM/100 m is observed between 569.9 and 796.4 mbsf in the clay-rich nannofossil chalks of Subunits IVA, IVB, and IVC . A sharp decrease in Cl^- occurs between 796.4 and 857.9 mbsf coinciding with the Gearle Siltstone and Muderong Shale equivalents of Subunits IVD, IVE, and Unit V (see "Lithostratigraphy," this chapter). Because poor sediment recovery and special sampling interests did not permit whole-round core sampling for interstitial waters, we are unable to determine precisely where in the sedimentary column the sharp Cl^- concentration drop actually occurs. The next interstitial-water sample (122-762C-82X, 140–150 cm) was well within the silty claystones of the lower Barrow Group equivalent, and the low Cl^- content suggests lateral transport of low-salinity water from the Australian continent at depth within the sediment. Similar occurrences of low-salinity waters and even freshwater have been previously reported in other DSDP sites such as Site 241 (offshore of Somaliland), where freshwater was observed approximately 300 km from shore (Gieskes, per. comm., 1989).

Salinity changes at Site 762 (Fig. 38) are similar to the Cl^- variations described above, except that the decrease in salinity begins immediately below the mudline and primarily reflects the depletion of Mg^{2+} and SO_4^{2-} in the sediments (Gieskes, 1974). The near-seawater salinity of 35.5 g/kg decreases progressively to 30.5 g/kg at 796.4 mbsf with an average gradient of −0.64 g/kg/100 m. A few small fluctuations in the generally steady decrease are observed, but probably are not significant. An exception occurs between

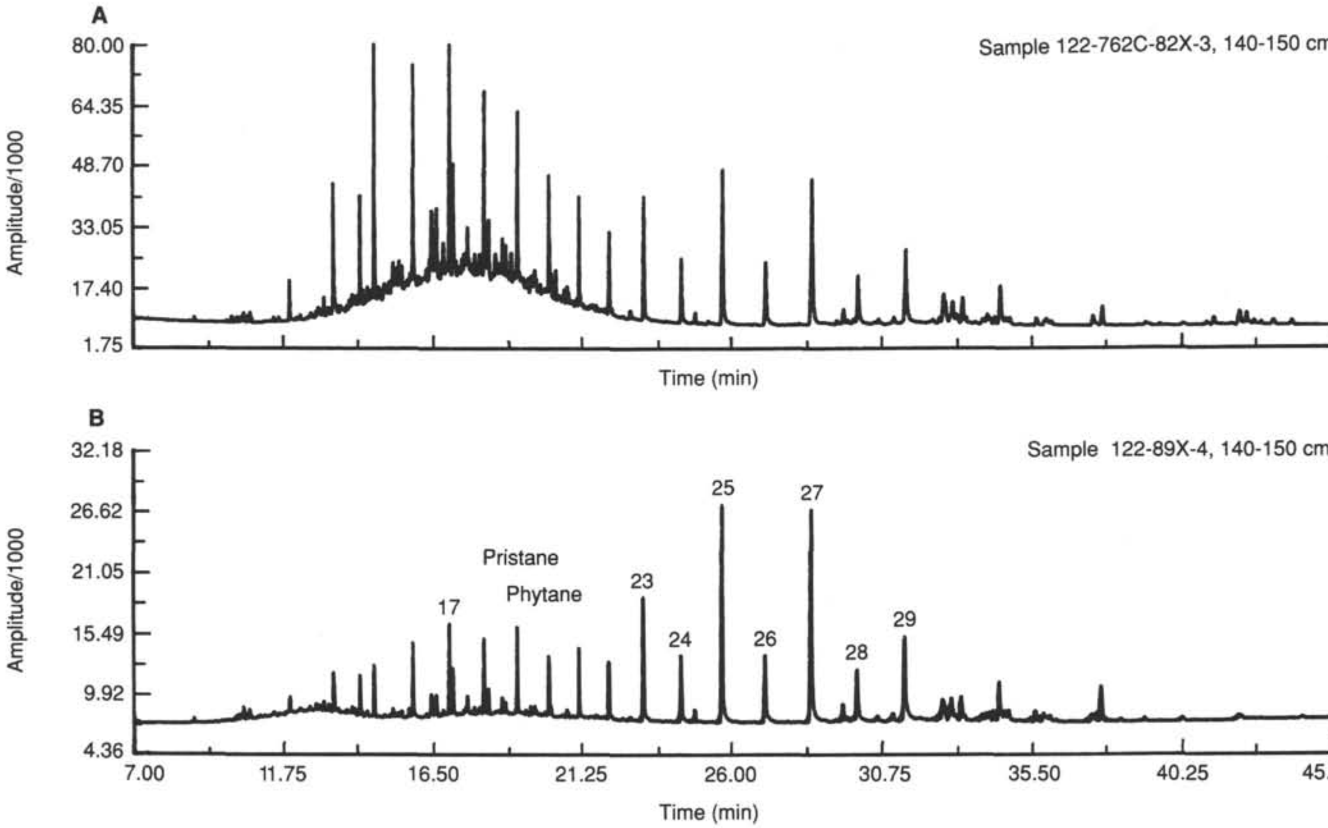

Figure 36. Chromatograms of extracted saturated hydrocarbon fractions. Straight-chain components are identified by the number of their carbon atoms. Vertical axis is flame ionization detector response and horizontal axis is chromatographic elution time increasing to the right. **A.** Sample 122-762C-82X-3, 140–150 cm. **B.** Sample 122-762C-89X-4, 140–150 cm.

318.5 and 403.9 mbsf, which reflects the previously discussed sharp increase in other dissolved constituents observed at the latter depth. The salinity minimum of 28.2 g/kg is reached at 857.9 mbsf in the sediments of the lower Barrow Group equivalent. Salinities below 31 g/kg generally do not result only from the depletion of Mg^{2+} and SO_4^{2-} and suggest seawater diluted by freshwater input (Gieskes, 1981). The low Cl^- concentrations observed near 900 mbsf support this hypothesis.

Alkalinity and pH

The alkalinity of interstitial waters in the upper 100 m of the sediments at Site 762 is approximately 50%–60% higher than surface seawater (Table 7 and Fig. 38); it then increases gradually to values between 4.0 and 4.5 mM by 156.4 mbsf and remains within this range down to 372.4 mbsf. A large spike in alkalinity occurs at 403.9 mbsf, below which it returns to the former range down to a depth of 599.9 mbsf. Below this depth the alkalinity varies between 2.0 and 2.9 mM. A sharp rise is also observed at 886.9 mbsf in sediments from the Barrow Group where the alkalinity reaches 6.6 mM. There are, however, no other data within the Barrow Group sediments and thus interpretation of this value is difficult. The first large alkalinity spike (403.9 mbsf) occurs in conjunction with increases in Ca^{2+}, SiO_2, SO_4^{2-}, and salinity, and a decrease in pH and Mg^{2+}. The second, however, is not associated with such widespread changes in other dissolved constituents.

Interstitial waters from Site 762 are characterized by pH values that range from 7.15 to 7.65, except for one sample (122-762C-26X-4, 140–150 cm), in which the pH drops to 6.90 (Fig. 38). Values generally drop from the surface value of 8.27 to 7.65 at 3.0 mbsf. They subsequently continue to decrease slightly downhole, except as noted above and between 655.4 and 685.4 mbsf coinciding with the last increase in SiO_2 just above the Gearle Siltstone equivalent. Alkalinity and pH generally mirror each other in the sediments of Site 762.

X-Ray Diffraction Analysis (XRD)

Bulk XRD studies were performed on the majority of squeeze cakes (28 samples) from Site 762 and other samples (8 samples) of interest to shipboard sedimentologists (Table 8). The mineralogy of Site 762 is dominated by calcite, in agreement with lithologic observations (see "Lithostratigraphy," this chapter). Trace to minor amounts of detrital minerals, such as chlorite, illite, smectite, and quartz (possibly of eolian origin) are found throughout the entire sedimentary sequence. Samples recovered between 193.5 and 569.9 mbsf also contain significant amounts of authigenic clinoptilolite and occasionally opal-CT, in addition to calcite and small amounts of detrital minerals. Between 599.9 and 796.4 mbsf only calcite and minor amounts of detrital minerals are found. Sediments of the Barrow Group equivalent reveal their terrigenous origin in the predominance of quartz, with kaolinite, feldspar, pyrite, smectite, and illite present in varying concentrations. Dolomite, which was reported by the sedimentologists, has not been found in the samples from Unit VI analyzed to date. This, however, does not preclude its presence because only the squeeze cakes from this section were studied and specific occurrences of apparently unusual mineralogy were not examined.

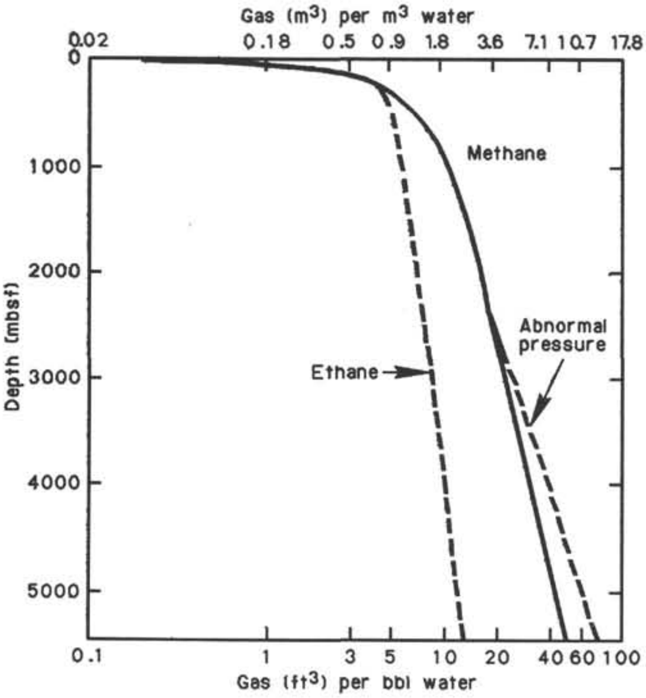

Figure 37. The solubility of methane and ethane in distilled water with depth assuming a pressure gradient of 0.46 psi/ft and a geothermal gradient of 1.5°F/100 ft (2.7°C/100 m). Salinities around 35 g/kg would reduce solubilities 10%–20%, depending on temperature. Abnormal pressure line calculated at 0.7 psi/ft and a geothermal gradient of 2°F/100 ft (3.65°C/100 m) starting at 7000 ft (2134 m). To convert ft^3/bbl to ppm, multiply by 127. To convert ft^3/bbl to mol fraction methane, divide by 7370. Data from Culberson and McKetta, 1951; figure modified from Hunt, 1979.

Conclusions

The chemistry of the interstitial waters of Site 762 is affected by diffusion processes throughout the unconsolidated carbonate oozes. Evidence of carbonate diagenesis and silica diagenesis is found in the Mg^{2+}, Ca^{2+}, and SiO_2 profiles of the upper 200 m of the sedimentary column. Below this depth diffusion processes are weaker and interstitial fluids appear to maintain compositions that reflect the local lithology. Sulfate reduction takes place down to 600 mbsf; thereafter no further depletion is observed. The mineral composition of sediments below 800 mbsf is characteristic of the input of terrigenous sediments and suggests a nearshore deltaic environment.

PHYSICAL PROPERTIES

Introduction

The physical properties measured on sediments from Site 762 on the Exmouth Plateau include compressional wave velocity, velocity anisotropy, thermal conductivity, and the index properties (bulk density, grain density, porosity, and water content) (see "Explanatory Notes" chapter, this volume). Two holes were drilled at this site. Hole 762B was drilled with the advanced piston corer (APC) to 175.4 mbsf. Hole 762C was washed down to 170.0 mbsf and drilled to 940.0 mbsf using the extended core barrel (XCB). Core recovery was excellent (average = 99.7%) with the APC, and thus it was possible to conduct all the physical-properties measurements to the bottom of Hole 762B with the exception of shear strength, which was discontinued at 127 mbsf due to brittle failure of the sediment. In Hole 762C, the sediment became progressively firmer, so only velocity and index properties could be measured below 380 mbsf. Both the GRAPE and the *P*-wave logger were used throughout Hole 762B, and the GRAPE was used for Hole 762C down to 293 mbsf (Core 122-762C-14X). The values of the various physical properties are listed in Tables 9 to 11 and their trends with depth are illustrated in Figure 39.

Velocity

The mean compressional velocity data from Site 762 (determined with the Hamilton Frame; Fig. 39) show a range from 1.52 to 3.56 km/s, with only four samples having velocities >2.8 km/s. There are two high-velocity samples: a 4.46-km/s chert at 210 mbsf (Section 122-762C-6X-2) and a 5.0-km/s limestone at 856 mbsf (Section 122-762C-82X-2), which are plotted off the figure as they do not represent a large percentage of the cored material. The relatively small velocity range is a result of the lack of highly lithified, high-velocity sandstones and limestones at Site 762, and is in stark contrast to the velocity data of Sites 759, 760, and 761 (Wombat Plateau), which display a large velocity range.

The general lithologies are mainly oozes at the top of the hole to about 350 mbsf, chalks down to about 840 mbsf, and clastics (shales and claystones) to the bottom of the hole at 940 mbsf. The oozes and claystones have relatively constant velocities (about 1.55 and 1.9 km/s, respectively). The chalk velocities are also within a narrow range (1.7–2.3 km/s) from about 450 mbsf until just above the Cretaceous/Tertiary boundary interval (554 mbsf), where there is a local velocity increase (from about 2.0 to 2.5 km/s). It is interesting to note that the chalks between about 600 to 700 mbsf exhibit a velocity decrease from about 2.3 to about 1.8 km/s as velocities usually increase with depth within the same lithology. Velocity then increases again to about 2.5 km/s (with two samples of 3.5 km/s at 808 mbsf) just before the chalk/clastic contact. Anisotropy in the velocity measurements (Fig. 39) is mostly positive and shows no consistent trend with depth.

Index Properties

Grain densities (Fig. 39) are relatively constant throughout the hole (about 2.68 g/cm^3), although some scatter is evident. One noted departure from the average grain density is a porcelaneous chert sample at 210 mbsf with a density of 2.2 g/cm^3, similar to the grain density of opal-CT. Bulk densities (Fig. 39) in the oozes increase relatively linearly with depth until about 320 mbsf. Between 320 mbsf and the first measurement on chalks at 360 mbsf, the wet-bulk density increases from 1.80 to 2.12 g/cm^3, a change not reflected by either the velocity data or any of the other index properties. Bulk density is generally constant at about 2.12 g/cm^3 from around 400 to 770 mbsf. Again, this trend is not evident in velocity or the other index properties. Below 770 mbsf, there is an increase in density to about 2.5 g/cm^3 with a corresponding increase in the velocity data. At the chalk/claystone contact (840 mbsf), wet-bulk density decreases sharply to a value of about 2.25 g/cm^3 in the underlying claystones. The decrease in velocity between about 600 and 700 mbsf is not clearly reflected in the bulk-density data.

Porosity and water-content values (Fig. 39) show good correlation throughout the borehole and an inverse correlation with velocity. Porosities are 74.3% at the top of the hole, and decrease nonlinearly to about 60% at about 100 mbsf. Porosity remains approximately constant at this level, although water content drops linearly down to the ooze/chalk contact. Porosity and water content decrease sharply in the chalks. Both properties decrease down to about 488 mbsf, and are relatively constant to

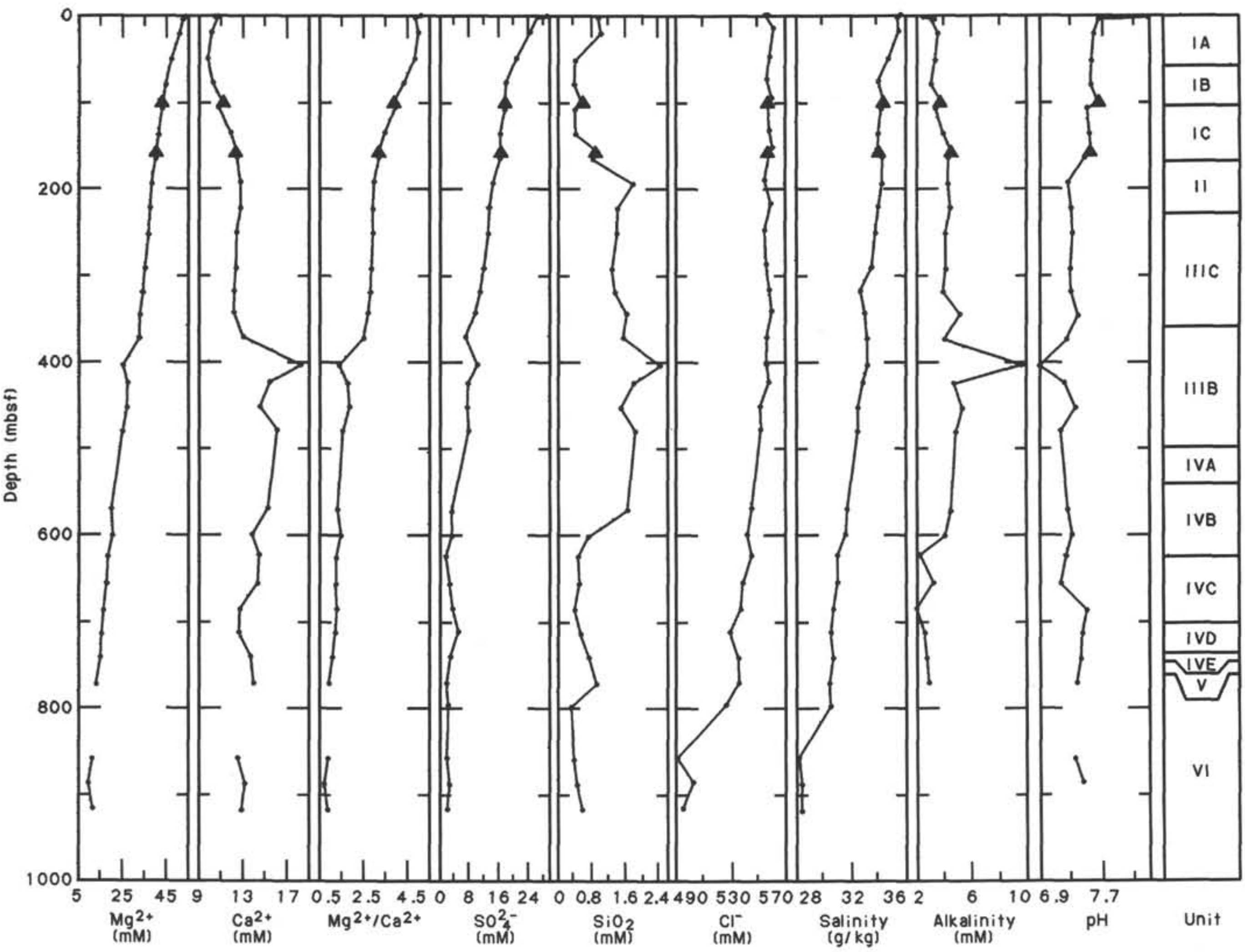

Figure 38. Interstitial water analyses plotted according to depth (mbsf), Site 762. Solid triangles indicate *in-situ* pore-water samples.

about 600 mbsf, although the data show some scatter. The data then gradually increase to about 700 mbsf. The increase of porosity and water content with depth between 600 and 700 mbsf is unusual as these properties usually decrease with depth within the same lithology in response to compaction. Porosity and water content sharply decrease below around 770 mbsf down to the chalk/claystone contact at about 840 mbsf, where they sharply increase again. Below this depth, porosity and water content gradually decrease.

Thermal Conductivity

Thermal conductivity (Fig. 40) was measured throughout Hole 762B and in Hole 762C to 373 mbsf, below which the sediments were too rigid to allow insertion of the temperature probes. The values display a general trend of increasing conductivity with depth, ranging from 1.033 W/m·K at the top of the hole to 1.804 W/m·K at 371.3 mbsf. This trend can be explained by a decrease in porosity and water content with depth, as previously described.

Formation Factor

Formation factor (Fig. 40) was measured in samples from Hole 762B and down to 345 mbsf in Hole 762C. Below this depth, the sediment became so resistive that no reading was registered by the instruments. Formation factor measured horizontally (perpendicular to the core axis) was generally higher than the formation factor measured vertically (parallel to the core axis). Values of formation factor show a generally increasing trend with depth, although there is some scatter in the data and three local maxima appear in the data at about 140, 170, and 320 mbsf. These local maxima correspond to small peaks in the wet-bulk-density and index-property data at the same depths.

Shear Strength

Shear strength (Fig. 40) was measured only in Hole 762B down to 95 mbsf. Below this depth, the sediment underwent brittle failure. Unfortunately, as there are not many data points and the data are scattered, no interpretation can be made.

GRAPE AND *P*-WAVE LOGGER

The *P*-wave logger data were collected from cores of Hole 762B (Fig. 41). Before the data were processed, there was a sharp velocity increase of 0.12 km/s at 50 mbsf that resulted from a mechanical malfunction in the *P*-wave logger. Therefore, a constant of 0.12 km/s was subtracted from all the *P*-wave logger data below 50 mbsf. The velocities are offset with respect to the Hamilton Frame velocities by about 0.1 km/s. This is also true for the *P*-wave logger velocities

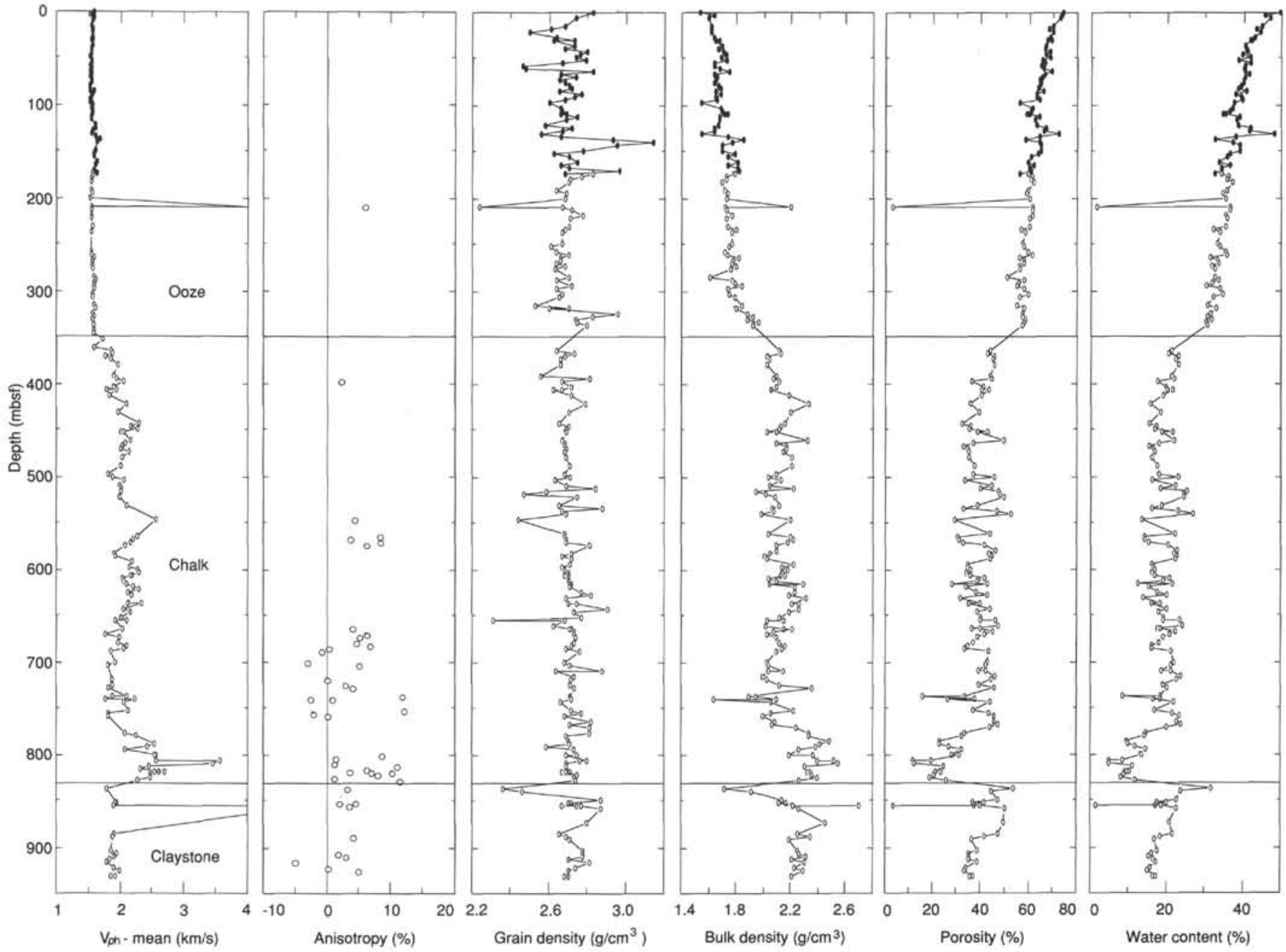

Figure 39. Physical-property data, Site 762 (mean compressional velocity, velocity anisotropy, grain density, bulk density, porosity, and water content). Solid symbols = Hole 762B; open symbols = Hole 762C. The major lithologies are indicated.

collected at Site 763. This offset may be the result of a calibration error in the *P*-wave logger; the Hamilton Frame was calibrated about every other day, but the *P*-wave logger was calibrated infrequently.

Owing to a calibration error, the GRAPE data for Site 762 are offset by exactly by 0.2 g/cm^3 from the data collected bygravimetric methods on individual samples. The GRAPE data from Hole 762B are also 0.2 g/cm^3 less than the GRAPE data from Hole 761B, although the lithology for both holes is mostly the same (nannofossil ooze). Because of these two circumstances, and because the GRAPE data from Sites 760 and 761 exactly coincide with the gravimetric data, we believe that it is valid to add 0.2 g/cm^3 to all the GRAPE data collected for Site 762.

The GRAPE data agree well with the gravimetric data in terms of magnitude and small variations between each measurement (Fig. 41). This is illustrated in the local minimum at 130 mbsf and the local maximum at 140 mbsf for both data sets. There is also a local maximum and minimum in the formation-factor data at the same depths. These perturbations of the properties at these depths correspond to a depositional hiatus at approximately 133 mbsf (see "Biostratigraphy," this chapter). There is a decrease in velocity just above the hiatus, and an increase in velocity just below. This is the same trend observed in the velocity record of Site 760 above and below the manganese crust in Sections 122-760A-9H-4 to -10H-1 (about 80 mbsf).

GRAPE data were also collected from cores of Hole 762C down to 293 mbsf (Fig. 41). As Hole 762C was cored using the XCB, the material was more disturbed than that of Hole 762B; thus the GRAPE data for Hole 762C show almost twice as much scatter as the data from Hole 762B. With the 0.2-g/cm^3 correction added, the GRAPE data agree almost exactly with the gravimetric data.

Heat Flow

Two temperature-probe measurements were conducted in Hole 762B, at 99.4 and 156.4 mbsf, with a calm sea state prevailing. At 99.4 mbsf, the probe stayed at the mudline for 5 min on both the ascent and descent, and remained on the bottom for 33 min. At 156.4 mbsf, the probe stayed at the mudline for 5–7 min on both the ascent and descent, and remained on the bottom for 30 min.

The bottom temperature at 99.4 mbsf was 14.5°C and at 156.4 mbsf was 15.4°C (Fig. 42). Both temperature values were characterized by an increase in temperature after insertion, followed by another increase that slowed toward an equilibrium value. This behavior is unusual for an area of normal continental heat flow. However, both measurements repeated the same increasing pattern and began to converge toward an equilibrium value; the results have thus been used to generate a temperature gradient of 100.4°C/km to 99.4 mbsf

Table 7. Composition of interstitial water, Site 762.

Core, section, interval (cm)	Depth (mbsf)	Vol. (cm^3)	pH	Alk. (mM)	Sal. (g/kg)	Mg^{2+} (mM)	Ca^{2+} (mM)	Mg^{2+}/Ca^{2+}	Cl^- (mM)	SO_4^{2-} (mM)	SiO_2 (mM)
122-762B-											
Surface seawater	0.0	100	8.27	2.506	35.6	53.6	10.5	5.13	557	29.3	0.043
1H-2, 145–150	3.0	25	7.65	3.326	35.5	52.3	10.7	4.88		28.1	0.972
1H-2, 145–150	3.0	50	7.65	3.152	35.4	52.4	10.7	4.89	555	26.7	0.963
3H-4, 145–150	19.9	50	7.59	3.563	35.5	50.8	10.1	5.02	561	24.6	1.022
6H-5, 145–150	49.9	45	7.55	3.354	34.7	47.1	9.7	4.83	558	20.8	1.412
9H-5, 145–150	78.4	40	7.55	3.088	34.0	44.7	10.3	4.35	556	18.2	0.392
12H-1, 0–10[a]	99.4	70	7.64	3.818	34.4	43.0	11.1	3.88	560	17.6	0.582
12H-5, 145–150	106.9	30	7.50	3.389	34.2	42.9	10.8	3.98	557	17.7	0.407
15H-5, 145–150	135.4	35	7.53	3.981	34.0	41.5	11.9	3.49	558	16.5	0.433
18H-1, 0–10[a]	156.4	70	7.55	4.531	34.0	40.1	12.4	3.23	560	16.4	0.935
18H-5, 145–150	163.9	30	7.47	4.328	34.3	39.9	12.5	3.21	558	16.3	0.832
122-762C-											
4X-3, 145–150	193.5	25	7.26	4.336	34.3	38.4	12.8	3.00	555	14.4	1.787
7X-3, 145–150	222.0	35	7.30	4.476	34.0	37.5	12.8	2.93	559	13.4	1.412
10X-4, 145–150	252.0	35	7.32	4.128	33.8	36.9	12.5	2.96	555	13.2	1.399
14X-5, 145–150	291.5	28	7.29	4.140	33.5	35.3	12.4	2.85	556	11.9	1.280
17X-4, 145–150	318.5	24	7.30	3.959	32.7	34.4	12.2	2.81	558	11.0	1.358
20X-2, 145–150	344.0	28	7.39	5.165	33.0	32.9	12.2	2.70	560	9.6	1.636
23X-2, 140–150	372.4	17	7.25	4.092	33.2	32.9	13.1	2.52	556	7.1	1.558
26X-4, 140–150	403.9	34	6.90	9.638	33.2	25.3	18.3	1.38	556	10.2	2.427
29X-2, 140–150	424.4	19	7.22	4.734	32.9	27.6	15.4	1.79	558	7.7	1.806
32X-2, 140–150	452.9	15	7.36	5.372	32.5	27.1	14.6	1.87	552	7.4	1.500
35X-1, 140–150	479.9	13	7.17	4.901	32.5	25.2	16.1	1.56	552	7.9	1.847
44X-4, 140–150	569.9	34	7.26	4.473	31.7	19.9	15.3	1.31	545	3.1	1.655
47X-5, 140–150	599.9	28	7.32	4.084	31.6	20.6	13.8	1.49	542	3.3	0.733
50X-2, 140–150	623.9	9	7.24	2.242	31.0	18.5	14.5	1.28	545	1.6	0.485
53X-4, 140–150	655.4	11	7.17	3.220	31.0	17.9	14.3	1.25	539	2.7	0.513
56X-5, 140–150	685.4	29	7.50	2.009	30.7	16.5	12.7	1.29	537	3.5	0.405
59X-4, 140–150	712.4	34	7.44	2.579	30.5	15.4	12.6	1.22	529	5.0	0.539
62X-4, 140–150	740.9	20	7.42	2.745	30.7	15.0	13.7	1.09	536	2.9	0.741
66X-4, 140–150	770.9	30	7.37	2.879	30.4	13.0	14.0	0.93	536	1.8	0.920
72X-1, 140–150	796.4	0.5			30.5				527	2.3	0.323
82R-3, 140–150	857.9	3	7.35		28.2	11.3	12.6	0.90	491	1.9	0.386
86X-3, 140–150	886.9	9	7.45	6.610	28.4	9.4	13.2	0.71	503	2.6	0.459
89X-4, 140–150	916.9	5			28.4	11.7	12.9	0.91	495	2.1	0.588

[a] *In-situ* pore-water sample obtained during downhole heat-flow measurements.

and 72.9°C/km to 156.4 mbsf (Fig. 43). Using thermal-conductivity measurements of 1.33 W/m·K (averaged over the upper 150 m of Hole 762B) heat flow was determined (Garland, 1979) as 129.8 mW/m^2 and 96.9 mW/m^2, respectively. These values are anomalously high for sediments above stable continental crust or Mesozoic ocean crust (Sclater et al., 1981). Further work is required to determine the validity of the Site 762 temperature data and to establish whether an unusual heat-flow pattern exists on the southwest Exmouth Plateau. See "Physical Properties," Site 763 chapter (this volume), for a summary of Leg 122 heat-flow results.

Discussion

The oozes and claystones of Site 762 have physical properties that do not vary greatly with depth. The physical properties of the chalks, however, are quite unusual, especially in the interval between approximately 600 and 700 mbsf (Subunit IVB), where the velocities *decrease* and the porosities *increase* with increasing depth. $CaCO_3$ content over this interval increases (see "Organic Geochemistry," this chapter), and smear-slide data indicate that the detrital quartz content decreases over this interval as well. This line of evidence suggests that the velocity decrease between 600 and 700 mbsf may be the result of an increase of porosity caused by the increased abundance of hollow, biogenic grains in the sediment. Future shore-based SEM work is needed to test this hypothesis.

The perturbation of physical properties above and below the depositional hiatus at around 133 mbsf is another observation that needs explanation. The sediment type seems to be the same above and below the hiatus (foraminifer nannofossil ooze). The same perturbation is seen near the manganese horizon (also a sedimentary hiatus) in Site 760 (about 80 mbsf). Though the hiatus and manganese horizon are not related chronologically, the variation in properties above and below these events probably have the same cause. Therefore it is suggested that the high bulk-density values below the hiatus at Site 762 are the result of additional water loss from the sediments during a period of nondeposition, and the low bulk-density values above the hiatus are caused by overpressuring (resulting from a rapid sedimentation rate). XRD work would be useful over this interval to determine if a significant mineralogical change is present, because smear-slide data indicate no such change.

SEISMIC STRATIGRAPHY

Introduction

The location for Site 762 was chosen using petroleum-industry multichannel-seismic-reflection data collected for Esso Exploration Ltd. in 1978 and 1979 and used in locating the Eendracht-1 well. The detailed industry seismic-reflection data was used in selecting the location of Site 762 because of the safety concerns regarding scientific drilling in a region of known substantial gas occurrence. The quality of the data was good and a number of strong regional reflectors were recorded in the Tertiary and Cretaceous section of Line X79B-1425, where Site 762 was located. This is consistent with the generally good quality of seismic-reflection data collected in the area. Site 762 was located on the central eastern Exmouth Plateau in an area of

Table 8. X-Ray mineralogy of Exmouth Plateau sediments.

Core, section, interval (cm)	Treatment[a]	Mineral phases present Major	Minor[b]
122-762B-			
3H-4, 145	UBN	Calcite	Smectite, illite, chlorite, (quartz)
6H-5, 145	UBN	Calcite	Quartz, pyrite, illite, chlorite
8H-2, 53	UBN	Calcite	Quartz
9H-5, 145	UBN	Calcite	Illite, chlorite, quartz
12H-5, 145	UBN	Calcite	Illite, chlorite, quartz
15H-5, 145	UBN	Calcite	Quartz, (illite, chlorite)
18H-5, 145	UBN	Calcite	Quartz, clinoptilolite, smectite, chlorite
122-762C-			
4X-3, 145	UBN	Calcite	Clinoptilolite, (quartz)
7X-3, 145	UBN	Calcite	Clinoptilolite, illite, smectite, quartz
10X-3, 145	UBN	Calcite	Illite, clinoptilolite, (quartz)
14X-5, 145	UBN	Calcite	Clinoptilolite, quartz
17X-4, 145	UBN	Calcite	Clinoptilolite, (quartz, smectite)
20X-2, 145	UBN	Calcite	Clinoptilolite, smectite, (quartz)
23X-2, 145	UBN	Calcite	Clinoptilolite, smectite, (quartz, feldspar)
26X-4, 140	UBN	Calcite	Clinoptilolite, smectite, illite, (quartz)
29X-2, 140	UBN	Calcite	Clinoptilolite, smectite, (quartz)
32X-2, 140	UBN	Calcite	Clinoptilolite, (quartz, smectite)
35X-1, 140	UBN	Calcite	Clinoptilolite, (quartz, smectite)
42X-5, 100	UBN	Calcite	Opal-CT, smectite, sepiolite?, quartz, (clinoptilolite)
42X-6, 110	UBN	Barite	Smectite
44X-4, 140	UBN	Calcite	(Clinoptilolite, quartz, smectite, feldspar)
47X-5, 140	UBN	Calcite	(Quartz, sepiolite)
50X-3, 140	UBN	Calcite	Quartz, (smectite, illite)
52X-6, 108	UBN	Calcite	Quartz, (smectite, illite, chlorite)
53X-4, 140	UBN	Calcite	Quartz, (smectite, illite, chlorite)
56X-5, 140	UBN	Calcite	Quartz, (smectite, illite, chlorite)
59X-4, 140	UBN	Calcite	(Quartz, smectite)
62X-4, 140	UBN	Calcite	(Quartz, smectite, illite)
66X-4, 140	UBN	Calcite	(Smectite, quartz)
72X-1, 140	UBN	Calcite	Quartz, smectite, (illite, feldspar)
73X-5, 17	UBN	Smectite	Calcite
77X-2, 4	UCN	Smectite, illite	Calcite, quartz
77X-2, 4	USN	Calcite, quartz	Illite
77X-2, 52	OCN	Smectite, illite	Calcite, quartz
77X-2, 52	USN	Calcite	Quartz, illite, (smectite)
82X-3, 140	UBN	Quartz, pyrite	Chlorite, feldspar, diopside?, illite, smectite
86X-3, 140	UBN	Quartz, chlorite, illite	Feldspar, pyrite, smectite, diopside?
89X-2, 0	UBN	Quartz, chlorite, illite	Pyrite, feldspar, diopside?, smectite
122-763A-			
1H-2, 145	UBN	Calcite	Quartz, (kaolinite)
2H-4, 145	UBN	Calcite	Quartz
3H-4, 145	UBN	Calcite	Quartz
4H-4, 145	UBN	Calcite	Quartz, (kaolinite)
7H-4, 145	UBN	Calcite	Quartz, illite, kaolinite, (feldspar)
9H-3, 70	OBN	Calcite	Quartz, chlorite, illite, smectite
9H-4, 140	UBN	Calcite	Quartz, illite, kaolinite
9H-5, 141	OBN	Calcite	Quartz, chlorite, illite, smectite
10H-4, 145	UBN	Calcite	Clinoptilolite, quartz
16H-4, 145	UBN	Calcite	Quartz, (illite)
122-763B-			
3X-4, 145	UBN	Calcite	Clinoptilolite, quartz
6X-4, 145	UBN	Calcite	Quartz
9X-4, 145	UBN	Calcite	Quartz, illite, kaolinite
10X-3, 140	UBN	Calcite	Quartz, smectite, illite
12X-3, 140	UBN	Calcite	(Quartz, clinoptilolite)
21X-1, 93	UBN	Calcite	Clinoptilolite, quartz, (smectite)
22X-1, 12	UBN	Calcite	Clinoptilolite, smectite, quartz
24X-5, 140	UBN	Calcite, clinoptilolite	Quartz, feldspar, (smectite)
26X-3, 8	UBN	Calcite, clinoptilolite,	Quartz, illite, smectite
29X-4, 44	UBN	Calcite, clinoptilolite, quartz	Smectite, illite

Table 8 (continued).

Core, section, interval (cm)	Treatment[a]	Mineral phases present Major	Minor[b]
30X-4, 140	UBN	Calcite	Clinoptilolite, quartz, (illite, feldspar)
33X-4, 140	UBN	Calcite	Clinoptilolite, (phillipsite?, quartz, illite)
36X-4, 140	UBN	Calcite	Clinoptilolite, quartz, (illite, feldspar)
42X-6, 140	UBN	Quartz, feldspar	Pyrite, clinoptilolite, (illite, smectite)
43X-4, 52	UBN	Quartz	Clinoptilolite, (heulandite?), pyrite, smectite, illite
46X-3, 90	UCN	Smectite/illite	Quartz, feldspar?
49X-4, 74	UBN	Quartz	Pyrite, kaolinite, illite, smectite, feldspar
50X-4, 140	UBN	Quartz, kaolinite, illite	Pyrite, feldspar, smectite
122-763C-			
6R-1, 140	UBN	Quartz, feldspar	Kaolinite, illite, smectite, pyrite, (clinoptilolite)
8R-2, 38	UBN	Quartz, kaolinite, illite, smectite	Feldspar
9R-4, 118	UBN	Quartz, siderite?, kaolinite, illite	Pyrite, smectite, feldspar
10R-4, 140	UBN	Quartz, kaolinite, illite, smectite	Feldspar, calcite, (siderite?)
11R-1, 124	UBN	Calcite, quartz	Kaolinite, pyrite, illite, smectite
13R-4, 140	UBN	Quartz	Kaolinite, feldspar, illite, smectite, pyrite
16R-5, 140	UBN	Quartz, kaolinite, illite, smectite	Feldspar, calcite
19R-4, 140	UBN	Quartz, kaolinite, illite, smectite	Pyrite, feldspar
20R-4, 140	UBN	Quartz, kaolinite, illite, smectite	Pyrite, feldspar
22R-4, 140	UBN	Quartz, kaolinite, illite, smectite	Feldspar, pyrite, (zeolite?)
25R-5, 140	UBN	Quartz, kaolinite, illite, smectite	Feldspar, pyrite
26R-4, 25	UBN	Smectite	Quartz
26R-4, 28	UBN	Smectite	Quartz, feldspar
29R-4, 101	UBN	Smectite, zircon	Feldspar
32R-5, 140	UBN	Quartz, kaolinite, illite, smectite	Pyrite, feldspar
34R-5, 140	UBN	Quartz, kaolinite, illite, smectite	Pyrite, feldspar
37R-5, 140	UBN	Quartz, kaolinite, illite, smectite	Feldspar, pyrite
41R-4, 140	UBN	Quartz, kaolinite, illite, smectite	Pyrite

[a] Key to treatment type: U = unoriented, O = oriented, B = bulk, C = clay fraction, S = silt fraction, N = no treatment.
[b] Minerals are listed in order of abundance estimated from peak intensities; parentheses indicate trace abundance or identification made on the basis of fewer than three reflections. The identification of chlorite versus kaolinite remains uncertain without heat treatments, pending additional shore-based analyses.

thick Tertiary and Cretaceous marine oozes and chalks, overlying a thin distal section of the late Jurassic to early Cretaceous Barrow Group equivalent. The Barrow Group overlies the Jurassic Dingo Claystone equivalent strata, which drape the tilted fault blocks of the Triassic Mungaroo Formation. Only minor normal faulting extends into the lower Cretaceous strata near Site 762. Site 762 is located in a slightly expanded section on the downthrown side of such a fault.

Radio navigation was used during collection of the industry seismic reflection data and consequently locations along Line X79B-1425 are accurately known. Most of the shipboard site-survey seismic-reflection Line 122-4 (collected to locate Site 762) was obtained while Global Positioning System (GPS) satellite navigation was available. Thus Line 122-4, designed to duplicate a segment of Line X79B-1425, was also accurately navigated and features on Line 122-4 correspond accurately with those on Line X79B-1425. Site 762 is located 2.5 km ENE of the Eendracht-1 well, at shotpoint 2625 on Line X79B-1425 and at 207.1819 on Line 122-4, at a water depth of 1330 m. The correspondence between seismic reflectors and velocity, density, and stratigraphy at Site 762 is shown in Figure 44.

Structure

The structural configuration of the region of Site 762 is made up of faults trending between north and north-northeast and dominantly downthrown to the west (Exon and Willcox, 1978; Barber, 1982). Normal faulting occurs at the level of the Mesozoic rift surfaces and exhibits throws on the order of hundreds of meters. Reactivation of these rift faults offsets seismic horizons corresponding to strata within the Cretaceous section. The fault reactivation that occurred within the Cretaceous resulted in fault throws on the order of tens of

Table 9. Physical-property data, Hole 762B.

Core, section, interval (cm)	Depth (mbsf)	V_{ph} (km/s)	Water content (%)	Bulk density (g/cm^3)	Grain density (g/cm^3)	Porosity (%)	Formation factor horizontal	Formation factor vertical	Shear strength (kPa)
122-762B-									
1H-1, 108	1.08	1.586	49.78	1.53	2.83	74.33	2.150	2.390	2.200
1H-3, 68	3.68	1.551	45.72	1.64		73.37	3.040	2.840	9.900
2H-2, 98	6.88	1.589	47.11	1.59	2.74	73.05	3.540	2.620	14.400
2H-4, 93	9.83	1.566					2.260	2.440	9.900
3H-2, 98	16.38	1.538	44.88	1.61	2.68	70.36	2.260	2.220	12.800
3H-4, 88	19.28	1.568	43.33	1.61	2.61	68.05	2.460	2.210	12.800
3H-6, 58	21.98	1.562	44.60	1.61	2.50	69.93	2.890	2.320	17.700
4H-2, 98	25.88	1.565	43.09	1.63	2.64	68.68	2.750	2.470	13.500
4H-4, 98	28.88	1.561	42.44	1.68	2.73	69.42	2.860	2.700	8.100
4H-6, 90	31.80	1.550	42.10	1.65	2.62	67.73	2.750	2.280	12.100
5H-2, 90	35.30	1.566	40.55	1.70	2.73	67.33	2.890	2.570	9.400
5H-4, 90	38.30	1.547	40.99	1.67	2.68	66.84	3.040	2.470	13.000
5H-6, 90	41.30	1.549	41.31	1.71	2.80	68.90	3.140	2.730	18.400
6H-2, 90	44.80	1.540	39.87	1.73	2.76	67.14	2.790	2.370	10.300
6H-4, 90	47.80	1.530	41.84	1.69	2.74	68.85	2.500	2.230	10.800
6H-6, 93	50.83	1.547	38.71	1.73	2.79	65.42	2.790	2.530	17.300
7H-2, 93	54.33	1.537	41.86	1.63	2.67	66.80	2.610	2.580	12.600
7H-4, 93	57.33	1.531	40.45	1.64	2.46	64.90	2.750	2.330	12.600
7H-6, 93	60.33	1.551	40.12	1.68	2.48	65.70	3.140	2.430	9.200
8H-2, 93	63.83	1.531	40.68	1.75	2.83	69.36	2.610	2.530	8.800
8H-4, 95	66.85	1.543	41.52	1.64	2.66	66.33	2.790	2.440	11.200
8H-6, 70	69.60	1.536	40.41	1.66	2.74	65.59	2.860	2.530	12.600
9H-2, 90	73.30	1.544	40.12	1.65	2.65	64.52	2.890	2.630	10.600
9H-4, 90	76.30	1.549	40.26	1.64	2.68	64.53	3.710	2.770	
9H-6, 90	79.30	1.531	39.43	1.67	2.70	64.25	2.860	3.430	16.600
10H-1, 17	80.57	1.536							
10H-2, 90	82.80	1.528	38.68	1.69	2.72	63.66	2.820	2.500	15.300
10H-3, 17	83.57	1.530							
10H-4, 16	85.06	1.588							
10H-4, 90	85.80		40.93	1.65	2.65	65.96			14.400
10H-5, 17	86.57	1.549							
10H-6, 86	88.76	1.562	38.05	1.69	2.77	62.95			11.000
10H-7, 7	89.47	1.539							
11H-1, 88	90.78	1.548							
11H-2, 75	92.15		39.25	1.65	2.73	63.06	2.140	2.160	13.900
11H-3, 88	93.78	1.533							
11H-4, 64	95.04	1.535	39.74	1.66	2.68	64.40	2.120	2.120	6.700
11H-5, 88	96.78	1.521							
11H-6, 88	98.28	1.549	37.42	1.54	2.60	56.14	2.270	2.270	
12H-1, 88	100.28	1.568							
12H-2, 88	101.78	1.543	37.26	1.69	2.66	61.37	2.400	2.510	
12H-3, 88	103.28	1.552							
12H-4, 88	104.78	1.566	36.56	1.70	2.67	60.78	2.270	2.970	
12H-5, 86	106.26	1.580							
12H-6, 88	107.78	1.570	34.83	1.74	2.69	59.11	2.650	2.750	10.200
13H-1, 74	109.64	1.576	35.57	1.72	2.66	59.87	2.850	3.180	10.600
13H-3, 80	112.70	1.540	38.99	1.68	2.75	63.97	2.260	2.230	
13H-5, 64	115.54	1.546	38.20	1.68	2.69	62.72	2.580	2.261	
14H-2, 88	120.78	1.617	38.68	1.67	2.58	63.11	3.320	3.650	
14H-4, 88	123.78	1.602	41.98	1.64	2.72	67.19	3.160	2.770	
14H-6, 88	126.78	1.578	41.43	1.64	2.67	66.24	3.550	3.810	
15H-2, 34	129.74	1.556	48.30	1.54	2.56	72.51	1.990	1.710	
15H-4, 54	132.94	1.620	38.04	1.74	2.66	64.44	4.380	2.510	
16H-1, 60	138.00	1.668	32.30	1.85	2.93	58.38	4.480		
16H-3, 70	141.10	1.644	37.11	1.77	3.14	64.17	4.010	3.550	
16H-5, 70	144.10		39.01	1.70	2.95	64.59	3.850	3.510	
17H-2, 70	149.10	1.604	39.11	1.70	2.78	65.08	3.130	2.740	
17H-4, 62	152.02	1.588	36.34	1.79	2.62	63.51	2.920	2.630	
17H-6, 62	155.02	1.585	35.74	1.74	2.70	60.59	2.650	2.780	
18H-3, 76	160.16	1.635	33.73	1.81	2.75	59.47	3.070	3.030	
18H-5, 60	163.00	1.603	36.47	1.74	2.66	61.85	3.520	3.150	
19H-1, 72	166.62		34.18	1.81	2.70	60.38	3.800	4.580	
19H-3, 62	169.52	1.582	34.20	1.82	2.97	60.80	3.750	3.700	
19H-5, 46	172.36	1.628	32.32	1.78	2.68	56.31	4.950		

meters. Reactivation of faulting decreased progressively into the Late Cretaceous and is rarely seen to displace the seismic horizon corresponding to the Cretaceous/Tertiary boundary. Minor fault reactivation above that level in the region may, however, be indicated by seismic diffractors (apparently associated with gas-saturated zones) that occur in some locations along the upward extension of the fault zones.

Sequence Stratigraphy

Using methods outlined in Vail et al. (1977), at least ten seismic sequences could be distinguished at Site 762. Identification of these sequences allows an interpretation of the seismic structure and seismic stratigraphy at Site 762, and a correlation with other data sets from the site (e.g., wireline logs; see Fig. 45).

Table 10. Physical-property data, Hole 762C.

Core, section, interval (cm)	Depth (mbsf)	V_{ph} (km/s)	V_{pv} (km/s)	Anisotropy (%)	Water content (%)	Bulk density (g/cm^3)	Grain density (g/cm^3)	Porosity (%)	Formation factor horizontal	Formation factor vertical
122-762C-										
2X-2, 105	172.55	1.560			34.23	1.79	2.83	59.69	4.160	4.740
2X-4, 80	175.30	1.564			36.14	1.73	2.77	61.07	3.720	3.510
3X-1, 80	180.30	1.555			35.87	1.73	2.71	60.49	3.750	3.890
3X-3, 104	183.54	1.542			37.31	1.70	2.70	62.06	2.750	2.600
4X-2, 80	191.30	1.538			35.64	1.72	2.64	59.77	2.640	2.350
4X-4, 85	194.35	1.560			34.82	1.74	2.69	59.10	2.940	2.830
5X-1, 90	199.40	1.534			35.48	1.73	2.68	60.00	2.650	2.560
6X-2, 19	209.69	4.458	4.203	5.897	1.42	2.20	2.24	3.05		
6X-2, 115	210.65	1.555			36.44	1.72	2.67	61.17	2.620	2.350
6X-4, 105	213.55	1.557			36.49	1.73	2.72	61.44	3.180	2.840
7X-1, 85	218.35	1.542			35.53	1.77	2.78	61.36	2.970	2.490
7X-4, 85	222.85	1.554			35.62	1.73	2.71	60.10	2.900	3.470
8X-2, 84	229.34	1.568			35.40	1.74	2.70	60.21		
8X-4, 90	232.40				32.15	1.80	2.68	56.51		
9X-1, 51	237.01	1.542			33.93	1.77	2.67	58.53		
10X-2, 95	248.45				33.15	1.77	2.67	57.23		
10X-4, 88	251.38				33.78	1.75	2.61	57.70		
11X-2, 80	257.80	1.543			35.49	1.72	2.64	59.73	2.830	2.910
11X-4, 48	260.48	1.537			35.88	1.74	2.70	61.08	2.640	2.460
11X-6, 100	264.00	1.580			31.53	1.82	2.66	56.12	3.230	3.860
12X-2, 88	267.38	1.568			33.38	1.78	2.66	57.93	3.350	3.260
12X-4, 88	270.38	1.569			33.47	1.77	2.64	57.71	3.120	2.950
12X-6, 88	273.38	1.563			31.73	1.80	2.68	55.81	4.200	3.540
13X-2, 88	276.88	1.576			32.60	1.76	2.63	55.98	2.860	2.840
14X-2, 78	286.28	1.594			32.30	1.60	2.70	50.58	3.610	3.330
14X-4, 88	289.38	1.604			33.55	1.77	2.64	57.90	3.900	3.090
14X-6, 98	292.48	1.600			31.80	1.79		55.49	3.300	3.650
15X-1, 94	294.44	1.596			30.36	1.84	2.72	54.64	4.130	4.210
15X-3, 31	296.81	1.586			34.00	1.74	2.64	57.88	3.230	3.230
16X-1, 90	303.90	1.570			34.83	1.75	2.67	59.49	3.310	2.920
16X-3, 82	306.82	1.572			32.02	1.79	2.65	55.97	4.070	3.940
17X-2, 123	315.23	1.587			30.61	1.84	2.53	55.09	4.830	4.280
17X-3, 98	316.48	1.597								
17X-4, 98	317.98				32.67	1.79	2.70	57.08	3.720	3.660
17X-5, 123	319.73	1.612			32.98	1.80	2.60	57.85	4.210	3.650
18X-2, 72	324.22	1.578			31.21	1.88	2.96	57.29	3.190	3.370
18X-4, 72	327.22	1.594			30.61	1.92	2.83	57.29	4.010	3.920
18X-6, 72	330.22	1.577			31.63	1.88	2.74	58.19	3.070	2.830
19X-2, 62	333.62				30.18	1.96	2.75	57.81	3.070	3.010
19X-4, 62	336.62	1.600			30.62	1.92	2.80	57.32	3.230	3.080
20X-2, 62	343.12	1.589							2.890	2.880
20X-4, 30	345.80	1.598							3.050	2.660
21X-CC, 16	353.14	1.729								
22X-1, 22	360.22	1.600								
22X-3, 40	363.40	1.857			21.07	2.12	2.64	43.57		
22X-5, 40	366.40	1.879			20.53	2.13	2.73	42.73		
23X-2, 62	371.62	1.771			22.96	2.02	2.68	45.31		
23X-CC, 20	373.63	1.856			22.44	2.04	2.66	44.68		
24X-1, 40	379.40	1.968			23.10	2.02	2.66	45.53		
25X-2, 30	390.30	1.907			21.21	2.10	2.56	43.51		
25X-4, 40	393.40	1.938			21.87	2.07	2.81	44.22		
26X-1, 31	398.31	2.066	2.022	2.162	17.62	2.12	2.67	36.38		
26X-6, 12	405.62	1.792			20.14	2.05	2.67	40.39		
27X-1, 48	402.98	1.902			19.89	2.10	2.72	40.87		
27X-3, 62	406.12	1.937			21.55	2.05	2.62	43.06		
28X-2, 6	413.56	1.836			18.91	2.19	2.72	40.39		
29X-1, 2	421.52	2.094			15.73	2.33	2.79	35.71		
30X-1, 77	431.77	1.967			18.32	2.20	2.70	39.30		
31X-2, 85	442.85	2.298			15.20	2.16	2.65	32.00		
31X-4, 85	445.85	2.158			17.15	2.13	2.70	35.66		
31X-6, 85	448.85	2.275			16.97	2.12	2.69	35.19		
32X-1, 91	450.91	1.998			21.55	2.02	2.68	42.50		
32X-2, 63	452.13	2.049			18.72	2.10	2.69	38.47		
33X-1, 90	460.40	2.159			21.96	2.32	2.67	49.65		
33X-3, 90	463.40	2.083			17.95	2.09	2.68	36.66		
33X-5, 88	466.38	2.034			15.36	2.17	2.68	32.55		
34X-2, 118	471.68	2.005			16.35	2.17	2.69	34.59		
34X-4, 29	473.79	2.134			16.64	2.15	2.68	34.99		
35X-1, 107	479.57	2.024			16.20	2.21	2.69	35.02		
36X-1, 22	488.22	2.006			17.43	2.21	2.71	37.59		
37X-1, 101	498.51	1.806			17.88	2.10	2.68	36.70		
37X-3, 98	501.48	1.879			22.96	2.03	2.17	45.48		
37X-5, 16	503.66	2.051			15.89	2.13	2.63	33.08		
38X-2, 18	508.68	1.994			22.30	2.04	2.69	44.34		
38X-4, 40	511.90	1.998			18.37	2.22	2.84	39.80		

Table 10 (continued).

Core, section, interval (cm)	Depth (mbsf)	V_{ph} (km/s)	V_{pv} (km/s)	Anisotropy (%)	Water content (%)	Bulk density (g/cm^3)	Grain density (g/cm^3)	Porosity (%)	Formation factor horizontal	vertical
38X-6, 40	514.90	2.001			25.04	1.94	2.59	47.46		
39X-2, 42	518.42				24.39	2.01	2.47	47.78		
39X-4, 42	521.42	1.991			24.37	2.08	2.75	49.54		
40X-4, 46	530.96	2.090			18.70	2.12	2.65	38.67		
40X-6, 38	533.88				16.18	2.06	2.88	32.46		
41X-2, 42	537.42				23.04	2.07	2.67	46.53		
41X-4, 23	540.23				27.14	1.98	2.69	52.33		
42X-1, 115	546.15	2.622	2.509	4.408	13.67	2.20	2.44	29.30		
43X-4, 115	560.15				22.21	2.03	2.68	44.02		
44X-1, 115	565.15	2.371	2.180	8.373	14.19	2.20	2.68	30.53		
44X-3, 33	567.33	2.239	2.155	3.806	14.38	2.22	2.69	31.18		
44X-5, 94	570.94	2.257	2.075	8.416	15.39	2.18	2.69	32.77		
45X-1, 10	573.60	2.130	2.000	6.300	20.43	2.09	2.81	41.70		
45X-4, 96	578.96				22.59	2.10		46.38		
46X-1, 35	583.35	1.890			21.83	2.04	2.72	43.44		
46X-2, 130	585.80	1.922			22.72	2.00	2.67	44.41		
46X-4, 65	588.15				22.38	2.02	2.72	44.08		
47X-1, 77	593.27	2.190								
47X-2, 77	594.77				15.95	2.22	2.71	34.63		
47X-4, 72	597.72	2.134			16.54	2.14	2.67	34.51		
47X-6, 66	600.66	2.269			16.69	2.18	2.68	35.51		
48X-1, 90	602.90	2.295			16.09	2.14	2.70	33.59		
48X-3, 94	605.94	2.174			16.91	2.13	2.68	35.09		
48X-5, 54	608.54	2.169			16.97	2.16	2.70	35.77		
48X-6, 68	610.18	2.035			20.97	2.03	2.70	41.62		
49X-1, 9	611.59	2.042			18.96	2.09	2.70	38.66		
49X-3, 77	615.27				12.54	2.29	2.72	28.04		
49X-4, 19	616.19	2.099			21.39	2.04	2.71	42.54		
49X-5, 133	618.83	2.202			15.41	2.23	2.71	33.60		
50X-2, 42	622.92	2.292								
50X-4, 92	626.42	2.116			17.42	2.23	2.77	38.01		
50X-6, 116	629.66	2.179			19.98	2.19	2.82	42.75		
51X-2, 68	632.68				14.02	2.31	2.69	31.64		
51X-4, 144	636.44	2.118			18.33	2.21	2.70	39.49		
51X-5, 146	637.96	2.327			15.95	2.26	2.75	35.16		
52X-2, 50	642.00	2.052								
52X-2, 76	642.26				19.95	2.26	2.91	44.04		
52X-4, 76	645.26	2.161			18.01	2.19	2.73	38.54		
53X-2, 20	651.20	1.997			19.15	2.12	2.77	39.60		
53X-4, 90	654.90	2.103			18.92	2.15	2.31	39.65		
53X-6, 8	657.08	1.917			23.31	2.02	2.68	45.90		
54X-2, 32	660.82				24.06	2.01	2.62	47.16		
54X-4, 49	663.99	2.064	1.982	4.068	17.37	2.15	2.72	36.43		
54X-4, 86	664.36				18.31	2.21	2.71	39.56		
54X-6, 104	667.54				22.34	2.07	2.73	45.15		
55X-2, 67	670.67	1.812	1.702	6.288	20.94	2.02	2.73	41.31		
55X-4, 7	673.07	2.029	1.930	5.011	18.91	2.10	2.74	38.74		
56X-1, 63	678.63	1.999	1.908	4.658	17.71	2.12	2.73	36.64		
56X-3, 89	681.89	2.162	2.020	6.791	16.22	2.16	2.72	34.27		
56X-5, 56	684.56	2.056	2.047	0.419	16.01	2.14	2.69	33.44		
57X-2, 57	689.57	1.852	1.865	−0.694	21.04	2.10	2.76	43.05		
58X-3, 103	701.03	1.894	1.950	−2.935	21.72	2.02	2.68	42.89		
58X-5, 12	703.12	1.846	1.754	5.138	21.29	2.03	2.71	42.16		
59X-2, 109	709.09				18.66	2.15	2.88	39.13		
59X-3, 148	710.98				21.17	2.03	2.64	41.93		
60X-1, 26	716.26				23.64	1.99	2.73	45.88		
60X-CC, 7	720.56	1.888	1.885	0.148	22.45	2.02	2.72	44.33		
61X-1, 3	725.53	1.913	1.860	2.830	18.84	2.12	2.71	38.92		
61X-2, 36	727.36	1.844	1.772	4.004	19.90	2.35	2.73	45.72		
62X-2, 127	737.77	2.103			18.15	1.89	2.71	33.48		
62X-3, 86	738.86	1.989	1.766	11.883	8.30	1.94	2.71	15.69		
62X-4, 35	739.85	1.735	1.781	−2.634	18.38	2.09	2.71	37.58		
62X-5, 38	741.38	2.231	2.217	0.621	16.33	1.64	2.72	26.11		
63X-1, 43	744.93	2.042			21.90	2.05	2.66	43.79		
64X-1, 14	754.14	2.244	1.989	12.035	16.96	2.22	2.72	36.68		
64X-3, 8	757.08	1.794	1.834	−2.194	21.58	2.05	2.77	43.18		
64X-4, 4	758.54	1.821	1.821	0.011	23.43	1.99	2.68	45.40		
66X-1, 29	765.29			22.53	2.53	2.08	2.82	45.80		
66X-3, 90	768.90				23.68	2.06	2.71	47.59		
67X-CC, 34	770.87				20.04	2.24	2.81	43.75		
68X-1, 138	776.38	2.071			14.71	2.33	2.81	33.49		
69X-1, 42	780.42	2.252			14.11	2.33	2.69	32.13		
69X-CC, 26	786.11				9.42	2.48	2.70	22.79		
71X-1, 56	790.56	2.525			9.73	2.41	2.71	22.86		
71X-2, 144	792.94	2.419			11.57	2.38	2.59	26.85		
72X-1, 42	795.42	2.067			14.66	2.26	2.73	32.36		

Table 10 (continued).

Core, section, interval (cm)	Depth (mbsf)	V_{ph} (km/s)	V_{pv} (km/s)	Anisotropy (%)	Water content (%)	Bulk density (g/cm^3)	Grain density (g/cm^3)	Porosity (%)	Formation factor horizontal	vertical
73X-2, 84	801.84	2.655	2.434	8.704	13.00	2.19	2.75	27.83		
73X-3, 6	802.56	2.536			13.52	2.36	2.69	31.20		
74X-2, 44	806.44	2.547			8.29	2.39	2.80	19.32		
74X-3, 24	807.74	3.587	3.540	1.319	4.88	2.51	2.76	11.97		
75X-1, 2	809.52	3.461	3.424	1.075	4.90	2.54	2.69	12.20		
75X-1, 90	810.40	2.687								
75X-3, 54	813.04	2.676								
75X-CC, 2	813.45	2.576	2.305	11.104	11.00	2.30	2.69	24.80		
76X-1, 57	815.07	2.389	2.246	6.166						
76X-3, 99	818.49	2.678	2.502	6.784	9.26	2.32	2.71	20.99		
76X-4, 82	819.82	2.738	2.641	3.603	10.11	2.34	2.67	23.14		
77X-1, 135	820.85	2.652	2.397	10.101	9.32	2.34	2.69	21.27		
77X-3, 129	823.79	2.569	2.373	7.951	8.92	2.35	2.75	20.49		
77X-5, 147	826.97	2.482	2.454	1.126	7.93	2.39	2.73	18.51		
78X-1, 91	829.91	2.392	2.133	11.456	11.52	2.26	2.74	25.41		
79X-1, 64	839.14	1.817	1.762	3.073	31.82	1.72	2.36	53.54		
79X-2, 109	841.09				23.80	1.91	2.46	44.43		
81X-1, 61	849.11				22.77	2.14	2.87	47.52		
81X-3, 107	852.57	1.982	1.891	4.714	17.51	2.17	2.72	37.04		
81X-3, 116	852.66	1.929	1.890	2.058	19.92	2.12	2.70	41.30		
82X-1, 111	854.61	1.939	1.871	3.554	17.31	2.21	2.75	37.28		
82X-2, 89	855.89	5.000			1.30	2.70	2.67	3.43		
82X-3, 70	857.20				18.46	2.22	2.77	39.93		
83X-1, 58	859.08				22.76	2.26	2.87	50.28		
85X-1, 114	874.14				20.81	2.45	2.80	49.67		
86X-2, 114	885.14	1.898			21.46	2.25	2.65	47.09		
86X-4, 84	887.84	1.925	1.847	4.146	18.14	2.34	2.69	41.44		
87X-2, 21	893.71				16.87	2.19	2.71	36.02		
88X-2, 126	904.26	1.860			17.61	2.25	2.78	38.74		
88X-4, 65	906.65	1.961	1.925	1.832	15.94	2.26	2.78	35.21		
88X-6, 100	910.00	1.937	1.876	3.205	15.43	2.31	2.78	34.82		
89X-2, 85	913.35	1.835			16.26	2.21	2.70	35.11		
89X-4, 28	915.78	1.737	1.827	−5.039	17.21	2.30	2.81	38.58		
90X-2, 81	922.81	1.909	1.906	0.183	15.53	2.23	2.74	33.82		
90X-4, 87	925.87	2.027	1.925	5.182	14.83	2.29	2.70	33.14		
91X-1, 85	930.85	1.917			17.07	2.21	2.70	36.90		
91X-2, 21	931.71	1.849			16.51	2.21	2.68	35.59		

Seismic Sequences

Sequence 1

This is the basal sequence at Site 762 (Fig. 44). It lies below approximately 2.75 s two-way traveltime (TWT), and the upper sequence boundary is a prominent unconformity near the top of a series of tilted fault blocks. This sequence is found throughout the Exmouth Plateau, and although not drilled at Site 762, it can be correlated to the upper part of the Triassic Mungaroo Formation (e.g., Barber 1982; Wright and Wheatley, 1979).

Sequence 2

This thin sequence lies approximately between 2.73 and 2.75 s (TWT) below sea level. It displays a conformable-to-onlapping relationship with the underlying Sequence 1. Drilling at Site 762 terminated around 50 m above the top of Sequence 2, but correlation to other seismic studies on the Exmouth Plateau (e.g., Barber, 1982; Wright and Wheatley, 1979) suggests that it is the Dingo Claystone of early to late Jurassic age. The top of Sequence 2 is commonly an erosional unconformity related to fault-block tilting and exposure.

Sequence 3

This sequence lies between 2.61 (847 mbsf) and 2.73 s (TWT) and occupies a northward-thinning wedge. It contains internal clinoforms that downlap onto Sequence 2 and toplap at the upper boundary of Sequence 3. Internal reflectors in Sequence 3 are of low amplitude, high continuity, and variable frequency. This description correlates well with black claystones drilled at Site 762 in Cores 122-762C-81X to -91X, and identified as the Barrow Group equivalent of Berriasian to Valanginian age. The top of Sequence 3 corresponds to a number of thin limestones that were first observed in Core 122-762C-82X and may contribute to generating the positive-amplitude peak that defines the top of Sequence 3. Definition is lacking within Sequence 3 near Site 762, but a division into at least two subunits appears to be possible, each of which may be a sequence.

Sequence 4

This thin sequence occupies only one cycle from 2.596 to 2.610 s (TWT), or 836–847 mbsf. It is conformable with Sequence 3 at Site 762, but thickens slightly nearby and appears to onlap Sequence 3 toward the east and the south. Correlation with Site 762 drilling results indicates that Sequence 4 consists of the Muderong Shale equivalent sediments of early Aptian age. Its upper boundary is a sharp velocity decrease from chalk downward into mudstone at around 838 m. This velocity decrease probably contributes to the large negative velocity anomaly at 2.6 s, but sequences are so closely spaced at this depth that the reflectors are complex interference composites.

Sequence 5

Like Sequence 4, this sequence is only one cycle wide and occurs from 2.578 to 2.596 s (TWT) below sea level, or 811–836 mbsf. The upper sequence boundary is a prominent erosional unconformity. This unconformity marks a change in seismic style from several high-amplitude, parallel reflectors below (each of which are sequence boundaries) to an overlying sequence of lower-amplitude, discontinuous re-

Table 11. Thermal-conductivity data, Site 762.

Core, section, interval (cm)	Depth (mbsf)	Thermal conductivity (W/m · K)
122-762B-		
1H-1, 110	1.10	1.033
1H-2, 70	2.20	1.219
1H-3, 70	3.70	1.222
2H-1, 70	5.10	1.223
2H-3, 70	8.10	1.258
2H-5, 70	11.10	1.223
3H-1, 70	14.60	1.310
3H-1, 70	17.60	1.210
3H-5, 70	20.60	1.199
3H-6, 30	21.70	1.218
4H-3, 70	27.10	1.269
4H-5, 70	30.10	1.296
4H-6, 70	31.60	1.291
5H-2, 49	34.89	1.291
5H-4, 49	37.89	1.282
5H-5, 49	39.39	1.311
5H-6, 50	40.90	1.312
6H-4, 70	47.60	1.311
6H-6, 70	50.60	1.297
6H-7, 20	51.60	1.254
7H-1, 70	52.60	1.495
7H-3, 70	55.60	1.294
7H-5, 70	58.60	1.253
7H-7, 30	61.20	1.313
8H-2, 70	63.60	1.307
8H-4, 70	66.60	1.301
8H-5, 70	68.10	1.326
8H-6, 70	69.60	1.306
9H-4, 70	76.10	1.443
9H-5, 70	77.60	1.392
9H-6, 70	79.10	1.443
10H-2, 70	82.60	1.292
10H-3, 70	84.10	1.358
10H-5, 70	87.10	1.345
10H-6, 70	88.60	1.341
11H-1, 70	90.60	1.407
11H-3, 70	93.60	1.380
11H-5, 70	96.60	1.319
11H-7, 25	99.15	1.369
12H-2, 70	101.60	1.452
12H-4, 70	104.60	1.401
12H-6, 70	107.60	1.469
12H-7, 35	108.75	1.328
13H-2, 70	111.10	1.710
13H-4, 70	114.10	1.384
13H-5, 70	115.60	1.419
14H-2, 70	120.60	1.410
14H-4, 70	123.60	1.376
14H-5, 70	125.10	1.316
14H-6, 80	126.70	1.287
15H-1, 70	128.60	1.284
15H-4, 70	133.10	1.335
15H-5, 70	134.60	1.408
15H-6, 70	136.10	1.367
16H-1, 60	138.00	1.551
16H-3, 60	141.00	1.470
16H-5, 60	144.00	1.361
16H-6, 60	145.50	1.401
17H-2, 60	149.00	1.416
17H-3, 60	150.50	1.339
17H-4, 60	152.00	1.399
17H-5, 60	153.50	1.409
18H-2, 60	158.50	1.274
18H-3, 60	160.00	1.485
18H-4, 60	161.50	1.550
18H-5, 60	163.00	1.481
19H-2, 60	168.00	1.435
19H-3, 60	169.50	1.487
19H-4, 60	171.00	1.404
19H-5, 60	172.50	1.512
122-762C-		
2X-2, 60	172.10	1.152
2X-3, 60	173.60	1.404
2X-4, 60	175.10	1.277
2X-5, 60	176.60	1.354
3X-1, 50	180.00	1.320
3X-2, 50	181.50	1.246
3X-3, 50	183.00	1.417
3X-4, 50	184.50	1.427
4X-1, 70	189.70	1.340
4X-2, 70	191.20	1.436
4X-3, 70	192.70	1.439
6X-1, 60	208.03	1.436
6X-3, 60	211.60	1.466
6X-4, 60	213.10	1.370
7X-4, 70	222.70	1.519
8X-2, 70	229.20	1.464
8X-4, 70	232.20	1.507
10X-2, 70	248.20	1.430
10X-4, 70	251.20	1.577
11X-2, 70	257.70	1.553
11X-4, 70	260.70	1.544
12X-2, 60	267.10	1.526
12X-4, 60	270.10	1.550
12X-6, 60	273.10	1.551
13X-2, 60	276.60	1.518
16X-1, 80	303.80	1.428
16X-2, 80	305.30	1.346
16X-3, 80	306.80	1.448
16X-4, 30	307.80	1.627
17X-2, 70	314.70	1.725
17X-4, 70	317.70	1.589
18X-2, 70	324.20	1.477
18X-5, 70	328.70	1.567
19X-2, 60	333.60	1.610
19X-4, 60	336.60	1.683
20X-2, 60	343.10	1.613
20X-4, 30	345.80	1.506
21X-1, 90	351.40	1.591
22X-2, 90	362.40	1.716
22X-5, 90	366.90	1.663
22X-6, 60	368.10	1.779
23X-2, 30	371.30	1.804
23X-3, 48	372.98	1.676

flectors cut by diffractors. Lithologically, this transition corresponds to the Turonian/Cenomanian boundary and may also mark the transition to a deep-water marine depositional environment. Sequence 5 at Site 762 corresponds to the Gearle Siltstone equivalent strata, where logging data show a prominent decrease in velocity and density at the top and a steadily increasing gamma-ray content below the base and into Sequence 4 (see "Downhole Measurements," Site 762 chapter).

Sequence 6

This sequence is composed of several broad reflectors of moderate amplitude that are largely parallel to the upper and lower sequence boundaries. These sequence boundaries occur at 2.38 and 2.578 s (TWT), or 555–811 mbsf. The sequence is characterized by numerous diffractors which make the internal reflectors appear to be locally discontinuous. The diffractors primarily originate from the upper sequence boundary, which at Site 762 (where it does not occur as an erosional unconformity) is identified as the Cretaceous/Tertiary boundary. The age of Sequence 6 is thus Maestrichtian to Turonian and includes the Toolonga Calcilutite equivalent and unnamed units that are time-equivalent to the Korojon Calcarenite and the Miria Marl. Lithologic nomenclature for these units is derived from outcrop and well data on the adjacent Northwest Shelf and coast (Quilty, 1980).

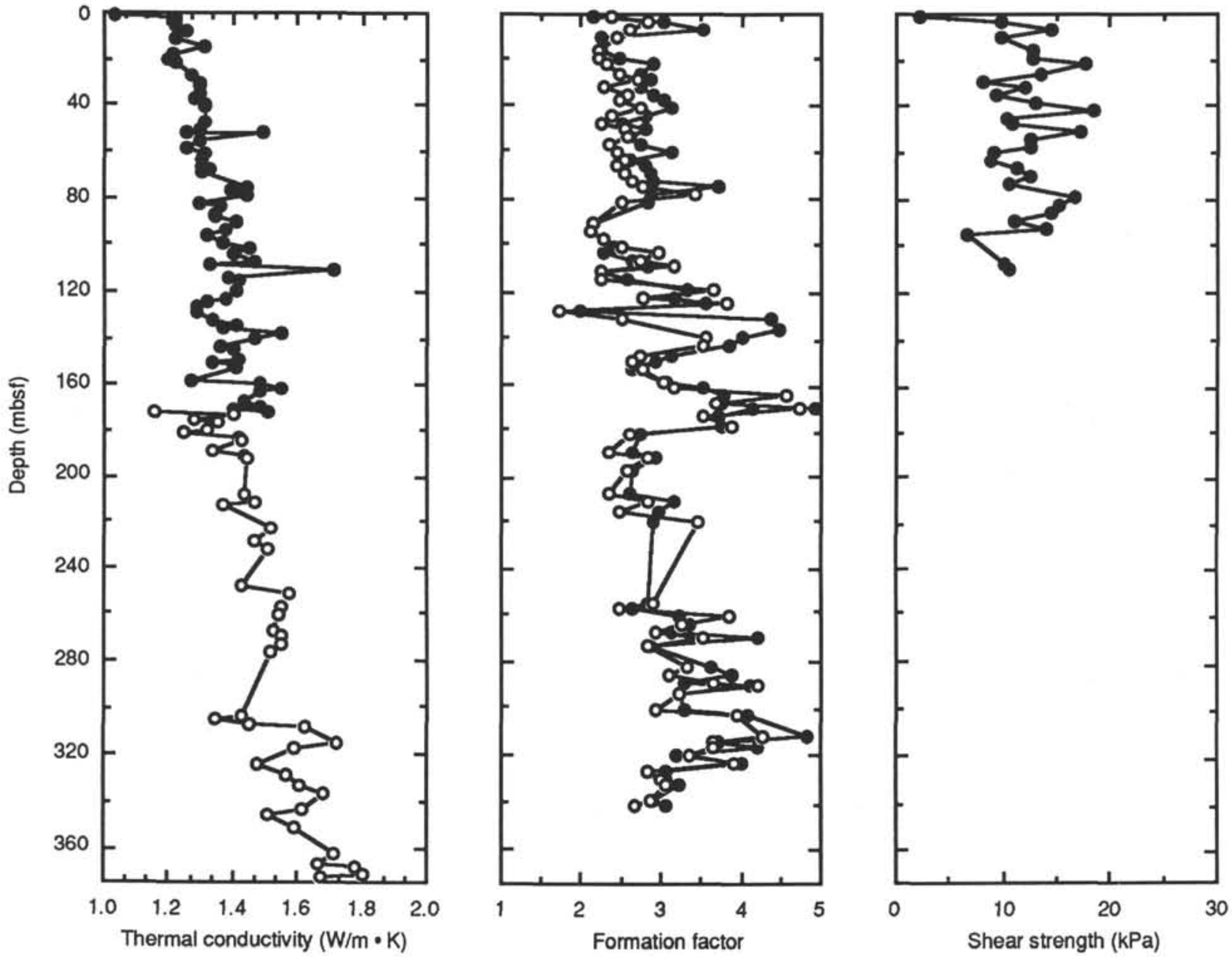

Figure 40. Physical-property data from Site 762. Thermal conductivity (measured through the core liner; solid circles = APC cores from Hole 762B, open circles = XCB cores from Hole 762C), formation factor (solid circles = measurements taken horizontally, or perpendicular to the core axis; open circles = measurements taken vertically, or parallel to the core axis), and shear strength.

Sequence 7

Sequence 7 immediately overlies the Cretaceous/Tertiary boundary and is similar in character to Sequence 6. The same broad, parallel, internal reflectors conform to the sequence boundaries, which occur at 2.27 and 2.38 s (TWT), or 427–555 mbsf, and are cut by numerous diffractions. The sequence is Paleocene in age and onlaps the Cretaceous/Tertiary boundary to the east. Like the sequences above and below, it is composed primarily of pelagic chalk and is age-equivalent to the Cardabia Group (Quilty, 1980).

Sequence 8

Characterized by highly discontinuous reflectors with variable amplitude and local relief of 50–100 ms, the boundaries of this sequence occur at 2.15 and 2.27 s (TWT) or at 317–427 mbsf. It also appears to contain diffractors similar to those in underlying sequences. The upper boundary is erosional and may indicate the presence of submarine erosional channels. The sequence is Eocene in age and is primarily pelagic chalk. The erosional relief is similar to that of other Eocene units on Exmouth Plateau, but this is not confirmed by the Site 762 drilling results, which indicate no hiatus in the Paleogene section.

Sequence 9

This sequence and the overlying Sequence 10 can be differentiated from those below by their relatively low-amplitude internal reflectors that display high continuity and have a high frequency content. This change in reflector character overlies, but is close to a lithological change at Site 762 from chalk to overlying ooze. Sequence boundaries occur at 2.02 and 2.15 s (TWT), or 172–317 mbsf. The upper boundary of Sequence 9 is an erosional unconformity of middle Miocene age and hence Sequence 9 extends from middle Miocene to Eocene.

Sequence 10

With very similar characteristics to Sequence 9, Sequence 10 onlaps the lower sequence boundary towards the east. Sequence boundaries occur at the seabed and 2.02 s (TWT), or 0–172 mbsf. It occupies the period from Quaternary to middle Miocene. The presence of an irregular seafloor with up to 100 ms of relief suggests the presence of erosional bottom currents or mass-wasting processes.

DOWNHOLE MEASUREMENTS

Operations

On 1 August 1988, a mini-cone was lowered to allow removal of the bit and pipe reentry for logging. Logging operations began at 2230 hr (all times are given in local time) with hole conditioning. Rig-up of the seismic stratigraphic tool string began at 0830 hr, 2 August. In this hole, the tool combination consisted of the digital sonic tool (SDT), the spectral gamma ray tool

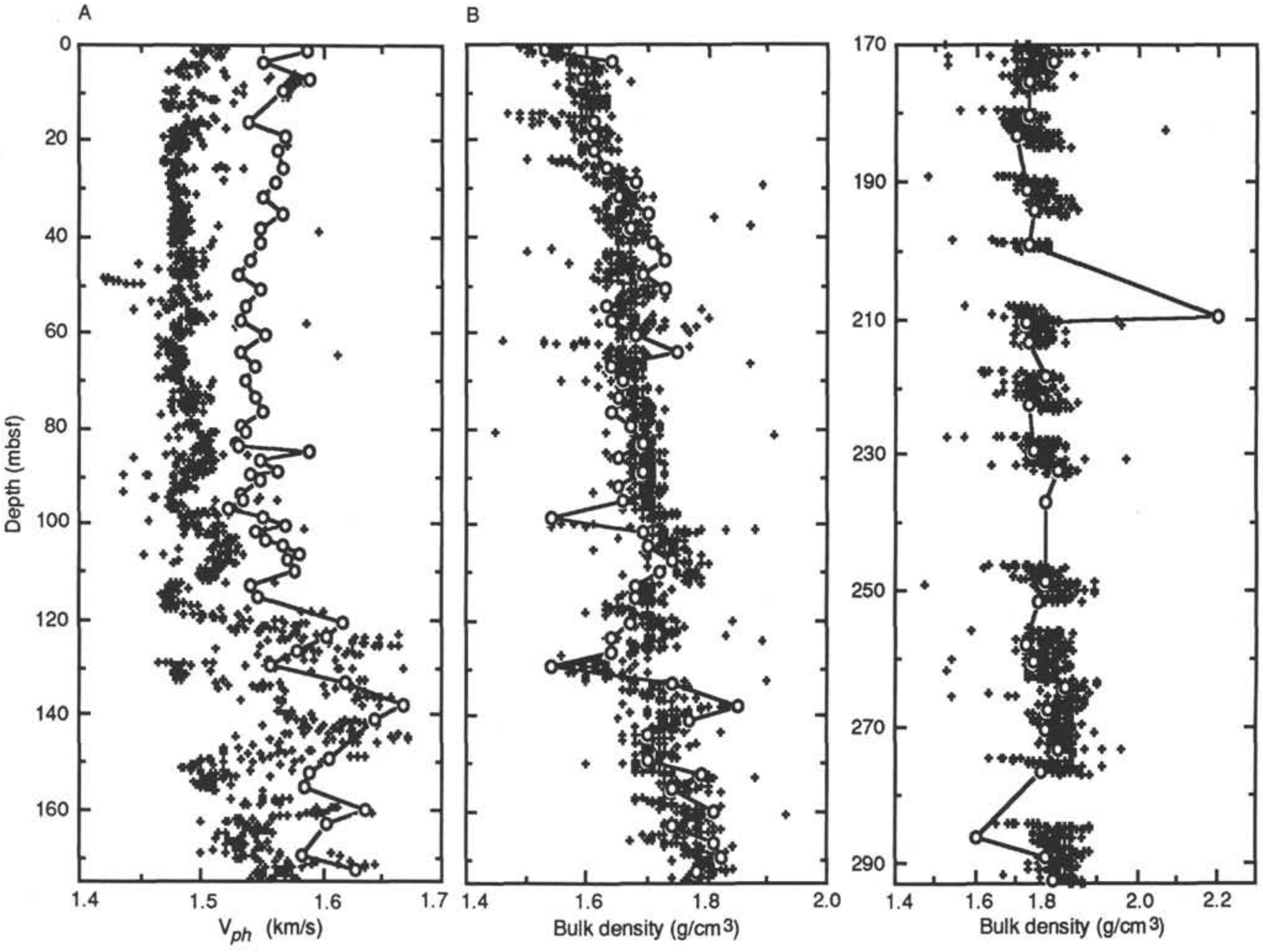

Figure 41. Velocity and density data, Site 762. **A.** *P*-wave logger data (small crosses) compared with Hamilton Frame measurements of individual samples (open circles), Hole 762B. **B.** GRAPE wet-bulk density measurements (small crosses) compared with gravimetric measurements of individual samples (open circles) for Holes 762B and 762C.

(NGT), phasor induction tool (DIT-E), and caliper (MCD). By 1345 hr, the tool string had been tested and rigged up below the sidewall-entry sub (SES). At 1705 hr, the logging tools were at the bottom of the hole (917 mbsf). Logs were recorded from total depth to the base of the pipe (180 mbsf). The tool string became stuck at the base of the pipe and was pulled into the pipe only after seawater was pumped to dislodge the obstruction. Rig-down of the SES and seismic-stratigraphic tool combination began at 2330 hr. By 0100 hr on August 3, the geochemistry tool string and SES were rigged up. After assembly was completed, the cable armor above the tool string had to be cut because it had unravelled.

Logging began at 0925 hr at 906 mbsf; because of the slow speed at which geochemical logs are run, logs were recorded only to 502 mbsf. By 1400 hr the geochemical tool combination was being rigged down. For safety considerations, the decision was made to run the porosity and density tools (lithoporosity tool string) to determine the presence of hydrocarbons. The tool string was rigged up at 1530 hr and was lowered to 903 mbsf by 1935 hr. The neutron porosity tool stopped functioning at the bottom of the hole; the gamma ray and density tools continued to record data. In attempting to reenter the pipe (180 mbsf), the tool string became stuck at the base of the drillstring. Pulling on the cable and pumping sea water failed to dislodge the obstruction. At 0150 hr on August 4, the decision was made to pull the pipe. The cable was cut and crimped every 30 m while pulling pipe in order to retrieve the tool string. When the drill string was brought to the moon pool, the tool string was not at the bottom of the pipe. Cable from the mini-cone float was wrapped around the bit and apparently caused the tool string to become stuck at the base of the pipe. A concerted effort was made to recover the logging tool. An overshot with a 3-3/8-in. grapple was appended to the drill pipe. The drill pipe was lowered to a few meters above the cone, and a search of the area around the cone was conducted using the television system. However, no indication of the tool was seen on the sea bottom. The hole was reentered and the drill pipe was run to the bottom of the hole; there was no indication of contact with the tools on the weight indicator. The drill pipe was pulled above the sea floor. Experience suggested that additional fishing was not likely to succeed.

Log Quality

Logs obtained with the seismic stratigraphic tool string included sonic, caliper, resistivity, total gamma ray, and the spectral logs for thorium, uranium, and potassium. These logs were obtained from 911 mbsf to 188 mbsf. Except for the two

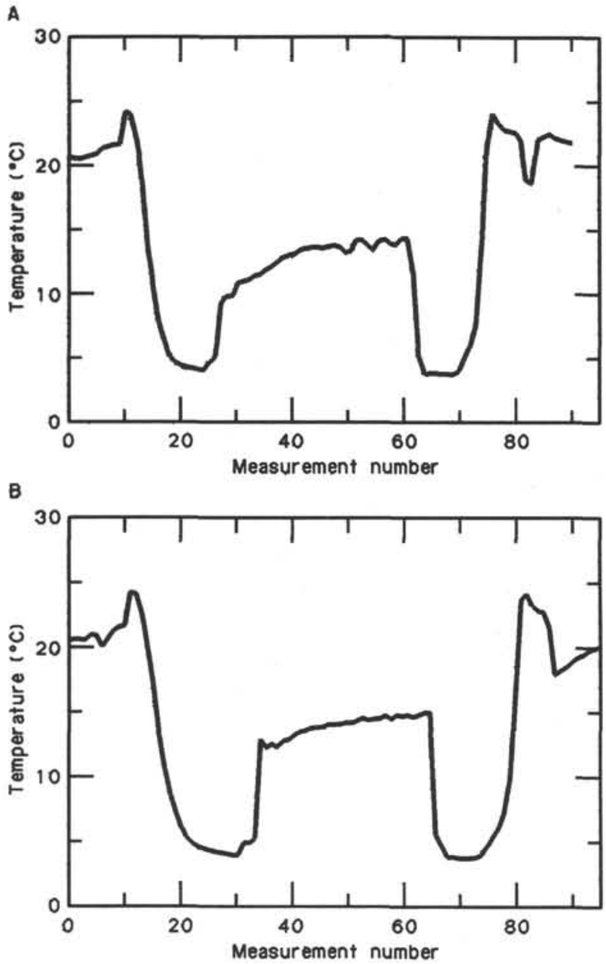

Figure 42. Temperature-versus -time record obtained with the temperature probe in Hole 762B. **A.** 99.4 mbsf. **B.** 156.4 mbsf.

sonic logs, the logs are of excellent quality. Both the near (DT) and the far (DTL) transit-time logs show cycle skips between the bottom of the logged interval (911 mbsf) to 842 mbsf. Above 842 mbsf, both transit-time logs are of good quality up to the Cretaceous/Tertiary boundary interval (554.3 mbsf). Above the boundary interval, the near and far transit-time logs read too low for approximately 20 m. The low values in the far transit-time logs are attributable to cycle skipping, while the low values on the near transit-time log are compatible with those observed for the same interval on the sonic log from the Eendracht-1 well. Above 302 mbsf, both transit-time logs are of marginal quality because of cycle skipping.

The caliper (MCD) encountered tight hole conditions between 218 and 237 mbsf, with hole size decreasing from 35 cm to 13.8 cm in that interval. This appears to have affected only the gamma-ray log, which has spurious low values within this interval (Fig. 46).

Logs obtained with the geochemical tool string included: (1) total gamma ray; (2) the spectra for thorium, potassium, and uranium; and (3) the elemental yields for silicon, calcium, sulfur, aluminum, iron, hydrogen, and chlorine. These logs were recorded from 906.5 to 505 mbsf, and are of good quality throughout the interval.

The third logging run included the neutron porosity, density, and gamma-ray tools. Neutron porosity was not recorded

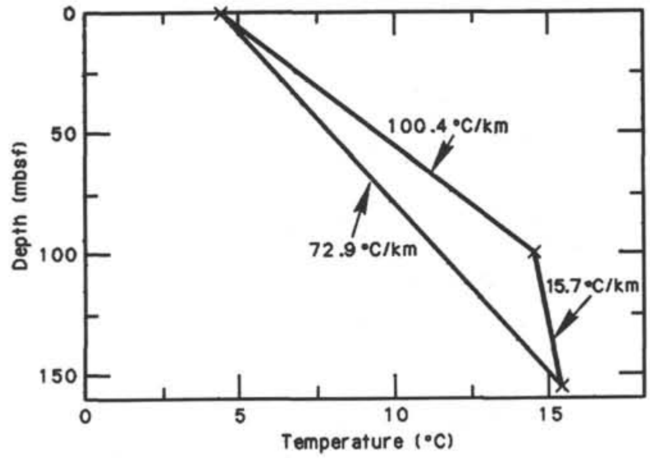

Figure 43. Temperature gradient in Hole 762B.

because of tool failure. Total gamma ray, density, and neutron porosity logs were recorded over the interval 903–182 mbsf.

Log Responses to Lithology

Lithologies at Site 762 include ooze from the seafloor to 187 mbsf, chalk from 187 to 838.5 mbsf, and claystone and clayey siltstone to total depth (940 mbsf). The first lithologic unit sampled by the logging tools was Unit II (187–265 mbsf), a white nannofossil chalk with no appreciable amounts of siliciclastic material. Log values are fairly monotonous over this interval, as indicated by low gamma-ray (10–12 API units), resistivity, and velocity values (Fig. 46).

The change from the white nannofossil chalk of Unit II to the light green-gray nannofossil chalk of Unit III at 265 mbsf is characterized by an increase in gamma-ray values to 15 API units and a positive shift in the resistivity values. Density increases from 1.7 to 1.81, and porosity calculated from density decreases from 60% to 47% below the lithological change. The thorium and potassium logs, which indicate clay content, show no change across this interval, implying that the nonbiogenic component encountered below this horizon is not clay, but probably consists of pyrite and accessory minerals.

Subunit IIIA (265.0–398.0 mbsf) consists of white nannofossil chalk with foraminifers, and shows very light green-gray to light green-gray color cycles. These bands are associated with fluctuating amounts of calcium carbonate versus inorganic components (i.e., quartz, pyrite, and clay), and increase in thickness towards the base of the subunit (see "Lithostratigraphy," this chapter). Below 300 mbsf, the color alternations (e.g., at 308 and 350 mbsf) correspond to very-low-amplitude spikes on the gamma ray and thorium logs (Figs. 46 and 47). Above 300 mbsf, the fine-scale cyclicity is not apparent on the logs because it is below the vertical resolution of the logging tools.

Subunit IIIB (398.0–554.8 mbsf) consists of light green-gray and white nannofossil chalk with the proportion of nonbiogenic material increasing towards the bottom of the subunit. Clay content, as indicated by the potassium and thorium logs, shows little change in the upper part of the subunit, but from 486 mbsf to the base of the subunit it increases significantly over a 25-m interval and remains fairly constant down to the Cretaceous/Tertiary boundary interval (554.8 mbsf). A similarly gradual change is observed in the velocity and resistivity logs, confirming the change to a clay-rich interval in the lower part of the subunit. Smear-slide

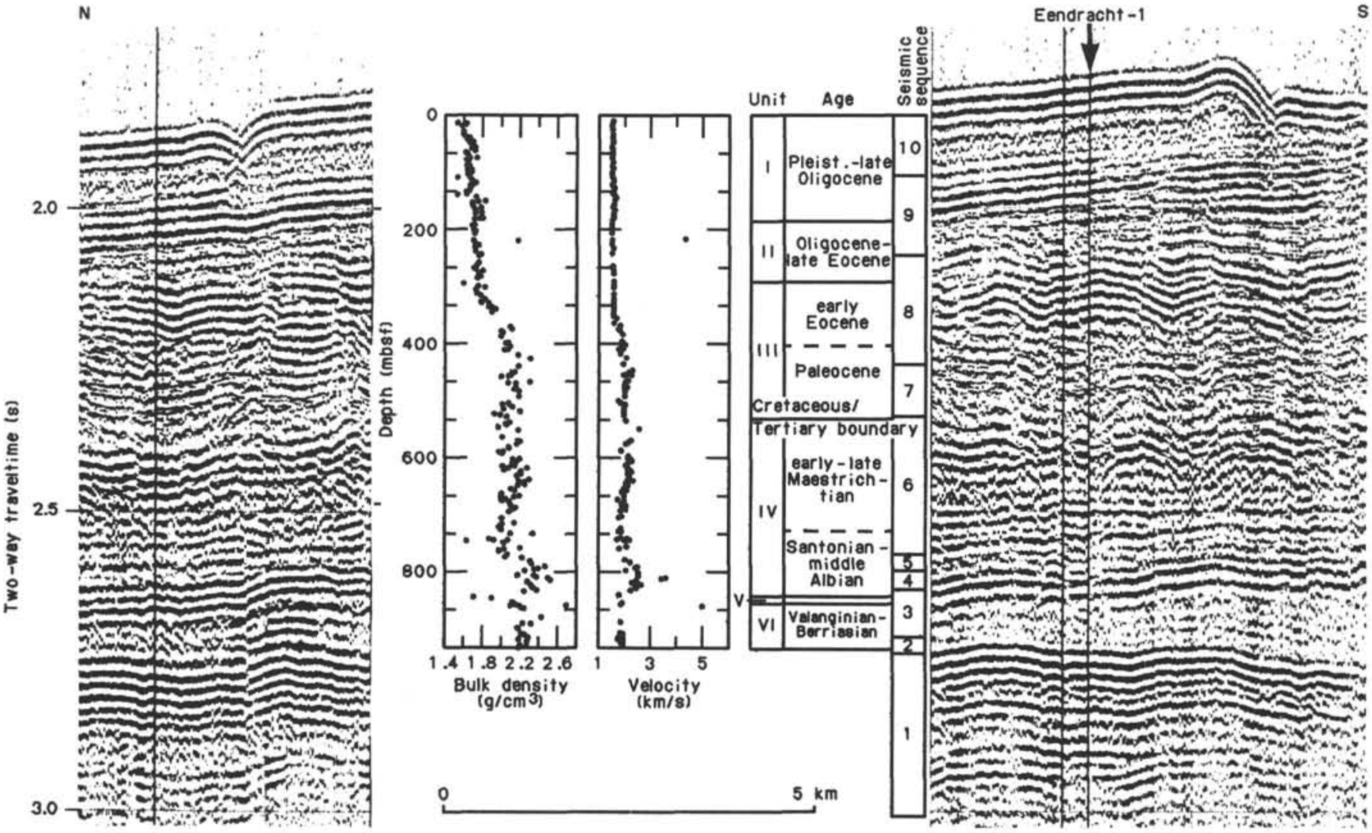

Figure 44. Correspondence between seismic sequences, seismic reflectors and velocity, density, and stratigraphy (derived both from logs and physical properties), Site 762. The seismic profile is a single-channel water-gun record recorded aboard the *JOIDES Resolution*, split at the location of Site 762. Also shown is the location of the Eendracht-1 well.

analysis of this interval indicates that the clay minerals, zeolite, pyrite, and plant debris account for more than 10% of the total sediment.

The base of Unit III (554.8 mbsf) is marked by the Cretaceous/Tertiary boundary and a lithologic change from clayey nannofossil chalk with gypsum near the base to nannofossil chalk below the unconformity. The log response to the chalk below the boundary is characterized by a decrease in gamma-ray values from 30 to 8 API units, a sharp resistivity increase, and a velocity increase from 2.05 to 2.7 km/s (Fig. 46). A porosity decrease from 50% to 40% below the boundary was determined by porosity calculated from density (Fig. 48), the porosity ratio (H/Ca + Si), and the velocity increase. Thorium, potassium, iron, and silicon values are also lower below the boundary, in response to the transition from a clay-rich to almost pure-carbonate sediment. As expected, calcium values are higher below the boundary (Fig. 49).

Log values below the Cretaceous/Tertiary boundary vary very little in the interval between 554.8 and 603.5 mbsf, which corresponds to Subunit IVA. Gamma-ray values are low (10 API units), indicating that the interval is a relatively uniform chalk with low clay content.

The transition from Subunit IVA to Subunit IVB is marked by a gradual downward increase in clay content, as indicated by the increases with depth of gamma ray and thorium, and the decrease in velocity, density, and calcium values (Figs. 46–49). Subunit IVB is characterized by gradational cyclic color changes representing changes between nannofossil chalk and nannofossil claystone (see "Lithostratigraphy," this chapter). Clay content varies between 8% and 60% of total sediment in this interval. Below 619 mbsf, clay content response can be identified on the logs as discrete peaks with wavelengths between 3 and 8 m in length. These responses are particularly obvious on the gamma-ray, resistivity, and silicon/aluminum-ratio logs.

At 697 mbsf, an abrupt decrease in gamma-ray values is associated with a downhole decrease in clay content. Core analysis indicates that the interval from 697 to 780 mbsf (Subunit IVC) consists of white to very light green-gray nannofossil chalk, with nannofossil claystone beds varying between 10 to 80 cm in thickness. These clay-rich beds are not observed on the logs throughout most of the interval and can only be differentiated as individual log responses towards the bottom of this subunit.

The largest log response in Unit IV is a major gamma-ray peak at 820 mbsf. This marks a distinct lithologic change associated with the Turonian/Cenomanian boundary and the top of the Gearle Siltstone equivalent identified in the adjacent Eendracht-1 well. The horizon separates the nannofossil chalks above from the clayey nannofossil chalks below. Gamma-ray values are higher below the boundary, increasing with depth from 12 to 30 API units. Likewise, thorium and potassium values increase, implying an increased clay abundance. However, quartz grains are also present, as suggested by the high Si/Al ratio for this interval (Fig. 49).

The pattern of change between nannofossil chalk and increased amounts of nonbiogenic material in Units III and IV can be easily detected in the logs. The log pattern of calcium-carbonate fluctuations is most obvious on the gamma-ray log (Fig. 50), which is sensitive to changes in the relative abundance of clay-rich material and heavy minerals. These changes are characterized by gradual increases in the relative

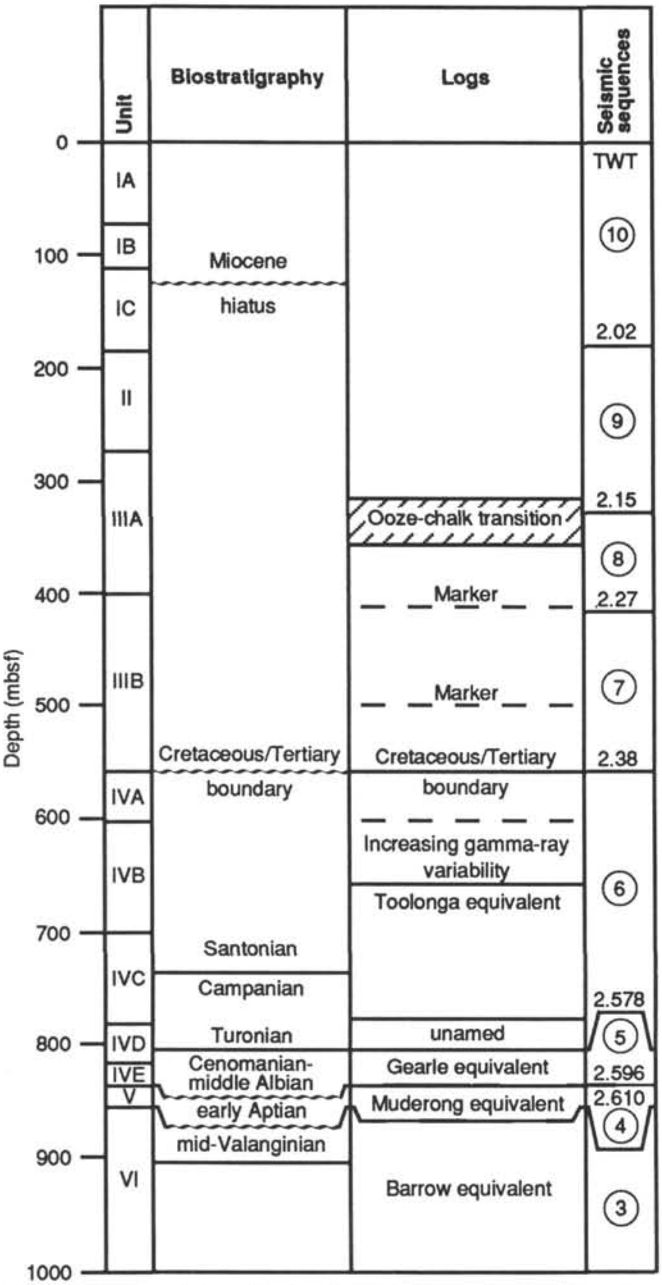

Figure 45. Correlation of seismic sequences, wireline log picks, biostratigraphy, and lithostratigraphy at Site 762.

abundance of inorganic material with an abrupt decrease at the base of each cycle. The gradual increase in detrital material is marked by an increase in gamma-ray values over an interval several tens of meters long. Three of the four cycles observed on the logs are illustrated in Figure 50.

The top of Unit V (838.5–848.5 mbsf) marks a sharp boundary between nannofossil chalk and claystone. The claystone is characterized by high gamma-ray values (80–110 API units), and a downhole decrease in velocity from 2.9 km/s in the chalk to 2.4 km/s in the claystone (Fig. 46). A porosity increase with depth is indicated by resistivity, porosity calculated from density, and the porosity ratio (Fig. 48).

Below the claystone, a change from clay to silt is clearly defined by a sharp decrease with depth in both gamma-ray and Si/Al-ratio logs. This horizon (842–848 mbsf) corresponds to an interval of poor recovery (recovery = 0.8%) and was not sampled. Below the claystone of Unit VI is a silty claystone and clayey siltstone (Unit VI, 848.5–940.0 mbsf), interpreted at this site as the northern extension of the Barrow Group strata (see "Lithostratigraphy," this chapter) and equivalent to the Barrow Group identified in the Eendracht-1 well. This unit is characterized by rapid and complex shifts in the gamma ray, resistivity, density, and the elemental logs (Figs. 46–48), indicating the variability of the sediments that make up this shelf margin prodelta sequence.

SUMMARY AND CONCLUSIONS

Introduction

Site 762 (proposed Site EP12P) is located on the western part of the central Exmouth Plateau at 19°53.24'S, 112°15.24'E, and at a water depth of 1360 m. The site is about 2.5 km northeast of the Eendracht-1 well site. Because of safety considerations, the site was designed to duplicate the upper part of the Eendracht-1 well to a depth of 940 mbsf. Hole 762B was continuously cored by APC to a depth of 175.4 mbsf with an excellent recovery rate of 99%. Hole 762C was washed to 170 mbsf and continuously cored with the XCB from 170 mbsf to a total depth of 940.0 m. The recovery in Hole 762B was moderate to fair, with 534.64 m recovered (recovery = 69%). A significant proportion of this recovery is in the form of sediment slurry between "biscuits" of actual sediments, which in our experience is more common while coring with the XCB than with the RCB.

The main objectives of drilling Site 762 were: (1) to provide documentation of Early Cretaceous to Quaternary depositional sequences and cycles of sea-level change in an area with excellent seismic-stratigraphic and commercial well control, and (2) to study the Cretaceous and Tertiary paleoenvironments during the late rift, juvenile ocean, and mature ocean stages of this sediment-starved passive continental margin. This site, together with central Exmouth Plateau Site 763 (EP7V), located more proximal to the source area of terrigenous influx, furnishes data to separate the tectonic, sedimentary, and eustatic signals for testing sequence-stratigraphic models, and enhances our knowledge about the area's Cretaceous paleoenvironmental evolution. This record was incompletely recovered from the Wombat Plateau transect (Sites 759 to 761) of this leg. The pre-site information from the Esso well Eendracht-1 (including seismic surveys and downhole logging) was helpful in planning Site 762. This was not only of advantage for predictions of stratigraphy, but was also a prerequisite of the JOIDES Pollution Prevention and Safety Panel (PPSP) to safeguard against hazards of drilling in an area of known substantial gas occurrence.

Stratigraphy, Paleoenvironment, and Sedimentation History

The stratigraphic results of Site 762 and some preliminary paleoenvironmental interpretations are summarized in Figure 2D, "Summary and Highlights" chapter, this volume (in back pocket). We discuss the important findings in stratigraphic order.

Berriasian to Early Valanginian Restricted Shelf Margin Prodeltaic Environment (Unit VI, 940.0–848.5 mbsf)

The oldest sediments cored at the base of Site 762 are black silty claystones and clayey siltstones of Berriasian age. These rocks come from just above the base of the Barrow Group equivalent sequence, which according to Eendracht-1 well data is only about 140 m thick at this setting (distal to the sediment source). The Berriasian-to-Valanginian clastic wedge prograded from southeast to northwest across Ex-

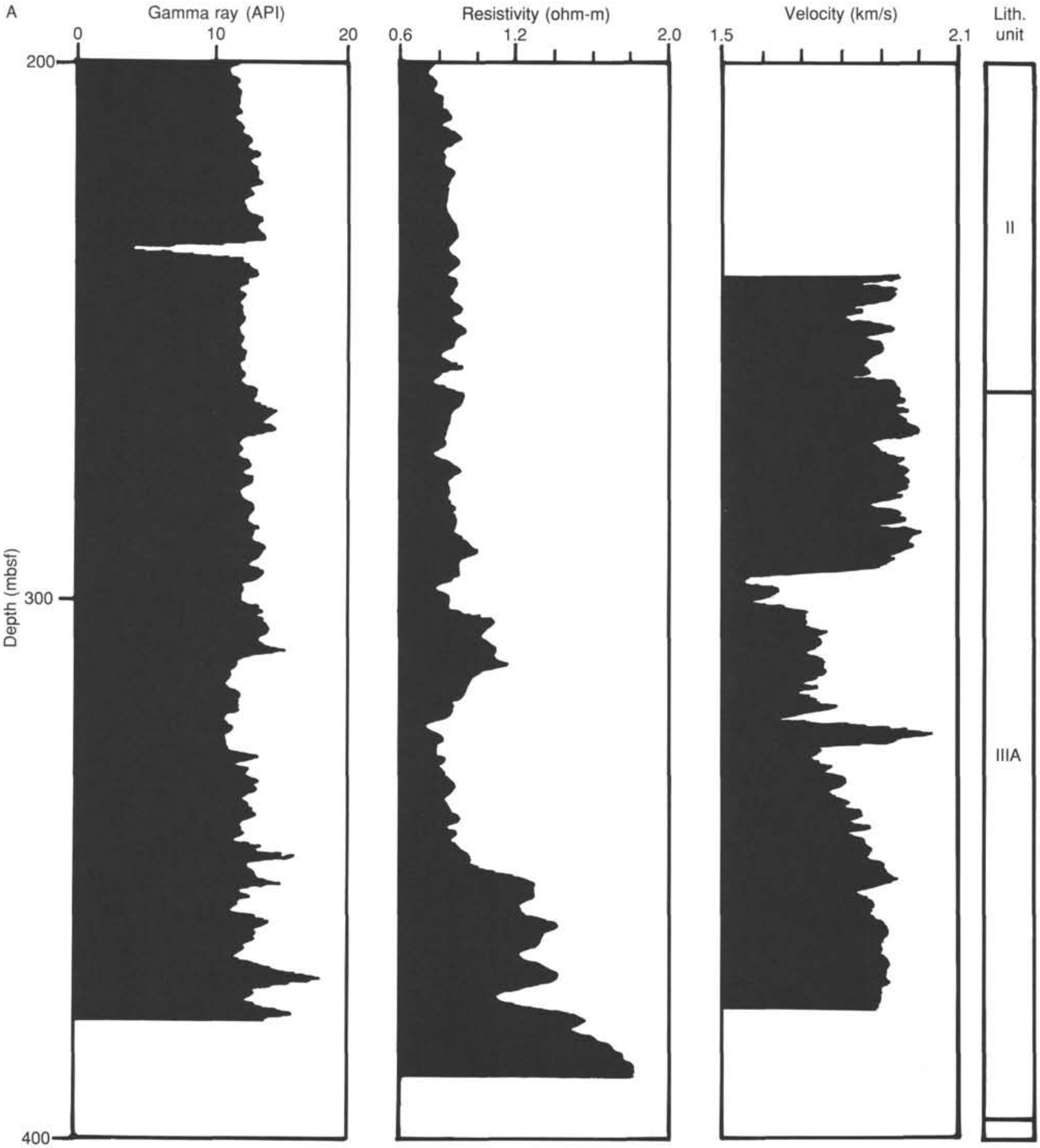

Figure 46. Total gamma-ray, resistivity, and velocity logs for the interval from 200 to 910 mbsf (note scale changes), Hole 762C. **A.** 200–400 mbsf. **B.** 400–610 mbsf. **C.** 610–910 mbsf.

mouth Plateau, and reached a maximum thickness of 1500 m on the central plateau east of Site 762 (Erskine and Vail, 1988). This clastic wedge, which was deposited in less than 7 m.y., is part of a system that included a variety of prograded siliciclastic continental margin deposits (e.g., alluvial plain, deltaic, submarine canyon/fan, and deeper basin-plain settings).

Shore-based studies will correlate the results of Sites 762 and 763 to the well-established seismic stratigraphy and biostratigraphic determinations both from this leg and from numerous commercial wells. This will eventually provide a three-dimensional view of this clastic continental margin wedge and a better understanding of its evolution during Berriasian to Valanginian time. The sequence-stratigraphic interpretation of this expanded, high-sedimentation-rate progradational wedge deposited between the Berriasian (128.5 Ma) erosional unconformity and the top-Valanginian (121 Ma) unconformity is given in Erskine and Vail. (1988). Site 762 is located at the most distal, basinward part of this wedge in a

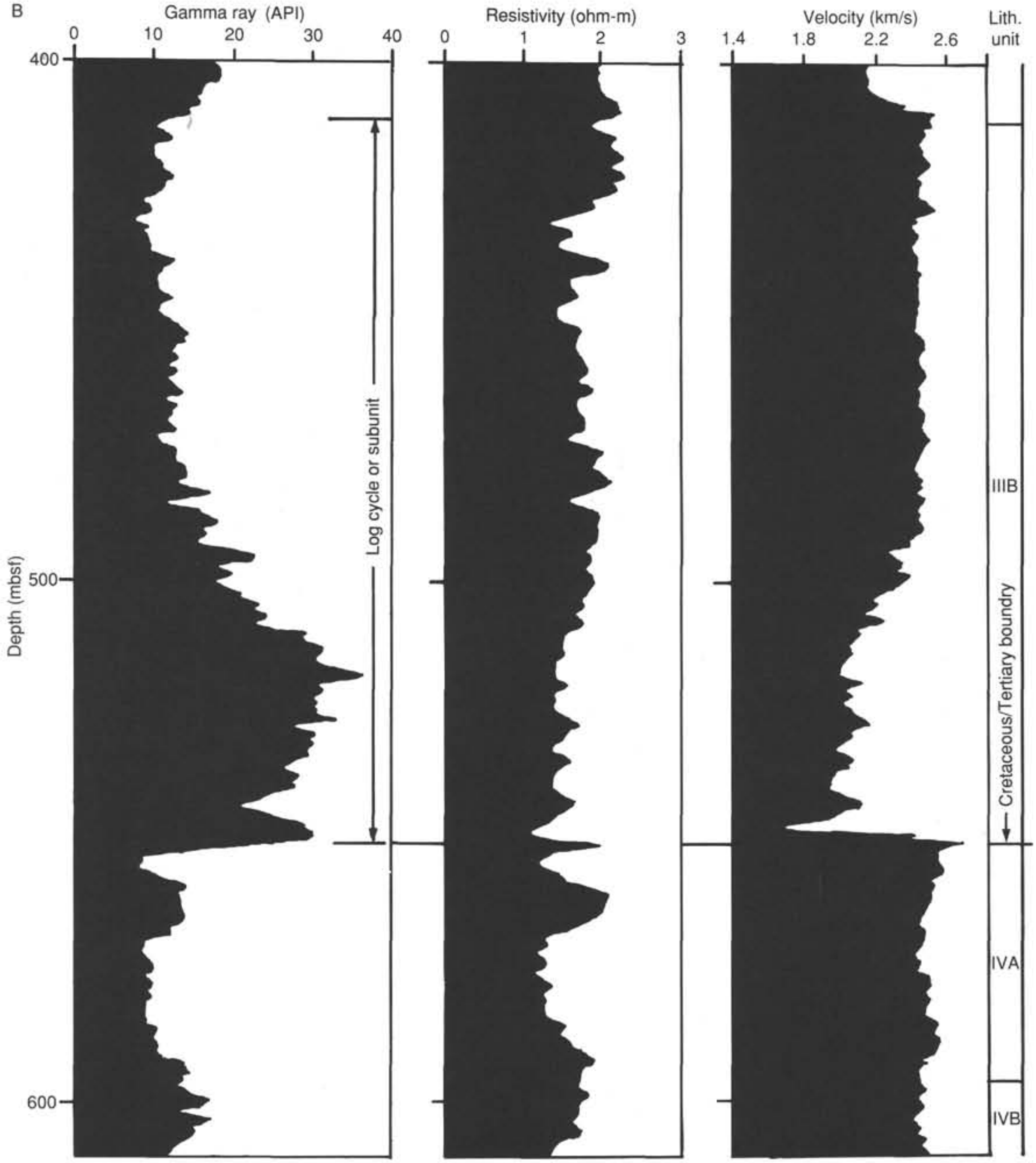

Figure 46 (continued).

"deep-water" (150–300 m), basinal, "shelf-margin prodelta" setting. Lower-than-normal (brackish?) salinities are indicated below 800 mbsf by pore-water chemistry (see "Inorganic Geochemistry," this chapter).

At the time of continental rifting, the central Exmouth Plateau was an epicontinental, restricted (semienclosed), marginal sea with a maximum depth of about 300 m (on the basis of seismic profiles with delta clinoforms), which might be compared to the present-day Yellow Sea (north China) in front of the Huangho delta or even the northwestern Black Sea in front of the Dnieper delta. The shelf break was almost at the site of commercial well site Investigator-1, with canyons and submarine fans north of this well, and a basin plain with silty claystones further seaward, as at the location of Site 762.

The silty claystones contain only 1%–5% carbonate (mollusk? debris and undetermined carbonates, including dolomite rhombs, siderite, etc.), and appreciable percentages of terrigenous quartz, mica, feldspar, glauconite, and pyrite. Clay minerals are the dominant constituent and include mainly kaolinite and illite (besides traces of smectite), a typical association of weathering products transported by rivers from continents in humid climates. Organic carbon content is between 0.6%–1.4%. Mollusk shells are common. Only terrestrial palynomorphs were found. Coccoliths are very rare below Core 122-762C-86X. Glauconite appears to increase with depth. A number of thin limestone beds were discovered in Core 122-762C-82X near the top of Unit VI. These might indicate a sea-level highstand (with cementation during sedi-

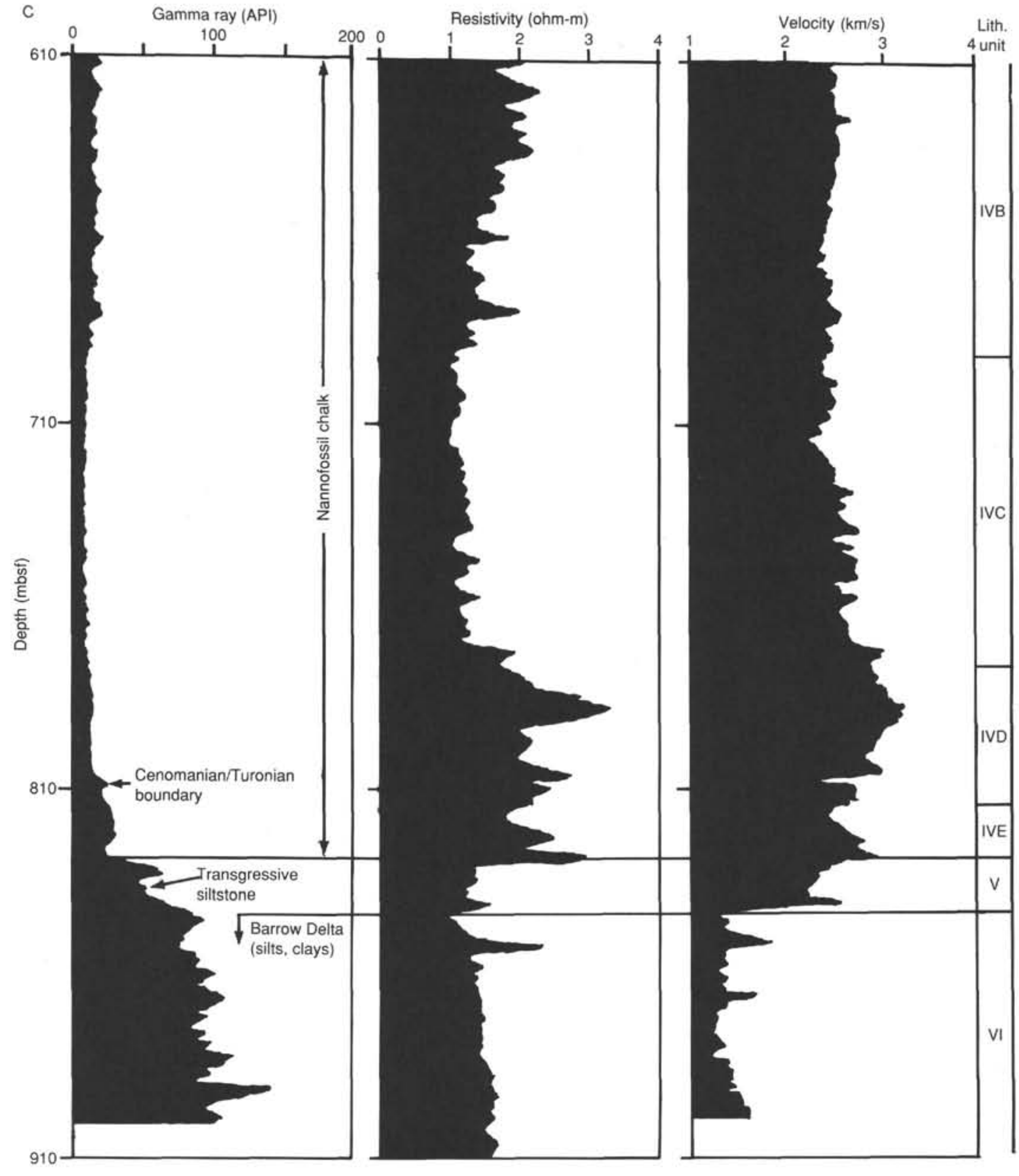

Figure 46 (continued).

ment starvation), preceded by transgressive sediments, and followed by a brief highstand systems track (see "Seismic Stratigraphy," this chapter). The gamma-ray logs show high counts and a frequent alternation of clay- and silt-rich layers. Many belemnites were found, especially in Core 122-762C-81X, which might be indicative of a condensed section within the highstand systems tract, as at Site 761.

Early Aptian Black Claystone (Muderong Shale equivalent, Unit V, 848.5–838.5 mbsf)

The Berriasian-to-Valanginian clastic wedge is truncated by an erosional unconformity, probably documenting a major earliest Aptian sea-level lowstand. The overlying black calcareous claystone of Unit V (early Aptian) is only 10 m thick, suggesting low input of terrigenous material in this transgressive marine unit during rising sea level (Erskine et al., 1988). The lower part of the unit is black, organic-matter-rich claystone (1%–4% $CaCO_3$, 0.8% C_{org}), and grades upward into lighter-colored, more calcareous material to the top. These sediments mark the onset of open-marine, "juvenile-ocean" sedimentation (Veevers and Johnstone, 1974) in a shelf or upper slope setting. The presence of the benthic foraminifer *Epistomina* might indicate shelf depths around or below 200 m, possibly indicating tectonic uplift as the cause of basin shallowing. The base of the unit was deposited under poorly oxygenated conditions, with oxygenation gradually increasing upsection. The presence of dinoflagellates and coccoliths indicates the gradual transition to fully marine conditions, documented by the transition from a siliciclastic to a carbonate-dominated environment.

Near the Valanginian/Hauterivian boundary (Magnetic Anomaly M10), sea-floor spreading commenced at the western and southern margins of the Exmouth Plateau, forming the Gascoyne and Cuvier abyssal plains and marking the final separation of "Greater India" from Australia. In this sense, the Aptian transgression of the central Exmouth Plateau

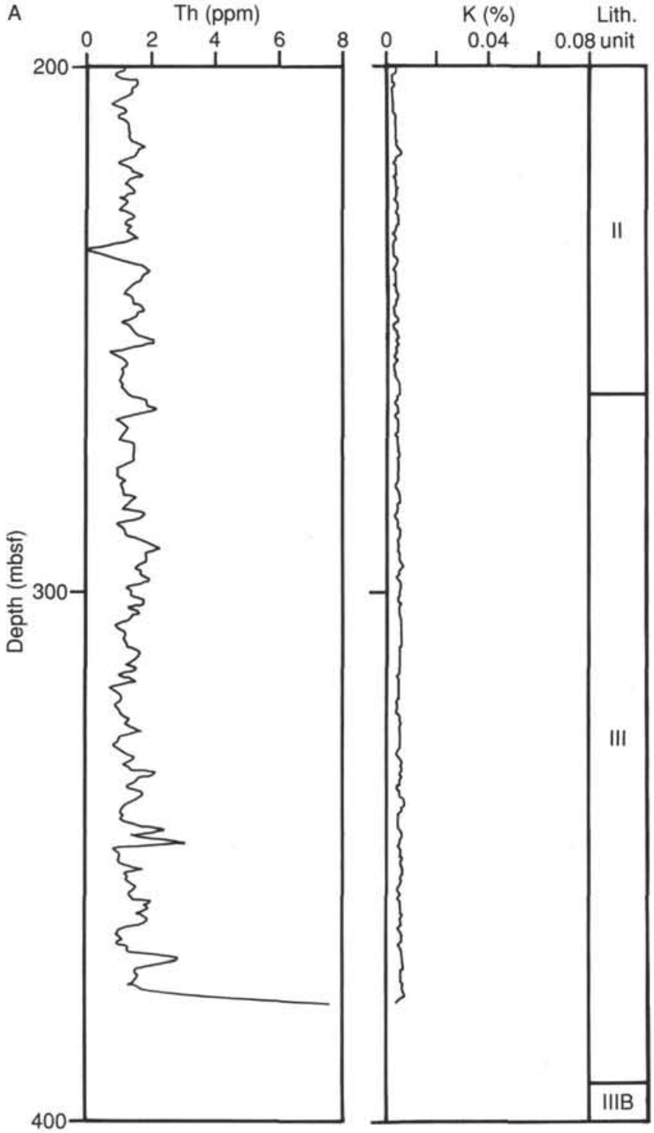

Figure 47. Thorium (Th) and potassium (K) logs for the interval from 200 to 910 mbsf (note scale changes), Hole 762C. **A.** 200–400 mbsf. **B.** 400–610 mbsf. **C.** 610–910 mbsf.

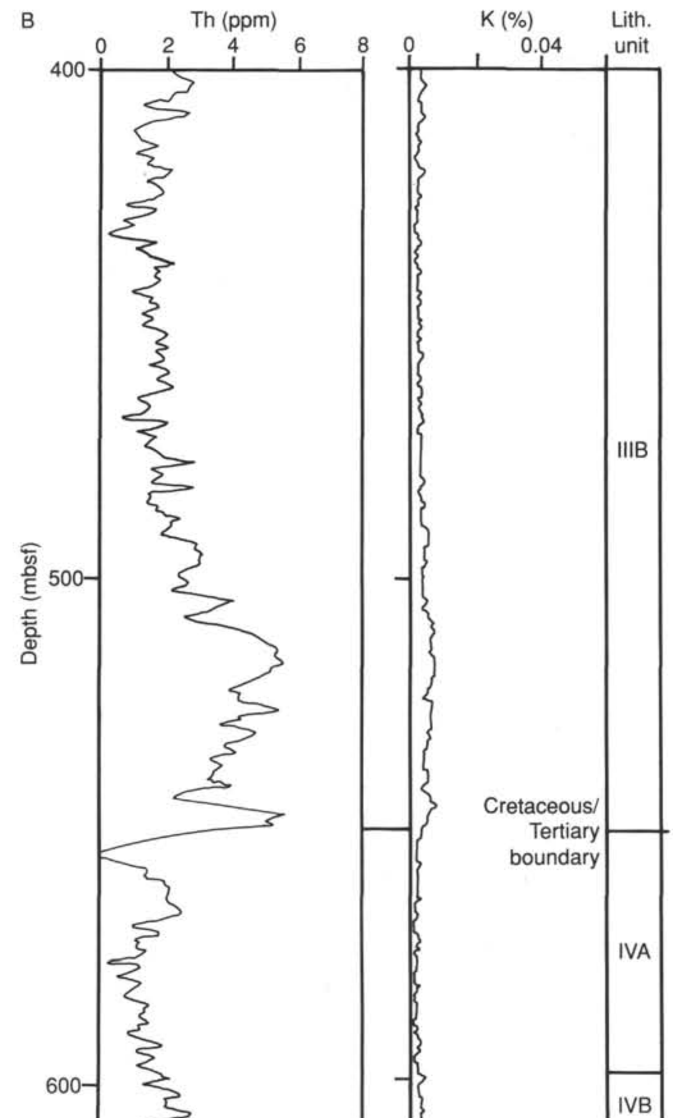

Figure 47 (continued).

postdates continental breakup and the unconformity underlying this unit could be called a "breakup unconformity."

Albian to Early Santonian Hemipelagic Calcareous Claystone/Chalk Sedimentation (Subunits IVD–IVE, 848.5–780.0 mbsf)

During the Aptian (as represented by the base of Subunit IVC), clayey nannofossil chalks (56%–83% $CaCO_3$) were first deposited on the Exmouth Plateau. A sharp downward velocity decrease seen between the chalk and the underlying mudstone is ascribed to changes in the degree of induration. The deposition of chalk marks the onset of carbonate sedimentation under open-marine, thermohaline circulation and productivity conditions, representing the continuation of the "juvenile-ocean stage" (Veevers and Johnstone, 1974). This development is indicated by the upward-increasing abundance of planktonic foraminifers and coccoliths, suggesting an epicontinental pelagic environment similar to the environment under which the northwestern European Late Cretaceous chalks were deposited. Sluggish circulation with oxygen-depleted (to anoxic?) conditions, like those experienced during the early Aptian Unit V, recurred at the Cenomanian/Turonian boundary. The "Cenomanian/Turonian Boundary Event," a global sea-level highstand and "stagnation" event, is marked by a 20-cm-thick organic-matter-rich (15% C_{org}) claystone and a thin (3 cm) black claystone layer in Core 122-762B-75X. Additional detailed shore-based work is necessary to interpret this event.

Subunit IVD (780.0–820.2 mbsf) is characterized by marked (10–30 cm thick) cycles of alternating light-colored chalks and dark-colored calcareous claystones. These cycles correspond to about 35–100 k.y. The minimum $CaCO_3$ values of the calcareous claystones increase from about 54% at the base of the unit to 78% at its top. Anastomosing pressure-suture seams or "microstylolites" in the chalks document pressure solution under high burial conditions. Microstylolites occur between 660 and 840 mbsf, decreasing in abundance upsection. Minimum prerequisites for the pressure solution of calcite at this site are (1) hydrostatic overburden of 660 m, (2) and the geochemical environment of a chalk/calcareous-claystone alternation, and (3) 80 m.y. duration.

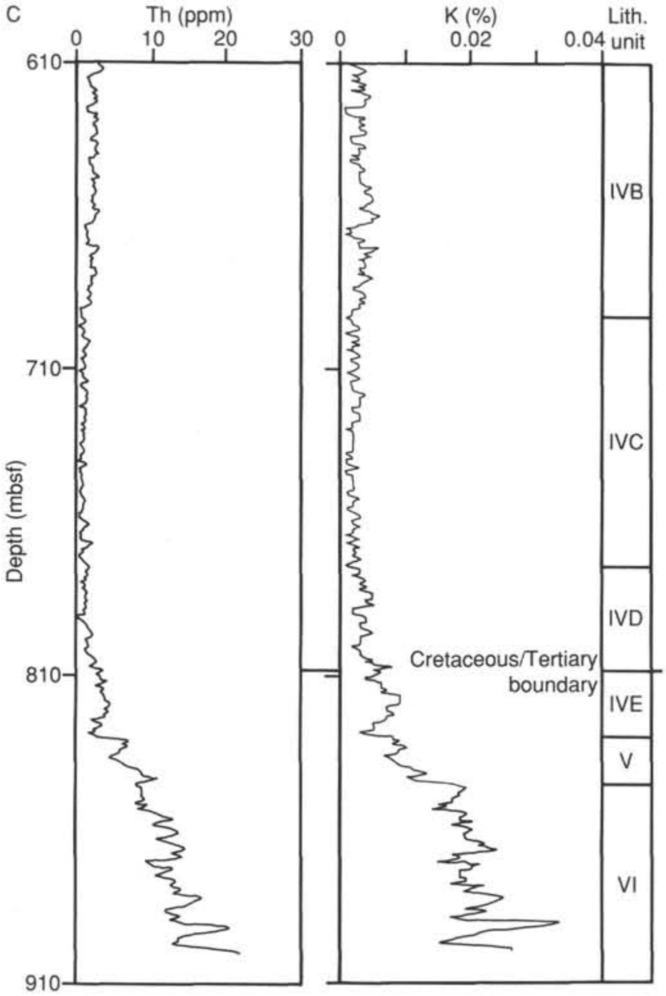

Figure 47 (continued).

Early Santonian to Early Campanian Pelagic Sedimentation (Subunit IVC, 780.0—697.0 mbsf)

Subunit IVC (697.0–780.0 mbsf) is characterized by light green to white, more or less homogeneous chalk (88%–92% $CaCO_3$) without chalk/calcareous-claystone cycles, interbedded with very thin (1–4 cm), green, calcareous claystone layers that might represent rare events of terrigenous input into a predominantly chalk environment.

Early Campanian to Early to Late Maestrichtian Eupelagic Chalk Deposition (Subunits IVA–IVB, 697.0–554.8 mbsf)

Slow, ongoing subsidence of the Exmouth Plateau during late Cretaceous times gradually changed the facies from siliciclastic-dominated (Units VI and V) to a transitional hemipelagic (Subunits IVC and IVD), and finally to eupelagic carbonate-dominated facies (Subunits IVB and IVA).

The early Campanian to early Maestrichtian Subunit IVB (603.5–697.0 mbsf) is characterized by a marked red-brown chalk that contrasts with the over- and underlying (light) green-gray chalks not only in color and composition (somewhat higher $CaCO_3$ contents), but also in the character of the gamma-ray log (higher, more variable counts). Again, color cycles of light-colored chalks (86%–93% $CaCO_3$) alternate with darker colored clayey chalks (60%–72% $CaCO_3$), with a cyclicity of about 20–50 cm. Pressure-solution features (microstylolites) are common in this unit, as in the underlying units. *Inoceramus* prisms are abundant. We observed an unusual downhole porosity increase and sonic velocity decrease in Subunit IVB that indicates a slightly overpressured interval. This unit was probably deposited in bathyal water depths around 1000 m, with more highly oxidizing bottom waters than either before or after this period. Whether the oxidizing paleoenvironment was caused by paleocirculation change, by sedimentation-rate decrease, or sea-level rise remains an open question.

The overlying late Maestrichtian Subunit IVA is characterized by high carbonate contents and light green colors, with alternations of chalks (82%–95% $CaCO_3$) and clayey chalks (56%–70% $CaCO_3$) in 20–50 cm cycles. The chalks are bioturbated, showing well-preserved *Planolites*- and *Zoophycos*-type burrows. Shore-based studies will address the question of whether these cycles were caused by changes in surface-water productivity, in the influx of terrigenous clay material, or in the intensity of bottom-water circulation (Ogg et al., 1987). Thin claystone interbeds spaced about 40–150 cm apart indicate periodic input of terrestrial clay into this carbonate-dominated eupelagic environment.

The Cretaceous/Tertiary Boundary

A possibly complete (although coring-disturbed) Cretaceous/Tertiary boundary interval was recovered at 554.8 mbsf. As at Site 761, the Cretaceous/Tertiary boundary interval is marked by a conspicuous color and compositional contrast; the upper Maestrichtian chalks are white (82%–95% $CaCO_3$) and the lowermost Paleocene clayey chalks are green-gray (50%–55% $CaCO_3$). There is also a distinct upward increase of the gamma-ray values at this boundary. Detailed biostratigraphic, magnetostratigraphic, chemostratigraphic, and isotope-stratigraphic studies will be performed from this critical interval.

Early Paleocene to Mid-Eocene Eupelagic Chalk/Calcareous-Claystone Deposition (Subunits IIIA–IIIB, 554.8–265.0 mbsf)

Subunits IIIA and IIIB document eupelagic carbonate deposition in bathyal water depths (>1000 m) with a high degree of bioturbation. Individual large *Zoophycos*-, *Planolites*-, and *Teichichnus*-type burrows, as well as small *Chondrites*, *Helmenthoidea*, and a great variety of as-yet-undetermined trace fossils were observed. Further shore-based study is necessary to ascertain the paleoenvironments that the trace fossil associations represent (e.g., nutrient supply, rates of clay accumulation, Eh conditions, etc.). Terrigenous clay input peaked during the early Paleocene, just above the Cretaceous/Tertiary boundary interval, with marls containing only 43%–63% $CaCO_3$. The paleoenvironmental significance of this comparatively high clay influx might be explained by a global sea-level lowstand in the early Paleocene, during which the site received resuspended sediments from a nearby shoreline. Upsection, the clay contents diminish rapidly, except for an interval around 400 mbsf (earliest Eocene) with slightly elevated clay content.

A well-developed rhythmicity in color alternations of chalk/marl cycles was observed in both Subunits IIIA and IIIB. In Subunit IIIA (sedimentation rates about 10 m/m.y.), the cycles have a thickness of approximately 50–100 cm. In Subunit IIIB, the chalk/calcareous-claystone cycles are thinner (about 35–60 cm). It is not clear whether these cycles are the result of changes in surface productivity (i.e., nannofossil input) or terrigenous clay input, or a combination of both factors.

Diagenetic changes in these sediments include porcellanite (opal-CT) in Cores 122-762C-21X (360 mbsf, early Eocene)

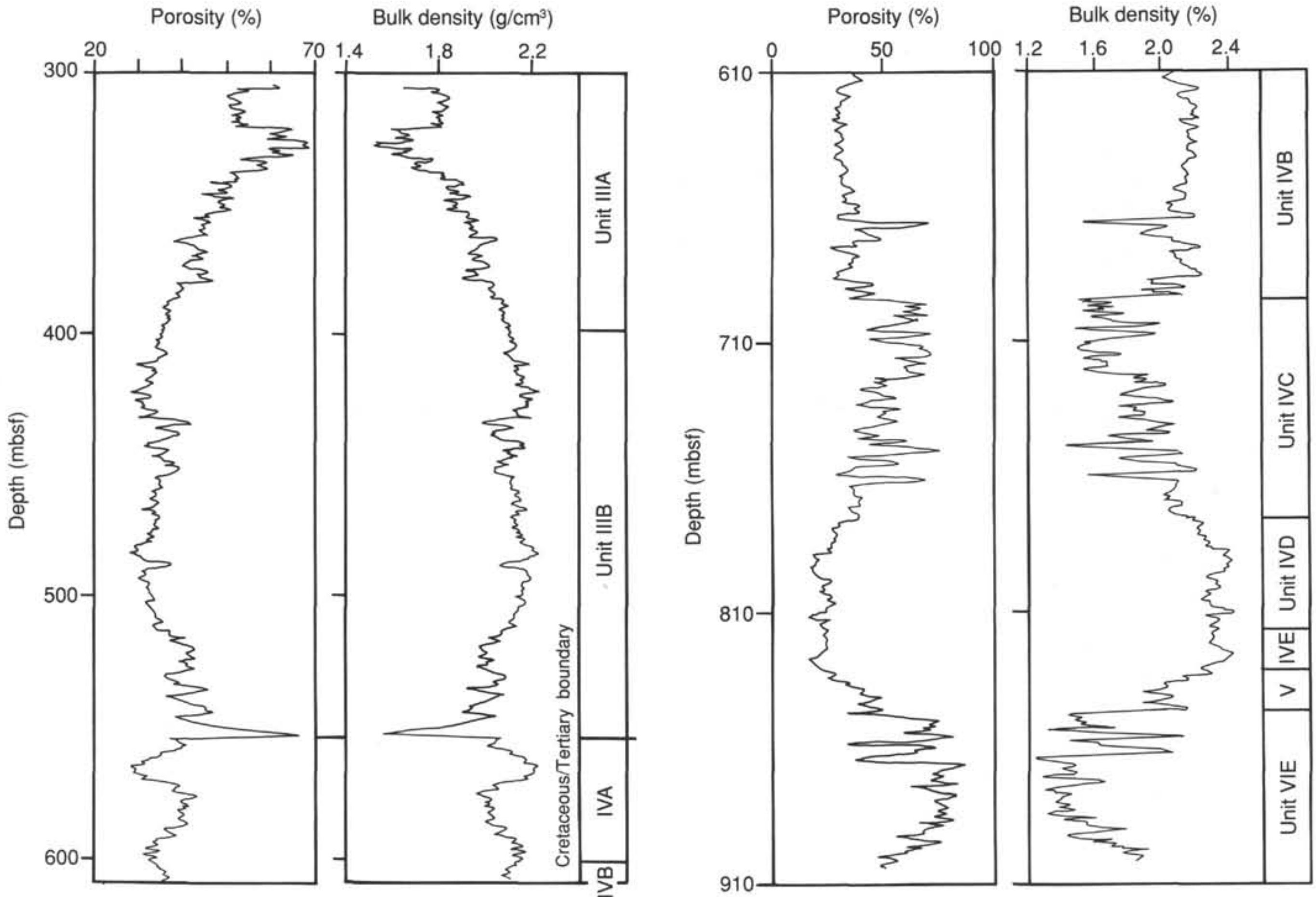

Figure 48. Porosity (calculated from density) and bulk density for the interval from 300 to 910 mbsf, Hole 762C.

and -42X (550 mbsf, early Paleocene), barite in Core 122-762-42X, and the zeolite clinoptilolite in Subunit IC. According to physical-property measurements, the ooze/chalk transition is at about 350 mbsf in Subunit IIIA.

Middle Eocene to Quaternary Nannofossil Ooze Deposition (Unit II–Subunit IA, 265.0—0.0 mbsf)

These units are characterized by eupelagic deposition of foraminifer nannofossil ooze in a bathyal environment, similar to the present situation wherein almost no terrigenous material reaches the isolated central and outer Exmouth Plateau. Sedimentation rates vary, but are generally lower in the Miocene-Oligocene than in the early Paleogene. The section is interrupted by several hiatuses (e.g., between the early and middle Miocene), documenting the activity of erosive bottom currents. A similar depositional regime currently exists on the top of the Exmouth Plateau, with very low deposition rates, winnowing, and periodic erosion.

Porcellanite nodules are present in the lower Upper Eocene (Cores 122-762C-6X to -9X), indicating the well-known global silicoplankton-fertility (and silica-preservation) peak. Subunit IC (118.4–181.5 mbsf) is a low-sedimentation-rate section spanning the middle Miocene to upper Eocene–lower Oligocene. Blooms of *Braarudosphaera bigelowii* in the upper Lower Oligocene to lowest Miocene might indicate a stressed environment (low salinity?). The unit is partly characterized by the additional input of terrigenous clay, mica, and quartz (dilution or lower plankton fertility?). In general, foraminiferal contents increase upward to the Quaternary section, which contains 20%–50% planktonic foraminifers. It is not clear whether this is a result of changes in the productivity of foraminifers versus a constant rate of nannofossil accumulation, or of winnowing by bottom currents, thereby removing the nannofossils and increasing the relative percentage of foraminifers.

Organic Geochemistry

Total organic carbon (TOC) analyses show that TOC contents are very low in the upper 840 m (generally <0.15%), and somewhat higher in the lower 100 m (up to 1.5% in the upper Barrow equivalent strata). Rock-Eval analysis of the lower section reveals the organic matter to be type III (land-derived, woody-coaly organic matter). The C_1–C_2 trend in the hole was as predicted by the nearby Eendracht-1 well: low in the Oligocene-Neogene oozes, considerably higher in the underlying Paleogene and Maestrichtian chalks and Toolonga Calcilutite equivalent strata (up to a maximum of >128,000 ppm), and then markedly lower in the Gearle Siltstone and underlying Muderong Shale and Barrow Group equivalent sediments. Two samples, from about 857 mbsf and 913 mbsf, were analyzed for higher-molecular-weight hydrocarbons; the sample from 857 mbsf contained a relatively large amount of C_{15}–C_{17} normal alkanes (see "Organic Geochemistry," this chapter).

Evaluation of geochemical logs from Site 762 confirmed that there were no hydrocarbon-bearing intervals in the cored section. Although high C_1 values (up to 128,000 ppm) were recorded from about 400–850 mbsf, no free-hydrocarbon intervals are apparent on the induction log, and resistivity

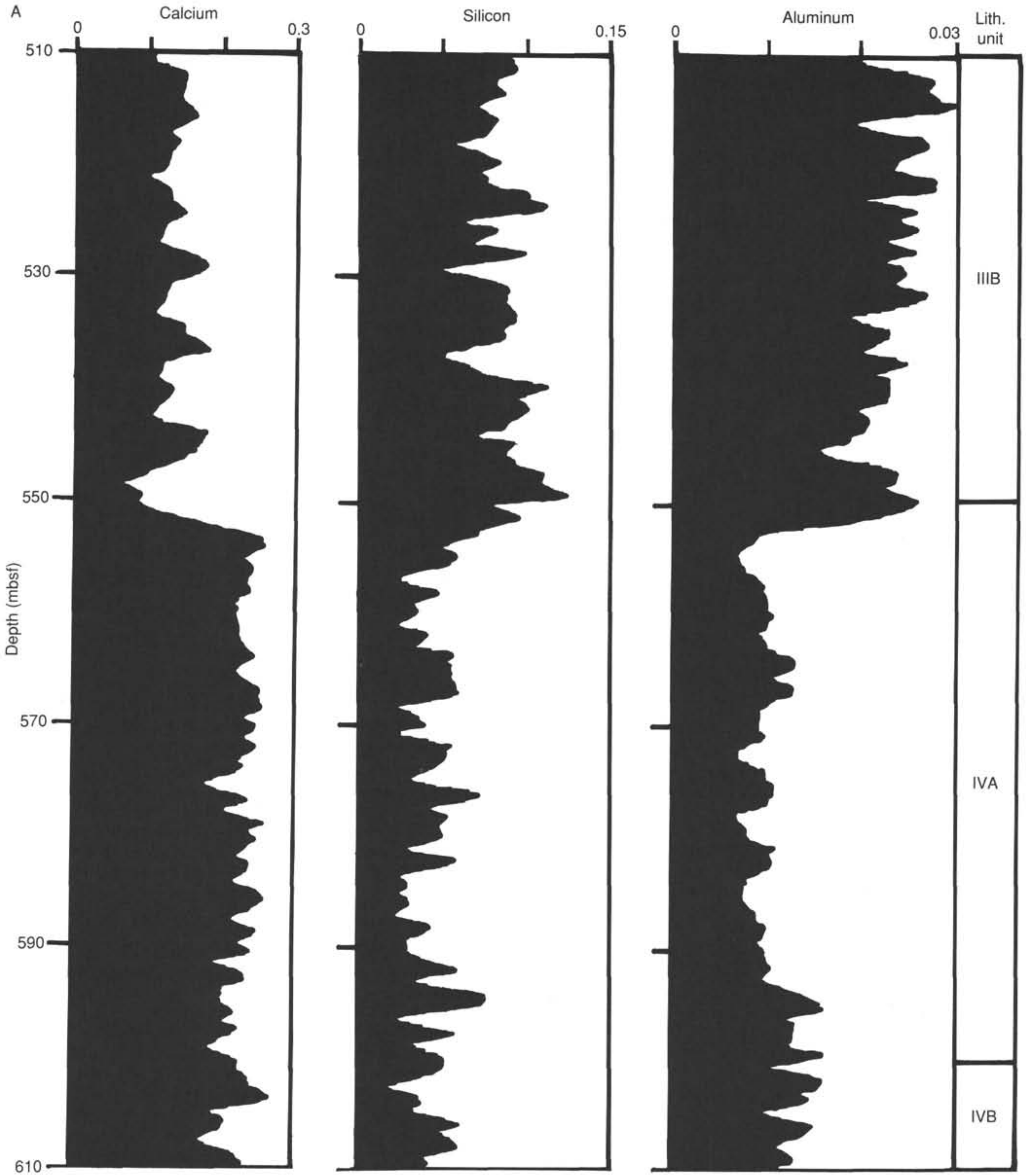

Figure 49. Calcium, silicon, aluminum, and silicon/aluminum ratio logs for the interval from 510 to 910 mbsf, Hole 762C. **A.** 510–610 mbsf. **B.** 610–910 mbsf.

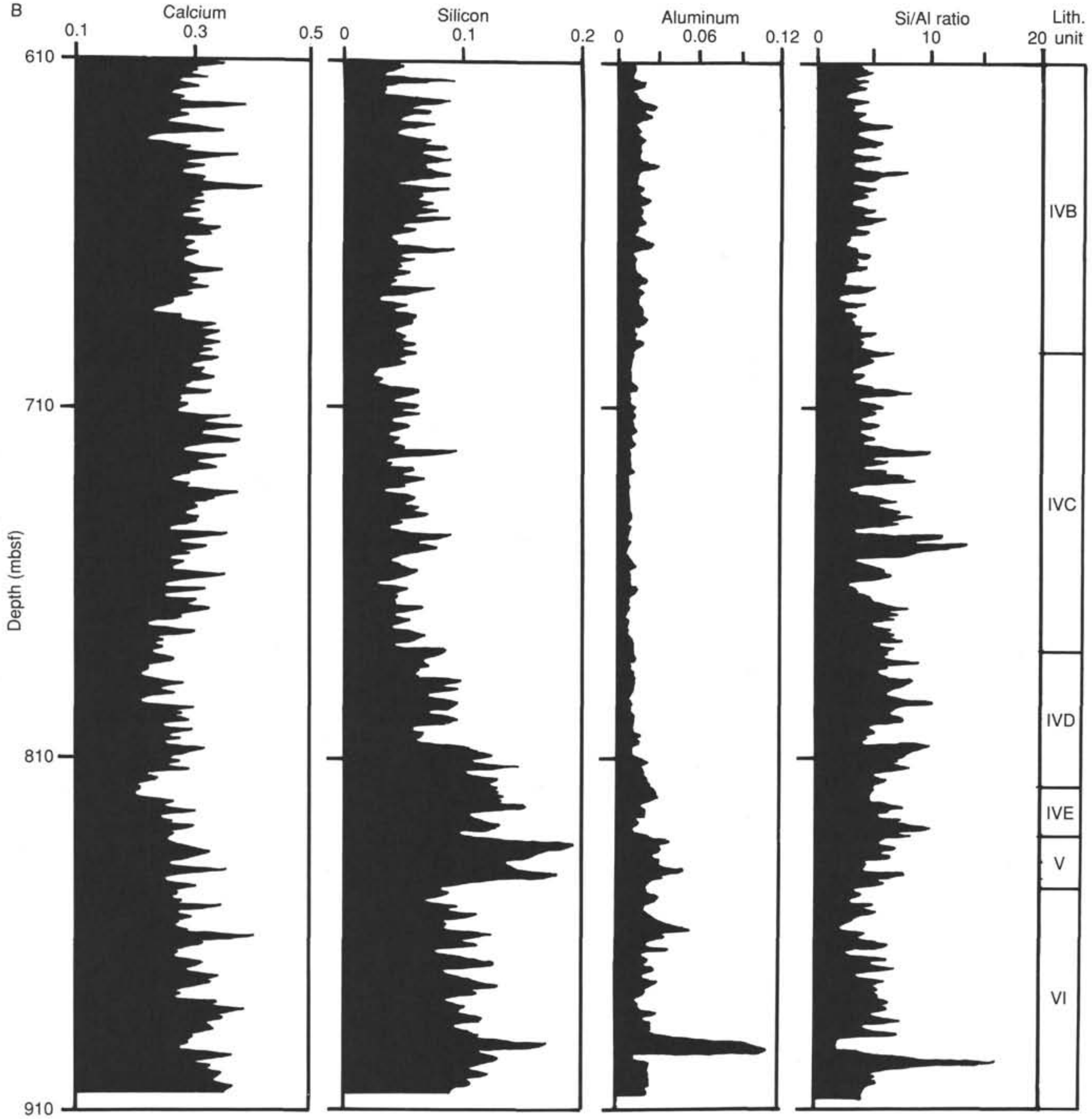

Figure 49 (continued).

values compare well with those obtained from the Eendracht-1 well. However, a downward increase in hole rugosity and the reversal in the normal compaction trend, indicated by the lower velocity and resistivity and the higher porosity between 600 and 715 mbsf, suggest the presence of a slightly overpressured interval. This may also explain the high gas values recorded in this interval.

Inorganic Geochemistry

The chemistry of Site 762 interstitial waters is affected by diffusion processes throughout the unconsolidated oozes. Evidence of carbonate diagenesis and silica diagenesis (e.g., dissolution of opaline skeletons, precipitation of authigenic silicates such as zeolites and opal-CT, and uptake of SiO_2 by clay minerals) is found in the Mg^{2+}, Ca^{2+}, and SiO_2 profiles. Below 200 mbsf, diffusion processes are weaker and interstitial fluids maintain compositions that reflect the local lithology. Sulfate reduction takes place down to 600 mbsf, and thereafter no further depletion is evident.

Physical Properties

The mean compressional velocity data from Site 762 generally show a range from 1.52 to 3.56 km/s. Oozes and claystones have relatively constant velocities (about 1.55 and 1.9 km/s, respectively). The velocities are also within a narrow range in the chalks from about 450 mbsf until just

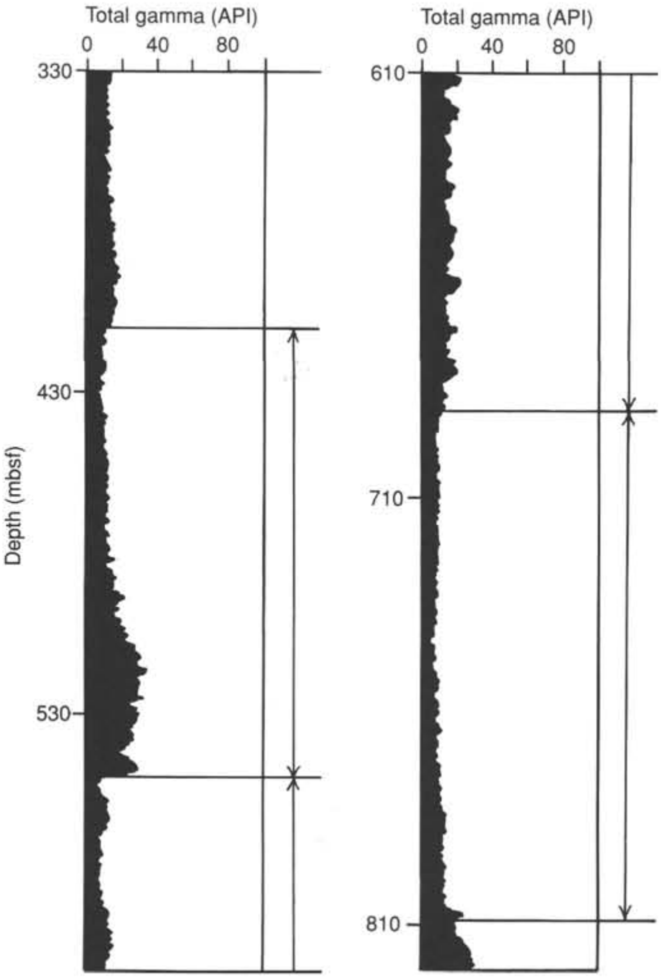

Figure 50. Gamma-ray response to an increase in clay abundance, and three of the cycles observed on the logs, Hole 762C.

above the Cretaceous/Tertiary boundary (554 mbsf) where there is a local velocity increase with depth (from about 2.0 to 2.5 km/s). Chalks between about 600 and 700 mbsf exhibit a downward velocity decrease from about 2.3 to about 1.8 km/s. Grain densities are relatively constant throughout the hole. Wet-bulk densities in the oozes increase relatively linearly with depth until about 320 mbsf. Between 320 and 360 mbsf wet-bulk density increases from 1.80 to 2.12 g/cm^3, is generally constant at about 2.12 g/cm^3 from around 400 to 770 mbsf (where there is an increase to about 2.5 g/cm^3), followed by a sharp decrease in bulk density at the chalk-claystone contact (840 mbsf).

Porosity and water-content values show good correlation throughout the borehole and an inverse correlation with velocity. Porosities start at 74.3% at the top of the hole and decrease with depth until around 600 mbsf. The data then show an unusual, gradual downward increase to about 700 mbsf—a reversal of normal compaction. Porosity and water content sharply decrease below around 770 mbsf, increase briefly at 840 mbsf and then continue to slowly decrease to the base of the hole. Thermal conductivity displays a general increase with depth, ranging from 1.033 W/m·K at the top of the hole to 1.804 W/m·K at 371.3 mbsf. GRAPE data agree well with the gravimetric data in terms of magnitude and small variations between each measurement.

The velocity and porosity response in chalks between approximately 600 and 700 mbsf (Subunit IVB) suggests an increase of porosity caused by the increased abundance of hollow, biogenic grains in the sediment. High wet-bulk density values below the hiatus around 133 mbsf at Site 762 may be the result of additional water loss from the sediments during a period of nondeposition, with low wet-bulk density values above the hiatus possibly caused by overpressuring that resulted from the rapid sedimentation rate.

Downhole Measurements

Three tool strings were run at Site 762. They consisted of (1) the seismic stratigraphic string (sonic, caliper, resistivity, total gamma ray and thorium, uranium, and potassium spectral logs), and (2) the geochemical string (total gamma ray, Th-K-U spectra, and elemental yields of Si, Ca, S, Al, Fe, H, and Cl), and the lithodensity string (neutron porosity, density, and gamma ray). All tools provided high quality data with the exception of the sonic logs which showed cycle skips and the density log, which failed to function.

In general, lithologic units at Site 762 showed good correlation with log data and also corresponded well with formation tops (Figs. 44 and 45) picked from the adjacent Eendracht-1. Logs were relatively flat and featureless down to the Cretaceous/Tertiary boundary. This boundary was clearly seen in all logs at 554.8 mbsf and was identified as a transition from an overlying clayey nannofossil chalk to an underlying nannofossil chalk with high carbonate content. This pattern of gradual downward increase in clay content followed by a decrease characterizes Site 762 from the Cretaceous/Tertiary boundary interval to at least the Cenomanian/Turonian boundary interval (810 mbsf). The pattern is seen on the logs as a gradual downward increase in gamma-ray values, and a decrease in sonic velocity, density, and calcium content, followed by reversal in trend for each log.

The Barrow Group equivalent below 850 m is a terrigenous mudstone with thin interbedded carbonate units and is characterized by high gamma ray, low sonic velocity, low Ca content, and local reversals in these values in the carbonate intervals. Between the Barrow Group of Valanginian-Berriasian age and the Aptian/Albian boundary at 835 mbsf, the Muderong Shale equivalent occupies a transition zone from clastic to carbonate-dominated environments. This transition is shown by an upward decrease in gamma-ray values and increases in velocity, resistivity, density, and calcium content. Interpretation of the major trends in log data at Site 762 indicates that the fluctuations in carbonate content reflect variations in sediment supply and that these may in turn be correlated to depositional sequences and possibly to sea-level cycles.

Biostratigraphy

At Site 762 a nearly complete Cenozoic section, including an expanded Paleocene, was recovered with well-preserved and abundant nannofossils and foraminifers. Minor hiatuses in sedimentation occur in the upper Lower Miocene and at the Cretaceous/Tertiary boundary. Calcareous plankton are less abundant and more poorly preserved in the Cretaceous part of the sequence than in the Cenozoic. *Braarudosphaera bigelowii* blooms, which represent stressed environments, occur in the lower Oligocene and the lowest Lower Miocene. Radiolarians occur in low numbers in the Quaternary and Eocene, with occasional poorly preserved specimens encountered in the Cretaceous. No Cenozoic palynomorphs were recorded. Dinoflagellates occur in the lower Valanginian through Aptian, and terrestrial palynomorphs in the Berriasian-Valanginian Barrow Group equivalent part of the section.

Magnetostratigraphy

Preliminary shipboard magnetic measurements on cores recovered at Site 762 demonstrate that a good paleomagnetic stratigraphy can be derived for the Quaternary and the middle Miocene part of the section. In addition, the middle Eocene interval may also yield a meaningful magnetic polarity record. However, whole-core analysis of other parts of the section proved inconclusive, and shore-based discrete sample analyses will be necessary to ascertain the presence of an unadulterated magnetic signal.

Seismic Stratigraphy

Most of shipboard-site-survey seismic-reflection Line 122-4 (collected to locate Site 762) was obtained while GPS navigation was available and was thus accurately navigated. Site 762 is located 2.5 km northeast of the Eendracht-1 well at shotpoint 2625 on Line X79B-1425 (petroleum exploration data shot for Esso Australia) and at 207.1818 on Line 122-4, at a water depth of 1360 m.

The structural configuration of the region of Site 762 is made up of north and north-northeast trending faults, predominantly downthrown to the west (Exon and Willcox, 1978; Barber, 1982). The faults were active in the late Triassic but the major movement along these faults may have been in the Callovian and resulted in fault throws on the order of hundreds of meters. The upthrown sides of the tilted fault blocks are commonly eroded, and upper Jurassic and Cretaceous strata infill half grabens and drape the fault blocks formed by rifting in the Callovian. Reactivation of the rift faults offsets seismic horizons corresponding to strata within the Cretaceous section, but reactivation decreased progressively into the late Cretaceous and is rarely seen to displace the seismic horizon corresponding to the Cretaceous/Tertiary boundary.

Using methods outlined in Vail et. al (1977), at least ten seismic sequences were distinguished at Site 762 (Fig. 44). From the three lowermost recovered, the following major implications for facies, environments, and sea level were derived. Two sets of prograding clinoforms in sequence 3 indicate northward sediment dispersal from a source along the southern margin of the Exmouth Plateau or from the adjacent southern block. The clinoforms are on a large scale with over 300 m of relief, and indicate deposition on a northward prograding continental margin/slope (Sangree and Widmier, 1977). Available log, lithostratigraphic, biostratigraphic, and seismic stratigraphic data suggest that the upper unit may occupy a full sea-level cycle of Valanginian age. In this case the limestone in this unit would represent a condensed section.

Sequence 4 appears to be a thin, distal clastic unit deposited in a deep basinal setting. Seismic resolution at Site 762 is only capable of defining one sequence and indicating an onlapping relationship with Sequence 3 below. Shipboard biostratigraphy dates this sequence as Aptian nannofossil Zone NK6, and lithostratigraphic results show that clastic influence decreases upward. These factors again suggest the presence of a single cycle, deposited primarily under rising relative sea level.

Sequence 5 is also a thin basinal unit with only a minor clastic input that decreases upward. Seismic data suggest that the sequence was deposited in a primarily deep-water environment with an onlapping relationship to Sequence 6 below. This indicates that, like Sequence 4, Sequence 5 occupies only one sea-level cycle at Site 762 and was deposited primarily under a rising sea level separated by lowstands at the upper and lower sequence boundaries. The age of Sequence 5 extends from Albian to Cenomanian. Above Sequence 5, sediments were deposited primarily in a pelagic environment and this is supported by the dominantly parallel, conformable, and continuous reflectors present in each sequence.

REFERENCES

Arthur, M. A., Dean, W. E., Bottjer, O., and Scholle, P. A., 1984. Rhythmic bedding in Mesozoic-Cenozoic pelagic carbonate sequence: the primary and diagenetic origin of Milankovitch-like cycles. *In* Berger, A., Imbrie, J., Hays, J., Kukla, G., and Saltzman, B. (Eds.), *Milankovitch and Climate* (Pt. 1): NATO ASI Ser. C: Math. Phys. Sci. 176:191–223.

Barber, P. M., 1982. Paleotectonic evolution and hydrocarbon genesis of the Central Exmouth Plateau. *APEA J.*, 22:134–44.

Borella, P. E., 1984. Sedimentology, petrology, and cyclic sedimentation patterns, Walvis Ridge transect, Leg 74, Deep Sea Drilling Project. *In* Moore, T. C., Jr., Rabinowitz, P. D., et al., *Init. Repts. DSDP,* 74: Washington (U.S. Govt. Printing Office), 645–662.

Bralower, T. J., 1987. Valanginian to Aptian calcareous nannofissil stratigraphy and correlation with the upper M sequence magnetic anomalies. *Mar. Micropaleontol.*, 11:293–310.

Bralower, T. J., Monechi, S., and Thierstein, H. R., 1989. Calcareous nannofossil zonation of the Jurassic-Cretaceous boundary interval and correlation with the geomagnetic polarity timescale. *Mar. Micropaleontol.*, 14:153–235.

Bukry, D., 1974. Coccoliths as paleosalinity indicators—evidence from Black Sea. *AAPG Mem.*, 20:335–353.

———, 1981. Cenozoic coccoliths from the Deep Sea Drilling Project. *Soc. Econ. Paleontol. Mineral Spec. Publ.*, 32:335–353.

Chamberlain, C. K., 1978. Recognition of trace fossils in cores. *In* Basan, P. B. (Ed.), *Trace Fossil Concepts*: Soc. Econ. Paleontol. Mineral., Short Course, 5:119–116.

Claypool, G. A., and Kvenvolden, K. A., 1983. Methane and other hydrocarbon gases in marine sediment. *Ann. Rev. Earth Planet. Sci.*, 11:299–327.

Culberson, O. L., and McKetta, J. J., Jr., 1951. Phase equilibria in hydrocarbon-water systems, Part 3: the solubility of methane in water at pressures to 10,000 psi. *Trans. Soc. Pet. Eng. AIME,* 192:233–226.

Emeis, K.-C., and Kvenvolden, K. K., 1986. Shipboard organic geochemistry on *JOIDES Resolution. ODP Tech. Note*, 7.

Erskine, R., and Vail, P. R., 1988. The Exmouth Plateau. *In* Bally, A. W. (Ed.), *Atlas of Seismic Stratigraphy* (Vol. 2). AAPG Stud. Geol., 27:163–173.

Exon, N. F., von Rad, U., and von Stackelberg, U., 1982. The geological development of the passive margin of the Exmouth Plateau off northwest Australia. *Mar. Geol.*, 47:313–152.

Exon, N. F., and Willcox, J. B., 1978. Geology and petroleum potential of the Exmouth Plateau area off Western Australia. *AAPG Bull.*, 62:40–72.

———, 1980. The Exmouth Plateau: stratigraphy, structure and petroleum potential. *Bull. Bur. Min. Resour. Geol. Geophys.*, 199:1–52.

Falvey, D. A., 1974. The development of continental margins in plate tectonics theory. *APEA J.*, 14:95–106.

Falvey, D. A., and Mutter, J. C., 1981. Regional plate tectonics and the evolution of Australia's continental margins. *BMR J. Aust. Geol. Geophys.*, 6:1–29.

Garland, G. D., 1979. *Introduction to Geophysics.* Philadelphia (Saunders).

Gieskes, J. M., 1974. Interstitial water studies, Leg 25, DSDP. *In* Heezen, B. C., and MacGregor, I. D., et al., *Init. Repts. DSDP,* 20: Washington (U.S. Govt. Printing Office), 813–829.

———, 1981. Deep-sea drilling interstitial waters: implications for chemical alteration of the oceanic crust, Layer I and II. *Soc. Econ. Paleontol. Mineral. Spec. Publ.*, 31:149–167.

Haq, B. U., Hardenbol, J., and Vail, P. R., 1987. Chronology of fluctuating sea levels since the Triassic. *Science,* 235:1156–1166.

Hays, J. D., Imbrie, J. and Shackelton, N. J., 1976. Variations in the earth's orbit: pacemaker of the ice ages. *Science,* 194:1121–1132.

Helby, R., Morgan, R., and Partridge, A. D., 1987. A palynological zonation of the Australian Mesozoic. *Mem. Assoc. Australas. Palaeontol.*, 4:1–95.

Hunt, J. M., 1979. *Petroleum Geochemistry and Geology:* San Francisco (W. H. Freeman).

Jenkins, D. G., 1985. Southern mid-latitude Paleocene to Holocene planktonic foraminifera. *In* Bolli, H. M., Saunders, J. B., and Perch-Nielsen, K. (Eds.) *Plankton Stratigraphy:* Cambridge (Cambridge Univ. Press), 263–283.
Kastner, M., and Gieskes, J. M., 1976. Interstitial water profiles and sites of diagenetic reactions, Leg 35, DSDP, Bellinghausen Abyssal Plain. *Earth Planet. Sci. Lett.,* 33:11–20.
Lemoine, M., and Trümpy, R., 1987. Pre-oceanic rifting in the Alps. *Tectonophysics,* 133:305–320.
Leythaeuser, D., Schaefer, R. G., and Pooch, H., 1983. Diffusion of light hydrocarbons in subsurface sedimentary rocks. *AAPG Bull.,* 67:889–895.
Leythaeuser, D., Schaefer, R. G., and Yukler, A., 1982. Role of diffusion in primary migration of hydrocarbons. *AAPG Bull.,* 66:408–429.
Martini, E., 1971. Standard Tertiary and Quaternary calcareous nannoplankton zonation. *Proc. 2nd Planktonic Conf.:* Rome (Ed. Technoscienza), 739–785.
Mauffret, A., and Montadert, L., 1987. Rift tectonics on the passive continental margin of Galicia (Spain). *Mar. Petrol. Geol.,* 4:49–70.
Milankovitch, M., 1938. Astronomische Mittel zur Erforschung der erdgeschichtlichen Klimate. *Handb. Geophys.,* 9:593–698.
Moullade, M., 1984. Intérêt des petits foraminiferes benthiques "profonds" pour la biostratigraphie et l'analyse des paleoenvironnements oceaniques Mésozoiques. *In* Oertli, H. J. (Ed.), *2nd Int. Symp. Benth. Foraminifera,* 429–464.
Mutter, J. C., Larson, R. L., and the NW Australian Study Group, 1989. Extension of the Exmouth Plateau: deep seismic reflection/refraction evidence for simple and pure shear mechanisms. *Geology,* 16:15–18.
Ogg, J. G., Haggerty, J., Sarti, M., and von Rad, U., 1987. Lower Cretaceous pelagic sediments of DSDP, Site 603, Western North Atlantic: a synthesis. *In* Van Hinte, J. E., Wise, S. W., Jr., et al., *Init. Repts. DSDP,* 93: Washington (U.S. Govt. Printing Office), 1305–1331.
Powell, T. G., 1978. *An assessment of the hydrocarbon source rock potential of the Canadian Arctic Islands.* Geol. Surv. Can. Pap., 78-12.
Quilty, P. G., 1980. Sedimentation cycles in the Cretaceous and Cenozoic of Western Australia. *Tectonophysics,* 63:349–366.
Ramsay, A.T.S., 1974. The distribution of calcium carbonate in deep sea sediments. *Soc. Econ. Paleontol. Mineral. Spec Publ.,* 20:58–76.
Riech, V., and von Rad, U., 1979. Silica diagenesis in the Atlantic Ocean: diagenetic potential and transformation. *In* Talwani, M., Hay, W., Ryan, W.B.F. (Eds.), *Deep Drilling Results in the Atlantic Ocean: Continental Margins and Paleoenvironment:* Washington (Am. Geophys. Union), 315–340.
Roth, P. H., 1978. Cretaceous nannoplankton biostratigraphy and oceanography of the Northwestern Atlantic Ocean. *In* Benson, W. E., Sheridan, R. E., et al., *Init. Repts. DSDP,* 44: Washington (U.S. Govt. Printing Office), 731–759.
Sanfilippo, A., Westberg-Smith, M. J., and Riedel, W. R., 1985. Cenozoic radiolaria. *In* Bolli, H. M., Saunders, J. B., and Perch-Nielsen, K. (Eds.), *Plankton Stratigraphy:* Cambridge (Cambridge Univ. Press), 631–712.
Sangree, J. B., and Widmier, J. M., 1977. Seismic interpretation of clastic depositional facies. *In* Payton, C. E. (Ed.), *Seismic Stratigraphy—Applications to Hydrocarbon Exploration.* AAPG Mem. 26:165–184.
Scheibnerova, V., 1974. Aptian-Albian benthonic foraminifera from Leg DSDP 27, Sites 259, 260, and 263, Eastern Indian Ocean. *In* Veevers, J., Heirtzler, J. R., et al., *Init. Repts. DSDP,* 27: Washington (U.S. Govt. Printing Office), 697–741.
Sclater, J. G., Parsons, B., and Jaupart, C., 1981. Oceans and continents: similarities and differences in the mechanisms of heat loss. *J. Geophys. Res.,* 86:11535–11552.
Sissingh, W., 1977. Biostratigraphy of Cretaceous calcareous nannoplankton. *Geol. Mijnbouw,* 56:37–65.
Thierstein, H. R., 1976. Mesozoic calcareous nannoplankton biostratigraphy of marine sediments. *Mar. Micropaleontol.,* 1:325–362.
Vail, P. R., Mitchum, R. M., Jr., Todd, R. G., Widmier, J. M., Thompson, S., III, Sangree, J. B., Bubb, J. N., and Hatlelid, W. G., 1977. Seismic stratigraphy and global changes in sea level. *In* Payton, C. E. (Ed.) *Seismic Stratigraphy—Applications to Hydrocarbon Exploration.* AAPG Mem., 26:49–212.
Veevers, J. J., and Johnstone, M. H., 1974. Comparative stratigraphy and structure of the Western Australian margin and the adjacent deep ocean floor. *In* Veevers, J. J., Heirtzler, J. R., et al., *Init. Repts. DSDP,* 27: Washington (U.S. Govt. Printing Office), 571–585.
Williamson, P. E., and Falvey, D. A., 1988. Preliminary post cruise report *Rig Seismic* research cruises 7 and 8 deep seismic structure of the Exmouth Plateau. *BMR Record 1988,* 31.
Wright, A. J., and Wheatley, T. J., 1979. Trapping mechanisms and hydrocarbon potential of the Exmouth Plateau, Western Australia. *APEA J.,* 19:19–29.

MS 122A-108

NOTE: All core description forms ("barrel sheets") and core photographs have been printed on coated paper and bound as Section 3, near the back of the book, beginning on page 387.